Australian National University

PhD THESIS

New techniques to assess ^{231}Pa and ^{227}Ac abundance and transfer in environmental media

Peter Medley

24 July 2025

A thesis submitted for the degree of Doctor of Philosophy of The Australian National University

Declaration

This thesis is the result of research undertaken part-time between February 2015 and November 2024 at the Department of Nuclear Physics & Accelerator Applications, Research School of Physics, College of Science, the Australian National University (ANU), Canberra, Australia, under the supervision of Associate Professor Dr Stephen Tims, Dr Michaela Froehlich and Dr Andreas Bollhöfer.

The material presented in this thesis is, to the best of my knowledge, original or is referenced. Parts of the results have been published and their references are given. Contributions of other parties are acknowledged in the text or the acknowledgements.

Peter Medley

24 July 2025

Acknowledgements

I would like to acknowledge the multitude of people that helped me to complete this PhD and make special mention of those that helped me throughout the study and along the way.

My supervisors Dr Andreas Bollhöfer, Dr Michaela Froehlich and Associate Professor Stephen Tims for their encouragement, patience and support throughout the thesis while juggling their own work, life and family commitments. Andreas as my manager at work was always supportive of my interest in undertaking scientific research despite it not being part of my defined role. As a supervisor for my Honours degree by research he was a great help in getting me started on the PhD and, despite moving to Germany early on, continued to provide advice and assistance throughout the many years of study. Michaela's advice, as the only chemist on the panel was invaluable in working through the difficult problems encountered and helped to ensure that the chemistry involved in the thesis came to the fore. Michaela's patience in working through challenges and willingness to provide direct and constructive criticism was instrumental in the substantial improvement in my research skills and writing, notwithstanding many more than 1 or two grammatical errors, throughout the project.

The Traditional Owners of the lands on which this project was undertaken, the Mirarr and other Bininj/Mungguy, Kungarakan and Warai, Larrakia, Jagera and Turrbal, Ngunnawal and Ngambri people.

As a mature age, remotely based, and part-time student I was acutely aware that the choice and selection of the chair of my supervisory panel was of paramount importance. I don't think it could have been possible to make a better choice for that role than Steve, and I credit that as one of the best decisions of my life. His support, both professional and personal throughout the project was appreciated beyond measure and fundamental to getting this project completed. Steve's family were also wonderfully friendly and generous hosts in the many times I stayed there while down in Canberra for study leave.

The people that have helped me get to the point of being able to undertake a PhD are many and varied, though there are a few without whom I would not have embarked on a career in nuclear science. Firstly, Michelle Iles, who let me know of an upcoming position and was my first supervisor along the path of becoming a nuclear scientist. Her support, patience, and more patience, with some forbearance thrown in for good measure was more than anyone can ask for. Early in my career, while still considering if I was taking the right path, a now good friend, John Pfitzner told me that I needed to decide if I wanted to be a radiochemist and that if I did,

then I should commit to it. Excellent advice, and a major factor in getting to this point today. I also need to thank Dr Paul Martin, a supervisor in my early career, who supported my involvement in research and had endless time to teach me the ins and outs of radiochemistry, alpha and gamma spectrometry, and numerous other areas of nuclear science and applications.

Early in the project, the ^{237}Np cow, the cornerstone of the research, developed a leak within hours after being prepared. This could have had disastrous consequences for the entire project, fortunately, some advice from my brother, Raymond Medley, an architectural modelmaker with extensive experience on handling plastics led to a quick and reliable fix that ensured stability through the remainder of the project. Ray also showed his dedication to helping by venturing into the jungle out the back of Humpty Doo to collect green ants and, in defiance of the angry, biting creatures, provided the 'Arthropod' sample and associated soil for the project.

The Environmental Research Institute of the Supervising Scientist (ERISS) for providing the financial support through study leave and conference attendance to present progress in the first several years of the project, as well as samples and laboratory access. In particular, I'd like to thank Dr Che Doering and John Pfitzner for providing data from ERISS databases and internal reports, and advice and training in gamma spectrometry, ERICA tool dose assessments and dose modelling for the Ranger Uranium Mine. Also, from ERISS, Fiona Evans and Jefferson Chen that kept the laboratory going, washed my glassware, prepared my solutions, and were always generous with their help for the project. Dr Melanie Trenfield of ERISS undertook the organic and inorganic carbon measurements, Dr Scott McMaster coordinated sample collection for a water sample and several soil samples analysed for the project.

Queensland Health, Radiation Sciences (RS), where I took up a new position part way through the project for continuing the financial support through study leave and conference attendance until its conclusion. My managers Dr Ross Kleinschmidt and then Drew Watson were always supportive of the project, despite major upheavals throughout its course. This included a major generational change with over 70% staff turnover in less than 18 months that was almost immediately followed by a global pandemic, leading to a permanent change in the way work was conducted. The RS laboratories were also made available, and the majority of the chemical, alpha and gamma spectrometric analysis was undertaken there. Again, from RS, the numerous laboratory staff that kept the laboratory going, washed my glassware, prepared my solutions, counted my samples, and were always generous with their help for the project Dimitri Nikolakopoulos, Sian Patterson, Kathy Coles, Dominique Scott, Michelle Thomas, Bradley Van Luenen, Sarah Mullins, Pushpendra Chauhan, Pierre Bouchereau de Pury, and Matthew

Wiggins. The various laboratory services coordinators at RS, Michelle Marshall, Mark Waterson, and Jessica Chorusch for getting paperwork completed, laboratory equipment and solutions delivered on time, and generally ensuring all the unseen jobs to keep things running smoothly were taken care of.

Dr Mat Johansen who coordinated access to the Australian Nuclear Science and Technology Organisation (ANSTO) Laboratories and Nicholas Howell for undertaking the autoradiography measurements at ANSTO.

The Australian Institute of Nuclear Science and Engineering (AINSE) provided several travel grants to attend conferences and present work undertaken as part of this thesis.

The numerous friends that let me stay while I attempted to thaw out when visiting Canberra to undertake the AMS aspects of the project (which somehow always happened to require leaving fantastic dry season weather in Darwin or late spring in Brisbane to a wintry cold snap in Canberra). Michael, an endless source of erudition on topics deep and varied, his wife Tracy and the family, Tim, a poet and general funkster, and his wife Jo and their family were my mainstays. Elaine and later Jim after he moved into his own wonderful house where many hours were spent enjoying a cold beverage or two over a fire in the backyard. Finally, John and Bess, Rhonda, and Lucy, also made a room available, which was deeply appreciated.

I'd like to finish here by thanking my partner Tida for her forbearance, patience, tolerance, and too many other virtues to count who has been a constant support over the many years, and I want to let you know that I'll be back soon.

Abstract

The focus of this thesis is on the Ranger Uranium Mine (RUM), which is now in a rehabilitation stage after ceasing all mining and milling in 2021. The RUM mining lease is surrounded by Kakadu National Park (KNP), a world heritage listed area for both natural and cultural reasons. The aim of rehabilitation is to return the land to the Indigenous Traditional Owners where traditional land usage post remediation will take place, including camping, hunting, and foraging.

An assessment of the potential radiological dose above the natural background from the RUM rehabilitated mining lease is required. This includes potential human exposure due to gamma radiation, radon and its progeny, inhalation of dust, and ingestion of radionuclides from traditional food items collected from the area. Radiological dose to the environment is also an important component of the dose assessment. The above background radionuclide concentrations of uranium and radioactive progeny in air, soil and water, and the expected occupancy of the site form the basis of the dose assessment.

Uranium has three naturally occurring radioactive isotopes with a high enough activity concentration to be relevant for radiological dose from U mining – ^{238}U, ^{235}U and ^{234}U. Both ^{238}U and ^{234}U are part of the ^{238}U decay series that has been studied extensively in the region. Uranium-235 is at the head of a unique decay series, which has received limited attention for dose assessment owing to the low relative abundance (about 5% by activity) compared to the ^{238}U series. It is thus generally assumed that the ^{235}U decay series will not make a significant contribution to radiological dose from uranium mining, however, this assumption has not been explicitly tested.

The most relevant radionuclides in the ^{235}U series are ^{227}Ac and ^{231}Pa, primarily as they have long enough half-lives for environmental migration and uptake into biota. The movement and partitioning of ^{227}Ac and ^{231}Pa in the environment, particularly in the study region, was largely unknown at the commencement of this thesis. Thus, the primary aim of this project was to assess the radiological dose from ^{227}Ac and ^{231}Pa to the environment, and to people via the ingestion pathway from traditional food items collected in and around the RUM mining lease post rehabilitation.

It was critical to develop separation methods for ^{227}Ac and ^{231}Pa from environmental samples as techniques with the desired detection limits for the sample matrices had not been previously published. This included methods for preparation of the yield tracers ^{225}Ac and ^{233}Pa, necessary

to assess losses of Ac and Pa throughout the sample preparation and chemical separation processes.

A technique was developed to prepare a ^{233}Pa generator (a ^{237}Np cow) for regular extraction of ^{233}Pa from the parent radionuclide ^{237}Np using ion chromatography. A published technique for separation of ^{227}Ac was adapted for extraction of ^{225}Ac from the parent radionuclide ^{229}Th to be used as a tracer. Novel methods were designed for sample preparation and separation of Pa from biological sample matrices using microwave-assisted wet-acid digestion followed by ion chromatography. Verification of the suitability of dry-ashing and published ion chromatography methods for separation of ultra-low levels of ^{227}Ac (<1 mBq kg^{-1} fresh weight) in high sample masses (up to 250 g wet weight) was also undertaken. A $Nd(OH)_3$ coprecipitation technique for actinides from a published method was adapted and optimised to produce Ac sources for alpha spectrometry.

Accelerator Mass Spectrometry (AMS) with the 14UD tandem accelerator at the Australian National University was used for the ^{231}Pa measurement after radiochemical separation. Both isotopes of Pa (^{231}Pa and ^{233}Pa) are analysed concurrently with AMS and ultra-low detection limits (<1 mBq kg^{-1} fresh weight) were achieved with a substantially lower mass (<10 g wet weight). This overcame some of the unique challenges with the chemistry of Pa for measurement of environmental samples. The Cs negative ion source of the 14UD AMS favoured production of PaO_2^- over PaO^-, with the opposite observed for UO_2^- and UO^- and thus isobaric interference from ^{233}U when measuring the tracer ^{233}Pa was significantly reduced, leading to an improvement over previously published techniques using AMS for ^{231}Pa measurement. Use of a time-of-flight system and a ‘fast-cycling’ system to more rapidly switch from measuring mass 231 to mass 233 improved sensitivity and precision respectively.

Concentration ratios (CR) were derived from measurement of bush foods and whole organisms, to allow prediction of ^{227}Ac and ^{231}Pa transfer to organisms on the rehabilitated RUM site. Similarly to ^{238}U series radionuclides, CRs derived for ^{227}Ac and ^{231}Pa spanned several orders of magnitude.

The radiological dose model of the ERICA (Environmental Risks from Ionising Contaminants: Assessment and Management) Integrated approach was applied using the ‘ERICA tool’ for environmental dose assessment. This approach is based on grouping broad ranges of ecologically significant organisms, including plants and animals, into ‘reference organisms’. Data from local species were used in the environmental dose assessment to conduct a

site-specific assessment, with default data from the ERICA tool used for other reference organisms. The limiting organism considering only the ^{235}U series were 'Insect Larvae' and 'Lichen and Bryophytes' for the freshwater and terrestrial environments respectively. The contribution to dose from the ^{235}U series to the limiting organisms 'Mollusc – Bivalve' (freshwater) and 'Reptile' (terrestrial) previously determined for the ^{238}U series was negligible.

Ingestion doses for human exposure from ^{227}Ac and ^{231}Pa were determined from measurements that covered more than three quarters of the traditional diet for the representative person. The estimated annual ingestion dose above background from ^{235}U radionuclides under the anticipated occupancy scenario of the RUM rehabilitated site by traditional owners was less than 1.6 µSv per year. The highest estimated doses were from the freshwater environment were from freshwater mussels for ^{227}Ac and magpie goose for ^{231}Pa. Yams were the highest contributors to estimated doses from the terrestrial environment for both ^{227}Ac and ^{231}Pa. The relative dose contribution from individual ^{235}U series radionuclides is relatively low, comparable to ^{238}U and ^{230}Th, with ^{210}Po, ^{226}Ra and ^{210}Pb remaining the highest contributors to dose from the ingestion pathway for the RUM rehabilitated site.

Measured activity concentrations of ^{227}Ac and ^{231}Pa demonstrated, through the first direct measurements of ^{231}Pa and quantifiable results of ^{227}Ac (e.g., above the limit of detection) from traditional food items, that there is a very low relative dose contribution from the ^{235}U series in the study region. This highlights that the radiological criteria for soil quality (being the medium for transfer to plants and animals) for mine closure, will essentially be limited by potential activity concentrations of ^{210}Po, ^{210}Pb and/or ^{226}Ra and not from ^{235}U series radionuclides.

Confirmation of the low contribution of ^{235}U series radionuclides to dose through direct measurement is an important aspect for communication of the rehabilitation success for the RUM site. Such direct measurements are unique in global dose assessment and can help to provide confidence for traditional landowners that reconnecting with country and with places of cultural significance on the site can be done safely.

Equally important is the contribution to demonstrating successful mine rehabilitation for RUM, which can provide the global community with assurances that the internationally significant and world heritage listed KNP is, and will remain, protected from the impacts of U mining.

Contents

Table of figures

List of tables

List of equations

Glossary

Abbreviations/acronyms

ADC	Analogue-to-digital convertor
AMS	Accelerator mass spectrometry/spectrometer
ANU	Australian National University
ARR	Alligator Rivers Region
Conc.	Concentrated
CR	Concentration ratio
$CR_{WO\text{-}Media}$	Concentration ratio for 'Whole organism' to environmental media
CRM	Certified reference material
DC	Dose coefficient (for inhalation or ingestion doses to humans)
DCC	Dose conversion coefficient (used exclusively for non-human biota)
DCRL	Derived consideration reference levels
EMCL	Environmental media concentration limits
ERISS	Environmental Research Institute of the Supervising Scientist
FWHM	Full-Width-Half-Maximum
GM	Geometric mean
HF	Hydrofluoric acid
HRGS	High-resolution gamma spectrometry
IAEA	International Atomic Energy Agency
ICP-MS	Inductively coupled plasma mass spectrometry
ICRP	International Commission on Radiological Protection
IR	Ionising radiation
KNP	Kakadu National Park
LDPE	Low density polyethylene
LNT	Linear-no-threshold
MCA	Multichannel analyser
MC-ICP-MS	Multi collector inductively coupled plasma mass spectrometry
MDL	Minimum detection limit
MS	Mass spectrometry
NIR	Non-ionising radiation
NIST	National Institute of Standards and Technology (United States)
NORM	Naturally occurring radioactive material

NT	Northern Territory (of Australia)
PDF	Probability distribution function
PES	Polyethersulfone
PET	Polyethylene terephthalate
PFA	Perfluoroalkoxy alkane
PIPS	Passivated implanted planar silicon
PMT	Photomultiplier tube
PP	Polypropylene
PTFE	Polytetrafluoroethylene
PVDF	Polyvinylidene
QA/QC	Quality assurance/quality control
REE	Rare earth elements (this includes the lanthanides, yttrium and scandium)
ROI	Region of Interest
RPA	Ranger Project Area
RQ	Risk quotient
RUM	Ranger Uranium Mine
TOF	Time-of-flight
UNSCEAR	United Nations Scientific Committee on the Effects of Atomic Radiation
XRF	X-Ray fluorescence spectroscopy

Definitions

General

Billabong: A branch of a river forming a backwater or stagnant pool, made by water flowing from the main stream during a flood.

Biological half-life: The time it takes to reduce the amount of an element in a specific organ or the whole the body to half its original value solely from biological processes.

Capacity factor (*k'*): A measure of the level of interaction with a solute and stationary phase in ion chromatography and ion exchange procedures.

Distribution coefficient (K_d): The equilibrium partitioning of a substance between two phases. In this thesis it refers to a solid phase (sediment) and liquid phase (water). The SI unit used for K_d is L kg^{-1}.

Radiation protection units

Absorbed dose: The energy in joules (J) deposited in a kilogram (kg) of a substance by radiation. Absorbed dose has the SI unit of Grays (1 J kg^{-1} = 1 Gy).

Annual effective dose: The effective dose summed for one year.

Equivalent dose: Absorbed dose multiplied by a radiation weighting factor for each type of radiation. Equivalent dose has the SI unit of Sieverts (Sv).

Effective dose: Equivalent dose multiplied by a tissue weighting factor to account for the sensitivity of different tissues and organs to radiation. Effective doses for all tissues and organs can be summed and then summed to give the whole-body effective dose. Effective dose also has the SI unit of Sieverts (Sv).

Committed effective dose: The total dose from an incorporated radioactive element expected to be delivered within a specified time. For members of the public this is the time integrated average over 50 years or to 70 years of age for children. Committed effective dose has the SI unit of Sieverts (Sv).

Radioactive decay and nuclear properties

Secular equilibrium: A situation whereby the quantity of a radioactive isotope remains constant because its production rate is equal to its decay rate. Secular equilibrium within a decay

series (e.g., the ^{238}U series) is when all radioactive isotope in the series can be considered to decay at the same rate (i.e., with the half-life of the parent radionuclide).

Non-SI units used

hr	Hours
d	Days
min	Minutes
yr	Years

Non-SI symbols used

k'	Capacity factor
K_d	Distribution coefficient (This is typically a unit less value, derived from dividing the activity concentration in a solid phase by that in the dissolved phase, however, it may sometimes be represented as L kg^{-1} to distinguish different units in the activity concentrations used)
M	Mean
SD	Standard deviation
t½	Half-life or half-lives

Nuclear decay data

Unless noted otherwise all nuclear decay data (e.g., half-life, alpha particle energy) reported throughout this thesis is taken from the Decay Data Evaluation Project (Dulieu et al., 2017).

Rounding, Tabulated blank data, and Reporting of uncertainty

Rounding is generally only to two significant figures, and to a maximal of three significant figures. The increased precision is used where measurements have been made as part of the present work. Rounding was done in accordance with Standards Australia (2003).

In tabulated data, where a field is left blank then no value is available for that field.

For reporting of uncertainty, unless noted otherwise:

- Uncertainty is reported as two standard deviations.

- Measurement uncertainty for analytical results for all measurements undertaken for this thesis has been reported as the expanded measurement uncertainty and calculated according to the principles of JCGM (2008).

Chapter 1 : The ^{235}U series in the environment and relevance for U mining dose assessment

Mining and milling of U is conducted in many parts of the world and has been for many years, with the first example of mining specifically for U occurring in the 1850s. This initial period of U mining was for production of colours and U glass. Uranium mining expanded in the early 19th century, primarily for the extraction of Ra after it was discovered by Marie Curie (Veselovský et al., 1997). Mining activity was reduced through the 1930s as the market for Ra diminished, and it was not until the 1940s that a resurgence in mining occurred. Large scale mining of U began after World War II directed at U extraction for production of nuclear weapons (Uranium in Plants and the Environment, 2020). The primary purpose of production pivoted in the late 1960s to the supply of nuclear fuel for civil purposes (e.g., energy generation, nuclear medicine, research and development) peaking in the late 1980s (Mudd and Diesendorf, 2008).

Environmental and social impacts from U mining and milling are many and varied and include those identified for many other types of mining operations (Darling et al., 2011). Though not exclusively related to U mining, the radiological dose[1] associated with U in the context of U mining is an important potential impact requiring explicit consideration (e.g., Darling et al., 2011; Ettenhuber, 2002). The UNSCEAR (2000) report, a comprehensive assessment of global sources and effects of ionising radiation, assessed the relative contribution to radiological dose from aspects of the nuclear fuel cycle, showing that U mining is a significant contributor to total collective dose to members of the public.

Assessment of the potential radiological dose arising from U mining and milling generally requires consideration of doses to workers and members of the public, both during operation and after mine closure (e.g., Bollhoefer et al., 2002; Doering and Bollhöfer, 2016b; Martin, 2000; Rweyemamu and Kim, 2020; Sarkar et al., 2019). Since 2003 radiation doses to the environment have also explicitly been considered. This was a change to previous practice based on an assumption that human radiation protection dose limits guarantee environmental protection that was no longer considered generally acceptable (ICRP, 2003). Doses from all

[1] Throughout this manuscript ‘dose’ refers to radiological dose arising from exposure to ionising radiation unless otherwise specified. Further discussion of dose calculation and the different units used is provided in Chapter 2.

potential pathways[2] should be considered for a comprehensive assessment (ICRP, 2006, 2008a), and this may include long-term assessment and monitoring to confirm dose limits are maintained (e.g., Carvalho, 2012; Landa and Gray, 1995). With 70% of global U deposits located on traditional lands (Dowie, 2009), it is also important to take into account the perspectives of Traditional Owners and the Indigenous population, including traditional cultural practices and activities when assessing potential impacts (Graetz, 2014; Lawrence and O'Faircheallaigh, 2022; Martin and Ryan, 2004; Rock and Ingram, 2020; Sarkar et al., 2019).

Naturally occurring radioactive material (NORM) is the term used to describe materials (such as U ores) containing radionuclides that exist in the natural environment. The radionuclides in NORM of most interest in radiation dose assessment include long-lived radionuclides ^{238}U, ^{235}U and ^{232}Th and their radioactive decay products (such as isotopes of Bi, Pb, Po, Ra and Rn), and the individual long-lived radionuclide ^{40}K. The parent radionuclides have half-lives ($t_{½}$) comparable with or larger than the age of the earth, so they have always been present in the earth's crust and within the tissues of all living species. Sometimes the term TENORM (technically enhanced naturally occurring radioactive material) is used for materials such as U mine tailings.

All living species are exposed to the natural radiation background arising from NORM, levels of which are not easily controlled. While background radiation levels vary across Australia, the average annual dose attributable to the natural background radiation of approximately 1.5–2 mSv for an adult (dose units are discussed in detail in Section 2.1.1). The annual background dose comes from several pathways, with the majority from external exposure to gamma radiation (i.e., from the decay of radionuclides in soils and rocks) at about 0.6 mSv, and internal exposure from inhalation of radon and progeny contributing 0.6–1.1 mSv (ARPANSA, 2008). Radiation from ^{40}K within the human body delivers 0.2–0.25 mSv whereas the estimated contributions from ingestion of food are less than 0.1 mSv for the average Australian diet (Sdraulig et al., 2019). An additional source of natural background radiation is derived from outside the planet, with 'cosmic radiation' contributing about 0.3 mSv (at sea-level) to members of the Australian public (ARPANSA, 2008). Annual background doses can vary by up to 0.5

[2] The capacity for consideration of all pathways for exposure to the environment presents unique challenges and, in many cases may be unachievable. More simplified dose models are used for exposures to the environment compared to human exposures and much more remains to be done on this front. See ICRP (2008a) for further information on this topic and refer to Chapter 2 for a discussion of environmental dose assessment relevant to this thesis.

mSv over distances of only a few kilometres and there appears to be no scientific evidence relating general variations in the natural radiation background to effects on human health (ARPANSA, 2008).

It is therefore relevant to highlight that any assessment of dose arising from planned operations, such as U mining and milling, must be considered in context of the background radiation levels that were present prior to the operation occurring (e.g., see Bollhöfer et al., 2014; Carvalho, 2012; Ettenhuber, 2002). Radiation dose limits will typically be set at a specific level above the natural background.

The research presented in this thesis is addressing a gap in dose assessment for members of the public and the environment from U mining and milling. The gap being a global lack of published information on radionuclides within the ^{235}U decay series for dose assessment (Medley et al., 2024). The focus of the research is on a specific mining region, the Alligator Rivers Region (ARR) in the Northern Territory of Australia, and mining operation, the Ranger Uranium mine (RUM). RUM was responsible for a substantial proportion of global U supply for around 40 years (World Nuclear News, 2021) and is wholly on Indigenous owned land. **The primary aim of this project is to determine the committed effective dose component of the annual effective dose through the ingestion pathway to the 'representative person'. This will be used to assess the relative contribution, and therefore relative importance, of isotopes in the ^{235}U series for determination of the annual effective dose from U mining and milling in the ARR from all pathways, with a focus on RUM.**

Section 1.1 The ^{235}U series: A data gap in dose assessment for U mining and milling

Uranium has five naturally occurring radioactive isotopes, ^{233}U, ^{234}U, ^{235}U, ^{236}U and ^{238}U. Of these, ^{233}U and ^{236}U occur only in trace amounts (Hain et al., 2020; Steier et al., 2008) and are of no significance from a dose perspective.

In stable geological compartments such as rocks, regolith and mineralised U it can be reasonably assumed that all radionuclides in a decay series will be in secular equilibrium. This is a point of time in which the activity concentrations of all radioactive progeny are essentially equal to that of the parent isotope. For such samples, measurement of the activity concentrations of any isotope in a decay series can give reliable information on the expected activity concentrations for the entire decay series. Natural weathering or industrial processes, such as mining and milling, can lead to the release of selected radioactive isotopes into the environment

(e.g., Ettenhuber, 2002; Landa and Gray, 1995). The number of radionuclides in each decay series, and the existing range of physical and chemical properties of the individual radionuclides within a decay series (e.g., differing solubilities, oxidation or physical states) in different media can lead to a substantial deviation from secular equilibrium in environmental systems. Under these circumstances, the assumption of secular equilibrium for a decay series cannot be maintained.

Both ^{238}U and ^{234}U are part of the ^{238}U decay series (Figure 1-1), along with other radionuclides including ^{226}Ra, ^{222}Rn (a radioactive noble gas) ^{210}Pb and ^{210}Po. The environmental occurrence and movement of isotopes in this series have been studied extensively (e.g., see IAEA, 2014a, 2017; UNSCEAR, 2000 and references therein), with ^{226}Ra and ^{210}Po the most widely studied for uptake (Tagami et al., 2012).

Uranium-235 is the parent isotope of a unique decay series, known as the actinium series or ^{235}U series (Figure 1-2). As the relative activity of ^{235}U (and hence progeny), is only about 5% compared to ^{238}U, it is often assumed that it will not contribute significantly to radiation dose (e.g., Beaugelin-Seiller et al., 2016; UNSCEAR, 2000; Vicente et al., 1991) and it is often overlooked in dose assessment for NORM (e.g., Caffrey et al., 2023; Gellermann et al., 2023). The assumption that the ^{235}U series does not contribute significantly to dose, does however not consider that significant differences in environmental transport, fractionation and accumulation can arise owing to differences in the chemistry, biochemistry or half-lives of the elements in the two decay chains. Vicente et al. (1991) concluded that the ^{235}U series should be considered in dose assessments associated with the nuclear industry and the more recent modelling by (Beaugelin-Seiller et al., 2016) has suggested that the relative contribution to environmental dose from radionuclides in the ^{235}U series may be higher than assumed, potentially up to 75% of the total dose. There is therefore a need to measure ^{235}U series radionuclides in environmental samples to facilitate more reliable dose assessments for the environment and human health. Although Lowe (1997) noted the necessity to include the ^{235}U decay series in dose assessments involving inhalation of natural U, the inhalation pathway is out of scope of this study.

It is important that comprehensive and defensible scientific decisions are made in relation to the nuclear industry, particularly for issues such as mine closure, where post-closure impacts may last for many years beyond initial assessments (O'Faircheallaigh and Lawrence, 2019). Effective communication of such decisions is equally as important to ensure business continuity, environmental and social risks associated with those decisions are addressed (Graetz, 2014; Graetz and Manning, 2011).

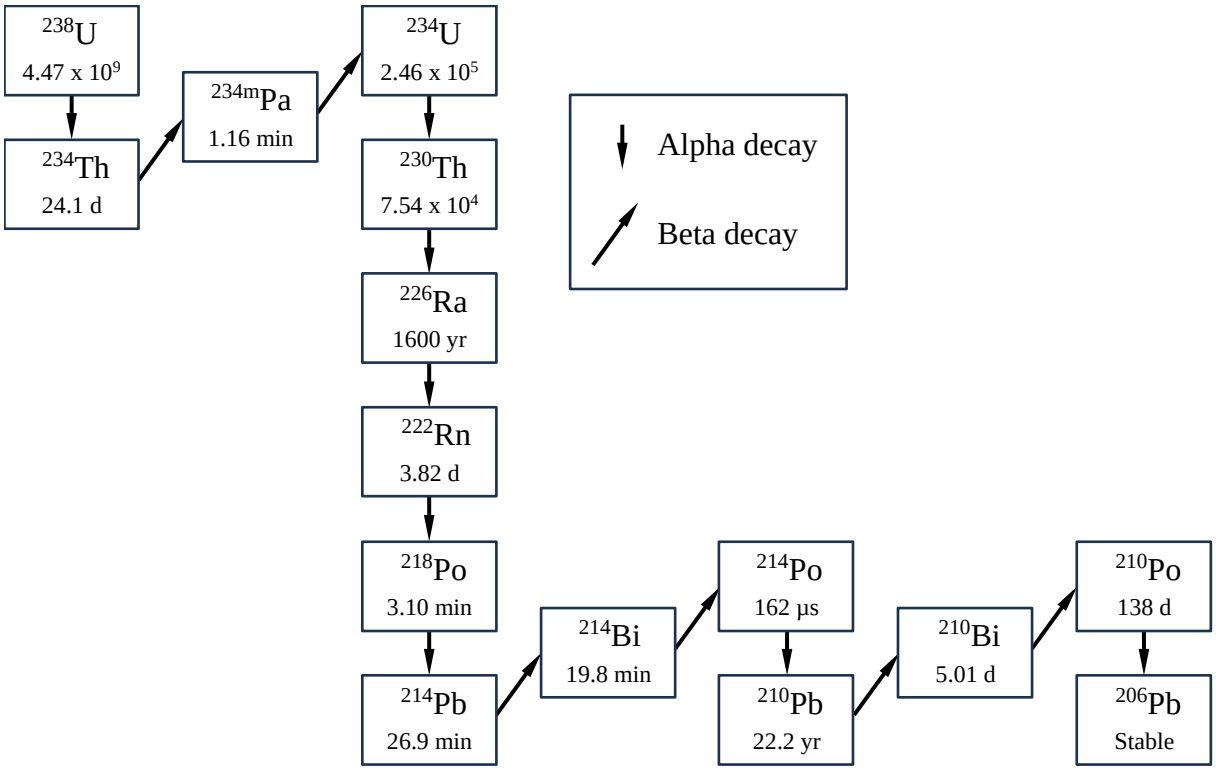

Figure 1-1 ^{238}U decay series.

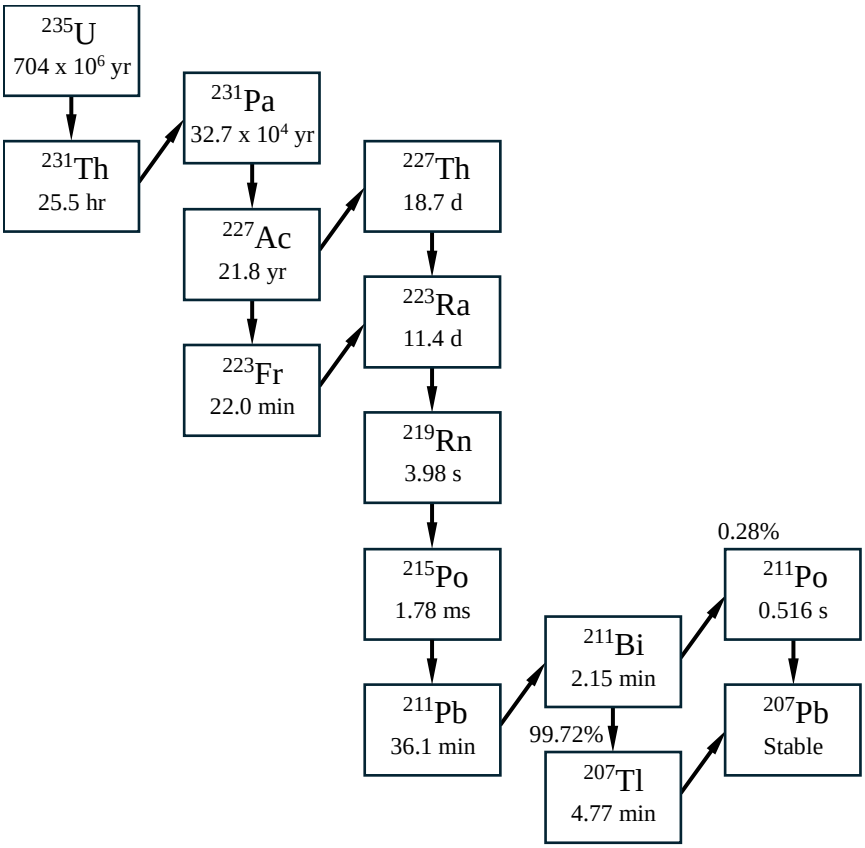

Figure 1-2 ^{235}U decay series.

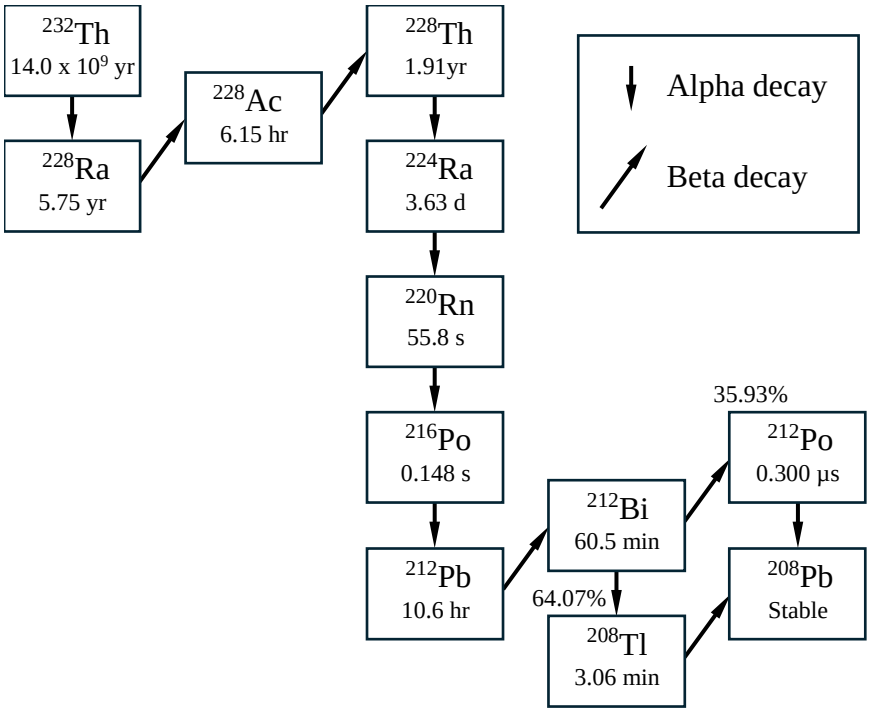

Figure 1-3 ^{232}Th decay series.

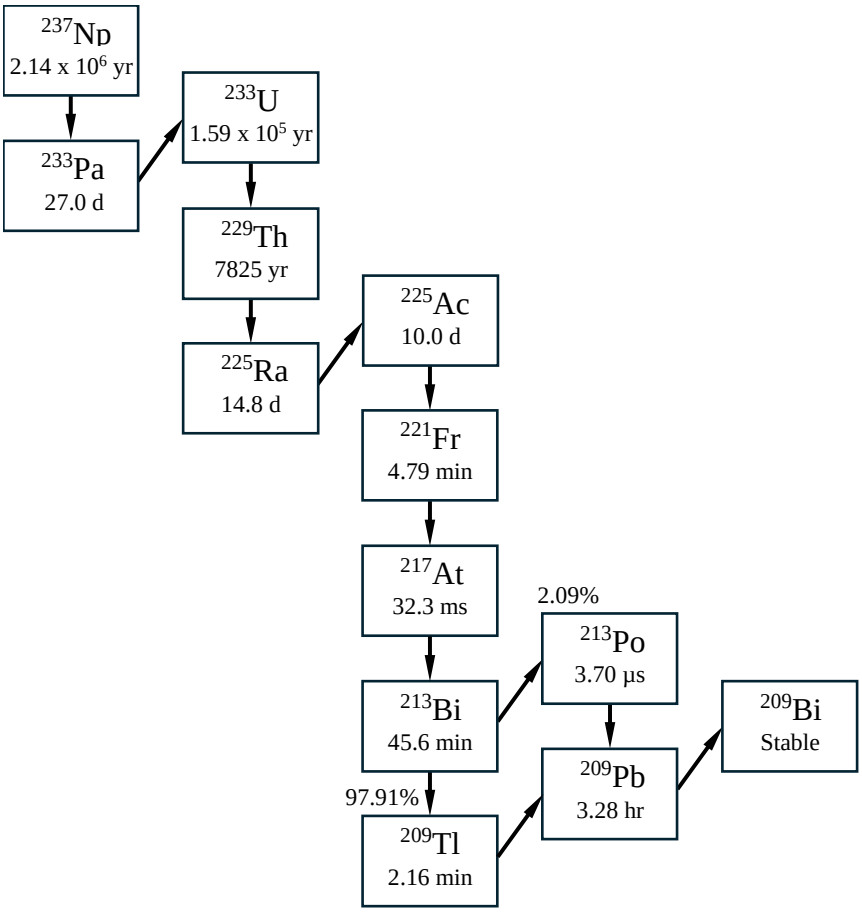

Figure 1-4 ^{237}Np decay series. Half-life of ^{229}Th taken from Essex et al. (2018).

Poor engagement and consultation with traditional owners by mining companies has a long history in Australia and globally, leading to a lack of trust and wariness within many Indigenous communities (Graetz and Manning, 2011). Heightened perceptions of risks specific to U mining, compared to the overall mining industry in Australia, necessitate a higher standard of engagement and consultation by U mining companies (Graetz and Manning, 2011). Although radiation doses from ^{235}U series radionuclides are assumed to be very low (e.g., Beaugelin-Seiller et al., 2016; UNSCEAR, 2000; Vicente et al., 1991) the knowledge underpinning these assumptions is scarce and technically complex. Site-specific measurements of food and environmental items for a comprehensive list of potential contributors to radiological dose, in consultation with Indigenous Traditional Owners, represents a high standard of engagement and consultation. Direct measurements to allow inclusion of site-specific dose estimates for ^{235}U series radionuclides can lead to greater engagement with traditional owners and improve trust in statements regarding the safety of people and the environment. Such measurements also have the advantage of providing relevant data for regional and global datasets where none currently exists.

1.1.1 The ^{235}U series

The ^{235}U decay series has eight radioactive isotopes that may contribute significantly to dose: ^{231}Pa, ^{227}Ac, ^{227}Th, ^{223}Ra, ^{219}Rn, ^{215}Po and ^{211}Bi and the decay chain parent ^{235}U (Figure 1-2). The short half-life of ^{219}Rn, ^{215}Po and ^{211}Bi (< 3 min) indicate that these isotopes do not need to be considered independently for the development of dose models. For these radionuclides, dose contribution is assessed based on an assumption of equilibrium with the parent isotope ^{223}Ra. Thorium-227 and ^{223}Ra are also not expected to bio-accumulate to significant levels independently of their closest parent isotope, ^{227}Ac ($t_{½}$ = 21.77 yr), owing to their relatively short half-lives of 18.7 d and 11.4 d respectively (e.g., Thiessen et al., 1999). Dose for ^{227}Ac therefore will typically include the dose derived from ^{227}Ac, ^{227}Th, ^{223}Ra and progeny (Brown et al., 2016; ICRP, 2012).

A substantial amount of information regarding the ^{238}U series in the Australian environment has been published (e.g., Doering, 2019a; Doering and Bollhöfer, 2016a; Doering et al., 2022; Johansen and Twining, 2010; Medley et al., 2017). This was highlighted in the review by Hirth (2014) of available radionuclide data for non-human biota inhabiting Australian U mining environments where no published ^{235}U series data was located by the author. There is also an abundance of ^{238}U series data published internationally (e.g., IAEA, 2010, 2014a, 2017, 2023). These data provide substantial information for dose assessment from naturally occurring

sources, however, they are not always suitable as a proxy for ^{235}U decay products for reasons outlined above and below.

The isotopes ^{227}Ac, ^{231}Pa and ^{235}U are the most relevant isotopes of the ^{235}U decay series for assessment of transfer to humans and non-human biota. This is because they have long enough half-lives for environmental migration and uptake into biota. Environmental release of ^{227}Ac can occur from practices associated with the nuclear fuel cycle, such as U mining, thereby potentially increasing the radiation dose to humans and to the environment (Beaugelin-Seiller et al., 2016; Vicente et al., 1991). This is also true for ^{231}Pa, where relatively high concentrations in the environment may be associated with U mining and milling (e.g., Beaugelin-Seiller et al., 2016; Medley et al., 2019; Terning, 1970). The natural ^{235}U:^{238}U isotope ratio in NORM varies to a negligible degree for consideration of uptake and ^{238}U can therefore be a reliable measure of ^{235}U activity concentrations (Richter et al., 2010).

With very little published data globally for ^{227}Ac and ^{231}Pa, the current state of knowledge for either isotope in the environment for dose assessment to members of the public and to the environment is very limited. Although references above indicate results exist for ^{235}U series radionuclides in the environment (e.g., Beaugelin-Seiller et al., 2016; Vicente et al., 1991), a common theme is the limited amount of published information on environmental concentrations (e.g., Geibert et al., 2008; Medley et al., 2024). There are no prior measurements of ^{231}Pa from the region assessed for this thesis, and only a small number for ^{227}Ac. As such, the contribution to dose to people and the environment in this region from ^{227}Ac and ^{231}Pa is largely unknown.

Beaugelin-Seiller et al. (2016) undertook a review and modelling exercise to estimate the relative importance of the ^{235}U series for radiation dose to wildlife. The results from that study challenged the assumption that ^{235}U series radionuclides make a negligible contribution to wildlife radiation doses and highlighted the need for measurement and assessment. Further conclusions from this work highlighted the need to ensure that high quality validated measurement methods for the measurement of radionuclides of the ^{235}U series are available. Many publications detail methods for analysis of radionuclides in environmental samples, including those of the ^{235}U series (e.g., Alharbi and Akber, 2017; Martin et al., 1995; Moore and Arnold, 1996; Regelous et al., 2004; Sill, 1978; Summerton, 1992a). However, successful application to the sample types (biota, soil, and water) required for this project, while achieving ultra-low limits of detection is not guaranteed. This is owing to the unique and challenging chemical behaviour of the two key radionuclides in the ^{235}U series, ^{227}Ac and ^{231}Pa, and to the very low expected activity concentrations in the biota and water samples. As such, there is a

necessity to validate methods adopted for this project. Development, validation, and verification of methods for analysis of these two radionuclides is a key component of this research and discussed in detail in Chapters 3 and 4.

Section 1.2 Current state of knowledge about the ^{235}U series in the environment

The two primary variables in dose assessment from NORM are the environmental activity concentrations of each radionuclide (both internal and external to the organism or population being assessed) and the dose per unit activity. Environmental concentrations are governed by chemical and physical properties, which determine environmental migration and transfer to plants and animals, including foods. Whereas dose per unit activity is determined only by the physical (radioactive) properties of the radionuclide.

A common assumption is that ^{235}U series radionuclides will not contribute significantly to radiological dose (UNSCEAR, 2000), however, some studies have made efforts to quantify the dose contribution (e.g., Beaugelin-Seiller et al., 2016; Doering et al., 2017; Vicente et al., 1991). The limited range of useful data to assess radiation doses, means such assessment reporting the potential significance of ^{235}U series isotopes for dose is poorly supported by evidence. The limitations of studies assessing the potential significance of ^{235}U series in radiological dose assessment and the relatively low traceability of values used for assessment are discussed in detail in (Medley et al., 2024). The use of chemical or isotopic analogues for estimating environmental concentrations of radionuclides in the ^{235}U series, and the potential relative contribution to dose is discussed below.

1.2.1 Analogues used to assess environmental concentrations of the ^{235}U series in radioecology

Where dose assessments for ^{235}U series radionuclides are undertaken, indirect methods of estimation are used to determine environmental activity concentrations, largely because of limited data availability. Radioecologists may estimate the activity of ^{235}U series isotopes in environmental media and non-human biota by assuming equilibrium with the parent ^{235}U (Beaugelin-Seiller et al., 2016). In other cases, chemical or isotopic analogues are used to estimate concentrations in sediments or water using sediment distribution coefficients (K_d values) (IAEA, 2004). Chemical or isotopic analogues are also used to determine concentration ratios (CRs) to predict transfer to plants and animals (e.g., Brown et al., 2016; Doering et al., 2017; IAEA, 2004; ICRP, 2009; Martin et al., 1998). The most recent work by (Beaugelin-Seiller et al., 2016) is the most comprehensive assessment from an environmental

perspective. The published data cited by (Beaugelin-Seiller et al., 2016) for assessing dose from the ^{235}U series, however, is not based on actual measurements of isotopes within the series but largely based on the use of analogues (Medley et al., 2024).

The use of analogues is primarily a result of the relative paucity of data regarding the uptake of ^{227}Ac and ^{231}Pa into plants and animals (Beaugelin-Seiller et al., 2016) which is partly due to the difficulty of chemical separation and measurement techniques (e.g., Berry et al., 1989; Dulaiova et al., 2013; Myasoedov et al., 2011; Sheppard and Herod, 2012; Sill, 1978). The relatively low abundance of ^{235}U at only 2% of the specific activity of natural U (Richter et al., 2010) is also a major contributing factor to the lack of research into isotopes of the ^{235}U series.

The chemical behaviour of ^{223}Ra, ^{227}Th and ^{235}U can be modelled through more commonly measured isotopic analogues such as ^{226}Ra, ^{232}Th/^{230}Th and ^{238}U respectively. From an uptake and accumulation perspective, isotopic analogues of ^{219}Rn, ^{215}Po and ^{211}Bi are irrelevant owing to the very short half-lives of these three isotopes. Similarly, the use of isotopic analogues to predict uptake of ^{227}Th and ^{223}Ra are unlikely to be accurate as ^{227}Th and ^{223}Ra are not expected to bio-accumulate to significant levels independently of their closest parent isotope, ^{227}Ac. The only radioactive isotopes of Ac and Pa in the ^{238}U decay series have half-lives of six hours and about one minute respectively. They therefore have a limited environmental mobility and cannot be used as analogues for ^{227}Ac and ^{231}Pa.

Where an isotopic analogue (e.g., ^{226}Ra for ^{223}Ra or ^{238}U for ^{235}U) does not exist, other elements are often used as chemical analogues for environmental migration (IAEA, 2010). The valence state and ionic radius of an element are important considerations when selecting potential chemical analogues, as are the chemical conditions, speciation and other parameters in the environment for which an analogue is selected (Varga et al., 2009).

The use of rare earth elements (e.g., Ce and Ln) as analogues for Ac is suggested owing to the similar chemical properties (i.e., +3 oxidation state) and is used in many publications (e.g., Chapman et al., 1968; Staven et al., 2003). For Ac, La and Th have been shown to be close analogues (Linsalata et al., 1991; Linsalata et al., 1989). Martin et al. (1998) considered Th to be an analogue for ^{227}Ac and later Doering et al. (2017) used U as an analogue for ^{231}Pa and Th for ^{227}Ac in developing CRs to estimate dose from ingestion of bush foods in the study region. The Ac ion has very similar chemical properties to La and many of the rare earths yet has a significantly higher atomic mass. With higher uptake of lanthanides associated with lower

atomic mass (Summerton, 1992a) the use of La as an analogue for Ac may likely represent a more conservative approach than the use of Th.

Gillberg-Wickman (1983) used Th as an analogue for the geochemical behaviour of ^{231}Pa, in the marine environment. In IAEA (2004) the use of Th as an analogue for Pa is suggested, whereas Am is used in Staven et al. (2003) and *in vivo* studies from Taylor et al. (1987) suggest Pu is a suitable analogue under physiological conditions. Baes et al. (1984) used both Ra and Th as analogues for ^{227}Ac, and Th and U as analogues for ^{231}Pa. In that case they were not considered directly analogous for all uptake parameters and instead an assumed systematic variation of analogue CR values based on atomic number was used.

Published international datasets for radionuclide CRs sometimes include CRs for Ac or Pa (e.g., ICRP, 2009 contains CRs for transfer to wildlife for Pa but not Ac), though they are often excluded for lack of available data (e.g., IAEA, 2010, 2014b). With very limited actual measurements for Ac and Pa, and the common use of analogues the quality of published CR values is challenging to assess or even questionable.

The almost complete lack of information regarding the environmental behaviour of Ac and Pa in tropical Australian environments makes the selection of a suitable analogue in the region of study for either Ac or Pa difficult.

Uncritical evaluation and acceptance of the published data may lead to a belief that measurements of Ac and Pa, although relatively uncommon, have been undertaken more often than they have. In turn, this may lead to assumptions that assessments undertaken to determine dose have a reasonable basis in fact when they do not. This highlights the need for direct measurements to ensure that reliable and traceable CRs can be developed for Ac and Pa. Without such measurements, the potential significance of dose contributions from the ^{235}U series will remain poor and dependent on the assumptions present in modelling.

1.2.2 Relative significance of the ^{235}U series for dose assessment

As noted above, only ^{227}Ac, ^{231}Pa and ^{235}U have long enough half-lives to bioaccumulate to significant levels independently of their closest parent isotope. All three of these isotopes emit alpha or beta particles, which can deposit more energy into tissues than other types of ionising radiation. This generally leads to a higher potential for internal dose from ingestion or inhalation compared to the external dose. Both ^{227}Ac and ^{231}Pa have comparatively high ingestion and inhalation dose coefficients (DCs; see Chapter 2 for a detailed discussion of dose assessment). This leads to a higher radiation dose per unit of radioactive decay if ingested or inhaled

compared to many other radionuclides. For ^{227}Ac, the relatively short time required to reach radioactive disequilibrium with decay products (all of which emit alpha or beta particles) is a major reason for the high DC. For both ^{227}Ac and ^{231}Pa the long biological half-life also plays an important role in contributing to a high relative dose. For ^{238}U and ^{235}U the DCs (ingestion and inhalation) are not substantially different and are relatively low. As such small variations in the relative abundance of these isotopes has negligible impact for dose assessment (NRC, 2001). Consequently, ^{227}Ac and ^{231}Pa are the most important radionuclides in the ^{235}U series for contribution to dose from naturally occurring sources.

1.2.3 Measurement techniques for ^{227}Ac and ^{231}Pa in environmental samples

The limited published data available from the region of study for this thesis for ^{227}Ac can be found in Martin et al. (1998) where 13 values for traditional food items and three values for surface water activity concentrations are reported. All results were, however, below the limit of detection at the 95% confidence (2σ) interval. Based on this, Martin et al. (1998) estimated detection limits required for measurement of environmental concentrations of ^{227}Ac were 1 mBq kg^{-1} for food items (wet weight) and 0.05 mBq L^{-1} in surface water. It is expected that requirements for ^{231}Pa detection limits are in the same range. As such, ultra-sensitive measurement techniques or techniques that allow for the analysis of large sample masses are required.

With the low number of actual published data of ^{227}Ac and ^{231}Pa in environmental samples, there is also a similar lack of published methods specifically for environmental samples. There are exceptions for the marine ecosystem where a range of measurements have been done on sediment and water in dating studies, particularly for ^{231}Pa (see Section 1.2.4.1 below). Development of methods for analysis of such low concentrations of ^{227}Ac and ^{231}Pa in environmental samples was a substantial part of the work undertaken for this thesis. The methods developed focussed on Australian native flora and fauna and included some measurements of soil and surface water samples. Method development for each isotope is discussed in dedicated individual chapters, each of which begins with a detailed discussion of the chemistry relevant for method development and sample selection.

Application of the developed methods to measure ^{227}Ac and ^{231}Pa in the environment from sources other than U mining is also a potential outcome of this research. A brief discussion of these other sources, and other uses for measurements of radionuclides in the ^{235}U series follows below.

1.2.4 Sources of ^{235}U series radionuclides in the environment not related to U mining and milling

1.1.1.1 ^{227}Ac

Studies in the petroleum and gas industries have shown that pipe scale and sludge may have high activity concentrations of ^{227}Ac, particularly associated with $CaCO_3$ scales (Al-Farsi, 2008; Kolb and Wojcik, 1985). Owing to similar chemical properties to the rare earth elements (REE), ^{227}Ac can be a significant radio-impurity in REE concentrates and wastes produced during extraction of REE (Kosynkin et al., 1995). Grench and Buchanan (1973) showed most of the radioactivity in La extracted from rare earth materials to be associated with ^{227}Ac. In cases where REE may be recovered from leach liquors produced during extraction of U, ^{227}Ac and progeny can account for over 99% of the total radioactivity in the REE concentrates produced (Rychkov et al., 2018). Thus, ^{227}Ac may potentially be released into the environment from industrial sources or contribute to occupational doses associated with REE production or in the petroleum and gas industries.

Deep ocean sediments can release ^{227}Ac into water in the deep ocean by diffusion from sediment with high activity concentrations of ^{231}Pa (Nozaki, 1984). This can lead to increased activity concentrations of ^{227}Ac in deep water relative to the open ocean.

During production of ^{225}Ac for nuclear medicine, ^{227}Ac may also be produced and is the most significant radio-impurity owing to it being chemically inseparable from ^{225}Ac (Aliev et al., 2014). This can lead to the generation of longer-lived radioactive wastes in the production of radiopharmaceuticals.

1.2.4.1 ^{231}Pa

Relatively high activity concentrations of ^{231}Pa in the environment may be associated with aspects of the nuclear fuel industry other than U mining and milling (e.g., Berry et al., 1989). Elevated concentrations can be associated with industries such as phosphogypsum production (van der Heijde et al., 1988), mineral sands extraction (Raje et al., 2001) and monazite mining (Dalvi et al., 2021). The Th-U fuel cycle has also generated interest in research into environmental migration of ^{231}Pa (Rekha et al., 2006), owing to ^{231}Pa being present in significant amounts in spent fuel from ^{231}Th produced by the (n, 2n) reaction on ^{232}Th (IAEA, 1980). A study on the potential migration of ^{231}Pa from a nuclear waste repository showed that ^{231}Pa very strongly and rapidly adsorbs to surfaces including the cement casing and surrounding rock (Berry et al., 1989), suggesting such repositories are unlikely to be a

significant environmental source of ^{231}Pa and thus present a negligible radiological risk in that context (Berry et al., 1989).

1.2.4.2 Other isotopes in the ^{235}U series

The parent isotope in the ^{235}U series, ^{235}U, is chemically indistinguishable from other U isotopes. A common assumption of a constant isotopic ratio of ^{235}U:^{238}U (i.e., 0.73% by mass) in the environment and that no significant fractionation occurs in environment processes is not always valid (Richter et al., 2010). However, the potential variability of up to 0.13% reported, is not significant from a dose perspective for natural material and the activity concentration of, and thus the radiation dose from, ^{235}U is readily obtained from measurement of ^{238}U.

The enrichment of U for nuclear fuel and weapons (leading to an increase in the ^{235}U:^{238}U activity ratio) is comprehensively documented (Murchie and Reid, 2020). Enriched U is highly regulated owing to the fissile nature and nuclear proliferation potential (Doyle, 2019). Therefore, environmental sources of enriched U and its decay products are expected to be extremely rare. As a byproduct from the enrichment process, depleted U, with a low ^{235}U:^{238}U activity ratio (around 0.25% ^{235}U, Rich et al., 1988) has found uses in armour piercing munitions and as a component of airplane stabilisers (NRC, 2001) which can lead to environmental release (IAEA, 2023).

Environmental transport of ^{227}Th and ^{223}Ra can occur independently of ^{227}Ac, though this does occur in a relatively short timeframe (days to months) and the source can be attributed to ^{227}Ac.

1.2.5 Potential uses for environmental data on the ^{235}U series not related to U mining and milling

1.2.5.1 ^{227}Ac

The release of ^{227}Ac by deep ocean sediments, combined with a half-life of a relevant time scale, leads to applications in measurement of deep mixing and upwelling of oceanic waters (Geibert et al., 2008). The use of radioactive disequilibria in the ^{238}U series and ^{235}U series also leads to use in geological dating techniques (Gascoyne, 1985; Shen, 1996). Nuclear forensics can also make use of ^{227}Ac as a means of aging nuclear material (Barry et al., 2022; Kayzar and Williams, 2015).

1.2.5.2 ^{231}Pa

There are several U-series dating methods based on measuring disequilibrium in the decay chains of both ^{238}U and ^{235}U (Grün, 2006). These can involve the use of ^{231}Pa, for which the long half-life makes it suitable for a range of dating techniques across broad time scales. Edwards et al. (1997) showed it could be used to date carbonates, such as those in corals, over

a range of 10–250,000 years. Similar ranges for dating human fossils were indicated by Grün (2006), with later work extending that date to 700,000 years in particular circumstances (Grün et al., 2010). Although very small amounts of material can be used for such dating, U-series dating methods are typically destructive. Non-destructive methods using gamma ray spectrometry (Simpson et al., 1998; Simpson and Grün, 1998) can be used for hominid samples that are too valuable to allow for destructive testing. Similarly to ^{227}Ac, ^{231}Pa can also be used to age nuclear material (Barry et al., 2022).

Measurement of ^{231}Pa is routinely undertaken for a range of studies in environmental transport, such as dating of deep ocean currents and sediments and particle transport processes (e.g., Gdaniec et al., 2018; Gherardi et al., 2009; Hayes et al., 2015). Such studies can also be used to measure impacts and links between changes in climate and environmental processes (e.g., Gherardi et al., 2009). These studies will be useful in reconstructing ocean circulation in the past and understanding present conditions to better predict potential impacts of changing climatic conditions on the world's oceans.

1.2.5.3 Other isotopes in the ^{235}U series

As one of 4 naturally occurring Ra isotopes, and with a half-life of 11.4 days, ^{223}Ra finds uses as an environmental tracer in short-term mixing of fresh water with coastal water (Moore and Arnold, 1996), groundwater (Smoak and Krest, 2006), in submarine groundwater discharge and coastal water circulation (Lamontagne et al., 2008; Stewart et al., 2015). The relatively short time taken to reach equilibrium with the parent radionuclides ^{227}Ac and ^{231}Pa also makes ^{223}Ra a useful isotope (and potentially easier to measure) in studies in which ^{227}Ac and ^{231}Pa are used as tracers of environmental processes (Moore and Arnold, 1996). Measurement of ^{219}Rn may be used as a proxy for direct measurement of ^{223}Ra (Moore and Arnold, 1996).

The relatively short half-life, alpha emission and bone-seeking properties also give rise to uses for ^{223}Ra in nuclear medicine for treatment of bone metastases (Bruland et al., 2006). More recently, nuclear medicine is also finding uses for ^{227}Th in targeted alpha therapy (Frantellizzi et al., 2020).

No documented uses of the remaining isotopes in the series, ^{215}Po and ^{211}Bi were found, likely owing to their very short half-lives.

Chapter 2 : Radiological dose assessments

Radiation is classified into 2 categories, ionising radiation (IR) and non-ionising radiation (NIR), where IR generally has a wavelength less than 100 nm and has enough energy to cause ionisation. Radio frequencies, infrared, visible and ultraviolet (UV) radiation are types of NIR, whereas alpha particles, gamma rays and high energy neutrons are types of IR. IR has more energy than NIR, enough to break chemical bonds, potentially damaging living tissue and DNA. Radiation from NORM is IR, comprising of alpha, beta and gamma and X-ray radiation, which are all relevant for dose estimation. When discussing radiation in this thesis it exclusively refers to IR.

Section 2.1 System of radiation protection – Human Health

2.1.1 Radiation dose units

Radiation protection is broadly defined on the principles of justification, optimisation and limitation. Optimisation and limitation require the definition of radiological protection quantities, in particular the specific units and methods for measurement (Menzel and Harrison, 2012). Radiation exposure is measured directly as an absorbed dose, which is equivalent to the energy in joules (J) deposited in a kilogram (kg) of a substance by the radiation. Absorbed dose has the SI unit of Grays ($1\ J\ kg^{-1} = 1\ Gy$) (Menzel and Harrison, 2012).

For external dose, primarily from gamma radiation, the **absorbed dose rate** is often measured as ‘air kerma’ (kinetic energy released per unit mass in air, per unit time) and this is the parameter often measured by field surface gamma radiation surveys ($Gy\ hr^{-1}$). Air kerma when measured is a combination of ‘terrestrial air kerma’ (i.e., coming from terrestrial sources, predominantly soil or rock with a small component associated with dust and radon) and cosmic radiation (i.e., radiation from space). Terrestrial air kerma can be derived directly from measurement of the activity concentrations of NORM in soil and rock samples and this is the process often used for prediction of external radiation dose (e.g., Kleinschmidt, 2017).

There are differences in biological effectiveness for different types of radiation (alpha is more damaging than beta and much more damaging than gamma) and differences in sensitivities of organs and tissues to potential health effects. For this reason, an additional dose unit, the Sievert (Sv) is used to give the quantity **equivalent dose**, which accounts for these differences. The equivalent dose is the absorbed dose multiplied by a radiation weighting factor for each type of radiation. Values of the equivalent dose are again multiplied by a tissue weighting factor to

account for the sensitivity of different tissues and organs to radiation and then summed to give the whole-body **effective dose**, also in Sieverts (Sv) (Menzel and Harrison, 2012). The **absorbed dose** from external exposure can be converted to an **effective dose**; UNSCEAR (2000) recommends applying a conversion factor of 0.7–0.9 Sv Gy^{-1} to the absorbed dose in air from terrestrial gamma rays depending on the age group and gamma ray source(s).

Internal dose comes primarily from alpha and beta radiation whereby radionuclides incorporated in the human body irradiate tissues over time periods determined by their radioactive and biological half-lives. The **committed effective dose** (also in Sieverts (Sv) from an incorporated radioactive element is the total dose expected to be delivered within a specified time. For members of the public this is the time integrated average over 50 years or to 70 years of age for children (ICRP, 2012). This is of particular importance for radionuclides with long radioactive and biological half-lives, e.g., those depositing in bones such as ^{227}Ac, ^{231}Pa, ^{226}Ra and ^{228}Ra (these radionuclides also have many short-lived alpha emitting decay products leading to further elevation of the dose).

2.1.2 Dose limits, constraints and reference levels

The equivalent and effective dose parameters allow doses from radionuclides incorporated into the body and from external sources to be summed. The fundamental purpose of this is to allow comparison with dose limits, constraints and reference levels that relate to stochastic risks of whole-body radiation exposure (Harrison and Day, 2008). Typical dose limits, constraints and reference levels are in reference to the **annual effective dose** (ICRP, 2007). For members of the public the **annual effective dose** is equal to the sum of the effective dose from external exposure and the committed effective dose from internal exposure over a year (ICRP, 2007). The annual effective dose is the fundamental unit for radiological protection of humans and enables (a) the implementation of optimisation processes intended to keep doses as low as reasonably achievable (ALARA) and (b) the setting of dose limits in a regulatory context. Annual effective dose is primarily intended for use at low doses for the management of stochastic (chronic exposure) risks. Discussion of deterministic (acute exposure) effects and radiological protection are not relevant for this project as very high doses that could potentially lead to these effects are not considered to be a possibility.

For radiation protection purposes, the ICRP (2007) recognises three types of exposure situations: planned, emergency and existing. Within these there are also three categories of exposure: Occupational, public and medical. These enable the principles of justification, optimisation and limitation to be applied for different circumstances.

The use of dose limits, constraints and reference levels is an important part of the system of radiological protection. Dose constraints and dose limits only apply in planned exposure situations where dose restrictions can be applied at the planning stages to ensure that they are not exceeded (ICRP, 2007). Dose limits apply to the sum of all sources or pathways of exposure in a planned exposure situation. Dose constraints apply to a specific radiation source or pathway, which must not exceed values that can cause the relevant dose limits to be exceeded when all sources or pathways of exposure are considered. This allows doses to be restricted by the application of ALARA optimisation processes on a source or pathway specific basis rather than by the dose limit (ICRP, 2007). Reference levels are used in the case of existing and emergency exposures where exposures may exceed the reference levels. In such cases, application of the optimisation process may be used to reduce exposures towards or below the reference level (ICRP, 2007).

For this project, the assessment is in relation to a planned exposure to members of the public where, as noted above, "*in practice, almost all public exposure is controlled by the procedures of constrained optimisation and the use of prescriptive limits."* (ICRP, 1991), in defining the actual constraints or limits to apply for a given planned public exposure situation *"It is often convenient to class together individuals who form a homogeneous group with respect to their exposure to a single source. When such a group is typical of those most highly exposed by that source, it is known as a critical group*" (ICRP, 1991). The concept of the critical group was replaced in the updated ICRP (2007) recommendations with that of the representative person. This individual, hypothetical or specific, for the purpose of protection of the public, is "*one whose dose can be used for determining compliance with the relevant dose constraint"* (ICRP, 2006). For prospective dose assessments, three categories of representative person are recommended, these are 0–5 years (infant), 6–15 years (child), and 16–70 years (adult). There are a range of techniques that can be used to determine the characteristics of the representative person for a given exposure situation, with the concepts of reasonableness, sustainability, and homogeneity to be considered when selecting an appropriate technique (ICRP, 2006). The definition of the critical group given above is a good description of the factors that should be considered when defining the representative person for a given dose assessment. The representative person defined for this project and the regulatory dose limit applied is detailed in Section 2.6.

2.1.3 Determining annual effective dose

To determine the annual effective dose for the representative person individual exposures are not generally measured, instead doses are estimated using modelling (ICRP, 2006). Models use input parameters such as environmental measurements of radioactivity in dwellings, air, food items or drinking water coupled with occupancy rates, breathing rates and dietary assessments (ICRP, 2006). Such models may use concentration ratios (CRs), which are also used in environmental dose assessments (see Section 2.4).

For the internal dose from ingestion or inhalation of a radioactive isotope, dose coefficients (DCs) are used which convert the activity (Bq) ingested or inhaled to a committed effective dose (Sv). DCs consider all radiations emitted by a given radionuclide, radioactive and biological half-lives, and partitioning within the body where different tissues may have different radio-sensitivities (ICRP, 2012). DCs are based on biokinetic models and are limited by the level of understanding of how different elements behave in the body (Leggett, 2001). This can lead to a high level of uncertainty in the biokinetic and dosimetric modelling for some elements and, given the lack of data for both Ac and Pa (see Sections 3.1.2 and 4.1.2), the DCs published for ^{227}Ac and ^{231}Pa may have a high level of uncertainty.

For external dose, calculations require modelling of the environmental radiation fields and computation of effective dose-rate coefficients for exposures to the range of gamma radiation emissions from a given radionuclide. Modelled values can vary with the distribution of radionuclides within the environment, as well as environmental properties, such as soil density. Generic age-dependent effective dose-rate coefficients are provided for the most probable external exposure scenarios for members of the public resulting from radionuclide contamination of soil, air, and water in (ICRP, 2020).

The primary aim of this project is to determine the committed effective dose component of the annual effective dose through the ingestion pathway to the representative person. This will be used to assess the relative contribution, and therefore relative importance, of isotopes in the ^{235}U series for determination of the annual effective dose from U mining and milling in the ARR from all pathways, with a focus on RUM.

The DCs for radionuclides in the ^{238}U and ^{235}U decay series are shown in Figure 2-1. The DCs for ^{227}Ac and ^{231}Pa are among the highest of all radionuclides in both series, however, when the relative activity concentration of each series (based on the natural activity ratio of ^{235}U:^{238}U of

0.0466:1) is taken into account (Figure 2-2) their relative importance may be substantially lower.

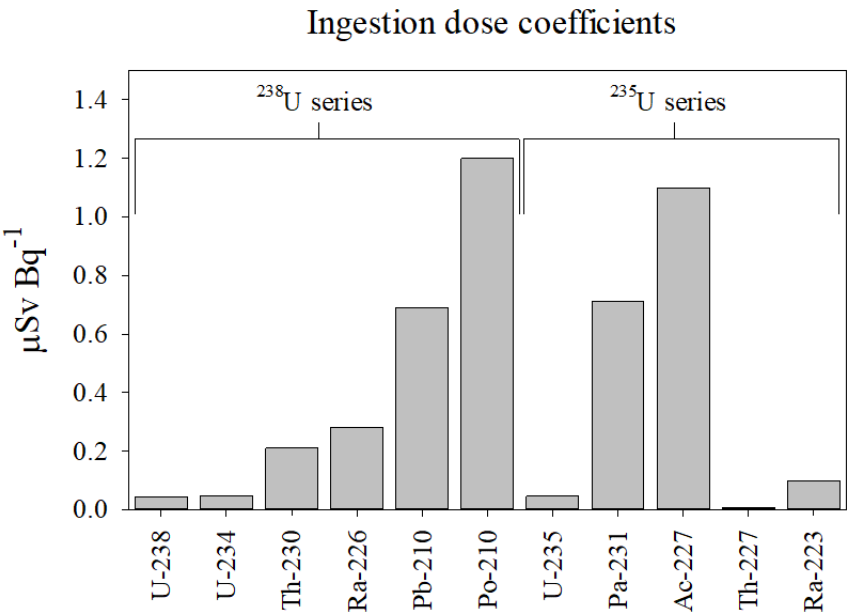

Figure 2-1 Ingestion dose coefficients for key radionuclides in the ^{238}U and ^{235}U decay series.

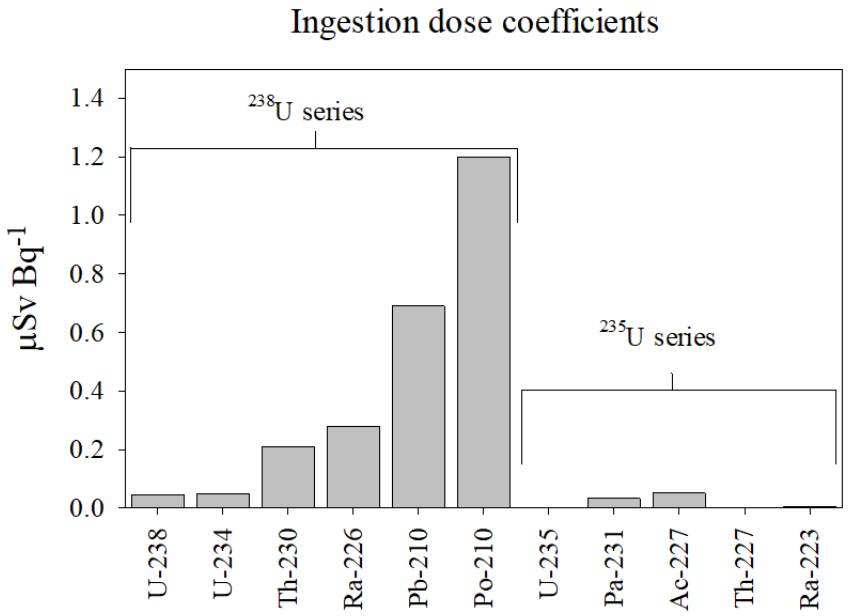

Figure 2-2 Ingestion dose coefficients for key radionuclides in the ^{238}U and ^{235}U decay series, corrected for the relative activity of the parent isotopes (^{235}U:^{238}U activity ratio of 0.0466:1).

Section 2.2 Limitations of effective dose and use in assessing radiation risk

There are known to be inherent problems associated with the use of effective dose for determination of risk. For example, there are known differences in age and sex related radiation risks. It is often confused with equivalent dose and the tissue-weighting factors used can be

considered subjective (Brenner, 2012). Although alternative proposals have been posited (e.g., Brenner, 2012 - age, gender, and organ specific with a focus solely on cancer risk) effective dose remains the current standard quantity used for the setting of dose limits. Effective dose uses sex and age averaged tissue weighting factors and is therefore not appropriate for determination of specific risk to an individual from a given radiation source but is applied to groups such as members of the public.

The setting of dose limits, constraints and reference levels using annual effective dose is based on the linear-no-threshold (LNT) model for determination of detriment/risk (ICRP, 2007). The effective dose is essentially an attempt to define a quantity which is proportional to the radio-biological detriment from low-dose radiation exposure (Brenner, 2012). Although detriment was intended to represent a balance between cancer risk, reduction in lifespan and hereditary effects, it is more commonly used as a proxy to directly estimate cancer risk by assigning a specific increased risk of cancer per unit of dose (Brenner, 2012).

The LNT model is based on the principle that there is no dose below which there is no risk of potential detriment, i.e., there is no 'threshold dose'. The LNT model has been seriously called into question in recent years (Boretti, 2023) and further detailed investigation may lead to development of a new paradigm in radiation protection (Okonkwo et al., 2022). Substantial work developing an improved understanding of the effects of radiation, particularly at low doses is being done. This includes recent studies investigating the interaction of organic compounds with radiation (e.g., Ren et al., 2022) and the effects of low dose on complex organisms (e.g., Belli and Indovina, 2020). The LNT model and the use of effective dose for assessing radiation risk, however, is the currently accepted basis of the regulatory framework upon which the system of protection from IR in Australia is based and has therefore been used for assessment in this project.

Section 2.3 System of radiation protection - The environment

An assumption that protection of the environment was assured through protection of humans prevailed in early international systems of radiological protection (ICRP, 1977, 1991, 2003). Diminishing acceptance of this assumption led to the recommendation for development of an international framework specifically aimed at environmental radiation protection (ICRP, 2003). This framework was scientifically and ethically based and provided the foundation for development of policies for protection of non-human species. The need for development of such policies was not based on specific identified hazards but was intended to fill conceptual

and knowledge gaps in radiological protection (ICRP, 2003). Since then, there has been a substantial amount of research dedicated to radiological protection of the environment. Given the enormous complexity of environmental systems and range of flora and fauna globally, these approaches seek to simplify the approach by grouping organisms into reference animals and plants (ICRP, 2008a), mirroring the approach of the 'representative person' in human radiological protection (ICRP, 2006).

"*The ICRP approach is based on the consideration of 12 more or less globally representative reference animals and plants, covering different life stages (e.g. fish egg, adult fish). This is a basis for systematically relating radionuclide exposure to radiological dose, and then dose (or dose rate) to different types of effect, for a number of organisms that are characteristic of different types of natural environment*" (IAEA, 2017)

There is still much debate regarding appropriate setting of effects criteria to determine ecological effects (e.g., Bréchignac, 2016; Bréchignac et al., 2016; Geras'kin, 2016), with the (ICRP, 2003) system (ICRP, 2003) and subsequent work focussing on organism level or biological effects rather than ecosystem effects. Biological effects, however, do not necessarily reflect ecologically relevant effects (Bréchignac, 2016). The increasing international importance of demonstrating radiation protection of the environment requires the development of a suitable means to properly assess environmental and ecological risk (Bréchignac, 2016). Such a system must include improving understanding of the extent of environmental contamination and the potential for ecological detriment.

The diversity of potential endpoints as ecologically relevant markers for assessing ecosystem or population effects is one complicating factor with developing such a system (Stark et al., 2017). Specific biological endpoints (e.g., reproduction, Fuller et al., 2018) are dependent on a range of factors such as tissue sensitivity, life-stage, and intra-species and inter-species differences within reference groups (Stark et al., 2017). Ecologically relevant markers may be dependent on more complex factors, such as alterations of trophic or host-pathogen relationships (Geras'kin et al., 2016). Such differences in the types of effects investigated for dose assessment of humans and the environment means that radiation weighting factors are not directly transferable between the two approaches[3]. Highly heterogeneous radionuclide

[3] There is, at present, no consensus on setting radiation weighting factors for biota dose assessments (Ulanovsky et al., 2008).

distributions within organisms can often occur[4]. Although doses to different tissue types may have substantially different impacts, dose to the environment is typically measured only as an absorbed dose rate (Gy hr^{-1}) and is not weighted for tissue types (ICRP, 2008a). In many environmental dose assessment models, a simplistic assumption for dosimetry is used, whereby a uniform distribution of radionuclides throughout an organism is assumed (Stark et al., 2017). These factors lead to a high degree of uncertainty in dosimetry for environmental protection (Stark et al., 2017).

As a direct result of these challenges and simplifications, consensus on setting threshold values or 'benchmark' dose rates (Andersson et al., 2009; Garnier-Laplace et al., 2010) below which an acceptable level of environmental protection is considered to be achieved is not universal (Bréchignac, 2016). Unlike radiological protection of humans, specific objectives in environmental protection may vary with the intended application (Real and Garnier-Laplace, 2020). For example, protection of threatened or endangered species may warrant protection of individuals as opposed to population or ecosystem protection (Real and Garnier-Laplace, 2020). Lower threshold values may also be justified in consideration of multiple stressors typical of the natural environment, where impacts such as predation of turtle hatchlings and competition for food are also present (e.g., Johansen et al., 2020). Although there is substantial variation in recommended benchmark values for environmental radiological protection, reference to benchmarks has value as a screening tool that reflects the relative effort required to demonstrate adequate protection (Real and Garnier-Laplace, 2020).

As a pragmatic approach to provide a level of guidance for decision making in the setting or application of benchmarks for environmental radiation protection, the ICRP (2008a) developed 'derived consideration reference levels' (DCRLs). These are defined as "*a band of dose rate within which there is likely to be some chance of deleterious effects of ionising radiation occurring to individuals of that type of Reference Animal or Plant*". The use of DCRLs allows a screening approach where there is a range of values for a given reference organism within which a more detailed approach to assessing dose is warranted (e.g., use of site-specific measurements or more detailed consideration of protection objectives for a particular species).

[4] E.g., Hosseini et al. (2010) noted preferential accumulation of Ra in fish skeleton and of ^{210}Po in fish liver and the hepatopancreas of crustaceans.

Within the Australian context, advice on specific assessment methods and associated tools enabling demonstration of radiological protection of the environment consistent with international best practice has been provided by the national radiation protection agency (ARPANSA), this is discussed in detail in (Hirth et al., 2018).

2.3.1 The ERICA integrated approach and assessment tool

The ERICA (Environmental Risks from Ionising Contaminants: Assessment and management) assessment tool was developed specifically for environmental radiation assessment using the ERICA integrated approach (Brown et al., 2016). This tool will be used to complete a Tier 2 ERICA environmental dose assessment for this thesis (see below for more details and Chapter 5, Section 5.3.4 for results and discussion).

The ERICA integrated approach is a generic framework for the assessment and management of environmental risks from IR (Larsson, 2008). It is based on the use of broad, non-taxonomic, groupings of ecologically significant plants and animals or 'reference organisms'. These reference organisms are defined across three ecosystems, marine, terrestrial and freshwater, the latter two of which are relevant for this study (Table 2-1).

Table 2-1 Reference organisms in the ERICA integrated approach for terrestrial and freshwater ecosystems.

Reference Organism and ecosystem			
Terrestrial		**Freshwater**	
Amphibian	Lichen and bryophytes	Amphibian	Mollusc – gastropod
Annelid	Mammal – large	Benthic fish	Pelagic fish
Arthropod	Mammal – small	Bird	Phytoplankton
Bird	Mollusc – gastropod	Crustacean	Reptile
Common Lizard	Reptile	Insect larvae	Vascular plant
Flying Insects	Shrub	Mammal	Zooplankton
Grasses and Herbs	Tree	Mollusc – bivalve	

The ERICA model uses a simple approach, representing reference organisms with an ellipsoid having a uniform radionuclide distribution. Unlike doses to people, the absorbed dose is used for environmental dose which is therefore a simple estimate of the energy deposited from

ionising radiation. The ERICA tool has dose conversion coefficients (DCCs) for a range of radionuclides that are used to calculate internal and external dose based on the radiation type and organism size (e.g., smaller organisms may get a reduced dose from high energy betas that have a greater chance of passing through the organism without losing all their energy, Ulanovsky et al., 2008). Default radiation weighting factors in the ERICA tool are ten for alphas, three for low energy electrons (<10 keV) and one high energy electrons, x-rays, and gamma rays (Ulanovsky et al., 2008). The unit for DCCs is μGy hr^{-1} per Bq L^{-1} or Bq kg^{-1} depending on the environmental medium.

Occupancy factors are also considered in ERICA assessments, these are the relative amount of time spent in an environmental compartment, and these affect the external dose calculated. For terrestrial environments these are 'on soil', 'in soil' and 'in air' and for freshwater they are 'water-surface', 'water', 'sediment-surface' and 'sediment' with default values for each reference organism. Default reference organisms are included in the ERICA tool and default distribution coefficients (K_d values) and concentration ratios (CRs, see Section 2.4 below) are provided. These can be used to determine activity concentrations of radionuclides for each reference organism from site activity concentrations in environmental media (Brown et al., 2016). However, where available, site and organism-specific data can provide a more realistic assessment (Goulet et al., 2022; Medley and Patterson, 2022; Thomas, 2000b). This is particularly true in Australia, where whole organism CR values ($CR_{WO\text{-}Media}$, where media refers to soil or water) for Australian wildlife have been shown to be higher than international datasets, with significant differences found where sufficient data is available for comparison (Doering and Bollhöfer, 2016b; Hirth et al., 2017; Rea et al., 2021).

Inherent in the use of CR and K_d values is the assumption of equilibrium in the concentration of radionuclides between organisms and the environmental medium allowing transfer to be modelled. This limits the validity of the approach to planned exposure situations (i.e., routine functioning consistent with equilibrium).

The ERICA integrated approach is a 3-tiered approach, where the first two tiers provide a conservative assessment with limited data requirements against a universal screening absorbed dose rate value. The default dose rate screening value is 10 μGy hr^{-1} which is considered to provide confidence that radiation related risks are negligible for all species (Andersson et al., 2009), however, alternative screening values, including custom values, may be entered. In Tier 1, media concentrations of radionuclides of interest are input and compared against pre-calculated environmental media concentration limits (EMCL). EMCLs are defined as the

"*activity concentration of a given radionuclide in media (soil, sediment, water) that will result in a dose-rate to the most exposed reference organism equal to the screening dose-rate*" (Brown et al., 2016). From these values a risk quotient (RQ) is generated for all organisms, with the 'limiting organism' being the most exposed reference organism for a given radionuclide (i.e., the one with the highest calculated dose rate relative to the screening dose rate). The limiting organism may vary for different radionuclides and may not receive the highest dose rate when doses from all radionuclides are summed. RQs are a fractional value of the EMCL, where a risk quotient of one means the media concentration is equal to the EMCL. Tier 1 assessments are typically used as screening assessments to evaluate relative risk and determine if a more detailed risk assessment is required. Where screening values are exceeded, Tier 2 or 3 assessments may be justified. These tiers allow a substantially more customisable assessment to be made. Of most relevance for this thesis, Tier 2 allows:

- Additional isotopes to be added (e.g., ^{227}Ac is not in the default list at Tier 1),
- Addition of representative organisms, such as Australian native species, through user-specified geometries,
- Modification of occupancy factors, and
- Use of calculated site specific CRs.

RQs are still used in Tier 2 assessments, however, internal and external dose rates for each reference organism are also calculated. For this thesis a Tier 2 assessment is used to allow addition of ^{227}Ac and native representative organisms as well as the use of site-specific CRs from measured activity concentrations in media and organisms. The dose rates calculated in a Tier 2 assessment also allow comparison with calculated dose rates from radionuclides in the ^{238}U decay series using the same customised aspects (e.g., site specific CRs and representative organisms). See Chapter 5, Section 5.3.4 for a more detailed discussion of the customised aspects of the assessment, and Appendix C for additional data and results.

Tier 3 allows the same customisation of the assessment as Tier 2, but also includes Monte Carlo simulations allowing full probabilistic calculations to be made. Default probability density functions (PDFs) for most inputs (e.g., CRs, K_d values, measured activity concentrations) are provided and several alternative PDFs are supported by the tool. There are further differences with a Tier 3 assessment allowing advanced users to undertake a more comprehensive assessment compared to Tier 2 (further information can be found in Brown et al., (2016) and associated references). However, the very low number of values for environmental

concentrations of ^{235}U series radionuclides in this thesis were not considered sufficient to enable PDFs to be assigned to provide a reliable Tier 3 assessment.

Section 2.4 Derivation of concentration ratios

Under the equilibrium approach, CRs are an integral part of human and ecological dose assessments and can be used to predict the uptake or transfer of a radionuclide from environmental media to flora and fauna. The relevant medium is dependent on the environmental compartment the organism typically inhabits, such as soil for terrestrial animals and plants, and water or sediment for aquatic organisms (Higley and Bytwerk, 2007).

A CR for terrestrial environments is typically defined as the ratio of the radionuclide activity concentration in an organism or specific tissue to the activity concentration measured in the plant root zone of the soil (Ehlken and Kirchner, 2002), see Equation 2-1.

Equation 2-1 Concentration ratio.

$$\text{Concentration ratio} = \frac{\text{Concentration in biota}}{\text{Concentration in medium}}$$

The CR is unitless, and the units used for the activity concentrations are generally Bq kg^{-1} for solid samples and Bq L^{-1} for aqueous samples, where the filtered fraction is typically used. For soil and sediment this is usually expressed as dry weight (e.g., Brown et al., 2016), whereas for biota fresh weight is more commonly used. Variations exist in the units used for CRs, such as dry or ashed weight for biota, or transfer from soil to tissue or herbage to tissue for edible animal products (e.g., IAEA, 2010, 2014b; Simon and Ibrahim, 1990). It is important to note that the CR is an integrated parameter supposed to account for all transfer pathways from a given medium to on organism or tissue.

For human dose assessments, CRs are used to predict transfer of radionuclides to food items from the surrounding environmental media and are targeted towards the edible tissues of biota consumed, such as fruit or meat (IAEA, 2010). For environmental dose assessments, CRs are based on the whole organism ($CR_{WO\text{-}Media}$) and these values are used in most models where the impact of IR on wildlife under chronic exposure conditions is assessed (Wood et al., 2013).

Compilations of CRs from Australia and the study region are in Hirth et al. (2017) and (Doering et al., 2018) respectively. Hirth et al. (2017) identified data gaps in published CRs, and associated biota and media activity concentration data, for freshwater, marine, and terrestrial environments. Subsequent papers have closed some data gaps in the marine environment,

e.g., MacIntosh et al. (2022) reported K_d values for ^{226}Ra, ^{228}Ra and progeny for pipe scales and Medley and Patterson (2022) reported CR values for ^{210}Po in crustacea. It is notable that none of these studies have discussed the knowledge gap for the ^{235}U series and as such the missing data is compounded by a lack of consideration. For this thesis, measurements of tissue, whole organism, and environmental media activity concentrations of ^{227}Ac and ^{231}Pa were undertaken (see Appendix B for results). CRs were derived to undertake a prospective dose assessment for people and the environment in the study area (see below and Chapter 5, Section 5.3.4) and to provide data for the ^{235}U series currently lacking in international datasets.

Most published radionuclide activity concentration data in flora and fauna were intended for use in human dose assessment and focussed on edible tissues (Yankovich et al., 2010). Use of CRs from single tissues ($CR_{Tissue\text{-}Media}$) may be inappropriate for direct use in deriving $CR_{WO\text{-}Media}$ values (Yankovich et al., 2010). Therefore, conversion factors for a range of reference organisms were developed to allow derivation of $CR_{WO\text{-}Media}$ values from measurements of single tissues (Wood et al., 2010; Yankovich et al., 2010). In the case of Ac and Pa, no such correction factors have been published, however, the use of conversion factors for chemical analogues may be appropriate where whole organism data is lacking and have been used in this thesis to increase the number of $CR_{WO\text{-}Media}$ values for environmental dose assessment. The cited references (Wood et al., 2010; Yankovich et al., 2010) and references therein provide further information and guidance on the use and appropriateness of conversion factors. Detailed discussion is out of scope of this thesis. The approach used to derive conversion factors for this thesis is consistent with the approach of Yankovich et al. (2010), see further discussion in Sections 2.7.2, 2.5.2 and 2.5.3.

A database of radionuclide activity concentrations measured in the ARR for the ^{238}U decay series (the 'CR Database'; Doering and Bollhöfer et al., 2016a) was updated for this thesis. A tool (the CR Tool) developed to query the CR Database was used to derive ^{227}Ac and ^{231}Pa CRs for reference organisms and bush foods, based on a range of criteria (Doering and Bollhöfer, 2016c). Variables used by the CR Tool include activity concentrations of radionuclides in bush foods, reference organisms and environmental media, spatial and temporal matching criteria for biota and media, and the approach for handling <MDL values. These aspects and application for this thesis are discussed in detail in Chapter 5, Section 5.2.

Section 2.5 Radiation exposure from NORM

2.5.1 Radiation exposure from NORM – To people

2.5.1.1 Ingestion

Doses received from ingestion of radionuclides in food are estimated as a 'committed effective dose' (Sv) owing to the potential for incorporation into the body. Over 90% of dietary dose comes from just nine radionuclides (IAEA, 2022), with three radionuclides from the ^{238}U decay series (^{210}Po > ^{210}Pb > ^{226}Ra) dominating the dose contribution (~75%). Therefore, where there is the potential for increased concentrations of these radionuclides in foods an understanding of potential ingestion doses can be important. The relative contributions to dose from ^{238}U series radionuclides found globally are similar to that measured in the study region, with the exception that doses from ^{226}Ra in the study region are typically higher than doses from ^{210}Pb (Bollhoefer et al., 2002; Martin et al., 1998). To estimate the dose from a given food item the activity concentration of each isotope in a food item is multiplied by the DC and the quantity consumed. This is typically estimated as an annual committed effective dose (Sv), therefore annual consumption estimates are needed. Cooking and preparation techniques can lead to variations in the activity of radionuclides in or associated with food between collection and consumption (e.g., Johansen et al., 2023). Doering and Bollhöfer (2016a) have shown from the study region that not washing food before cooking can lead to higher activities ingested, reflecting variations in traditional food preparation techniques used. Results from unwashed samples in this case includes radionuclides associated with soil attached to the food item and are typically higher than those from washed samples. Where possible, assessment of dose should reflect the activity concentration of consumed foods, however, this may not always be achieved.

2.5.1.2 Inhalation

Similarly to ingestion, inhalation of radionuclides leads to potential incorporation into the body and doses are measured as 'committed effective dose' (Sv). Inhalation doses can occur through the inhalation of long-lived radionuclides bound to dust (Doering et al., 2019b). However, the highest dose pathway for NORM radionuclides is typically from inhalation of radon and radon decay products (e.g., Doering et al., 2022; Hanfi et al., 2021; Rweyemamu and Kim, 2020) though inhalation doses from dust have the potential to be the largest contributor to occupational dose in operational phases of mining (Ralph et al., 2020). The two radon isotopes of relevance for radiological exposure from NORM are ^{222}Rn (^{238}U decay series; $t_{½}$ = 3.8 days) and ^{220}Rn (^{232}Th decay series; $t_{½}$ = 56 s). Although there is a Rn isotope in the ^{235}U series (^{219}Rn), with a half-life of 3.8 s, the potential for migration into the atmosphere is negligible.

2.5.1.3 External exposure

External radiation exposure from NORM is primarily through exposure to gamma radiation (UNSCEAR, 2000). The consequent external dose rates are proportional to the activity concentrations of NORM radionuclides in environmental media (USEPA, 2019). As such, knowledge of activity concentrations of NORM in various media is required to determine the effective dose from external radiation.

2.5.2 Radiation exposure from NORM - To the environment

As for human dose assessment (Section 2.5.1) external dose to the environment from NORM is mostly from gamma radiation, whereas internal dose is mostly from alpha and beta radiation. Variations in organism size can affect this general pattern, with external dose rates higher and internal dose rates lower with decreasing organism size (Howard et al., 2013).

Trends in the relative dose contribution to reference organisms from NORM radionuclides are not universal. This is hardly surprising given:

- the limitations in understanding dose effects, and data gaps for dose assessment of the environment noted in Sections 2.3 and 2.4,
- the wide variation in potential exposure scenarios (e.g., high background U or Th, different waste or legacies from different industries), and
- the wide range of modelling approaches and parameters that are currently applied (Goulet et al., 2022).

In addition to this, the highest dose rates do not necessarily determine the most exposed or 'limiting organism' as the varying screening benchmarks proposed for different reference organisms also need to be taken into account. This variance in proposed benchmarks is a result of the observed variations in the effects of ionising radiation for different reference organisms (Garnier-Laplace et al., 2008; UNSCEAR, 2008).

There are diverse studies investigating potential dose rates to reference organisms in different environments and exposure situations, some of which are noted below. In these studies, where internal and external doses are reported, the internal dose is the highest contributing pathway.

Modelling by Koppel et al. (2023) showed the most exposed organisms from NORM contaminated subsea oil and gas infrastructure to be Phytoplankton (^{226}Ra, ^{210}Pb, ^{228}Ra, and ^{228}Th), and Sea anemones and True corals (^{210}Po).

In areas impacted by mining where ^{238}U series radionuclides have been demonstrated to be above natural background levels (e.g., phosphate or U mining), ^{226}Ra and ^{210}Po have been shown to be the highest contributors to dose in freshwater and terrestrial environments (e.g., Doering and Bollhöfer, 2016b; Doering et al., 2019a; Medley et al., 2017; Thomas, 2000a; Vandenhove et al., 2015). Strong bioaccumulation of ^{226}Ra in bivalve molluscs can lead to higher dose rates compared to other species for a given activity concentration in environmental media. This can be a strong determining factor for which reference organism is the limiting organism in a freshwater ecosystem (e.g., Doering et al., 2019a). Despite this, aquatic plants were determined to be the limiting organism in U mining regions of central Asia with internal alpha doses from uranium generally making the highest contribution to the predicted dose (Oughton et al., 2013).

Internal dose rates from ^{226}Ra and ^{210}Po were highest for a terrestrial environment impacted by a coal fired power plant (Ćujić and Dragović, 2018) and a coal ash and slag disposal site (Skoko et al., 2019). Of relevance to this thesis and in contrast to most other studies, the latter study also assessed ^{235}U series (using default Th and Ra CRs for ^{227}Th and ^{223}Ra and assuming secular equilibrium with ^{227}Ac). Non-negligible dose contributions of up 11% in some reference organisms with an average of 7% were reported. Internal dose from ^{226}Ra was also shown to be the major pathway for dose contribution, with reptile being the limiting organism.

In a Belgian site impacted by phosphate production and nuclear industry effluents, ^{226}Ra followed by ^{210}Pb were the highest contributors to dose for the terrestrial environment, with ^{228}Ra highest for the freshwater environment (Sweeck et al., 2024). Natural dose rates in Australian arid environments were highest from ^{226}Ra and ^{210}Po and for grasses and shrubs (Rea et al., 2021).

A simple Tier 2 assessment was undertaken for this thesis, using default inputs (e.g., CRs, K_d values, radiation weighting factors) in the ERICA tool (version 2.0[5]) to determine limiting organisms for different environments and the relative contributions from radionuclides in the ^{238}U and ^{235}U series to each reference organism. All environments were assessed, and environmental media concentrations of 1 Bq L^{-1} or 1 Bq kg^{-1} (sediment, soil and water) were input for all ^{238}U series radionuclides with half-lives greater than 10 days. Likewise, environmental media concentrations of ^{235}U series radionuclides were entered as 0.047 Bq L^{-1}

[5] Version 2.0 of the ERICA tool is meant when the ERICA tool is referred to in this thesis.

or Bq kg^{-1} to reflect the natural activity ratio of ^{235}U:^{238}U. All boxes were checked for selecting the ERICA default CR values and the DCCs for ^{227}Ac were derived using the 'Add Isotope' function (see Section 2.7.2 for further details). The limiting organism and associated radionuclide are shown in Table 2-2. If the dose contribution from all radionuclides is summed, the limiting organism still receives the highest dose for each ecosystem (except 'Mollusc – gastropod' which is no longer one of the reference organisms with the equal highest dose, see Table 2-2). The relative dose contribution from the ^{235}U series if the dose from all radionuclides in the ^{238}U and ^{235}U series is summed is also shown in Table 2-2.

Table 2-2 Comparative assessment of limiting organism and ^{235}U series contribution.

Environment	Radionuclide/Limiting organism(s)	^{235}U series contribution (%)	
		To limiting organism	To all reference organisms
Freshwater	^{226}Ra: Insect larvae, Mollusc – bivalve, Mollusc – gastropod, Zooplankton	4% (for all organisms)	3–35%
Marine	^{230}Th: Phytoplankton	19%	0.1–36%
Terrestrial	^{226}Ra: Lichen and bryophytes	5%	3–15%

The results from the ERICA assessment referred to in Table 2-2, showed that for most reference freshwater and terrestrial organisms ^{226}Ra was the highest contributor to dose with ^{210}Po and ^{210}Pb the next highest. However, ^{227}Ac and ^{230}Th were the third highest contributors for several reference organisms. For the marine environment, ^{210}Po was the highest contributor for most organisms, with ^{210}Pb second. However, ^{227}Ac was the highest for Macroalgae and Vascular plant and, surprisingly, ^{230}Th was the highest for the limiting organism, Phytoplankton.

In separate ERICA assessments undertaken for the study area (Section 2.6) 'Mollusc – bivalve' and 'Reptile' were determined to be the limiting organisms for the freshwater and terrestrial environments respectively, with ^{226}Ra being the highest contributor to dose (Doering and Bollhöfer, 2016b; Doering et al., 2019a). In these studies, site-specific CR data was used and highlighted the value in not using default parameters as site-specific CRs can impact conclusions from environmental dose assessments, such as the limiting organism or whether screening dose rates are exceeded (Doering and Bollhöfer, 2016b; Skoko et al., 2019).

Section 2.6 The study area – The Alligator Rivers Region

The Alligator Rivers Region (ARR; Figure 2-3) of the Northern Territory (NT) of Australia covers approximately 28,000 km^2. It is situated east of Darwin and can be loosely defined as encompassing the catchments of the West, South, and East Alligator Rivers (Martin and Ryan, 2004). The Arnhem Land Aboriginal reserve covers approximately 8,000 km^2 of the eastern portion of the ARR, with most of the remainder forming Kakadu National Park (KNP) (Martin and Ryan, 2004). KNP is world heritage listed for both its natural and cultural values owing to unique ecosystems and species, including rare and endemic species and Ramsar listed wetlands. The Aboriginal heritage of Australia is one of the oldest living cultures in the world and dating evidence indicates hunting and gathering traditions in the area date back more than 60,000 years (Commonwealth of Australia, 2016).

The area contains several remediated legacy mine sites, a large mine undergoing rehabilitation since mining ceased in 2021 (RUM) and several undeveloped U deposits. The vast majority of the ARR is Aboriginal owned land and includes KNP. Due to the nature of the land tenure in the ARR usage of land may include traditional hunting and gathering of food on old and rehabilitated mine sites (Martin and Ryan, 2004). Mining activities can cause dispersion of NORM into the environment leading to NORM exposure to people and the environment above natural background levels.

2.6.1 Traditional owners and relevant radiation risks

Aboriginal people, collectively known as the Bininj-Mungguy people, have lived in the ARR for over 60,000 years (Leger and Fisk, 2016). This is a culturally diverse group comprising several different clans and languages and, to some degree, following different traditions (DCEEW, 2021). The traditional owners of the RUM lease and surrounding areas are the Mirarr people and, eventually, the RUM lease will be returned to the Mirarr people (ERA, 2023).

Activity concentrations of NORM above natural background levels on former mining sites or areas impacted by mining can increase the risk of radionuclide contamination of bush foods. Where traditional activities of Aboriginal people, such as hunting and gathering of traditional bush foods for consumption, may occur on these sites it can lead to radiation doses to people that are above natural baseline levels.

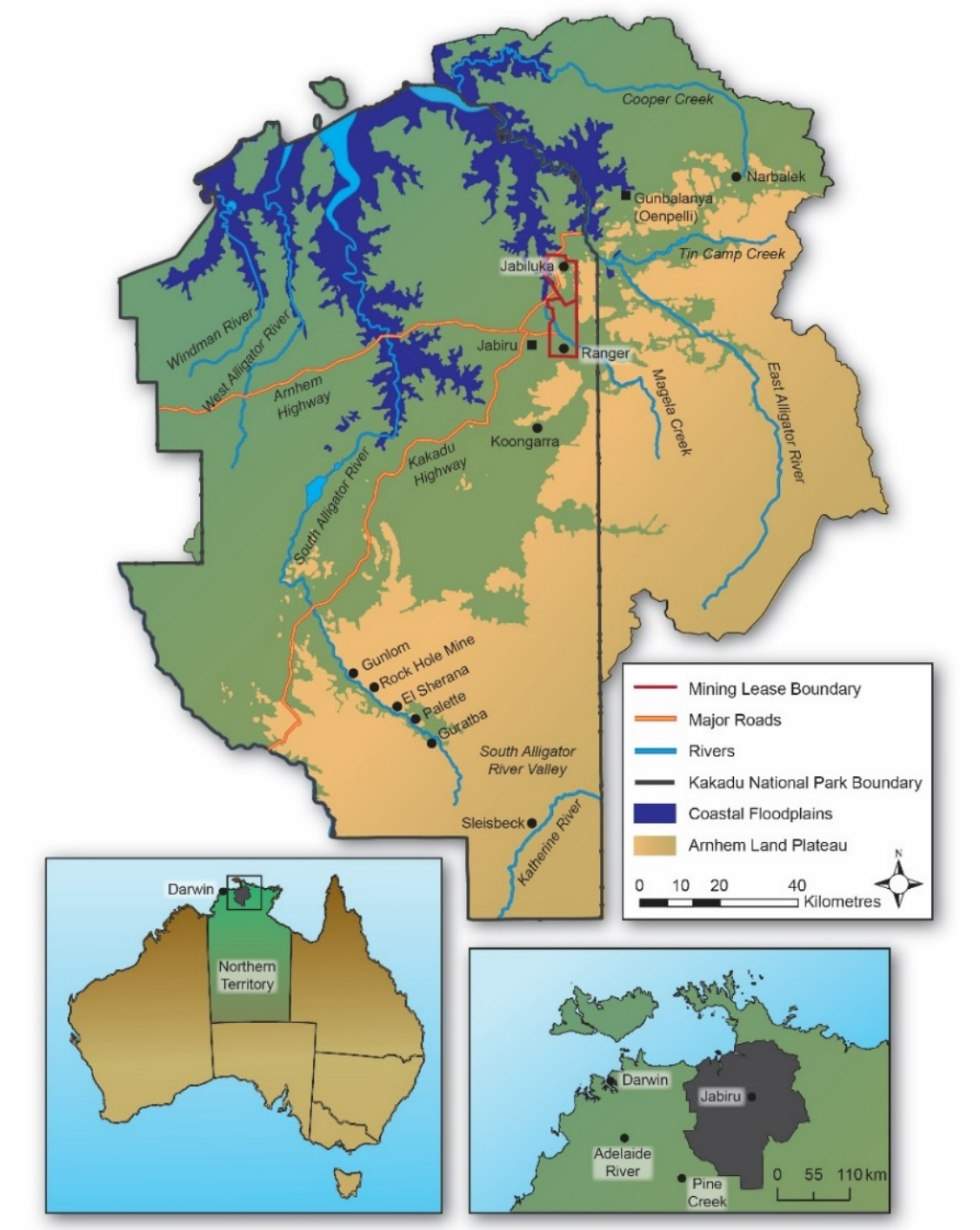

Figure 2-3 Location of the ARR and the Ranger Project Area (RPA).

Environmental risk factors such as those present in environmental media and food are often excluded from studies into Indigenous health outcomes owing to a lack of exposure data[6] (Knibbs and Sly, 2014). An area known as the Alligator Rivers U field, which is part of the

[6] Even where exposure data may be available, investigation may often be unable to explicitly determine the role of environmental factors such as IR where multiple risk factors are present (Schultz, 2021).

Pine Creek Geosyncline (Ferguson and Goleby, 1980), contains the former Nabarlek U mine and the three mineral leases of Ranger, Jabiluka, and Koongarra lie within, but are not a part of KNP[7].

The fact that for many Indigenous communities there is no distinction between environmental and social impacts, for whom the two are inextricably linked (Lawrence and O'Faircheallaigh, 2022), highlights that environmental impacts may also have social impacts. The social aspects of NORM related activities, including in relation to U mining, are also often overlooked (Turcanu et al., 2022).

Gathering site-specific information on exposure pathways for both people and the environment can allow better inclusion of exposure data to people in studies investigating Indigenous health impacts from sites affected by mining and improve communication of risks that can be directly related to the environment being assessed.

2.6.2 The Ranger Uranium Mine

The RUM was the longest operating U mine in Australia's history and produced over 132,000 tonnes of U ore concentrate, a feat achieved by only two other mines worldwide (ASNO, 2021). Mining and milling at the mine ceased on 8th January 2021 and a remediation phase is underway (ERA, 2023). Detailed environmental requirements for operation of the RUM were established and include provisions for the operational phase of the mine as well as rehabilitation (Commonwealth of Australia, 1999). The RUM mining lease, or Ranger Project Area (RPA), covers an area of 79 km^2 (Figure 2-4; see also Figure 2-3 for geographical location). Within this, there is a disturbed area covering 10.6 km^2 (Figure 2-4**)**, which included mining pits, stockpiles, a tailings storage facility, areas where mining waste water was applied, a processing plant and other infrastructure (ERA, 2023). To facilitate rehabilitation, the tailings and infrastructure are planned to be transferred to a mined-out pit (ERA, 2023). A final landform is planned to cover this disturbed area with an overlay of several metres of low U grade waste rock (Doering, 2019a; ERA, 2023). The remainder of the RPA is generally undisturbed, however, exploration activities were undertaken in the area and monitoring wells, sampling stations, roads and tracks are still present (ERA, 2023).

The statutory requirements for rehabilitation of the RUM mining lease are specified in the 'Environmental Requirements of the Commonwealth of Australia for the Operation of Ranger

[7] Koongarra was initially excluded from KNP but was incorporated into KNP in 2013.

Uranium Mine' (the 'Environmental Requirements'; Commonwealth of Australia, 1999). A committed aim of remediation is for the RPA to eventually be incorporated into KNP (Brady et al., 2021).

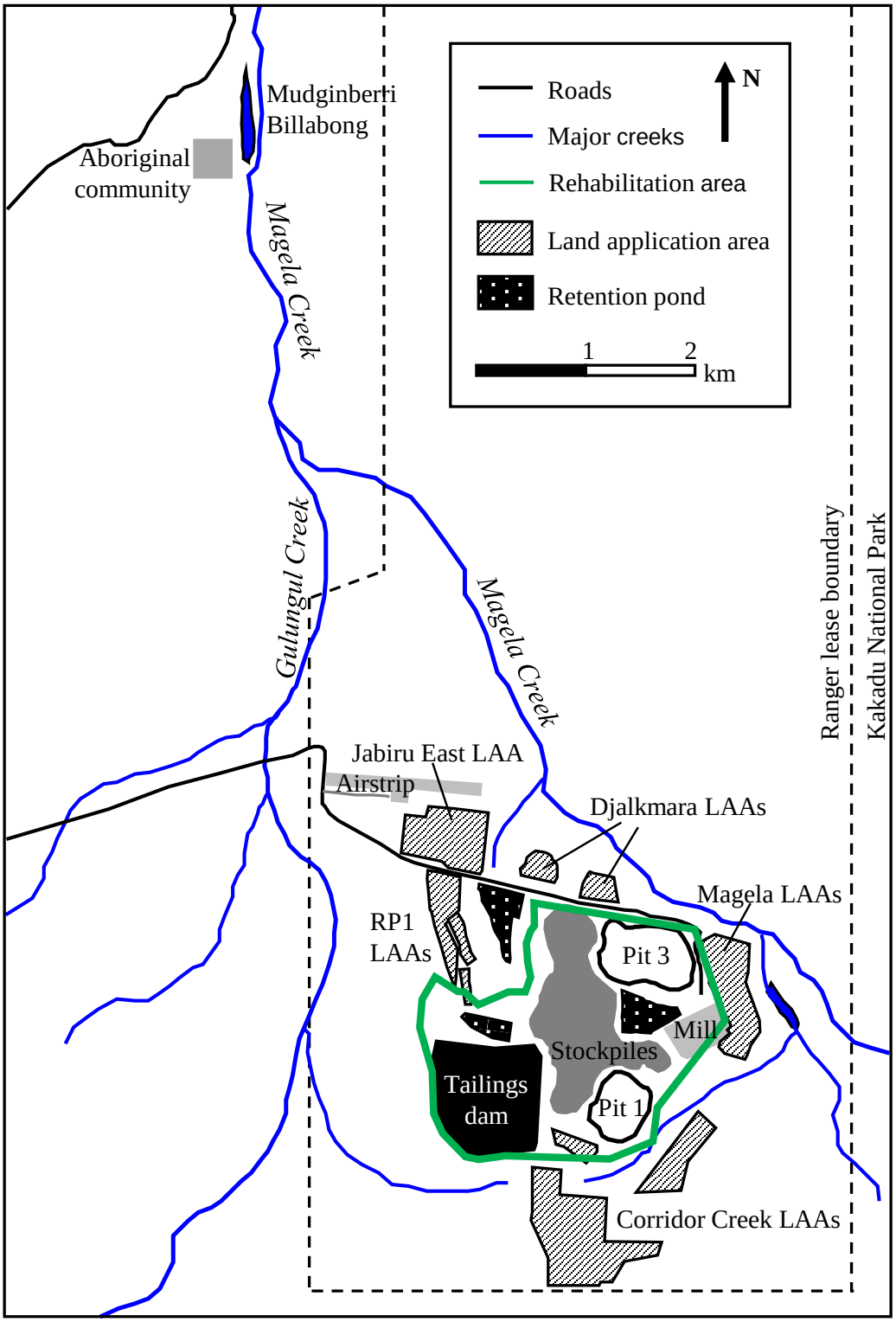

Figure 2-4 Location of disturbed areas on the RPA, Magela and Gulungul Creeks and Mudginberri Billabong (which is downstream of RUM).

The Environmental Requirements establishes primary and secondary environmental objectives, covering aspects of the operation and rehabilitation of RUM. The fundamental purpose is to ensure protection of:

(a) People by *"ensuring that exposure to radiation and chemical pollutants is as low as reasonably achievable and conforms with relevant Australian laws"*, and

(b) The environment such that the rehabilitated area can be incorporated into KNP and attributes for which KNP was inscribed on the World Heritage list are maintained.

The major objectives for rehabilitation specifically relevant to radiation of people are:

"…stable radiological conditions on areas impacted by mining so that, the health risk to members of the public, including traditional owners, is as low as reasonably achievable; members of the public do not receive a radiation dose which exceeds applicable limits recommended by the most recently published and relevant Australian standards, codes of practice, and guidelines; and there is a minimum of restrictions on the use of the area…" (Commonwealth of Australia, 1999).

The above background annual effective dose limit for members of the public in Australia is 1 mSv (ARPANSA, 2020a, b). Restrictions on access may apply if this dose limit cannot be achieved. The stated limit[8] is effectively the minimum requirement, and it is explicitly stated within the Environmental Requirements (Commonwealth of Australia, 1999) that *"Nothing in these Environmental Requirements must be interpreted to prevent or discourage the company from attaining higher environmental standards than those specified."*. This above background annual effective dose limit will apply to the representative person, which for RUM rehabilitation has been defined in ERA (2023) through consultation with Traditional Owners as an:

"*… Aboriginal person using the site for traditional activities including transient camping and the gathering of traditional bush foods for consumption"*.

This will be the definition used in this thesis and although different age classes are not specified in (ERA, 2023), doses across different age classes will also be considered. Achieving the stated

8 Note that the application of a limit indicates this is a planned exposure situation (ICRP, 2007). Note also that a dose constraint of 0.3 mSv has been adopted by ERA (2023), despite there being relatively few other exposure pathways outside of the RPA.

rehabilitation goals for RUM requires detailed understanding of the potential exposure pathways and activities of the representative person.

The following objective is also implicitly relevant to radiation protection of non-human biota:

"*…that operations at Ranger do not result in…change to biodiversity, or impairment of ecosystem health, outside of the Ranger Project Area. Such change is to be different and detrimental from that expected from natural biophysical or biological processes…*".

Aspects covering environmental radiation protection are discussed in (Section 2.7.2) below.

In addition to the legislated rehabilitation requirements, there has been consideration of the aspirations of the Mirarr people for rehabilitation of RUM. These aspirations relating and radiation protection of people and the environment are included in specific rehabilitation standards (Supervising Scientist, 2018a, b):

"*Mirarr Traditional Owners desire that animal and plant populations will persist within off-site ecosystems and recolonise on-site ecosystems of the Ranger Project area after rehabilitation. It is implicit that radiation should not impact on the achievement of these aspirations.*" (Supervising Scientist, 2018a)

"*The Mirarr Traditional Owners desire that residual radioactivity in the environment after rehabilitation will not make it unsafe to access or use the land (including water bodies) on or outside of the Ranger Project Area for their activities, such as collecting and consuming bush foods, seasonal camping, recreation, land management and monitoring, rituals and ceremonies.*" (Supervising Scientist, 2018b)

In addition to these, in both standards it is highlighted that the Mirarr "*…Traditional Owners desire that, after rehabilitation of the Ranger Project Area, the cover design for the mined-out pits and the construction of the final landform will achieve a level of radiation no higher than the pre-mining level.*".

It is important to note that expectations are that rehabilitation meeting all of the noted aspirations will not be achieved in practice (ERA, 2023). Where what can be achieved differs from the aspirations of the Mirarr people, it is imperative that comprehensive and defensible scientific decisions are made. Such decision should be made with consideration of the ability to communicate those decisions and associated risks effectively. This can be achieved by direct measurements of food and environmental items for a comprehensive list of possible contributors to radiological dose.

Section 2.7 Whole-of-site dose models for RUM

The dose model for the representative person and the environment for the RUM rehabilitated site is shown schematically in Figure 2-5. Total dose is dependent upon several factors, these are:

- The above-background component of radionuclide activity concentration in surface waste rock and surface water,
- Occupancy on and around the rehabilitated site, and
- Dietary consumption of bush food items (dose to the representative person only).

The RUM dose model for people includes external exposure arising from gamma radiation, internal exposure from inhalation of dust and Rn and its decay products[9], and ingestion of radionuclides from bush food items collected in the area (estimated as committed effective dose, see Section 2.1.1).

The RUM dose model for the environment is the sum of external and internal exposures calculated within the ERICA assessment tool. These are based on radionuclide activity concentrations in environmental media (soil and water) and whole organisms, occupancy factors and reference organism geometry.

These dose models can be used to assess whether mine closure criteria for radiation will be achieved. If they cannot be achieved, restrictions may need to be placed on access or activities on the site for the representative person, although no such restrictions are possible for wildlife.

To achieve this, several dose model input parameters require clarification, including:

- For dose to people: Characterisation of the ingestion pathway for radionuclides. This is a large part of the dataset required for the development of the dose model for people to assess contribution from impacted soil and water on rehabilitated sites in the region.
- For dose to the environment: Whole organism activity concentrations for some reference organisms and some radionuclides that have not been previously measured.

[9] Note that dose from inhalation of dust for environmental dose assessment is implicit in the CR approach for determining dose. The inhalation of Rn and decay products for reference organisms is complex and not relevant for all reference organisms and has not been included in the whole-of-site dose model presented here, however, it was considered with specific reference to burrowing animals in determination of the limiting organism for RUM (Doering and Bollhöfer, 2016b). External exposure to gamma radiation from water (e.g., from fishing, boating, swimming) has been excluded as it is considered to be negligible. Note that, owing to the presence of saltwater crocodiles in the region and potential for them to inhabit all waterbodies in the former RUM mine site, swimming is a very low probability activity.

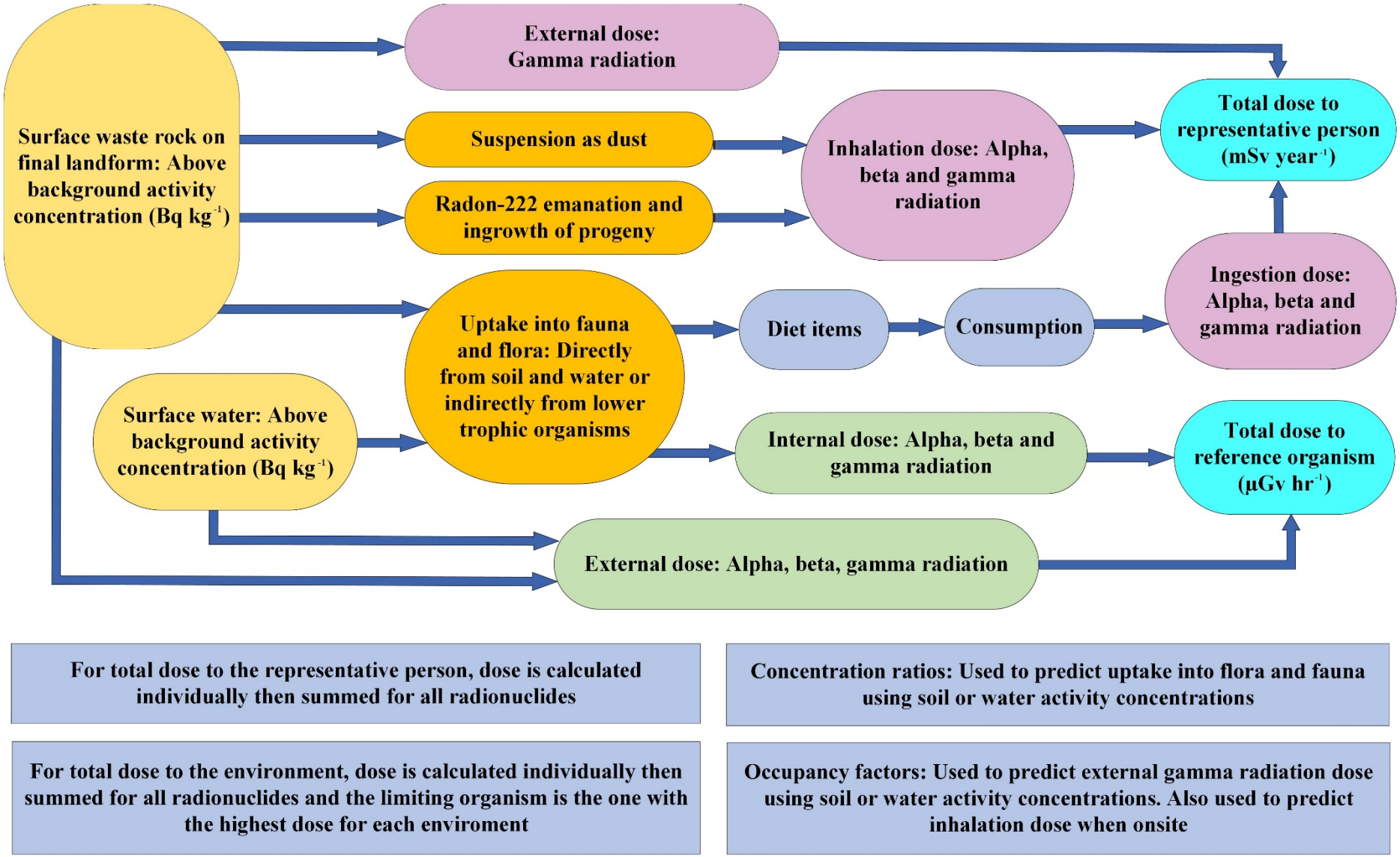

Figure 2-5 RUM Radiological dose conceptual model for exposure to humans and to the environment.

- For dose to people and the environment: Derivation of CRs to allow prediction of activity concentrations of radionuclides in bush foods and whole organisms based on soil and water activity concentrations.

With sufficient knowledge of these parameters, a prospective dose assessment can be undertaken to estimate above background dose from all relevant pathways for the rehabilitated RPA to people and the environment based on the expected activity concentrations in soil and water after remediation.

2.7.1 Representative person dose model

Several values covering dose rate per unit activity concentration in surface waste rock and surface water for each exposure pathway (i.e., ingestion, inhalation and external exposure) for human health above have been published. These values include external exposure from gamma radiation (Doering, 2019a), exposure from inhalation of dusts (Doering et al., 2019b) and Rn progeny (Doering et al., 2022). Occupancy estimates have been detailed in a recent mine closure plan prepared by the Ranger mine operators (ERA, 2023). This plan highlights a desire of Traditional Owners, following 35+ years of access restrictions and a period of rehabilitation, to continue visitation of the site and to reconnect with country and with places of cultural significance (ERA, 2023). Activities that may be expected to occur include:

- Hunting, fishing, bush food gathering,
- Land management and monitoring activities,
- Cultural site visitation, ritual responsibilities,
- Recreation and intergenerational knowledge transfer, and
- Camping along Magela Creek (Figure 2-4), bushwalking and swimming (see footnote 9 regarding potential dose from swimming).

Occupancy estimates based on these activities are shown in Table 2-3 and will be used in determining potential doses to people accessing the site post-rehabilitation[10]. Actual occupancy is contingent on demonstrating satisfactorily that the area is safe to enter and occupy.

[10] Note that actual areas within the rehabilitated landform where access is expected to occur are detailed in the Ranger Mine Closure Plan (ERA, 2023). Also note that the occupancy estimates differ slightly from Doering (2019a) and may be amended in future updates of the Ranger Mine Closure Plan.

Table 2-3 Estimates of occupancy periods on the rehabilitated RPA. Data reproduced from ERA (2023).

Activity	Days per year	Hours per day	Hours per year
Hunting and food gathering (day trips)	30	6	180
Seasonal camping (extended camping)	20	24	480
Recreation	10	24	240
Land management and monitoring	10	8	80
Ritual	5	12	60
Total	75		1040

2.7.1.1 Background dose contribution

The Environmental Requirements note that dose assessment is to be determined from above background dose levels (Commonwealth of Australia, 1999). Utilisation of waste rock material from mining operations as a surface substrate is planned for the rehabilitated landform (Figure 2-4), covering an estimated 8.0 km^2 (ERA, 2023). In the absence of detailed pre-mining radiological baseline studies, an important facet in developing a dose model was the determination of the pre-mining radiological conditions. Retrospective analysis allowed a pre-mining radiological baseline to be determined from historic airborne gamma surveys (Bollhöfer et al., 2014) through correlation with ground-based terrestrial gamma dose rate surveys from an undisturbed radiological anomaly. Results from this survey were used to determine an average pre-mining ^{238}U activity concentration at the surface of 260 Bq kg^{-1} (Doering, 2019a). In this context, the ^{235}U activity concentration is assumed from the natural activity ratio (^{235}U:^{238}U = 0.0466:1) and all radionuclides in the ^{235}U and ^{238}U series are assumed to be in equilibrium. The U content in waste rock is high relative to typical soils, up to 0.02% U_3O_8, equivalent to a ^{238}U activity concentration of 2,100 Bq kg^{-1} for (Lawrence et al., 2009). The expected activity concentration of material across the Ranger final landform post rehabilitation is expected to be less than 0.007% U_3O_8, a ^{238}U activity concentration <728 Bq kg^{-1} (ERA, 2023). This indicates that people using the site and wildlife colonising the site will receive

elevated radiation exposures compared to the natural background[11] (e.g., Doering, 2019a; Doering and Bollhöfer, 2016b; Medley et al., 2017).

2.7.1.2 Diet model for Traditional Owners and ingestion doses

The diet of Aboriginal people living in the ARR comprises both bush foods and food purchased from retail outlets (Ryan et al., 2008). The most comprehensive dietary study for estimating consumption rates of bush foods for the region is by (Altman, 1984), which covers a range of plant and animal species consumed. In the more than 30 years since this study, additional information has been gathered through questionnaires and direct engagement with Aboriginal people (Doering et al., 2017). This research has helped estimate doses throughout the operational phase of RUM. Beyond this phase, a model diet was developed specifically for dose assessment post-remediation in which total consumption of bush foods was estimated at 320 kg per year (Ryan et al., 2008). The model diet reduces the variety of bush foods consumed to key items and food types, and a recently updated model diet is shown in Table 2-4. Samples of all diet items were not available for this thesis, however, those available accounted for over three quarters of the estimated consumption in the model diet (Table 2-4).

Table 2-4 Model diet of Aboriginal bush food consumption adapted from ERA (2023) showing where sample material was available for analysis of ^{227}Ac and/or ^{231}Pa for this thesis.

Bush food group	Compartment	Consumption[a] kg yr^{-1}	Availability for this thesis
Freshwater bush foods			
Crocodile	Flesh	3	Available
File snake	Flesh	3	Available
Fish group 1[b]	Flesh	10	Not available
Fish group 2[b]	Flesh	20	Available
Magpie goose	Flesh	20	Available
Other waterfowl	Flesh	3	Not available
Mussel	Flesh	4	Available

[11] Radionuclides in the ^{232}Th decay series are not considered relevant to the Ranger mine context, because the ore is not naturally elevated in these radionuclides.

Bush food group	Compartment	Consumption[a] kg yr^{-1}	Availability for this thesis
Turtle (pig nose, long neck and snapping)	Flesh	5	Not available
Turtle (long neck only)	Liver	0.5	Not available
Waterlily	Rhizome	3	Not available
Drinking water	Unfiltered	2000[c]	Limited
Terrestrial Bush Foods			
Buffalo	Flesh	5	Available
Buffalo	Kidney	0.5	Available
Buffalo	Liver	0.5	Not available
Emu	Flesh	2	Not available
Fruit	Flesh	3	Available
Flying fox	Flesh	5	Not available
Goanna	Flesh	2	Not available
Pig	Flesh	25	Available
Wallaby	Flesh	20	Available
Yam	Flesh	20	Available

[a] Annual consumption given in the table is for an adult, and for a 10-year-old child is assumed to be half the amount.

[b] Fish were split into 2 groups based on significant differences in CRs between species, with Group 1 having CRs a factor of 2–10 times higher than Group 2 (Martin et al., 1998). The single fish sample measured for this study was a barramundi (*Lates calcarifer*) classified as a Group 2 species.

[c] Annual drinking water intake used to determine ingestion doses during the early operational phase of mining in the model diet (Johnston, 1987) and continued through subsequent assessments until very recently (e.g., Doering et al., 2017; Martin, 2000) was 600 L.

Given the diversity of Aboriginal communities within KNP, detailed study of actual consumption rates where bush foods form a large part of the diet is considered to be not only impractical, but unacceptably intrusive for those people being studied (ERA, 2023). Evidence gathered from interviews with residents from relevant communities and through observation

during bush food collection indicate that the data in Ryan et al. (2008) is still generally applicable. However, there are some changes in the model diet used here taken from the latest RUM mine closure report (ERA, 2023). The most significant changes are a substantial reduction in consumption estimates for water buffalo tissues sourced from the region (revised down from 146 kg for flesh, and 18 kg for kidney and liver) in acknowledgement that most water buffalo is sourced from an alternative location. Ingestion of water from local creeks has also been increased from 600 to 2,000 L $year^{-1}$, which may be more realistic for the local climate. Other changes include the addition of emu, flying fox and waterfowl other than magpie goose as food sources, noting that organs are eaten for several species, and a variation in the consumption estimate for crocodile from 2 to 3 kg per person per year.

Bush food samples for this thesis were provided from previously collected material and there was limited capacity for additional sample collections. As such, not all food groups were measured and for some samples, with limited sample material, only one isotope (either ^{227}Ac or ^{231}Pa) was measured (see Table 2-4 and Chapter 5, Section 5.3.3). Despite this, most food groups were measured.

It is expected that the Traditional Owners will source drinking water from both the rehabilitated RPA and downstream of the RPA from creeks that flow through the RPA (ERA, 2023). There are two such creeks, Magela and Gulungul creek, that merge and flow into the Magela floodplain after passing through the Mudginberri billabong (Figure 2-3). This billabong is a source of drinking water and bush foods for the permanent settlement (also called Mudginberri) adjacent to the billabong (Martin, 2000). The population of the Mudginberri settlement was deemed to be the 'critical group' during the operational phase of RUM, owing to the consumption of freshwater mussels (*Velesunio angasi*) which strongly bioaccumulate ^{226}Ra (Martin, 2000). Long-term water quality monitoring of ^{226}Ra has been conducted in the Magela (since 2001) and Gulungul (since 2011) creeks, both upstream and downstream of the mine (Figure 2-4). In addition, long-term monitoring of Ra isotopes, ^{226}Ra and ^{228}Ra, has been conducted in freshwater mussels collected from Mudginberri billabong (since 1982). Analysis of the monitoring data indicates no increase in Ra activity concentrations, in either water or freshwater mussels attributable to RUM (Doering, 2018). Monitoring of these pathways is ongoing (Supervising Scientist, 2023). The water sample and freshwater mussels analysed for this thesis were collected from Mudginberri billabong.

2.7.1.3 Inhalation exposure

Inhalation doses from dust from the Ranger rehabilitated site, including doses from all radionuclides in the ^{235}U and ^{238}U decay series, were assessed by Doering et al. (2019b) with an assumption that all radionuclides in a decay series were in secular equilibrium. This assessment used an assumed average ^{238}U activity concentration on the final landform of 800 Bq kg^{-1} and a background of 260 Bq kg^{-1}. The annual effective dose from inhalation of dust was estimated to be 5.3 µSv yr^{-1} under a 'worst case' scenario. This is very low compared to potential inhalation doses from the most significant inhalation dose pathway, inhalation of ^{222}Rn progeny (0.11 mSv $year^{-1}$ for the worst case scenario; Doering et al., 2019b; Doering et al., 2022).

In the analysis for dose from inhalation of dust by Doering et al. (2019b) ^{235}U series radionuclide activity concentrations were based on ^{238}U values assuming the natural activity ratio (^{235}U:^{238}U = 0.0466:1), however, the relative contribution from the ^{235}U series was not reported (Doering et al., 2019b).

The relative contribution in the reported inhalation doses from dust attributable to the ^{235}U series was determined for this thesis by comparing the DCs (ICRP, 2012) of the ^{238}U and ^{235}U decay series radionuclides used in the modelling[12] by Doering et al. (2019b) and assuming the U natural activity ratio. For this thesis, the above background dose contribution from the ^{235}U series was determined to be equivalent to 23.5% of the total dose from inhalation of dust. The annual effective dose thus calculated for the ^{235}U series is detailed in Chapter 5, Section 5.3.3.1, with corrections to the dust inhalation dose estimate of Doering et al. (2019b) made to account for a revised estimate of the average ^{238}U activity concentration on the final landform.

2.7.1.4 External exposure

Above background gamma dose rates were also estimated by Doering (2019a) using published external gamma dose coefficients for the ^{238}U and ^{235}U series radionuclides. The natural activity ratio for ^{235}U:^{238}U of 0.0466:1 with both decay chains in secular equilibrium with progeny was assumed. Only 1.3% of the external dose was attributable to the ^{235}U series (see Chapter 5, Section 5.3.3.1).

[12] Radionuclides ^{210}Pb, ^{210}Po, ^{226}Ra, ^{230}Th, ^{234}U and ^{238}U in the ^{238}U series and ^{227}Ac, ^{231}Pa and ^{235}U in the ^{235}U series. This list represents all radionuclides with half-lives greater than 30 days, with dose from progeny with half-lives less than 30 days included in dose calculated from that of the parent isotope (Doering et al., 2019b).

2.7.2 Environmental dose model

As noted above, $CR_{WO\text{-}Media}$ values for Australian wildlife have been shown to typically be higher than the equivalent in international datasets for several reference organisms where data is available (Doering and Bollhöfer, 2016b; Hirth et al., 2017; Rea et al., 2021). Australian species can exist in different environmental conditions (most international data is from temperate environments) and have very different biology and metabolism compared to species used to provide $CR_{WO\text{-}Media}$ data for reference organism (e.g., marsupial and placental biology are rather different, Sánchez-Villagra, 2013). This may lead to differences in the uptake of radionuclides in Australian species compared to those used to provide default data for environmental dose assessment. An example is the 'Large Mammal' reference organism where data in the ERICA assessment tool is derived from roe deer, elk, moose and other large placental mammals. However, in the NT of Australia an "Agile Wallaby" is more relevant to use as a basis for data input in the dose model for a 'large mammal'. Australian native species investigated in this work and their equivalent reference organism in the ERICA assessment tool are shown in Table 2-5.

Table 2-5 Northern Territory Species used as representative of reference organisms in the ERICA assessment. Only those reference organisms where sample material was available for this thesis are listed.

Terrestrial ecosystem		**Freshwater ecosystem**	
ERICA Reference Organism	**NT equivalent representative organism**	**ERICA Reference Organism**	**NT equivalent representative organism**
Arthropod	Green Ant *Oecophylla smaragdina*	Bird	Magpie Goose[a] *Anseranas semipalmata*
Bird	Rainbow lorikeet *Trichoglossus moluccanus*	Mollusc – bivalve	Freshwater mussel *Velesunio angasi*
Grasses and Herbs	Native herbaceous plants[b] (various spp.)	Pelagic fish	Barramundi[a] *Lates calcarifer*
Mammal – large	Agile wallaby[a] *Macropus agilis*	Reptile	Freshwater crocodile[a] *Crocodylus johnstoni*
Mammal – small-burrowing	Bandicoot *Isoodon macrourus*		

	Flying fox *Pteropus* sp.
Reptile	Green tree snake *Dendrelaphis punctulata*
Shrub	Native shrub[b] (various spp.)

[a] $CR_{WO\text{-}Media}$ values for these were derived from tissue concentrations by applying a tissue to whole-organism conversion factor for a chemical analogue (see Appendix C, Section C-2).

[b] $CR_{WO\text{-}Media}$ values derived from above ground parts of plants cut approximately 1 cm from the ground (Supervising Scientist, 2022).

Owing to sample unavailability not all reference organisms are listed as sample material for this thesis.

It is also important to define the level at which environmental impacts on the Ranger rehabilitated landform may arise to understand the protection goals needed for setting appropriate benchmark values. In this context the relevant primary environmental objective for RUM rehabilitation is to (Commonwealth of Australia, 1999):

"*maintain the natural biological diversity of aquatic and terrestrial ecosystems of the Alligator Rivers Region, including ecological processes*"

The potential impacts for which protective benchmarks are considered therefore apply to the aquatic (freshwater only) and terrestrial ecosystems of the region, as opposed to individuals or specific representative organisms (such as threatened species or populations). In this case the 10 µGy hr^{-1} numeric benchmark default in ERICA is likely to be over-protective as it integrates a conservative safety factor in the prediction of dose rates below which deleterious impacts are unlikely to occur (Garnier-Laplace et al., 2008).

An environmental dose rate of 100 µGy hr^{-1} is noted by UNSCEAR (2008) as the point below which doses "*to the most highly exposed individuals would be unlikely to have significant effects on most terrestrial animal communities*". Similarly, UNSCEAR (2008) reports that "*maximum dose rates of 400 µGy/h to a small proportion of the individuals in aquatic populations of organisms would not have any detrimental effect at the population level*".

It is from this that the RUM mine closure plan derives benchmark dose rates, specifying 100 µGy hr^{-1} for the most highly exposed terrestrial plants and animals, and 400 µGy hr^{-1} for aquatic plants and animals (ERA, 2023). These benchmark dose rates have been approved as

closure criteria for rehabilitation of RUM and were used in previous environmental dose assessments for RUM (Doering and Bollhöfer, 2016b; Doering et al., 2019a). Radiation levels below the benchmark dose rates are considered unlikely to have significant effects on most terrestrial communities or detrimental effects at the population level for aquatic organisms (UNSCEAR, 2008). If dose rates exceed these benchmarks, there are few reasonably achievable actions that could be taken to reduce dose rates (Doering and Bollhöfer, 2016b). However, exceeding a benchmark may justify continued monitoring for deleterious impacts on affected populations and may also trigger further assessment. Such assessment may include comparison of the assessed dose rates for any organism exceeding the benchmark value against more specific effects data published for that type of organism.

Whole organism results are required for an ERICA assessment. Although whole organism samples for some reference organisms were available for this thesis, for several other reference organisms tissue to whole organism conversion factors were used to derive whole organism activity concentrations from results for single tissues. Several studies have reviewed published data to determine tissue to whole organism conversion factors (Wood et al., 2010; Yankovich et al., 2010), including one study from the ARR (Doering et al., 2019a). Although none of these studies included measurements of ^{227}Ac or ^{231}Pa, conversion factors for chemical analogues commonly used for ^{227}Ac and ^{231}Pa were published. In this thesis, tissue to whole organism conversion factors were used to derive whole organism activity concentrations of ^{227}Ac and/or ^{231}Pa for several organisms, where relevant tissues results were available. As no conversion factors for Ac and Pa have been published, chemical analogues were used for ^{227}Ac and ^{231}Pa. These chemical analogues included Am, Th and U for both ^{227}Ac and ^{231}Pa, and Ce, Eu, La and Lu for ^{227}Ac only, and Pu for ^{231}Pa only. To derive a whole organism activity concentration, the tissue-specific activity concentration is multiplied by the tissue to whole organism conversion factor (see footnote to Table 2-5). Results are shown in (Chapter 5, Section 5.2.3).

Organisms can be added to the ERICA tool where sizes may differ from the default organism. Although variations in size makes minimal difference to the calculated dose rate, particularly for terrestrial organisms (Howard et al., 2013), using locally relevant values can assist in communication of results. Region-specific organism data were used to define region-specific representative organisms in the ERICA assessment tool in place of default reference organisms where results for ^{227}Ac or ^{231}Pa were available. Added organism input parameters include new DCCs, which are interpolated from the DCCs of the default reference organism ellipsoids in the ERICA tool. The new DCCs are then used for dose calculation (Medley and Patterson,

2022). Details of the region-specific organisms and a comparison of interpolated DCCs with those from ERICA reference organisms is in (Chapter 5, Section 5.3.4.1 and Appendix C, Section C-1, Table C-2).

The dosimetric model integrated into the latest version of the ERICA tool was developed by the ICRP, using the ICRP recommended dosimetric system for non-human biota (ICRP, 2017). The ERICA tool is linked to a radionuclide decay and emission database (ICRP, 2008b) and a software tool 'BiotaDC', complementary to ICRP (2017). BiotaDC is used to derive DCCs in the ERICA tool and allows addition of radionuclides not included in the ERICA tool by default using the 'Add Isotope' function (e.g., ^{227}Ac). An integration period of one year is assumed in deriving DCCs for internal and external dose, which accounts for dose from ingrowth of progeny, this is particularly relevant for ^{227}Ac. A limitation of this approach is that ^{227}Ac can generally be considered to be in equilibrium with progeny in soils, therefore an integration period will underestimate external dose rates. This will have a minimal impact for ^{227}Ac and progeny as internal dose is generally the major dose pathway for the terrestrial environment (see results also in Chapter 5). Another limitation is in the case of organisms with lifespans of less than one year, in which case dose rates are likely to be overestimated.

2.7.3 Details specific to the RUM whole-of-site dose models

A database containing radionuclide activity concentrations in tissues, whole organisms, soils and surface water for the ARR was published in (Doering and Bollhöfer, 2016a). Subsequent to this, a tool that utilises the database for calculation of CRs was also published (Doering and Bollhöfer, 2016c). It is noted that, during the operational phase of the Ranger mine, the primary radiation exposure pathway to people was from freshwater systems and, as such, data from routine sample collection from this ecosystem dominates the database (e.g., fish, freshwater mussels and water; Doering and Bollhöfer, 2016a). Sampling for terrestrial biota was less targeted and mainly involved opportunistic sampling, including fresh roadkill, feral animals culled by KNP rangers, and by researchers accompanying Aboriginal people on hunting and gathering trips. Soil, sediment and water samples were collected with biota samples and as part of environmental characterisation studies (Doering and Bollhöfer, 2016a). Some samples were collected after publication of this database, in particular to target missing data for specific reference organisms in environmental dose assessment (e.g., arthropods in Medley et al., 2017).

CRs for the ingestion pathway are available for all foods in the Aboriginal bush food diet (Table 2-4), for relevant elements of the ^{238}U decay series[13] (Pb, Po, Ra, Th and U). For environmental dose assessment, data for a range of reference organisms for the above elements from the ^{238}U decay series have been published in (Doering and Bollhöfer, 2016b; Doering et al., 2019a; Doering et al., 2018; Medley et al., 2017).

Despite the extensive range of data published, $CR_{WO\text{-}Media}$ values for many reference organisms are still lacking for the ^{238}U decay series[14]. This includes, amphibians, annelids, flying insects, lichen and bryophytes and mollusc – gastropod for the terrestrial ecosystem. In addition, amphibian, crustacean, insect larvae, mollusc – gastropod, phytoplankton, vascular plant and zooplankton are missing for the freshwater ecosystem.

Except for ^{235}U (using ^{238}U as an isotopic analogue), there were no CR data available for the ^{235}U series at the commencement of this study. This substantial data gap highlights the importance of the work undertaken in this thesis.

For this thesis terrestrial samples from the above collection types, where sample material remained, were made available and additional soil samples representing the approximate areas of collection were re-sampled. Green ants (*Oecophylla Smaragdina*) to represent the arthropod reference organism, and samples comprising a mixture of "Grasses and Herbs" and "Shrub" as specific reference organisms in the ERICA tool with associated soils were sampled in 2021 and included in the assessments performed for this thesis. Data for Pb, Po, Ra, Th and U has only been published as a technical advice to ERA (Supervising Scientist, 2022). Freshwater mussel samples, collected as part of the annual monitoring program at Mudginberri Billabong (downstream of Ranger), were also provided and a large volume (30 L) water sample was collected from this billabong specifically for this thesis.

As plants have relatively variable rooting depths depending on the size and species of plant, instead of the real rooting depth a standardised soil layer is adopted by the (IAEA, 2010, 2014b). In these publications a depth of 10 cm for grasses or 20 cm for fruiting trees is recommended for general determination of CRs (IAEA, 2010), whereas the 'ideal' depth suggested for wildlife CRs is 10 cm (IAEA, 2014b). Although results for a range of soil depths is reported in Doering

[13] Results from radionuclides ^{210}Pb, ^{210}Po, ^{226}Ra and ^{238}U in the ^{238}U decay series were measured, whereas ^{232}Th was measured as an isotopic analogue for ^{230}Th in most data (Doering et al., 2017).

[14] Note that site-specific data for flying insects and phytoplankton has been generated but is yet to be published (Pers. Comm Che Doering, 13 March 2024).

and Bollhöfer (2016a) and used with the associated CR tool for calculation of CRs (Doering and Bollhöfer, 2016c), the most common collection depth was 10 cm. Soil samples for the recent collections noted above were all to a depth of 10 cm.

To complete the final dose assessment the activity concentration of radionuclides in the waste rock capping for the final landform and surface water are required. These will not be available until determined by the mine operator. In addition, as noted above, estimated occupancy by Traditional Owners may vary from current estimate in (ERA, 2023).

Section 2.8 The importance of ^{227}Ac and ^{231}Pa in ^{235}U series dose assessment

As noted in Chapter 1, Section 1.1.1, the most relevant isotopes in the ^{235}U series are ^{235}U, ^{231}Pa and ^{227}Ac. The extent to which the subsequent radiologically significant decay products in the series are present in biological systems is controlled by the chemical properties of these three elements in the environment, and their biological uptake. This is particularly so for species with life cycles in the order of years. This is of relevance to the radiation dose received by humans through ingestion of bushfoods which typically have longer life cycles (e.g., fish, wallaby, tree fruits). The relevance of ^{235}U can be appropriately modelled using ^{238}U as an analogue as the behaviour of both isotopes is the same. As noted in Section 1.1.1, there are no suitable isotopic or stable analogues of Ac and Pa for ^{227}Ac and ^{231}Pa, and the validity of chemical analogues for the transport through the environment and accumulation in environmental media is largely untested owing to the very low number of environmental measurements for either isotope (Medley et al., 2024). The total dose (internal plus external) from NORM for both people and the environment is dominated by the internal dose component (see Section 2.5 above). As such measurements of ^{227}Ac and ^{231}Pa activity concentrations in foods and water for human dose assessment and in whole organisms for environmental dose assessment are likely to be the key pathways.

Section 2.9 Scope of analysis – ^{235}U series in the ARR

2.9.1 Background information on the ^{235}U series in the ARR

The water activity concentration of ^{227}Ac was measured in the tailings dam at RUM in the 1990s which showed a value of 7.5 Bq L^{-1} (Paulka et al., 1993), this provides evidence that ^{227}Ac can be liberated in mineral extraction processes and could therefore be mobile in the environment at mining impacted sites. Later work by Martin and Akber (1996) showed that concentrations of ^{227}Ac in groundwater impacted by seepage from this tailings dam had increased. The

potentially higher mobility of ^{227}Ac in the ARR than might be predicted from the environmental chemistry was illustrated by Golian et al. (1984), where observations of excess ^{223}Ra in groundwater in the region were seen as evidence of ^{227}Ac mobility. Payne et al. (1992) measured ^{227}Ac in groundwater in the study region (Koongarra deposit) using ^{227}Th as a proxy. Their work showed that ^{227}Ac was not readily mobilised in the filtered fraction of water, however, a higher mobility was shown in the <0.1 µm fraction, possibly adsorbed to colloids or fine clays. The activity ratio for ^{226}Ra:^{210}Po:^{227}Ac of 10:1:1 was measured in retention pond water (RP2) at RUM and this water was used for irrigation of land application areas on the RPA (Akber et al., 2011; Martin and Ryan, 1995). Again, this highlights the potential mobility of ^{227}Ac in waters and release of ^{227}Ac from mineral matrices through operations at RUM.

Martin et al. (1998) and Martin (2000) reported 17 measurements of ^{227}Ac (four in water samples and 13 in biological samples) collected from the ARR, however, all of these were effectively below the limit of detection. A dose assessment for the critical group[15] for RUM during the operational phase undertaken by Martin (2000) included ^{227}Ac, however, Th was used as an analogue for Ac when defining CRs and the assessment did not include ^{231}Pa.

2.9.2 Contribution of this thesis to addressing information needs and dose assessment

The present work included development and application of novel methods for analysis of ^{227}Ac and ^{231}Pa at environmental concentrations such that reliable CRs could be derived for bush foods and reference organisms. The methods developed for analysis of ^{227}Ac and ^{231}Pa will also allow future analysis to fill gaps remaining.

Activity concentrations of ^{227}Ac and/or ^{231}Pa were measured for the bush food and reference organisms shown in Tables 2-4 and 2-5. Actinium-227 was measured in a water sample from Mudginberri billabong (Figure 2-4) and both ^{227}Ac and ^{231}Pa were measured in several soil samples from the ARR. The potential environmental mobility of ^{227}Ac and ^{231}Pa was inferred from the soil and water activity concentrations. CRs were derived for bush foods and region-specific organisms then used to undertake prospective dose assessments for human health and environmental protection. The outcomes provide valuable input to inform closure criteria developed for RUM rehabilitation. This included an assessment of the relative

[15] In this assessment the critical group was an Aboriginal population of around 50 people living near the Mudginberri billabong Figure 2-4, i.e., downstream of the Magela and Gulungul creeks passing through the RPA.

contribution to dose from the ^{235}U series compared to the ^{238}U series and the applicability of using chemical analogues for dose assessment for ^{227}Ac and ^{231}Pa in the ARR.

Chapter 3 : Chemistry of ^{231}Pa and method development

Section 3.1 Chemistry of ^{231}Pa

There are 29 known isotopes of Pa, only three of which have had relevance for chemists, naturally occurring isotopes ^{231}Pa and ^{234}Pa, and reactor-produced ^{233}Pa (Myasoedov et al., 2011). The most abundant isotope of Pa, ^{231}Pa, is rare in the environment with an abundance in the earth's crust typically around a few parts per trillion (NCBI, 2022). The chemical isolation of ^{234m}Pa, the metastable state of ^{234}Pa (half-life 6.7 hours) led to the discovery of Pa in 1913 (Myasoedov et al., 2011), initially called 'brevium' owing to the short half-life of 1.15 minutes. With half-lives of 32,600 years (^{231}Pa) and 27.0 days (^{233}Pa), only ^{231}Pa and ^{233}Pa have seen substantial further use for studying the chemical properties of Pa (Kirby, 1959).

Investigating the chemistry of Pa is a significant challenge owing to the relatively low natural abundance. In 1961 approximately 127 g of ^{231}Pa, was prepared in the UK from 60 tons of pitchblende sludge and is believed to be the largest amount ever produced (Myasoedov et al., 2011). Despite the bold prediction of Kirby (1959) that "*It is safe to predict that the 1960's will see much of the mystery and witchcraft eliminated from protactinium chemistry*", there still remains much to be understood about the chemistry of Pa.

The chemical behaviour of Pa is similar to both, actinides and transition metals, with a pentavalent oxidation state like Nb and Ta, but also, under reducing conditions, a tetravalent state like other actinides (Wilson, 2012). Transition metals are characterised by chemistry associated with their d shells, whereas actinides by their f shells (Hübener, 2003). As the first actinide it possesses a 5f orbital, which has almost the same energy as the 6d orbital, leading to two stable ground-state electron configurations with $[Rn]5f^2 6d^1 7s^2$ only slightly more stable than $[Rn]5f^1 6d^2 7s^2$. These are similar to the ground-state electron configurations of Th ($[Rn]6d^2 7s^2$) and U ($[Rn]5f^3 6d^1 7s^2$) leading to chemical properties that transition between those of Th and U (Hübener, 2003; Wilson, 2012).

In addition to the hybrid chemical properties between actinide and transition metals, Pa has several other unique tendencies that make the chemistry of this element challenging. The extreme tendency of Pa to hydrolyse in dilute solutions of most common acids, except sulfuric and hydrofluoric acid, is a common theme running through published research (e.g., Knight et al., 2016; Myasoedov et al., 2011; Regelous et al., 2004; Sill, 1978). Other properties, including the formation of difficult to dissolve refractory species and polymers (Myasoedov et al., 2011;

Sill, 1978), high particle reactivity in aqueous solution and affinity for Si in the absence of F^- ions (Regelous et al., 2004) further complicate chemical separation from complex matrices. The chemistry of Pa when present in ultra-trace amounts can also be significantly different compared to higher concentrations (e.g., at concentrations greater than 10^{-6} M Pa(V) can start to form insoluble oxide polymers; Jerome et al., 2018; Myasoedov et al., 2011). Thus, development and validation of analytical techniques should be undertaken with quantities in the same range as those intended to be measured by the technique.

3.1.1 Environmental Chemistry

Protactinium-231 occurs in the environment in ultra-low concentrations relative to other metal ions (with a crustal abundance of 0.87×10^{-6} ppm it is similar to ^{226}Ra; Myasoedov et al., 2011), which leads to the extraction chemistry being largely determined by the chemical and physical properties of the sample (Myasoedov et al., 2011). Although it has been used advantageously in the development of Pa separation schemes (Myasoedov et al., 2011; Ostapenko et al., 2017; Regelous et al., 2004), the high affinity for Si can be problematic for separation of Pa from some sample types, such as soils and sediments. Particle reactivity rather than chemistry seems to be the primary environmental process impacting Pa concentrations and behaviour, particularly in marine studies (e.g., Anderson et al., 1983a; Anderson et al., 1983b), however, the environmental behaviour in terrestrial systems is poorly documented.

3.1.2 Biochemistry

Pa has a range of possible valence states and although it is most stable in the +5 state, Taylor et al. (1987) have shown that, in biological systems, it is likely to quickly convert to the +4 state and will follow the same biochemical pathways as other quadrivalent actinides (e.g., Np, Pu, Th and U), which may therefore be suitable analogues. Protactinium is known to be a 'bone-seeker' in humans (Grossmann et al., 2008; Sill, 1978) with up to 40% of ^{231}Pa that enters the blood stream being deposited in the bones. In some cases, U has been shown to be an analogue of the essential element Ca (Sheppard and Sheppard, 1985), and biologically, this may also be the case for ^{231}Pa. Hence, several bone samples and freshwater mussels, with relatively high concentrations of Ca were included in this study. The freshwater mussels are also known for Ra accumulation associated with similarity in chemistry to Ca (Bollhöfer et al., 2011), which was an important consideration for sample chemistry.

For Pa, the data are scarce on direct effects from exposure or biokinetics within the human body. Systemic uptake and retention of ^{231}Pa was assessed by Newton and Brown (1974) in a

man exposed to ^{231}Pa via a puncture wound (exposure was also to ^{227}Ac which is discussed in Chapter 4, Section 4.1.2). Deposition was primarily in bone and the liver, with 20–30% removed from the body within 1000 days, and the remainder having a biological half-life of 70–125 years. Data from several rat studies (generally with ^{233}Pa) support the human data in that most absorbed Pa is deposited in the skeleton, however, there are some reported differences. For example, Taylor et al. (1987) and Hamilton (1948) reported relatively high retention in rat liver whereas low Pa retention in neonatal rat liver was found by Sullivan et al. (1983). The fractional absorption of Pa in the gastrointestinal tract of rats is similar to the currently used ICRP (2012) value for humans, however, a study with hamsters suggests this value is underestimated (Harrison and Stather, 1981).

The ICRP provide radiological age-specific dosimetric and biokinetic models for a range of radionuclides, including ^{231}Pa (see ICRP (2012) and Chapter 2, Section 2.1.3 for details). For Pa, actinide analogues for which substantially more biokinetic information is available, are often used. For example, in ICRP (1995) doses to the lung for members of public, and in ICRP (2019) occupational doses from Pa inhalation, are assigned the biokinetics of Th. However, a relatively simplistic model is still used for uptake via ingestion for members of the public: 0.05% is assumed to transfer from the gastrointestinal tract to the blood (ICRP, 2012). Of this, 40%, l5% and 2% are deposited in bone, the liver and the kidneys respectively, with the remainder being directly excreted (ICRP, 1981). These transfer values are a synthesis of the studies of Pa uptake in rats and humans (including those noted above). The relatively long physical half-life, high skeletal transfer leading to a long biological half-life, and decay via alpha emission lead to relatively high ingestion dose coefficients (DCs) for ^{231}Pa (ICRP, 2012).

The behaviour of Pa is expected to differ in reference organisms compared to that in humans. A range of elements have been used as analogues to derive CRs for Pa, depending on the biological system for which CRs are being developed. For example, ICRP (2009) uses Th for marine fish, Pu for freshwater fish and Pu or Am for a range of terrestrial biota. Protactinium-231 was also shown to be one of four main contributors to radiological dose from mussel ingestion as a result of marine discharge of phosphogypsum into a North Sea ecosystem (van der Heijde et al., 1988), again supporting the possibility that Pa may behave similarly to Ca. Given that both Pa and U have demonstrated similarity in biochemical behaviour to Ca, the selection of U is likely to be the closest potential analogue for Pa in the environment.

3.1.3 Radiochemistry

The chemistry of protactinium can make the measurement of ultra-low quantities a challenge and I cannot state this better than Berry et al. (1989):

"*The great difficulty of maintaining Pa in aqueous solution without hydrolytic precipitation or, at the very low concentrations that have been studied, loss of a large portion by adsorption on container surfaces or particulate impurities is perhaps the best known feature of the aqueous chemistry of this element.*" (p. 339).

Hydrolytic precipitation also tends to inhibit extraction of Pa from aqueous solution into organic solvents (Raje et al., 2001). Adsorption to any precipitate present in solution or container walls is common (Raje et al., 2001), in particular the affinity of Pa to silica means that glass vessels should be avoided (Sill, 1978). As such, chemical analysis techniques essentially require stabilisation of Pa in aqueous solution via complexation, avoidance of the use of organic solvents where possible, and the use of plastic containers such as polypropylene (PP) or fluoropolymers such as polytetrafluoroethylene (PTFE) or (perfluoroalkoxy alkane) PFA.

One of the most stable aqueous complexes of Pa is with fluoride ions (e.g., Knight et al., 2016; Myasoedov et al., 2011; Regelous et al., 2004; Sill, 1978). A particular challenge for this thesis was the intention to avoid the use of HF where possible as exposure can pose serious local and systemic hazards (Dennerlein et al., 2016). In environmental samples, the need to separate ultralow levels of Pa from much larger masses of other elements exacerbates the challenges associated with hydrolysis of Pa (Raje et al., 2001) and affinity of Pa for silica (often present in the sample, e.g., in soils and sediments). Pa forms stable fluoro- and sulfato- complexes in aqueous solution and this is commonly used to maintain stable solutions for chemical analysis. However, Myasoedov et al. (2011) reports that if the concentration of Pa $\leq 10^{-5}$ M, freshly prepared solutions are stable in 1–4 M HNO_3. Work by Sill (1978) details a method indicating stability of ^{233}Pa in a 25% (5.6 M) HNO_3 solution for at least 58 days, and ^{231}Pa for at least 2 years was demonstrated. At environmental concentrations, Pa may behave unpredictably; the use of stable carriers including Nb and Ta can alleviate this, however, some measurement techniques (particularly mass spectrometry, Jerome et al., 2018) may be adversely affected by using these carriers.

The necessity for removal of interfering ions is dictated by the measurement technique used (e.g., removal of alpha emitters for alpha spectrometry or isobaric interferences for mass spectrometry). A complete discussion on the radiochemistry of Pa is considered out of scope

for this thesis but comprehensive reviews can be found in e.g., Myasoedov et al. (2011) and Kirby (1959) with a discussion of more recent advances in Ostapenko et al. (2017) and references therein.

However, the radiochemistry of Pa specific to the needs in this thesis, including tracer isotope selection, its production and relevance for the measurement technique selected are discussed in Section 3.2 below.

Section 3.2 Method Development for the Separation of Pa

3.2.1 Selection of a chemical tracer and measurement technique

An advantage of measuring radionuclides in naturally occurring decay chains is that in some circumstances it is possible to measure a parent or daughter radionuclide as a proxy for the radionuclide of interest. For example, the daughter isotope ^{227}Th has been used as a proxy for the ^{231}Pa measurement (Gascoyne, 1985; Shen, 1996). However, this requires the assumption that the parent and daughter isotopes are in equilibrium. Although this can reasonably be assumed in some sample types (e.g., geological samples), it may not always be true (Gascoyne, 1985) and for environmental samples, such assumptions become more difficult to sustain. In the study region for this thesis, disequilibrium with the intermediate in the decay chain between ^{231}Pa and ^{227}Th (i.e., ^{227}Ac) was shown in (Golian et al., 1984) and thus invalidates the use of ^{227}Th as a proxy for ^{231}Pa in environmental samples.

To accurately assess concentrations of trace elements in a complex sample matrix chemical separation and a way of monitoring the recovery from this process is required. Recovery is often measured by use of a yield tracer which, to be effective, must exhibit the same chemical behaviour as the analyte. Thus, isotopes of the same element are commonly used as yield tracer for elemental or radioisotopic analysis (Harvey and Lovett, 1984).

For the measurement of ^{231}Pa, the most used yield tracer is ^{233}Pa (e.g., Edwards et al., 1997; Knight et al., 2014; Regelous et al., 2004). Neptunium-237 (t½ 2.14×10^6 yr) is the parent isotope of the Neptunium series decay chain (Figure 1-4) and ^{233}Pa, with a half-life of 27.0 days, is the immediate decay product. Therefore, in even a slightly aged purified ^{237}Np solution, the presence of ^{233}Pa is guaranteed, as is the direct progeny of ^{233}Pa, ^{233}U. Due to the much longer half-life of ^{233}U (1.59×10^5 yr) there is no significant ingrowth of further isotopes in the decay chain in such a solution. Production of ^{233}Pa can also arise through neutron irradiation of ^{232}Th and subsequent beta decay of the ^{233}Th produced (t½ 22.2 min), however, separation of ^{233}Pa from ^{237}Np is a more commonly employed technique for the preparation of ^{233}Pa tracer solutions

(e.g., Knight et al., 2014; Mendes et al., 2013; Regelous et al., 2004). For this thesis, neptunium oxide (NpO_2) was available to use as a material for the extraction of ^{233}Pa. Therefore, a suitable technique for chemical separation of Np and Pa was required.

Mass concentrations of actinides, such as ^{231}Pa, in the environment require highly sensitive methods for precision measurement. The sensitivity of the intended measurement technique is an important consideration when developing procedures for measurement of environmental concentrations of actinides and selection of an associated yield tracer. A range of measurement techniques have been employed for measurement of ^{231}Pa, including decay counting and mass spectrometric methods. Alpha spectrometry was used by Knight et al. (2014), single collector ICP-MS in ion counting mode by Süfke et al. (2018), sector field ICP-MS by Agarande et al. (2005), secondary ion MS by Schmitt (2007), Thermal Ionisation MS by Edwards et al. (1997), Fietzke et al. (1999) and Shen et al. (2003), and Multi-Collector ICP-MS by van Calsteren and Thomas (2012). The first reported use of Accelerator Mass Spectrometry (AMS) to measure ^{231}Pa was by Christl et al. (2007) using the ETH/PSI-AMS TANDY facility, operating at about 300 kV. Importantly, although Christl et al. (2007) could not calculate a precise detection limit, due to interference in the tracer measurement from the ^{233}U progeny of ^{233}Pa, they estimated that detection limits significantly lower than 10 fg could be achieved.

A comparison of different measurement techniques by Hellborg and Skog (2008) highlights that AMS techniques are more sensitive for the measurement of longer-lived radionuclides and less sensitive for shorter lived radionuclides with a cut-off point around 10–100 years. For example, Fifield (2008) estimated that AMS is at least two orders of magnitude more sensitive than alpha spectrometry for the measurement of $^{239}Pu/^{240}Pu$ (t½ of 24,100 and 6,561 yr, respectively). For ^{241}Am, with a half-life of 433 years, Aggarwal (2018) demonstrated a sensitivity of 1–2 orders of magnitude[16] better than alpha spectrometry. It is important to understand all aspects of the measurement process to make a true determination of the most sensitive technique, including for example the blank count rate, sample preparation and suitable radiochemical separation techniques. Other factors, including economic ones, need also be

[16] Assuming a typical limit of detection for alpha spectrometry of 1 mBq and calculating a detection limit of 0.015 mBq (0.12 fg) from (Aggarwal, 2018). The sensitivity of decay counting techniques varies with radionuclide decay properties however, alpha spectrometry often has a sensitivity 2–3 orders of magnitude better than gamma spectrometry for measurement of NORM (Saïdou et al., 2008).

considered in the final selection of a measurement technique and the typically higher cost of AMS limits its general application (Fifield, 2008; Hellborg and Skog, 2008).

AMS is likely to be significantly more sensitive for ^{231}Pa (t½ 32,670 yr) than alpha spectrometry. AMS can offer advantages over typical decay counting and other mass spectrometric techniques for the measurement of actinides (e.g., Brown et al., 2004; Fifield, 2008). In AMS the background caused by molecular interferences (e.g., ^{232}ThH for mass 233) is almost completely removed in the stripper and is therefore of little concern (Christl et al., 2007; Fifield, 2008), this provides a distinct advantage over conventional mass spectrometry.

Although AMS is likely to be far more sensitive for the ^{231}Pa measurement than decay counting techniques, this is not the case for the ^{233}Pa tracer. The short half-life of ^{233}Pa leads to the need for the addition of a higher activity of ^{233}Pa for AMS to achieve the same precision (i.e., a similar number of ^{233}Pa atoms) on the yield tracer measurement compared to high sensitivity decay counting techniques such as alpha spectrometry (and therefore a relatively high activity of the parent ^{237}Np from which to produce the ^{233}Pa).

The relatively short half-life of ^{233}Pa requires separation chemistry to be relatively rapid for any technique measuring ^{233}Pa directly. As ^{233}Pa decays to a longer-lived isobar (^{233}U) which has a different ion counting efficiency, the time delay from chemical separation to sample analysis has further implications for measurement accuracy of mass spectrometric methods. Christl et al. (2007) found a higher negative ion yield for UO^- compared to PaO^-, (dubbed an 'enhancement factor'). Furthermore, the enhancement factor also differed significantly between runs (ranging between 2.00±0.09 and 2.32±0.07). This required the enhancement factor to be determined for each run. This can be done by using a standard with a ^{233}Pa to ^{233}U isotope ratio that is the same as samples and blanks, which can be achieved by ensuring that standards, samples and blanks are prepared at the same time and in an equal manner.

It is also important to note that the most suitable chemical tracer and measurement technique is also contingent on the effectiveness of the applied chemical separation procedure, which may vary between sample types and matrices.

3.2.2 Selection of a chemical separation procedure for Pa

In the present work the possibility of using a ^{237}Np cow was explored. A so-called 'cow' follows the 'loading' of ^{237}Np onto a resin bed where it is retained in a stable condition, with the ability to extract ^{233}Pa when needed. Because of the potential production of organic wastes from repeated solvent extractions of ^{233}Pa from ^{237}Np only extraction chromatography and ion

exchange techniques were considered, with an approach targeted at effectively separating ^{233}U in addition to ^{237}Np. This had the advantage of preventing the production of organic wastes from solvent extraction and minimising recurrent losses of ^{237}Np with repeated extractions.

Any sample from which Pa must be separated may have other alpha emitting isotopes present, which potentially interfere with alpha spectrometric measurements. Elements close in mass to 231 and 233 may also be present, which will potentially interfere with mass spectrometry measurements. Consequently, the sample type and technique used to measure Pa (decay counting or atom counting) directly impacted which isotopes were most likely to lead to interference in the measurement and how effectively they needed to be removed during radiochemical separation.

In the case of alpha spectrometry, the most likely isotopes in the environmental samples from the ARR that could have interfered with ultra-low-level measurements of ^{231}Pa were ^{210}Po, ^{226}Ra and ^{234}U. For example, freshwater mussels have been shown to have high activity concentrations of ^{226}Ra (Bollhöfer et al., 2011) and in crustacea, ^{210}Po (Fowler, 2011). Uranium-234 has a similar alpha particle energy to ^{231}Pa and, although activity concentrations of ^{234}U are typically rather low in biological samples, they can be relatively high in soil samples (e.g., Doering and Bollhöfer, 2016a; Vera Tome et al., 2002). The separation of Pa from the sample matrix would therefore need to take these isotopes into consideration.

For mass spectrometric techniques, the isotope ^{230}Th, arising in the ^{238}U decay series, ^{232}Th as the parent isotope of the thorium decay series, and ^{233}U from decay of ^{233}Pa, were the most likely similar mass nuclides to interfere with ^{231}Pa measurement, whereas ^{232}Th, and ^{234}U from the ^{238}U decay series, had the greatest potential for interference in ^{233}Pa measurement due to their high abundance. Results from ICP-MS for ^{232}Th and ^{238}U were available for most samples analysed for ^{227}Ac and ^{231}Pa in this thesis (see Appendix B). Activity concentrations ranged from <0.001–2 mBq g^{-1} for ^{232}Th and <0.006–2.4 mBq g^{-1} fresh weight for ^{238}U. Furthermore, although ^{234}U results were only available for a limited number of samples they were close to equilibrium values (i.e., 1:1 activity ratio of ^{234}U:^{238}U). The activity concentrations of ^{232}Th and ^{234}U equate to a range of $<6 \times 10^{11} – 1 \times 10^{15}$ atoms g^{-1} and $7 \times 10^{7} – 3 \times 10^{10}$ atoms g^{-1} respectively. Activity concentrations of ^{230}Th were measured in only four samples analysed for ^{227}Ac and ^{231}Pa, three of these measurements were <MDL for the respective samples (owing to low chemical recovery). The activity concentration in the fourth sample was 0.016 Bq kg^{-1} fresh weight which equates to 5×10^{7} atoms g^{-1}. Given the low activity concentrations of ^{230}Th expected and the fact that the half-life of ^{230}Th is over five orders of magnitude lower than for

^{232}Th, methods that effectively separate interference from ^{232}Th in mass spectrometric techniques are expected to also do so for ^{230}Th.

Other naturally occurring isotopes in the ^{232}Th (Figure 1-3) and ^{238}U decay series (Figure 1-1) that have similar mass to 231 and 233 include ^{234}Th (t½ 24.1 d), ^{231}Th (t½ 25.5 hr), ^{234}Pa (t½ 6.70 hr) and ^{234m}Pa (t½ 1.16 min). These all have half-lives too short to have substantial biological uptake and activity concentrations in biological samples are therefore governed by the parent radionuclide ^{235}U for ^{231}Th, and ^{238}U effectively for the other three isotopes. At the highest activity concentration for ^{238}U in samples for this thesis this would lead to <200 atoms of ^{231}Pa from decay of ^{231}Th and <70,000 atoms of mass 234 at the time of measurement, with <800 atoms of ^{234}U from decay of both ^{234}Pa and ^{234m}Pa. In addition, sample preparation includes steps that would further reduce ^{231}Th and ^{234}Th to even lower levels. Thus, potential interference from ^{234}Pa, ^{234m}Pa, ^{231}Th and ^{234}Th can be expected to be negligible, particularly given that atoms with mass 234 will be heavily suppressed when measuring mass 233 and the quantities at mass 231 would likely be below the detection limit for AMS systems.

The half-life of ^{233}U is much longer than ^{233}Pa, and hence ^{233}U alpha activity resulting from ingrowth from ^{237}Np (Figure 1-4) will be negligible over the time frames relevant to the present work. However, when ^{237}Np is used to prepare the ^{233}Pa tracer solutions for mass spectrometric techniques, the relative number of ^{233}U atoms needs to be considered and indeed will exceed the number of ^{233}Pa atoms when the time after extraction for ^{233}Pa tracer preparation is greater than 62 days.

It is also important to note that for AMS, the measurement process itself separates interfering isobars or elements at various stages (see Section 3.10), which can make criteria for the selection and development of a chemical separation method less stringent.

Based on the considerations from this section and Section 3.2.1, AMS was the method of choice with the use of ^{233}Pa as a tracer. The better detection limit of AMS compared to alpha spectrometry was a major factor in this decision. Implications for the choice of AMS were:

- ~1 × 10^{10} atoms of ^{233}Pa (3 kBq) tracer were desired per sample at the time of measurement,
- Effective and repeatable radiochemical separation method(s) of ^{233}Pa from ^{237}Np was needed for the preparation and use of a ^{237}Np cow,
- ^{233}U required effective separation from ^{233}Pa to minimise interference in tracer measurement,

- There was a requirement to keep a chronological record of key steps in the procedure to accommodate the impact of ^{233}U ingrowth, and
- ^{232}Th and ^{234}U were the primary isotopes requiring a high degree of separation to minimise interference with ^{231}Pa and ^{233}Pa measurement via AMS.

Therefore, chemical separation methods were developed:

- The first method involved preparation of a ^{237}Np cow and the techniques to repeatedly isolate ^{233}Pa from ^{237}Np to yield the ^{233}Pa tracer. This was further refined to remove ^{233}U extracted with ^{233}Pa from the ^{237}Np cow.
- The second method was aimed at efficiently extracting ^{231}Pa and ^{233}Pa from the sample material ensuring ^{232}Th and ^{234}U were sufficiently removed.

Section 3.3.1.1 provides a summary of the experimental work for optimising the separation of ^{233}Pa and ^{237}Np, with Section 3.3.1.2 detailing repeated extractions of ^{233}Pa with 3 M HNO_3 from a prototype ^{237}Np cow. This is followed in Section 3.4 which presents results from development and production of the 'ANU ^{237}Np cow'[17], prepared from 19.2 mg of NpO_2 (440 kBq ^{237}Np) which provided the ^{233}Pa tracer added to all environmental samples analysed in the present work. Section 3.4 also details results from milking of the ANU ^{237}Np cow for ^{233}Pa tracer preparation, and its long-term stability. Section 3.5 describes characterisation of the ANU ^{237}Np cow, identification of specific contaminants present and purification of ^{233}Pa tracer solutions. Section 3.6 to Section 3.9 present results and discuss development of the method for extracting ^{231}Pa and ^{233}Pa from environmental samples.

Section 3.3 Production of the ^{233}Pa Tracer

Although Pa can form a number of stable complexes in aqueous solution (Myasoedov et al., 2011; Sill, 1978), the stability of the Pa fluoro-complexes and resistance to hydrolysis (Brown and Maddock, 1963; Myasoedov et al., 2011) has led to HF solutions being commonly used for the wet extraction of Pa (e.g., Agarande et al., 2005; Eppich et al., 2013; Gies et al., 1984; Knight et al., 2014; Regelous et al., 2004; Sakamoto et al., 2002). Although HF is used at relatively weak concentration which reduces the associated risks of HF in general handling,

[17] The 'ANU ^{237}Np cow' was used for tracer preparation throughout the present work and is identified with this name to prevent confusion with prototypes prepared in the method development process. An unopened container of NpO_2 from an ANU chemical store was deemed suitable, however, it was noted the only documentation regarding this material related to the date it was received (1964) at ANU.

there is still a significant risk in the preparation of extraction solutions from concentrated HF. As noted above (Section 3.1.3), an aim of this thesis was to avoid using HF where possible for occupational health and safety reasons.

Many solvent extraction techniques have been developed and used for the separation of Pa, (e.g., Knight et al., 2014; Myasoedov et al., 2011; Sill, 1978). These techniques have the problem of generating radioactive organic waste when high activity solutions are used. Some techniques take advantage of the high affinity Pa has for silica, by allowing Pa to bind to silica while removing other elements and then extracting Pa from the silica (Regelous et al., 2004; Sakamoto et al., 2002). These separation methods, however, elute other elements, including Np, prior to elution of Pa. This is not optimal for a cow technique where Np is best retained on the resin. The method by Regelous et al. (2004) also has the disadvantage that, in addition to the use of HF, it also uses potentially explosive $HClO_4$ for Pa separation. Ion exchange separation techniques have received some attention (e.g., Eppich et al., 2013; Mendes et al., 2013 which all use AG1-X8 resin), and more recently studies evaluated the use of extraction chromatography for separation of Pa from Np (Knight et al., 2016; Ostapenko et al., 2017). The extraction chromatography methods have the advantage that they have eliminated the use of HF and $HClO_4$ for Pa separation and use only reasonably common and less hazardous acids such as HNO_3 and HCl. Ostapenko et al. (2017) studied the retention behaviour of Pa and Np on Eichrom® DGA®, TEVA®, TRU® and UTEVA® resins in HNO_3 and HCl, building on earlier similar work (e.g., Horwitz et al., 1995; Mendes et al., 2013). In these studies, the retention behaviour of Np was observed to be strongly dependent on the oxidation state of Np. The behaviour for both elements was shown to be similar in all resins except for the TEVA® resin. Notably, separation of Np and Pa without HF by Ostapenko et al. (2017) used the TEVA® resin. Indeed, Sill (1978), Knight et al. (2014), Knight et al. (2016) and Ostapenko et al. (2017) all developed techniques for Pa separation without the use of HF, though each had limitations that prevented their use in the present work[18].

[18] The method described in Sill (1978) used a potassium fluoride fusion, which is converted to a pyrosulfate fusion generating HF vapour, and the effectiveness of Np separation was not assessed. The work of Knight et al. (2014) used a solvent extraction method for Np/Pa separation, leading to organic waste generation. The method of Knight et al. (2016) was less promising as a separation method as Np was eluted before Pa, and it used a resin comprised of 1-octanol impregnated onto a solid phase support that was developed in-house and not commercially available when this thesis was commenced. Limitations of the Ostapenko et al. (2017) method are that losses of Pa to the surfaces of labware were up to 15%, in the weak acid concentrations used for Pa extraction and Np was also eluted before Pa.

A HF-free method that overcomes the limitations has been developed as part of this thesis. It allows separation of ^{233}Pa from ^{237}Np on a TEVA® resin column, while retaining Np, and simultaneously extracts Pa in a stable solution (3 M HNO_3). The method also shows minimal losses of Pa onto the surfaces of labware. The ANU ^{237}Np cow was prepared using the method developed which is given in Appendix F (Section F-1), and ^{233}Pa tracer solutions were extracted from it for the thesis. The main limitation of the method developed for ^{233}Pa tracer production is that the process does not separate Th and U from Pa, but only isolates Pa from Np, as such ^{233}U was present in the ^{233}Pa tracer solutions. Accordingly, after the tracer has been added to the sample, ^{233}U is separated when separating Pa from U (and other elements) from the sample. Several challenges were encountered with development and use of the ANU ^{237}Np cow, including substantial concentrations of ^{241}Am and Pu isotopes in the NpO_2 and, owing to the age of the NpO_2, an initially high abundance of ^{233}U atoms were encountered. Repeated extractions of Pa removed the contaminant nuclides but also showed a decline in the overall recovery of ^{233}Pa, which started at close to 100% but declined following subsequent extractions, stabilising at about 50%.

3.3.1 Method development and prototype ^{237}Np cow

A method was identified (Eichrom Technologies Inc., 2006) that met the desired criteria for the separation of ^{233}Pa and ^{237}Np as described in the previous sections. That is, retention of ^{237}Np, as Np(IV), with probable effective separation of Pa without the use of HF on an ion chromatographic resin, such as TEVA® (based on the capacity factors for Pa(V) reported in Mendes et al., 2013). A set of tests was undertaken to assess and optimise separation of ^{233}Pa and ^{237}Np. The tests also assessed the suitability of the method for creating a '^{237}Np cow' from which ^{233}Pa could be repeatedly 'milked' after a suitable time to allow for ingrowth of ^{233}Pa between extractions. Specifically assessed were the stability of the resin in the relatively strong acid used (3 M HNO_3) and the ability to effectively separate ^{233}Pa while retaining ^{237}Np with repeated extractions over time[19].

3.3.1.1 Separation of ^{233}Pa and ^{237}Np on TEVA®

In acidic solutions, Np exists in oxidation states from III to VI (Kitatsuji et al., 2010), which must be converted to Np(IV) to ensure high retention of Np on TEVA® resin (Horwitz et al., 1995). Several methods to reduce Np for separation using ion chromatography have been

[19] Although it was expected that the time needed for a ^{237}Np cow to remain stable was several years, these tests assessed stability only over a period of 251 days (Table 3-3).

published (e.g., Eichrom Technologies Inc., 2005, 2006; Horwitz et al., 1992; Horwitz et al., 1995). In the present work two different reducing solutions from Eichrom Technologies Inc. (2005) and (2006) were tested (Table 3-1).

The methods were selected as the load solutions were prepared in 2.5 M and 3 M HNO_3 (with reducing agents) which were stable solutions for Pa (according to Myasoedov et al., 2011) and Pa was expected to be eluted in this fraction while Np was retained. In these methods after loading the Np, 2.5 M and 3 M HNO_3 solutions (without reducing agents) are then used to elute interfering elements, and it was expected this would include Pa. As it was not clear that the Np(IV) would remain stable with addition of sufficient 2.5 M or 3 M HNO_3 to fully extract Pa, or if complete extraction of Pa could be achieved, the 2.5 M HNO_3 solution with a reducing agent (ferrous sulfamate, see Table 3-1) was tested as an extraction solution for Pa to maintain Np in the +4 oxidation state in case the HNO_3 solution alone was ineffective. In these methods Fe(III) is used in the load solutions to more effectively reduce Np.

Although retaining Np on the column was the aim of the method under development, removal of Np at the completion of the thesis may also be required. However, HF solutions were used to extract Np in both the Eichrom Technologies Inc. (2006) and (2005) procedures. To avoid using HF for extraction of Np, 0.05 M HNO_3 was tested as an extraction solution for Np based on the poor retention of Np(IV) on TEVA® in weak HNO_3 solutions ($k' < 10$) as summarised by Mendes et al. (2013). Results of testing the two different load solutions are shown in Table 3-1, elution profiles are shown in Figure 3-1. Recovery was determined by high-resolution gamma spectrometry (HRGS) using the 29.4 keV and 311.9 keV emission energies of ^{233}Pa and ^{237}Np, respectively. Individual aliquots of the eluted solutions were taken throughout the procedure to develop elution profiles, with partial recoveries for each aliquot summed to determine recovery for each test. Details of the HRGS procedures are given in (Appendix H).

Table 3-1 Results of Tests 1 and 2 conducted for separation of ^{237}Np and ^{233}Pa with TEVA® resin with different load and extraction solutions.

Test ID	**Test description**	**Recovery (%)**	
Test 1		**^{233}Pa**	**^{237}Np**
Load solution	1 mL ^{237}Np tracer in 4 M HNO_3 + 1.25 mL 1.5 M ascorbic acid, 0.5 mg Fe(III) (in 0.1 mL solution) and 0.5 mL 1.5 M sulphamic acid in 3 M HNO_3 + 1 mL 8 M HNO_3 to make total load solution to 3.85 mL 3 M HNO_3	18±1	<1
Extraction solutions	^{233}Pa 10 mL 3 M HNO_3		
	^{237}Np 10 mL 0.05 M HNO_3	80±4	99±3
Test 2			
Load solution	1 mL ^{237}Np tracer in 4 M HNO_3 made to total load solution volume of 3.85 mL as 0.1 M ferrous sulfamate in 2.5 M HNO_3	11±2	2±1
Extraction solutions	10 mL 0.1 M ferrous sulfamate in 2.5 M HNO_3		
	10 mL 0.05 M HNO_3	89±6	100±7

Tests of the different load solutions showed poor recovery of ^{233}Pa (18%) with an elution volume of 10 mL 3 M HNO_3 and even lower recovery (11%) with 10 mL 2.5 M HNO_3/0.1 M ferrous sulfamate. However, excellent retention of ^{237}Np (>97%) on the TEVA® resin was achieved with the reducing agents in the load solution, followed by high recovery in 10 mL of 0.05 M HNO_3. This demonstrated that ^{237}Np could be effectively reduced to Np(IV) and maintained in that state, leading to retention on TEVA® resin. Best retention of ^{237}Np and most rapid recovery of ^{233}Pa were with the load solution from Test 1' with Pa eluted in 3 M HNO_3 (Table 3-1).

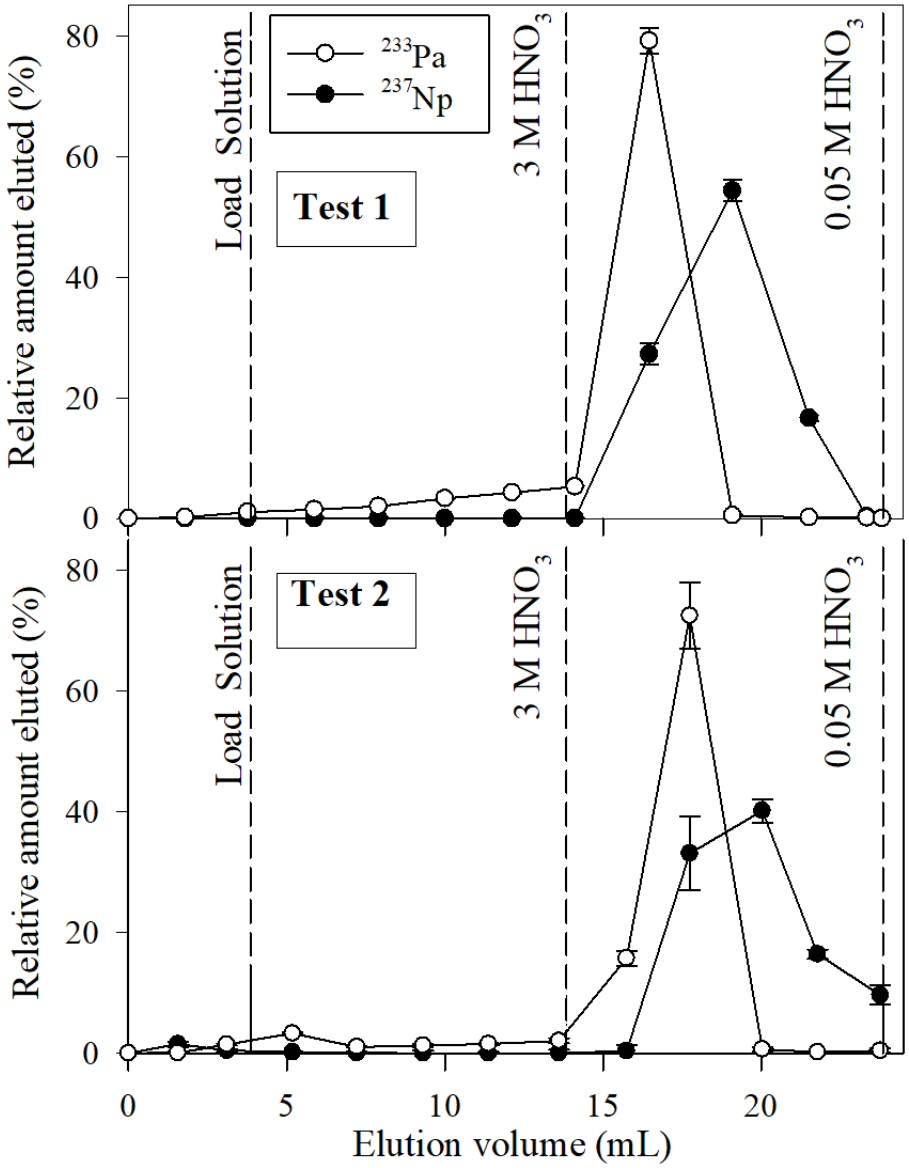

Figure 3-1 Elution profiles for Tests 1 and 2 conducted for separation of ^{237}Np and ^{233}Pa with TEVA® resin with different reducing and extraction solutions. Volume for Test 1 is on the bottom x-axis.

To confirm that 3 M HNO_3 would yield high recovery as an eluant for ^{233}Pa, a further four tests (Tests 3–6) were conducted to optimise the separation of ^{233}Pa and ^{237}Np using TEVA® resin. For these tests, the load solution from Test 1 was used, with extraction of ^{233}Pa in 3 M HNO_3. In these tests the volume of 3 M HNO_3 and 0.05 M HNO_3, were varied, with the final test (Test 6) also assessing the impact of flow rate on extraction efficiency. Results are shown in Table 3-2, with elution profiles shown in Figures 3-2 and 3-3. Recovery and elution profiles were determined by HRGS (Appendix H).

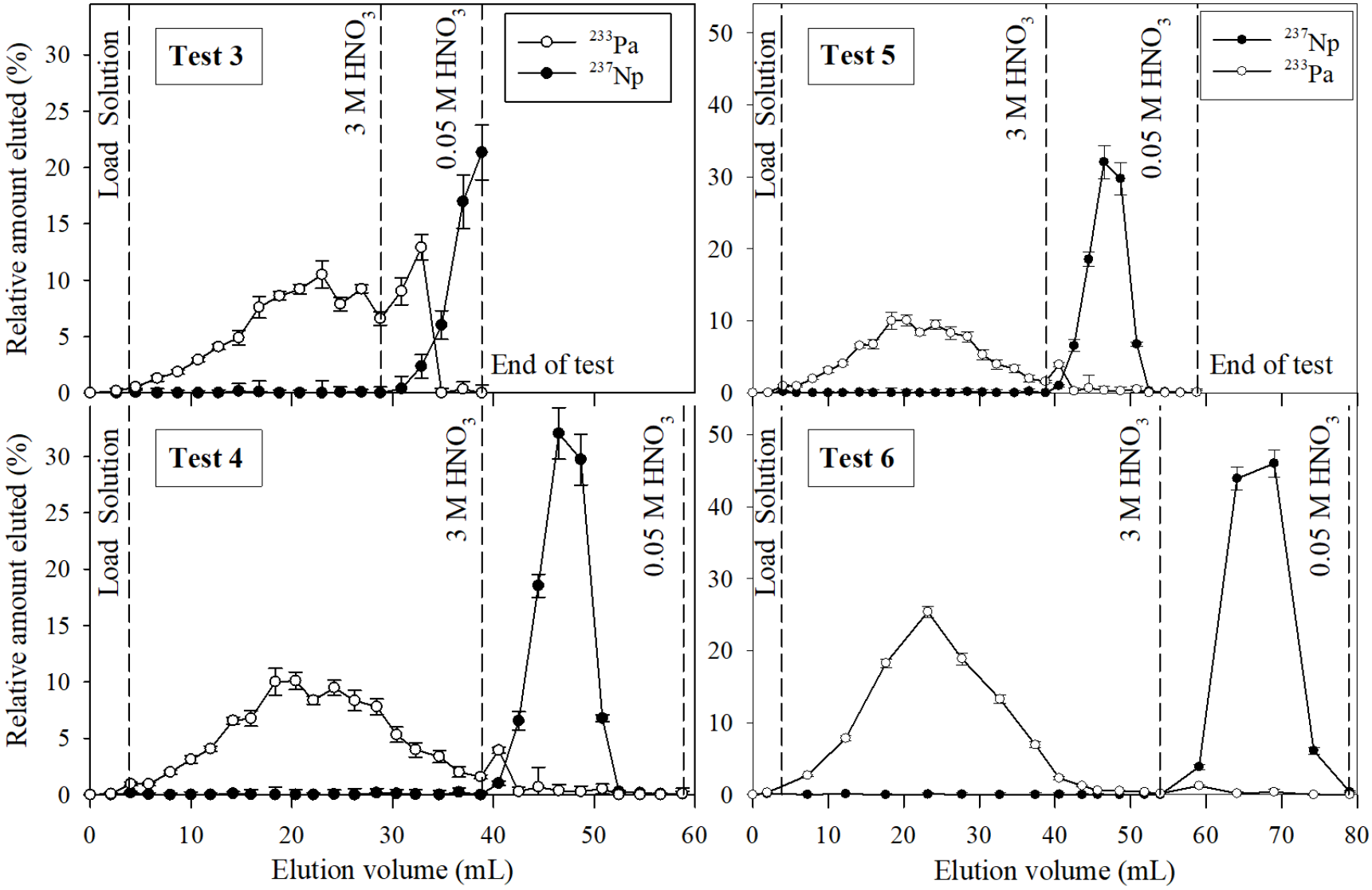

Figure 3-2 Results of four tests to optimise separation of ^{237}Np and ^{233}Pa with TEVA® resin. The full method developed for preparation and milking of a ^{237}Np cow with repeated separation of ^{233}Pa and ^{237}Np is given in Appendix F (Section F-1). Elution volume shown on the bottom x-axis also applies to Test 3 and 5.

Table 3-2 Results of Tests 3–6 to optimise separation of ^{237}Np and ^{233}Pa with TEVA® resin. The full method developed for preparation and milking of a ^{237}Np cow with repeated separation of ^{233}Pa and ^{237}Np is given in Appendix F (Section F-1).

Test ID	Solution volume (mL)		3 M HNO_3 recovery (%)		0.05 M HNO_3 recovery (%)	
	3 M HNO_3	0.05 M HNO_3	^{233}Pa	^{237}Np	^{233}Pa	^{237}Np
Test 3	25	10	75±2	<2	22±2	47±4
Test 4	35	20	95±2	<2	6±2	95±3
Test 5[a]	50	25	99±1	<1	1.8±0.3	100±3
Test 6[a]	50	25	100±2	<1	2.2±0.3	99±3

[a] Activity of ^{237}Np was increased to ~60 Bq to improve the precision on the ^{237}Np measurement compared to ~20 Bq in Tests 1–4.

An improved recovery of ^{233}Pa, approaching 100%, was achieved by increasing the volume to 50 mL 3 M HNO_3 (Tests 5–6). Recovery of ^{237}Np was only 47% in Test 3 and this was attributed to the increased volume of the 3 M HNO_3 rinse which may have strengthened the binding of ^{237}Np to the TEVA® resin. Increasing the volume of the 0.05 M HNO_3 solution from 10 to 25 mL improved recovery of ^{237}Np leading to ~100% recovery of ^{237}Np. Elution was gravity fed for Tests 3–5, with flow rates of 0.4–1 mL min^{-1} throughout each test. The highest flow rates occurring when the reservoir was loaded with 15–20 mL of rinse solution. An Eichrom® vacuum box (Appendix F, Section F-4.1, Figure F-1) was acquired for use with Test 6 to achieve a constant flow rate of 1 mL min^{-1} as recommended[20] (Eichrom Technologies Inc., 2006). Results showed that flow rate had a negligible impact on the elution profiles and the high recoveries obtained for ^{233}Pa and ^{237}Np (Figure 3-3).

The relationship between the cumulative percentage of ^{233}Pa eluted and the volume of 3 M HNO_3 rinse used showed a distinct sigmoidal distribution. A logistic function was fit to the distribution using SIGMAPLOT® 14 data analysis software to model the relationship between the ^{233}Pa recovery and volume of 3 M HNO_3 solution.

[20] Flow rate can influence the elution behaviour through modifying the interaction time between the mobile and stationary phases.

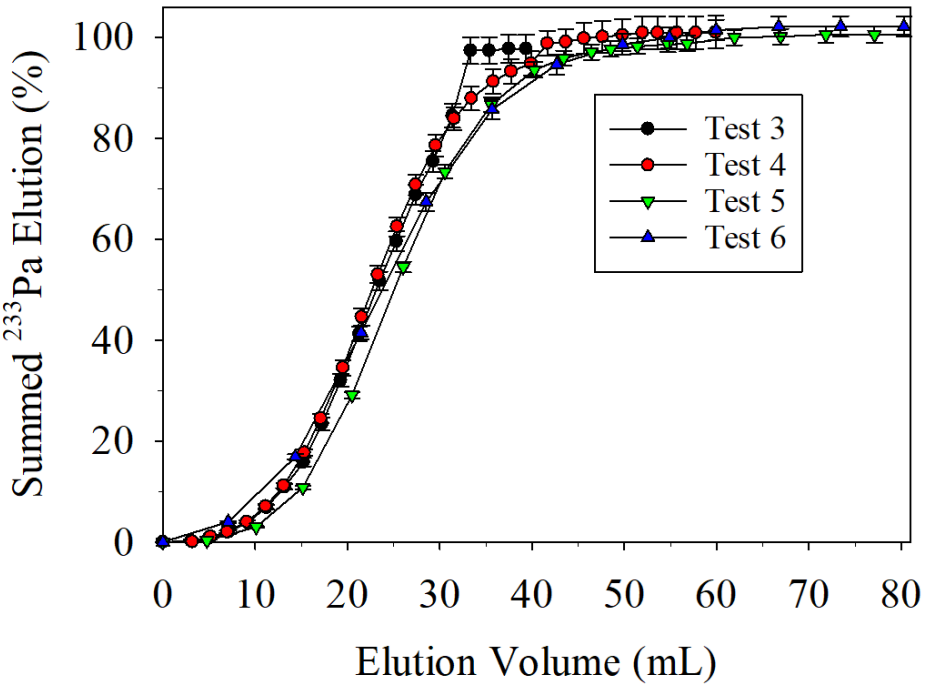

Figure 3-3 Cumulative elution profiles for tests 3–6.

Despite the slightly poorer fit, only results from Test 3 were used to fit the function as lower volume aliquots of 3 M HNO_3 were collected, providing a better resolution for curve fitting. The logistic function fitted is shown in Equation 3-1.

Equation 3-1 Logistic function used to model the relationship between ^{233}Pa eluted (%) and volume of eluant (3 M HNO_3; mL).

$$f(x) = \frac{L}{1 + e^{-k(x - x_0)}}$$

Where:

$f(x)$ = Cumulative ^{233}Pa eluted (%)

L = Maximum ^{233}Pa that can be eluted, or 98.4% with the fitted model

x = Volume of 3 M HNO_3 eluant passed through the column (mL)

x_0 = 22.2 (the function mid-point; mL)

k = 0.201

The fitted function yields an expected recovery of 98.0% from an elution volume of 50 mL 3 M HNO_3. This suggests that further increasing the 3 M HNO_3 elution volume will have a negligible impact on the ^{233}Pa recovery and that there is likely some interaction between Pa and the functional groups in the stationary phase of the TEVA® resin.

The optimised procedure used for preparing the ANU ^{237}Np cow (in Section 3.4) consequently was (complete method details are in Appendix F, Section F-1):

- Taking a known mass of a calibrated ^{237}Np tracer solution in secular equilibrium with ^{233}Pa, add the following reagents to reduce Np(V) to Np(IV) (Note this combined solution is referred to as the 'load solution').
    - 0.5 mL of 1.5 M Sulphamic acid, swirl to mix.
    - 1.25 mL of 1.5 M ascorbic acid, swirl to mix then wait for 3 minutes before proceeding to the next step.
    - 0.1 mL of 5 mg mL^{-1} Fe solution.
- Add 8 M HNO_3 to bring the load solution concentration to 3 M HNO_3. Allow the prepared solution to rest for 30 minutes prior to adding to the resin.
- Precondition the TEVA® resin (100–150 μm) with 10 mL of 3 M HNO_3 then add the load solution.
- Elute ^{233}Pa, by rinsing the resin with 50 mL 3 M HNO_3.
- To recover ^{237}Np after completion of the present work, if necessary, it could be achieved by rinsing the resin with 25 mL 0.05 M HNO_3.

In all six of the tests described above, a light brown colour was observed in the initial eluant fraction (the first ~5 mL containing ^{233}Pa), becoming darker over several days and forming a thin film on the walls of the bottles. The colouration was consistent with the initial presence of ascorbic acid and slow oxidation with nitrous acid. Hence, the carbon content (total, organic and inorganic carbon) in the eluant from Test 3, containing ^{233}Pa, was measured. This was done with a Non-Dispersive Infra-Red detector (Shimadzu TOC-V CSH) on the first five bottles from Test 3 (Figure 3-4). These five bottles contained the first 11.2 mL of eluant, made up of the load solution and a portion of the 3 M HNO_3 rinse. The elution of organic carbon (as a measure for ascorbic acid) was rapid, reducing to effectively zero in the fourth and fifth eluant bottles. This is consistent with the ascorbic acid not being bound and passing through the column with the load solution. Total carbon, though it decreased more slowly, dropped sharply after the third bottle (7.7 mL), however, it did not reach zero, with concentrations of 5.1 and 6.4 mg L^{-1} measured in bottles 4 and 5. The total mass of carbon added in the ascorbic solution was 135 mg and the summed total mass of organic carbon measured in the five eluant bottles was 137 mg. This, combined with the darkening of the solution indicative of slow oxidation of

dissolved ascorbic acid, suggests that the organic carbon is a measure of the elution of ascorbic acid, whereas the inorganic carbon is likely to be coming from another source (e.g., as a minor contaminant in the reagents or from dissolved atmospheric CO_2 in the reagent water).

The formation of the thin film on the walls of the ^{233}Pa solution containers was of concern as it had the potential to adsorb Pa or incorporate Pa from the solution during formation, leading to instability of the ^{233}Pa tracer solutions needed for this thesis. This problem was addressed by use of 30% H_2O_2 to treat ^{233}Pa solutions, which is effective at decomposition of ascorbic acid in solution and assisted in stabilising ^{233}Pa tracer solutions (see Section 3.3.1.3 for further details).

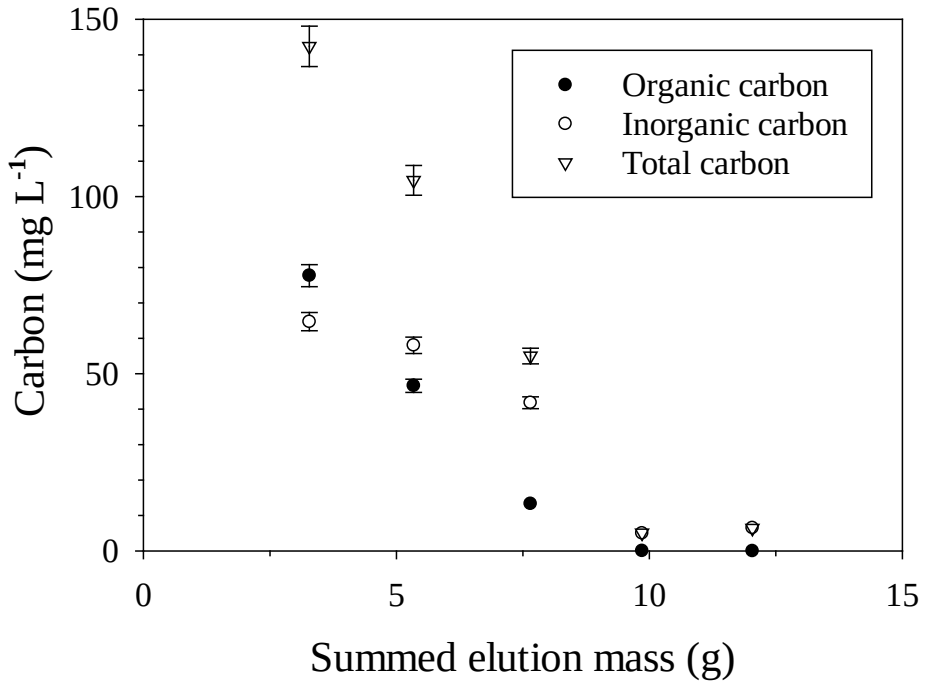

Figure 3-4 Organic carbon, Inorganic carbon and Total carbon measured in Test 3, eluant bottles 1–5 (first 11.2 mL of extraction solution). Where not indicated the uncertainty is smaller than the size of the plotted symbol.

3.3.1.2 ^{237}Np prototype cow preparation and assessment

The next two tests (Tests A and B) were conducted on two separate TEVA® resin columns and were aimed at finding the most reliable method for producing a ^{233}Pa tracer solution:

Test A: Separate Pa and Np using TEVA® resin (method in Appendix F, Section F-1, omitting step 11 where the first few mL of eluant is loaded back onto the column). Pa was eluted in 3 M HNO_3 then Np was eluted in 0.05 M HNO_3, which was evaporated to dryness, then taken up in 1 mL 4 M HNO_3 to maintain Pa in solution for storage. After ingrowth of Pa separation

of Np and Pa was repeated with a new TEVA® resin column[21]. This test assessed extraction and reuse of the ^{237}Np solution.

Test B: Separate Pa from Np using TEVA® resin (method in Appendix F, Section F-1, extracting only Pa and omitting step 11 as above). Np was not eluted but was retained on the TEVA® resin column (the '^{237}Np prototype cow'). Pa was eluted ('milked') again after ingrowth. This test assessed stability of a ^{237}Np cow for repeated extraction of ^{233}Pa.

Results for two separations conducted for Test A and four separations conducted for Test B are shown in Table 3-3.

Table 3-3 The recovery of ^{233}Pa and ^{237}Np eluted in the 50 mL 3 M HNO_3 and 25 mL 0.05 M HNO_3 eluant fractions for Test A (Elutions 1–2) and recovery of ^{233}Pa in 50 mL 3 M HNO_3 only for Test B (Elutions 1–4).

Test ID	Elution ID	Days since first separation	3 M HNO_3		0.05 M HNO_3	
			Recovery[a] of ^{233}Pa (%)	Recovery of ^{237}Np (%)	Recovery[a] of ^{233}Pa (%)	Recovery of ^{237}Np (%)
A	1[b]	N/A	100±5	0.3±0.2	2.0±0.3	100±5
	2	42	53±3	5.5±0.5	1.5±0.2	84±4
B	1[b]	N/A	100±4	0.5±0.3		
	2	42	85±5	1.4±0.6		
	3	161	77±4	3.9±0.8		
	4	251	65±4	<0.6		

[a] As secular equilibrium between ^{233}Pa and ^{237}Np were not reached by the time the second through fourth elutions were performed, and losses of ^{237}Np occurred, corrections for equilibrium conditions and losses of ^{237}Np have been accounted for in the recovery values.
[b] To make it easier to control flow rates for concurrent tests, an Eichrom® vacuum box (Appendix F, Section F-4.1 Figure F-1) was used to control flow rates for Elution 1. Subsequent elutions were conducted individually, and gravity flow was used.

Excellent recovery of ^{233}Pa was achieved from Elution 1 in both tests (Table 3-3). However, the ^{233}Pa recovery was poor for Elution 2 from Test A (53±3%). This highlights the potential for substantial losses of ^{237}Np through repetition of this method and suggests extraction and

[21] A third test (Test C) was also undertaken to evaluate the reuse of the same TEVA® column for subsequent extractions (to limit overall waste generation, including potentially radioactively contaminated waste columns). However, a leak in the TEVA® column prevented reuse. The ^{233}Pa solution prepared from Test B was also used later in Section 3.3.1.3 to demonstrate effective stabilisation of ^{233}Pa solutions by treating with 30% H_2O_2.

reuse of the ^{237}Np solution with the method developed is not an optimal approach. A low activity of ^{233}Pa (1.5–2% relative to the ^{237}Np activity loaded) was observed in the ^{237}Np (0.05 M HNO_3) fraction (Table 3-3). However, this is within the range expected from ingrowth of ^{233}Pa between separation from ^{237}Np and HRGS measurement.

The repeated extraction of ^{233}Pa from ^{237}Np retained on the TEVA® resin column for Test B showed a reduction in the chemical recovery of ^{233}Pa with each successive elution of ^{233}Pa. This was a potential concern for longer-term use of a more active ^{237}Np cow prepared for sample analysis. However, analysis of the ^{233}Pa chemical recovery from the more active cow prepared (the ANU ^{237}Np cow) showed that recovery stabilised (at 53±7%, see full details in Section 3.4, Table 3-5).

There was low breakthrough of ^{237}Np in the ^{233}Pa solution (3 M HNO_3) in Elution 1 for each test with 0.3–0.5% of the ^{237}Np loaded measured in this fraction and a substantial increase in the ^{237}Np breakthrough was observed in Test A, Elution 2. The cause of this increased breakthrough is unknown.

Elution profiles were collected for Test B, Elutions 2–4 for ^{237}Np and are shown in Figure 3-5. Increased breakthrough of ^{237}Np was noted for Test B, Elutions 2 and 3, with ^{237}Np eluted in the very first few mL of eluant (Figure 3-5).

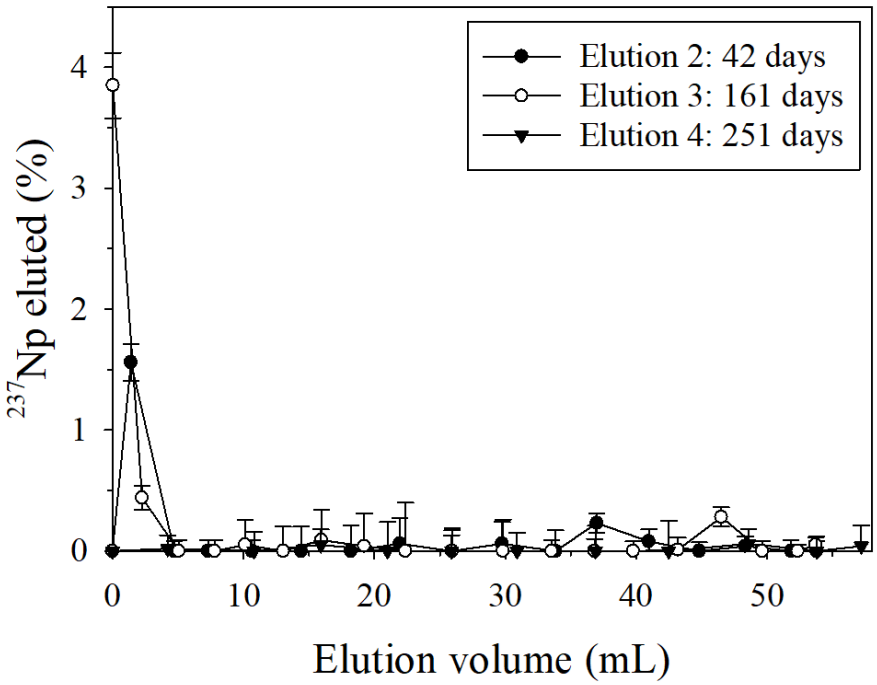

Figure 3-5 Elution profile in 3 M HNO_3 for ^{237}Np from Test C, Elutions 2–4, conducted 42, 161 and 251 days after Elution 1 respectively. Values are relative to the calculated amount of ^{237}Np remaining on the columns after correction for losses of ^{237}Np.

The breakthrough of Np was considered to be attributable to Np that was no longer retained on the column as Np(IV), potentially caused by:

- Leaching of ^{237}Np into the 3 M HNO_3 solution in which the resin bed is stored, or
- Incomplete reduction of ^{237}Np retained on the column at the 'front' of the loading solution passing through the column.

To assess the first potential cause, for Elution 4 of Test B, the first ~7.5 mL of eluant[22] was collected and loaded back onto the column to reduce breakthrough of ^{237}Np. This approach was considered successful as the breakthrough of ^{237}Np for Test B, Elution 4 was <MDL (Table 3-3). As such, this step was incorporated into the method for milking the ANU ^{237}Np cow (see Appendix F, Section F-1 and Section 3.4).

Elution profiles were also collected for ^{233}Pa for Test B, Elutions 2–4 are shown in Figure 3-6. These elution profiles showed consistent extraction behaviour of ^{233}Pa with repeated 'milking' and demonstrated the stability of the ^{237}Np prototype cow over time in the relatively strong acid solution (3 M HNO_3) in which it was stored.

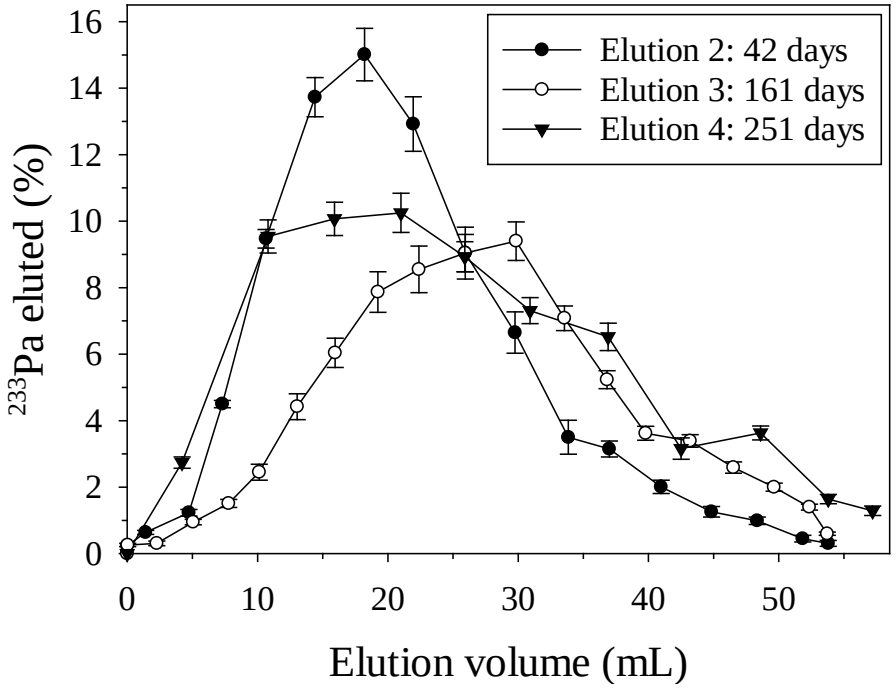

Figure 3-6 Elution profile from Test B, Elutions 2–4, conducted 42, 161 and 251 days after Elution 1 respectively. These values are relative to the calculated amount of ^{233}Pa on the columns based on ingrowth since the last extraction and corrected for losses of ^{237}Np from prior extractions.

[22] This is equivalent to approximately four column volumes (i.e., the interstitial space in the resin bed) plus the 2 mL.

3.3.1.3 Stability of ^{233}Pa extracted solutions

For Tests A and B above (and Test C referred to in footnote 21), the ^{233}Pa solutions from Elution 1 were stored for several weeks prior to treatment with 30% H_2O_2 to assess the stability of the solution. As in the previous tests, discolouration on the walls of the bottles containing the ^{233}Pa eluant was observed in all Elution 1 solutions from Tests A–C.

The stability of these solutions was assessed by sub-sampling and HRGS measurements over several weeks to observe changes in ^{233}Pa remaining in solution, with losses observed (Table 3-4). A sub-sample of the solution from Test A was filtered and indicated losses of ^{233}Pa with particulates filtered from the solution.

Table 3-4 Stability of ^{233}Pa eluant solutions from Tests A–C.

Test ID	Days since solution collection	^{233}Pa recovery (%)		Sample treatment
		Unfiltered	Filtered[a]	
Test A	0	100±5		
Test A	14	76±3		
Test A	29	48±5		
Test A	30	49±3	37±2	
Test A	32	100±2	98±2	30% H_2O_2
Test B	0	100±4		
Test B	9	66±4		
Test B	29	80±7		
Test B	37	100±4		30% H_2O_2
Test C	0	100±5		
Test C	29	46±8		
Test C	37	98±3		30% H_2O_2

[a] Filtered with a 0.45 µm PVDF disposable syringe filter.

Two potential explanations for the loss of ^{233}Pa from solution were investigated. These were:

- The tendency of Pa to hydrolyse may have led to the formation of insoluble polymers which formed a suspension or precipitated from solution, and

- The presence of ascorbic acid may have led to the formation of carbon in suspension, creating a thin film of carbon on container walls which adsorbed Pa.

Although the formation of insoluble polymers of hydrated Pa oxides (Myasoedov et al., 2011) has proved exceedingly challenging to reverse, the breakdown of ascorbic acid can be achieved with a strong enough oxidiser. To this end, 3 mL of 30% H_2O_2 was added to each solution (after 32 and 37 days, respectively) followed by heating overnight at 90°C. Removal of the colour in the solution was observed and subsequent HRGS measurement of a sub-sample showed ^{233}Pa was returned into the solution. This suggests carbon had been effectively removed from suspension. A sub-sample of the solution from Test A was filtered after treatment with H_2O_2 and showed no loss of ^{233}Pa (Table 3-4).

3.3.1.4 Semi-quantitative estimate of the distribution of ^{237}Np on the TEVA® resin

Before and after Elution 3 for Test B, a semi-quantitative estimate of the distribution of ^{237}Np on the TEVA® resin column was performed (see Appendix H for HRGS procedure used). Results are shown in Figure 3-7.

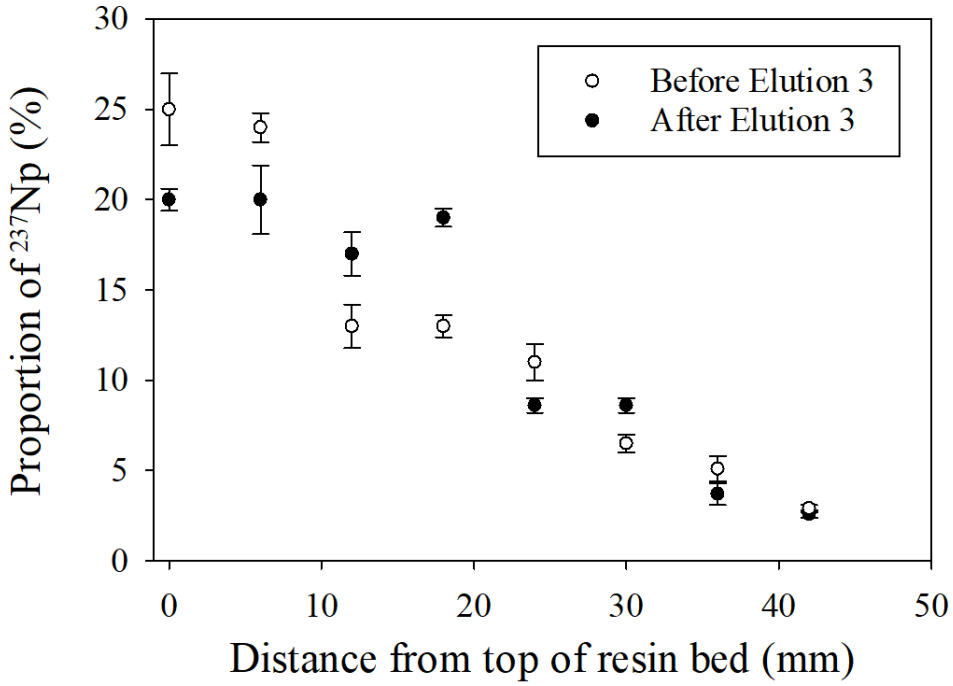

Figure 3-7 Test B: Distribution of ^{237}Np on the TEVA® resin column before and after Elution 3. Measurement uncertainty is from counting statistics only.

The distribution showed that 40–50% of the ^{237}Np was retained in the upper 5 mm of the column, with the majority in the top 20 mm, though some ^{237}Np did travel further down the column during Elution 3. This indicated a potential problem for repeated extraction of ^{233}Pa, however, the strong retention in the top 20 mm after four elutions indicated a ^{237}Np cow

produced in the same manner would likely remain sufficiently stable for the required production of ^{233}Pa tracer solutions for this thesis.

Section 3.4 Preparation of the ANU ^{237}Np cow

The ^{237}Np cow used throughout the present work for optimisation of the AMS measurement process and analysis of samples, was prepared from 19.2 mg of NpO_2 at ANU (referred to as the 'ANU ^{237}Np cow'). Preparation of the ANU ^{237}Np cow involved converting the NpO_2 powder to a $Np(NO_3)_4$ solution which was then loaded onto a TEVA® resin column under reducing conditions (see Appendix F, Section F-1). Separation of ^{233}Pa was done by eluting with 50 mL of 3 M HNO_3.

The solubility of NpO_2 in aqueous solution depends on whether it was formed through ignition or precipitation (Lieser et al., 1985). For ignition methods, the temperature of formation (Burney and Harbour, 1974; Xu et al., 2013) also influences solubility, with temperatures above 500–600°C being more resistant to chemical dissolution. The mode of production was unknown for the NpO_2 used for this study. Prior to the preparation of the ANU ^{237}Np cow, some experimental work was required to find an appropriate method to dissolve NpO_2 as research on dissolution of NpO_2 has seen limited attention (Xu et al., 2013).

Several methods for dissolution of NpO_2 have been described, with strong HNO_3 solutions (>8 M) generally suitable, with catalysts including fluoride and Hg sometimes necessary (e.g., Burney and Harbour, 1974; Kyser, 2009; Xu et al., 2013). The USEPA (2024) suggests NpO_2 is soluble in concentrated HCl, $HClO_4$ and HNO_3. Where HF is used as a catalyst in HNO_3 solution, F^- is a stronger ligand than NO_3^- which may lead to formation of Np fluorides (Xu et al., 2013).

Reports on individual methods tend to contain insufficient detail to reproduce successful dissolution. Hence, to dissolve the NpO_2 and convert to a $Np(NO_3)_4$ solution, a stepwise approach was undertaken, starting with the simplest and most direct method progressing to more complex methods. This started by weighing 19.2 mg of NpO_2 powder into a 50 mL HDPE centrifuge tube (equivalent to 440 kBq ^{237}Np).

First, dissolution of the NpO_2 in concentrated HNO_3 was attempted (the desired acid type for loading onto the TEVA® resin column). This was followed by an attempt to dissolve the NpO_2 in concentrated HCl, both approaches were unsuccessful. As such, although it was an intention of this thesis to avoid the use of HF, it was considered necessary at this stage and, finally, dissolution of the NpO_2 in concentrated HF was successfully undertaken. The Np fluoride

formed was dried and treated with concentrated HNO_3 to convert to a nitrate. This was again evaporated and taken up as $Np(NO_3)_4$ in 3 M HNO_3.

To create the ANU ^{237}Np cow, the 3 M HNO_3 solution of ^{237}Np was prepared as a reducing solution (Reducing solution 1 from Table 3-1, method as described in Section 3.3.1.1 and Appendix F, Section F-1). The solution was loaded onto TEVA® resin with the grey colour on the resin bed remaining after loading consistent with the position of ^{237}Np determined on the TEVA® resin column from method development (see Appendix H, Section H-2). A further 50 mL of 3 M HNO_3 was used to elute ^{233}Pa with the eluate collected in two containers[23]. The first 5–6 mL comprised the load solution and the first 1 mL of 3 M HNO_3 (Container 1), and the second the remainder of the 50 mL 3 M HNO_3 (Container 2). The ^{233}Pa solutions in Containers 1 and 2 were treated with 1 mL of 30% H_2O_2 and heated to break down ascorbic acid as per method in Appendix F, Section F-1.

The completeness of NpO_2 dissolution in the load solution was assessed by HRGS measurement of the centrifuge tube (in which the NpO_2 was dissolved and the load solution subsequently prepared) after a scan with a dosimeter indicated ~10% of the original activity remained in the centrifuge tube. The HRGS measurement confirmed that the activity was due to the presence of ^{233}Pa and no ^{237}Np peaks could be identified. A typical $^{237}Np/^{233}Pa$ HRGS spectrum is shown in Figure 3-8, with the HRGS spectrum from counting the centrifuge tube shown in Figure 3-9.

Subsequent HRGS measurement of the eluant was undertaken to determine recovery of ^{233}Pa and breakthrough of ^{237}Np. Chemical separation of ^{233}U was also performed followed by measurement using alpha spectrometry to determine potential interference during AMS measurement, further detail is given in Section 3.5.3 below. The ANU ^{237}Np cow was sealed in a plastic bag and stored in a bottle for later use.

The presence of ^{241}Am as a contaminant radionuclide was identified in the HRGS measurement of the ^{233}Pa solution (via the presence of the 59.5 keV gamma ray). The first AMS measurements of the solution prepared from milking the ANU ^{237}Np cow also showed a substantially higher than expected concentration of ^{233}U. The ANU ^{237}Np cow was milked nine times, the elution behaviour of ^{233}Pa and ^{237}Np is summarised in Table 3-5. The method used for milking the ANU ^{237}Np cow is given in Appendix F, Section F-1, aspects of these extractions

[23] The purpose of this was to collect a small amount of relatively pure ^{237}Np for a separate unrelated project.

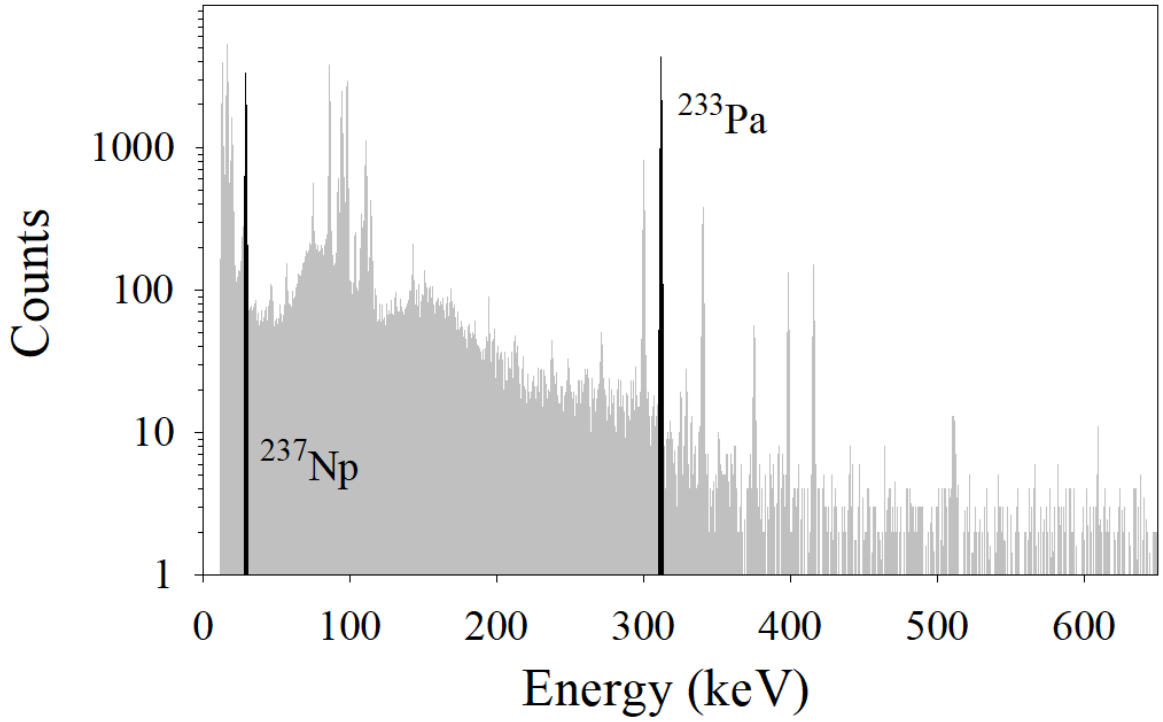

Figure 3-8 Typical HRGS spectrum of ^{237}Np and ^{233}Pa in secular equilibrium. The gamma emissions used for activity determination throughout this thesis are highlighted (29.4 keV for ^{237}Np and 311.9 keV for ^{233}Pa).

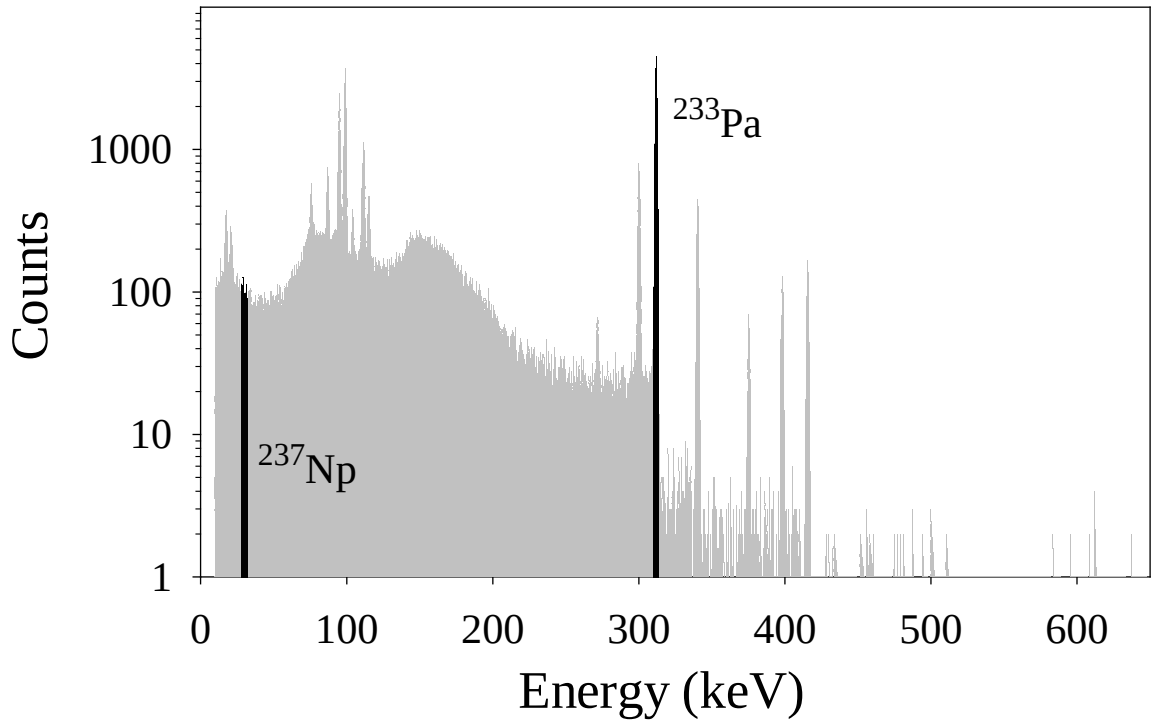

Figure 3-9 HRGS spectrum from counting the centrifuge tube after loading dissolved NpO_2 onto the ANU ^{237}Np cow. Note there is no observable peak of ^{237}Np.

regarding contaminants, including ^{237}Np and ^{233}U in ^{233}Pa tracer solutions are discussed below in Section 3.5.The chemical recovery of ^{233}Pa in successively milked solutions from the ANU ^{237}Np cow were generally consistent with the behaviour of the ^{237}Np prototype cow results (Section 3.3.1.2), with recovery initially high and stabilising after several extractions. There was one exception, with 11±1% recovery of ^{233}Pa where the solution was milked only eight days after the previous elution. The stability of the ANU ^{237}Np cow over a period of at least four years indicates this is an effective method for producing ^{233}Pa tracer solutions for measurement of ^{231}Pa.

Section 3.5 ANU ^{237}Np cow assessment regarding radionuclide contamination

Several contaminants were identified in extracts from the ANU ^{237}Np cow through alpha spectrometry, AMS and gamma spectrometry measurements. Further purification of the solution was required to remove these contaminants to make the ^{233}Pa solution suitable for use as a tracer for ^{231}Pa analysis with AMS. The provenance of the NpO_2 source material, including the preparation date and source material was unknown and there was no initial information regarding the source of contaminants.

3.5.1 ^{241}Am contamination

The presence of ^{241}Am was noted in the original NpO_2 container when counted via gamma spectrometry at ANU, and the presence of other radioactive isotopes with low gamma emission intensities was possible though none were identified. Quantification of the ^{241}Am contamination in solutions milked from the ANU ^{237}Np cow was done using HRGS. The ^{241}Am was detected in the eluant fractions from the first milking of the ANU ^{237}Np cow in both the first 5–6 mL of eluant and the remaining eluant making up the ^{233}Pa fraction (Containers 1 and 2 from Section 3.4 respectively).

In the first 5–6 mL, 2.4±0.2 kBq of ^{241}Am was measured, with a total activity of 2.7±0.4 kBq in containers 1 and 2 eluted with the first milking of the ANU ^{237}Np cow. The capacity factor of ^{241}Am is only ~0.4 in 3 M HNO_3 on the TEVA® resin (Horwitz et al., 1995) which indicated the majority of ^{241}Am should have been removed in this first milking. This was confirmed with only 1.2±0.7 Bq measured in the next milking 263 days after preparation (Table 3-5), a three order of magnitude reduction, and ^{241}Am was below the limit of detection in subsequent extractions.

Table 3-5 Behaviour of ^{237}Np, ^{233}Pa and ^{233}U with repeated extractions from the ANU ^{237}Np cow.

Days since ^{237}Np cow preparation	Initial activity (kBq)[a]: ^{237}Np | ^{233}Pa	^{237}Np Breakthrough (kBq)	^{233}Pa Extracted (kBq)	^{233}Pa recovery (%)	^{233}U activity in ^{233}Pa solution (Bq): Measured[b]	Estimated[c]	Purpose of extraction
–	440±2 | 440±2	0.36±0.03	356±5	81±1	74±21	102±1	ANU ^{237}Np cow preparation
263	440±2 | 440±2	0.34±0.01	282±14	64±3		1.42±0.01	ANU ^{237}Np cow milking test
272	440±2 | 216±3	0.15±0.01	23±1	11±1		0.224±0.002	ANU ^{237}Np cow milking test
431	439±2 | 435±1	0.2±0.01	228±10	52±2	3.3±1.3	0.924±0.004	Excess ^{233}U measurement; UTEVA® and TK400® resins Pa separation tests
774	439±2 | 439±2	0.85±0.04	207±9	47±2	1.68±0.05	1.89±0.01	Separation of Pa with TK400® resin
858	438±2 | 415±1	0.4±0.02	214±13	52±3	0.18±0.02	0.56±0.01	Sample measurements
1367	438±2 | 438±2	0.54±0.04	297±12	68±3	1.3±0.7	2.75±0.01	Sample measurements
1501	437±2 | 428±1	0.005±0.002	223±9	52±2	N/A	0.77±0.01	Sample measurements
1962	437±2 | 437±2	3.6±0.1	216±37[d]	49±8	5.4±0.6	2.5±0.01	Sample measurements

[a] Measurement uncertainty for initial activity of ^{237}Np is based on the balance range limit used for weighing and assuming a uniform distribution. Other contributions to measurement uncertainty are considered negligible and the material weighed was assumed to be pure NpO_2.

[b] The ^{233}U results are not available for ^{233}Pa solutions prepared 263, 272 (not measured) and 1501 (measurement failed owing to low recovery) days after ^{237}Np cow preparation.

[c] Based on the recorded date for the receipt from the manufacturer of the NpO_2 being 1964, ^{233}U activity was estimated from 1 July 1964 (a uniform distribution was assumed with an uncertainty of ±6 months). Estimated ^{233}U activity is determined from ingrowth between extractions and assumes that all ^{233}U activity is removed with each extraction.

[d] The chemical recovery of ^{233}Pa solution prepared 1962 days after ^{237}Np cow preparation initially showed an activity of 130±5 kBq, however, subsequent measurement of the solution after purification showed a substantially higher activity. The initial low value may reflect a temporary change to the set-up of the HRGS system (placement of a cap on the detector head), however, the exact reason could not be confirmed. The value presented here is an estimate based on the average chemical recovery of the purified solutions from the three prior ^{233}Pa extractions.

3.5.2 ^{237}Np contamination

The ^{237}Np activity in ^{233}Pa solutions milked from the ANU ^{237}Np cow was determined from HRGS measurement (Appendix H). It is noteworthy that of the 0.36±0.03 kBq of ^{237}Np eluted when the ANU ^{237}Np cow was first milked (Table 3-5), the majority (0.35±0.03 kBq) was in the first 5–6 mL (Container 1 in Section 3.4) which, in this instance was not reloaded onto the ANU ^{237}Np cow. A much smaller fraction was in the subsequent 50 mL of 3 M HNO_3 (Container 2 in Section 3.4, with 6.2±0.3 mBq). There was some variability in the range of ^{237}Np activities in the ^{233}Pa solutions with subsequent milking of the ANU ^{237}Np cow (0.15–0.85 kBq, Table 3-5), where the process of collecting and reloading the first ~7 mL of eluant was used to reduce breakthrough of ^{237}Np (as shown for the ^{237}Np prototype cow in Section 3.3.1.2). These results suggest that the reloaded solution was still the source of most of the ^{237}Np eluted in the ^{233}Pa fraction. Variability in ^{237}Np breakthrough increased with the final two times the ANU ^{237}Np cow was milked, when a low activity was recorded (5.1±2.2 Bq) followed by a much higher value in the final extraction (3.6±0.1 kBq). The high value was almost 2,000 days after the initial preparation of the ANU ^{237}Np cow and may reflect a degradation of the TEVA® resin after a long storage period in a strong acid with a relatively high alpha and beta activity present. Consequently, the integrity of the ^{237}Np cow should be assessed if it is to be used following the completion of this thesis.

3.5.3 ^{233}U and other alpha emitting contaminants in the ^{233}Pa solution following preparation of the ANU ^{237}Np cow

The ^{233}Pa solution obtained from milking of the ANU ^{237}Np cow the first time was used directly after elution for testing of the AMS system for Pa measurement (see Section 3.11.1). In this initial testing, a much higher ion count rate than expected was observed in the 233 mass-region. This was attributed to a high concentration of ^{233}U in the ^{233}Pa extract. The information available for the NpO_2 source (written on the outer container) indicated a preparation date no later than 1964. Assuming 53 years between the ANU ^{237}Np cow preparation in 2017 and manufacture of the NpO_2 in 1964, approximately 7.4×10^{14} ^{233}U atoms (102 Bq; Table 3-5) would have been present when the ANU ^{237}Np cow was prepared. This was more than two orders of magnitude higher than the estimated 1.5×10^{12} atoms of ^{233}Pa and required further investigation to assess the effectiveness of separation of Pa from U prior to further AMS measurements.

Gamma emission probabilities from decay of ^{233}U are low (Nichols et al., 2008), the highest being 0.018% at 54.7 keV. This made HRGS unsuitable for the ^{233}U determination in solutions

milked from the ANU ^{237}Np cow. Accordingly alpha spectrometry was used to assess ^{233}U activity concentrations. Measurement of ^{233}U was further complicated by the known breakthrough of ^{237}Np as the dominant alpha decay energies are 4.78–4.82 MeV for ^{233}U and 4.77–4.79 MeV for ^{237}Np (Appendix D) which cannot be resolved in a typical alpha spectrum.

An initial attempt to separate ^{233}U was undertaken using the AG1-X8 anion exchange step for U separation from Martin and Hancock (2004) followed by electrodeposition for U. Although ^{237}Np was not fully separated it was evident that additional alpha-emitting isotopes were present that had not been identified using HRGS. The most probable contaminant isotope(s) were thought to be either one or a combination of ^{239}Pu and ^{240}Pu given the alpha emission energies (these two isotopes have alpha energies that cannot be easily resolved).

A review of the method on which separation of ^{233}Pa from ^{237}Np was based (Eichrom Technologies Inc., 2006) indicated that the method should be effective for separation of both Np and U from Pa. Evaluation of U separation with TEVA® resin using the method developed for Np/Pa separation (Appendix F, Section F-1) was tested using a $UO_2(NO_3)_2$ solution. The concentration of U in the aliquot tested gave an approximately equivalent loading (~20 mg) to the NpO_2 used to prepare the ANU ^{237}Np cow, and thus allowed assessment of U separation under similar load conditions[24] to the ANU ^{237}Np cow. As expected, U was not strongly bound and was quickly eluted from the TEVA® resin with 3 M HNO_3, with 100±4% eluted with the full elution volume (^{233}Pa and ^{235}U measured with HRGS). The elution profile is shown in Figure 3-10, with a typical elution profile of Pa under the same conditions overlayed for comparison.

Initial studies by Horwitz et al. (1995) indicated a capacity factor of approximately three for U(VI) on TEVA® with 3 M HNO_3, and ~0.6 with 0.05 M HNO_3. As such, after the initial 50 mL of 3 M HNO_3 used to elute U (Pa in the Np/Pa separation), 25 mL of 0.05 M HNO_3 was used to elute any U remaining on the column (i.e., the full developed method was used, including the rinse step normally used for elution of ^{237}Np). A ^{232}U tracer was added to the 0.05 M HNO_3 fraction which was evaporated and deposited for U analysis via alpha spectrometry using the electrodeposition method from Martin and Hancock (2004).

[24] 20 mg is a relatively large mass for the volume of resin and therefore had the potential to saturate the column and reduce the effectiveness of separation.

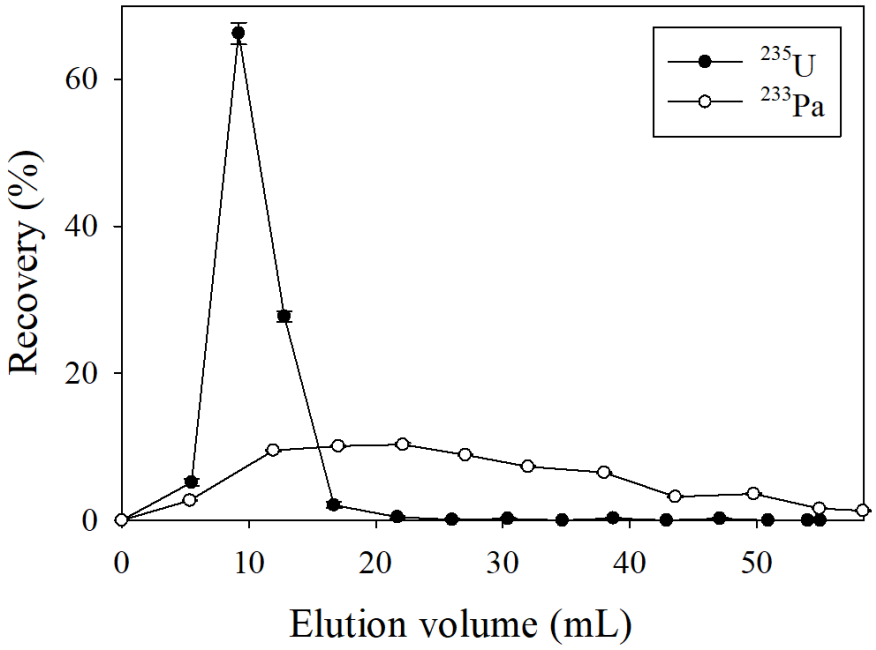

Figure 3-10 Elution profile of U on TEVA® using the Np/Pa separation method. Elution volume includes initial column volume, load solution and 50 mL 3 M HNO_3 rinse.

The use of 25 mL of 0.05 M HNO_3 was intended to provide an indication of the likely amount of ^{233}U that will be eluted when ^{237}Np is recovered from the ANU ^{237}Np cow after completion of this thesis. Although almost all U was eluted in the 3 M HNO_3 eluant, 0.67±0.04% was still eluted in the second step with the 25 mL 0.05 M HNO_3. This suggests strong elution of U in 0.05 M HNO_3 and that when ^{237}Np is recovered from the ANU ^{237}Np cow during decommissioning, all U present is likely to be recovered with ^{237}Np unless removed by initial elution with 3 M HNO_3.

The full method developed for separation of ^{233}Pa and ^{237}Np (see Appendix F, Section F-1) was used to remove U from an aliquot of the ^{233}Pa fraction (Container 2) of the milked solution after the addition of a ^{232}U tracer. The electrodeposition technique from Martin and Hancock (2004) was used to prepare an alpha source for alpha spectrometry from the 3 M HNO_3 fraction. The alpha spectrum from the analysis of the 3 M HNO_3 fraction is shown in Figure 3-11.

It is unlikely there is any significant contribution from ^{237}Np to the peak associated with ^{233}U decay based on the effectiveness of Np retention on TEVA® resin. The presence of Pu isotopes in the milked solution was confirmed from the peak in the alpha spectrum attributable to ^{239}Pu and/or ^{240}Pu decay, however there was no clear evidence for other Pu isotopes. The alpha particle energies of ^{241}Am and ^{238}Pu are difficult to resolve, however, the measurable presence of ^{241}Am in the NpO_2 and in both fractions of the milked solution indicate ^{241}Am decay was the main source of this peak. Plutonium-241 is a beta emitter, and alpha peaks associated with ^{242}Pu

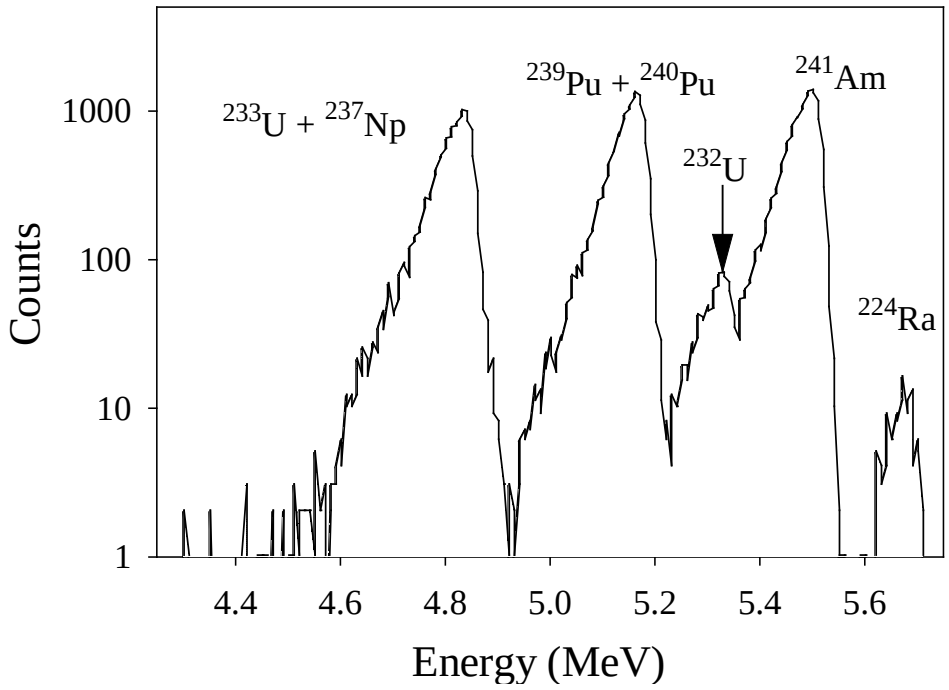

Figure 3-11 Alpha spectrum from TEVA® separation of ^{233}Pa fraction of milking solution (Log scale). Labels correspond to the parent isotopes responsible for each peak.

decay were not visible in the alpha spectrum. Pu has oxidation states ranging from +2 to +7, and the method used to separate ^{237}Np and ^{233}Pa (Eichrom Technologies Inc., 2006) notes that the addition of ascorbic acid will reduce Pu(IV) and Pu(VI) to Pu(III) and that the addition of $NaNO_2$ is required to fix the oxidation state at Pu(IV). The modified method used omitted the $NaNO_2$ and therefore it is expected that the Pu will remain in the Pu(III) state. However, work by Kim et al. (2004) suggests that some Pu may be retained in the +4 state (and therefore in the resin) with addition of ascorbic acid and with subsequent rinsing of the TEVA® resin with 3 M HNO_3. As there was no Pu tracer added, quantification of the activity of Pu present in the solution from milking the ANU ^{237}Np cow was not possible. However, no discernible peaks in the ^{239}Pu and ^{240}Pu region were observed when analysing ^{233}U in subsequent extractions from the ANU ^{237}Np cow using alpha spectrometry (see Figure 3-12).

The alpha peak associated with decay of the ^{232}U tracer used was difficult to resolve from the large peaks from Am and Pu isotopes in the alpha spectrum, however, a peak tailing correction was made to estimate counts attributable to ^{232}U decay in the spectrum shown in Figure 3-11. This was done by setting ROIs in the ^{239}Pu and ^{240}Pu region (where no significant contribution from other isotopes known to be present were expected) that were equivalent (i.e., the same width) to a ROI set for ^{232}U and the main body of the peak due to ^{241}Am. A peak tailing of 0.18±0.08% for contribution of ^{241}Am decay counts to the ^{232}U ROI was estimated and used to

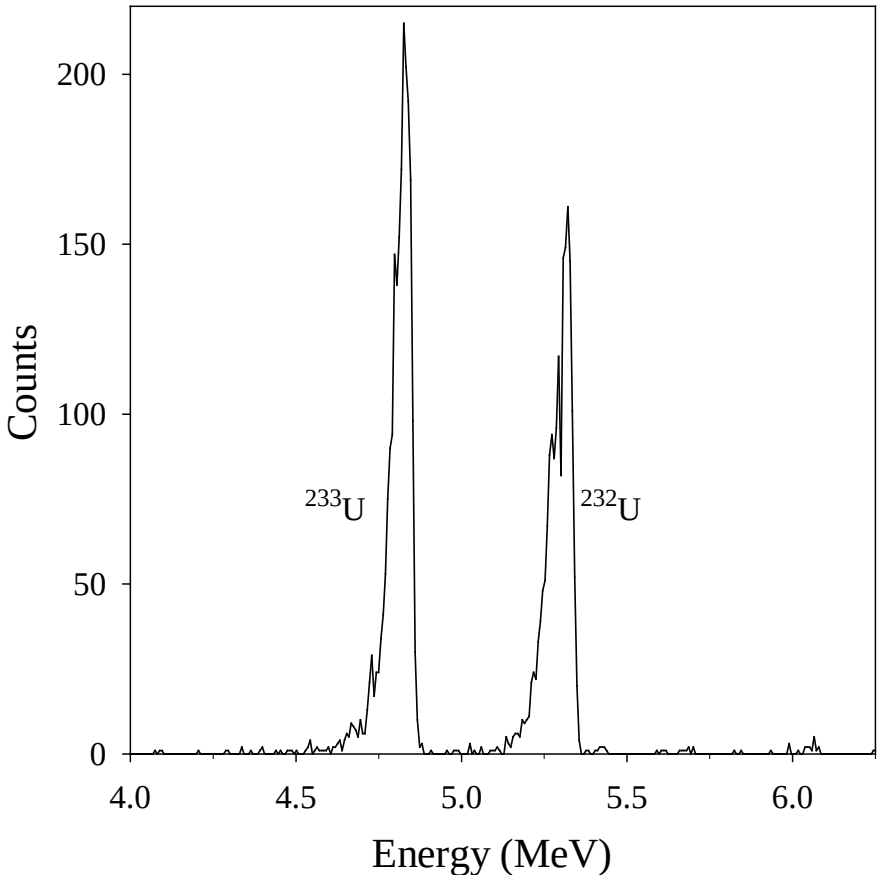

Figure 3-12 Example ^{233}U alpha-particle spectrum with ^{232}U tracer from analysis of ^{233}Pa tracer solution milked from the ANU ^{237}Np cow.

correct the counts measured in the ^{232}U ROI. The estimated ^{233}U extracted during preparation of the ANU ^{237}Np cow determined from this method was 74±21 Bq which was slightly lower than expected to be present in the NpO_2 used (102±1 Bq; see Table 3-5), although the precision of the measurement was low (28%).

Measurement of ^{233}U was undertaken in additional ^{233}Pa solutions milked from the ANU ^{237}Np cow coinciding with purification of these solutions for Pa separation method development and is discussed below.

3.5.4 Purification of ^{233}Pa tracer solutions milked from the ANU ^{237}Np cow

Owing to operational issues, measurement of alpha-emitting contaminants in the ^{233}Pa solutions milked from the ANU ^{237}Np cow 263 and 272 days after preparation was not undertaken. The contaminants ^{241}Am, ^{239}Pu and ^{240}Pu were effectively removed from the ANU ^{237}Np cow by the next elution conducted 431 days after preparation of the ANU ^{237}Np cow.

Purification of the ^{233}Pa solutions milked from the ANU ^{237}Np cow from 431 days after preparation onwards was undertaken for several reasons:

- to break down traces of ascorbic acid from the load solution remaining after initial treatment with 30% H_2O_2 used to stabilise the ^{233}Pa,
- to remove ^{237}Np from the solution. Although this was not a significant concern for this thesis, it was intended to minimise the potential for cross contamination of the ANU clean laboratory which is used for ultra-trace measurement of ^{237}Np in the environment, and
- to reduce the ^{233}U concentration in ^{233}Pa and provide confidence in calculating the ^{233}U contribution to the ^{233}Pa tracer measurement for sample analysis.

All ^{233}Pa solutions milked from the ANU ^{237}Np cow from 431 days after preparation onwards (see Table 3-5) were evaporated to dryness to allow uptake in the solutions required to proceed with separation chemistry. After drying, a black residue from the reaction of ascorbic acid with the acid remained which was removed by treating the residues with 30% H_2O_2 in 3 M HNO_3 until no significant colour remained.

Purification of the ^{233}Pa tracer solutions milked from the ANU ^{237}Np cow to remove ^{237}Np was undertaken for solutions milked 431 and 774 days after preparation (see Table 3-5) using the TEVA® resin separation method (Appendix F, Section F-1).

For solutions milked 858 days after preparation of the ANU ^{237}Np cow onwards, purification was undertaken to remove both ^{237}Np and ^{233}U. A combination of the TEVA® resin separation method to remove ^{237}Np followed by the TK400® resin separation method to remove ^{233}U was used for this solution. For all subsequent solutions only the TK400® resin separation method was used as it was observed that both ^{237}Np and ^{233}U were effectively removed.

Measurement of the ^{233}U activity in the ^{233}Pa tracer solutions used for sample analysis was needed to ensure the contribution of ^{233}U to the ^{233}Pa tracer measurement could be accurately quantified. This was undertaken on ^{233}Pa solutions milked from the ANU ^{237}Np cow from 431 days after preparation of the ANU ^{237}Np cow onwards. Aliquots of these solutions were removed and ^{233}U was measured using alpha spectrometry, though different chemical separation methods for U were used and all methods are described in Appendix F.

Approximately 2% of the estimated initial activity of ^{233}U on the ANU ^{237}Np cow was measured in the ^{233}Pa milked 431 days after preparation (after accounting for ingrowth since the previous extraction; note that the measurement uncertainty is high). The results for ^{233}U in the ^{233}Pa tracer solutions prepared from 858 days after preparation of the ANU ^{237}Np cow onwards indicate that the initial high activity of ^{233}U measured in the first extraction solutions had been removed

by the time sample measurements were made and that the measured activity concentrations of ^{233}U were similar to the estimated ^{233}U activity concentrations attributable to ingrowth alone (Table 3-5).

Section 3.6 Sample preparation for ^{231}Pa AMS measurement

For this thesis, the sample types for AMS analyses included biological, soil/sediment, and water samples. Each of these sample types present different challenges in preparation for analysis and have different processes impacting the behaviour of Pa and its progenitors in the environment.

Within a closed system (e.g., mineralised matrices, rocks, ores) the assumption of equilibrium for naturally occurring radionuclides within a decay series can often be made. However, with environmental migration of radionuclides, the chemical behaviour is largely governed by adsorption/desorption processes (Saint-Fort, 2018). This is especially true for Pa, which tends to be highly particle reactive (Gdaniec et al., 2018). This can lead to difficulties with preconcentration of Pa from biological samples into a stable solution for analytical chemistry.

3.6.1 Preparation and preconcentration techniques

For alpha spectrometry and AMS analysis of natural radioactivity, biological, soil/sediment and water samples need to be prepared in a liquid form to allow for radiochemical separation. This requires decomposition of the sample matrix to completely release the analyte of interest, which can then be solubilised in a form suitable for the separation method selected (Lamble and Hill, 1998). Typical sample preparation and preconcentration steps are discussed below for different sample types.

Water samples: Filtration and evaporation are used, with samples typically filtered through a 0.45 µm pore size filter to remove suspended particulates. The filtered sample is acidified to maintain metals in solution and prevent them from plating on container surfaces or precipitating. Ashing of filtration residues is then undertaken, with techniques like those for biological or soil/sediment samples below depending on requirements. After addition of a yield tracer, coprecipitation is a common technique used to preconcentrate metals in solution. There are a wide range of techniques available with the general principle aimed at removing soluble salts (i.e., group I and II metals, and major anions; see e.g., Ko, 2020; Michel et al., 2008; Rogers and Watrous, 1955).

Biological samples: Soil, dust or sediment particulates are removed by washing the surface (e.g., Medley and Bollhöfer, 2016; Medley et al., 2017). The material may then be dissected to obtain different organs (e.g., Medley and Patterson, 2022), and/or other preparation may be

warranted. Fresh samples are then dried to remove water and milled to homogenise the sample. Drying can involve air-drying, oven-drying or freeze-drying, each of which have different advantages and disadvantages. Freeze-drying, which is more expensive and time consuming, can lead to a finer powder when milled, leading to more complete digestion. Dried samples are weighed, then a yield tracer is added followed by ashing to remove organic components and decompose the sample matrix such that it can be solubilised (usually in a strong acid) for chemical separation. This is typically done through either dry- or wet-ashing. With dry-ashing, samples are heated typically to 450–500°C to remove organic matter as CO_2 and H_2O via oxidation with oxygen in the air (Barnes et al., 2014; USTUR, 1995). The remaining 'ash' contains primarily metallic oxides as well as other non-volatile compounds (e.g., sulphates, phosphates, and silicates; Barnes et al., 2014). The high temperatures can remove some volatile elements[25] (e.g., As, Hg and Se; Hoenig, 2001), for example ^{210}Po is volatile and dry-ashing is not recommended for this isotope (IAEA, 2017). There is a vast array of techniques for wet-ashing (also known as wet-acid digestion) of biological samples, substantial detail is included in Hoenig (2001), Wolf (2006), Lamble and Hill (1998), and references therein. The principal remains the same as for dry-ashing, which is oxidative removal of organic matter. Concentrated HNO_3, a mixture of concentrated HNO_3 with and H_2O_2, and aqua regia, in combination with heating are common techniques. Often several techniques are combined in sequence to completely release the analyte of interest. Microwave-assisted wet-ashing can involve higher temperatures and pressures than achievable with e.g., a hotplate, leading to more complete decomposition of the sample.

Soil/sediment samples: samples are usually oven dried to remove water, then milled to a coarse powder to homogenise. Dry-ashing may be undertaken to remove organic components (as for biological samples, however, the soil/sediment mineral matrix is not substantially affected in the dry-ashing process). Where there is not a substantial organic component this step is often skipped. Again, there is a vast array of different techniques for wet-ashing of soil/sediment samples (Hoenig, 2001; e.g., Michel et al., 2008). The most important distinction between wet--ashing for soil/sediment samples and biological samples is the high potential for silicate content and refractory fractions in soil/sediment samples. For complete digestion, the use of HF is generally required to break Si–O bonds and release silicate bound elements (Chao and

[25] There is the potential for losses of non-volatile elements through heating too quickly and thus rapid generation of smoke or sample ignition. Ensuring that a tracer is added prior to ashing can minimise this as a potential issue.

Sanzolone, 1992). Fusion techniques can also be used to solubilise Si (Chao and Sanzolone, 1992), however, further preconcentration is required to remove the Si from the sample for radiochemical separation. Unless a complete digest procedure is used, wet-ashing of soil/sediment samples should be considered to produce an acid-soluble or similar fraction dependent on the wet-ashing technique used.

For this work, biological and soil samples were provided dried and milled to a fine powder, except for four samples (whole organism or bone) that were provided as dry-ashed[26] samples (see Table B-1 in Appendix B, Section B-1). All soil samples, and biological samples collected before 2012 were oven dried at 60°C. Biological samples collected after 2012 were freeze dried[27]. Where known, information regarding whether samples were washed or otherwise prepared prior to analysis is provided (Appendix B, Table B-1).

Section 3.7 Preconcentration of ^{231}Pa – Method optimisation tests

In some cases, sample preparation techniques can be somewhat effective at sample preconcentration to remove major matrix elements prior to solubilisation for chemical separation (e.g., by removing organic compounds by dry-ashing). However, further preconcentration of solubilised samples must generally be performed before chemical separation can be undertaken to remove the bulk sample matrix remaining after sample preparation. To optimise the preconcentration of ^{231}Pa from biological and soil/sediment samples several tests were undertaken. As no water samples were available for ^{231}Pa measurement for this thesis, details of water sample preconcentration (for ^{227}Ac analysis) are in Chapter 4, Section 4.4.1.1. Unless otherwise specified all tests used PTFE equipment for handling solutions.

Two coprecipitation methods for preconcentration of metals in solution were initially tested using a ^{233}Pa tracer solution with no sample material. These methods were $Fe(OH)_3$ and MnO_2 coprecipitation from Martin and Hancock (2004). Chemical recoveries determined by HRGS for three sub-samples for each technique were 94±2% ($Fe(OH)_3$) and 98±2% (MnO_2), indicating both were suitable for analysis of Pa. The MnO_2 coprecipitation technique was used in subsequent testing as the recovery was slightly higher and experience has demonstrated it

[26] Dry-ashing was done by an external laboratory, the maximum temperature reached was not specified, however it is expected to be in the range of 450–500°C.

[27] Except samples DN15008 and DN15009, which were oven dried at 100ºC.

was less prone to difficulties with biological digest samples. Coprecipitation with $PbSO_4$ was also assessed after processing the first batch of samples to improve separation of Fe from the sample prior to ion chromatographic separation of Pa using the TK400® resin (Section 3.9.1.3).

3.7.1 Biological samples

For biological sample decomposition dry- and wet-ashing techniques are commonly used (Hoenig, 2001). Dry-ashing requires high temperatures and, in the presence of O_2, may lead to the formation of Pa oxides (which are difficult to solubilise, even in strong acids, without HF, according to Myasoedov et al., 2011). As such, only wet-ashing (wet acid digestion) techniques were considered and both hotplate and microwave assisted digestion techniques were assessed. Whereas simple hotplate digestion techniques can use relatively large sample masses[28], microwave assisted digestion can easily reach much higher pressures and higher temperatures. The oxidising strength of HNO_3 is increased at higher temperature/pressure and is further enhanced by the addition of H_2O_2 which adds oxygen to the reaction vessel (Nóbrega et al., 2012).

In tests of wet acid digestion, prior to HRGS measurement for chemical recovery (Appendix H) all digest solutions were diluted to 4 M HNO_3 to maintain Pa in solution then filtered through 0.45 µm to ensure only solubilised Pa was measured.

Two hotplate digest techniques were tested, concentrated (conc.) HNO_3 only, and a two-step method with a conc. HNO_3 digest followed by a combined conc. HNO_3/30% H_2O_2 digest. Samples masses of 1 g and 1.5 g were used for each method respectively (see Appendix E, Section E-7). In both tests more than 50% of Pa was lost, either bound to particulates attached to beaker walls or lost during filtration of the dissolved fraction, also likely bound to particulate matter. Hotplate digestion techniques were therefore considered unsuitable for ^{231}Pa analysis of biological samples.

A microwave-assisted digestion technique using ~0.5 g (dry weight) of sample combined with 9 mL of conc. HNO_3 and 1 mL of 30% H_2O_2 was tested, initially as a test of only the decomposition and then followed with a combined digest and MnO_2 coprecipitation. A final test with the same technique using a larger sample mass in each digest vessel (~2.3 g) to

[28] This essentially depends on beaker size and is thus technically unlimited. Biological samples >10 g are routinely digested for ^{210}Pb, ^{210}Po, Ra, Th and U isotopes in the laboratories in which the present work was undertaken. All microwave-assisted digestion was conducted in an ETHOS™ Milestone Microwave digestion system with SK-15 rotor using 100 mL PTFE digestion vessels, standard methods for organic materials for this instrument typically use <1 g of sample material.

improve achievable MDL was also undertaken (Appendix E, Section E-6). Both freshwater mussel flesh and prawn tissues were assumed representative of biological samples, with samples freeze dried and milled to a fine powder before digestion. Results for all tests are shown in Table 3-6.

The microwave assisted wet acid digestion technique showed excellent recovery (99±5%) for four prawn tissue samples. The combined wet acid digestion followed by MnO_2 coprecipitation showed no difference within uncertainty (98±6%) for five freshwater mussel flesh samples. The increased mass in a single digest vessel (~2.3 g) in the final test led to over pressurisation of the microwave digestion vessels, with some loss of digest solution through venting.

Table 3-6 Chemical recovery of ^{233}Pa after microwave-assisted digestion for dried prawn tissues and microwave-assisted digestion followed by MnO_2 coprecipitation for freshwater mussel flesh. Mass is dry weight.

Sample ID	**^{233}Pa Recovery (%)**					
Sample # **Sample Type (mass)**	**Average**	**1**	**2**	**3**	**4**	**5**
Prawn tissues (~0.5 g)	99±5	100±6	100±7	99±7	97±5	
Freshwater mussel flesh (~0.5 g)	98±6	100±10	98±9	100±10	99±9	93±8
Prawn flesh[a] (~2.3 g)	98±9	100±10	90±7	93±9	100±10	100±8

[a] Sample 5 was a spiked blank (i.e., only tracer solution with no prawn flesh).

Although chemical recovery was still high (98±9%) this procedure was not considered safe for routine use. The success of the microwave-assisted digestion techniques suggests effectively complete or near complete digestion of the samples with minimal potential loss of Pa bound to particulates. The technique used for the remainder of this thesis was therefore microwave assisted digestion with 0.5 g of sample material. Where analysis of a greater sample mass was possible, separate 0.5 g sub-samples were digested and combined prior to radiochemical separation. An equal activity of ^{233}Pa tracer was added to each sub-sample to ensure differential losses in digestion were appropriately accounted for (Appendix E, Section E-6).

3.7.2 Soil/sediment samples

Fusion was tested as a potential method for digestion of soil/sediment samples. Fusion involves sample dissolution through high temperature heating to break down mineral matrices and allow

solid samples to be more readily dissolved in aqueous solutions for chemical separation (Chao and Sanzolone, 1992). Much higher temperatures can be achieved with fusion compared to acid digestion techniques owing to the low boiling temperature of acids (Chao and Sanzolone, 1992). Fusion is commonly used for soil and sediment samples as it allows complete dissolution of silicates and other refractory minerals (Chao and Sanzolone, 1992) without the use of HF which removes Si by volatilisation of SiF_4 (Vlastélic and Piro, 2022). Borate fusions are a well-established technique for the dissolution of soil and sediment samples, including for the analysis of actinides (Braysher et al., 2019; Chao and Sanzolone, 1992). The use of borate fusion techniques for analysis of ^{227}Ac and ^{231}Pa for soil dissolution was trialled in this thesis. Although dissolution was achieved, subsequent attempts to yield a suitable precipitate for radiochemical separation of Ac or Pa were unsuccessful. Soil and sediment samples were therefore sent to an external laboratory for HF digestion[29].

Section 3.8 Ion chromatography for radiochemical separation of ^{231}Pa

At the start of the present work commercially available resins from Eichrom® were considered potentially suitable for the separation of Pa from environmental samples, including TRU®, UTEVA® and TEVA®. Of these resins, UTEVA® was selected for two reasons. Compared to TRU® resin, UTEVA® has a low relative affinity for Fe which is typically in moderately high concentrations in environmental samples and can interfere with retention of actinides by occupying binding sites (Vajda et al., 2003). UTEVA® is more sensitive to U than TEVA® and there are several published methods that show it can be used for effective separation of U and Th. Numerous tests with the UTEVA® resin were unable to separate Pa from U as highlighted in a typical elution profile from tests conducted for the present work (Figure 3-13).

Fortunately, during this thesis, major improvements in the separation of Pa from environmental samples was achieved. This was largely due to the development of a novel extraction chromatography resin based on the 1-octanol impregnated resin first reported by Knight et al.

[29] The HF digestion was similar to that described in Appendix E, Section E-7, with a HNO_3/HF/HCl digest step followed by a HNO_3/$HClO_4$ step. Samples were provided as 2 × 1 g sub-samples, with equal activities of ^{233}Pa tracer solutions added. The sub-samples were returned as semi-dried digest residues. A small fraction of particulates remained indicating incomplete digestion. The dissolution of the digest residues is described in Appendix E, Section E-8, with the 2 × 1 g sub-sample fractions combined prior to chemical separation.

(2016), which lead to the commercialisation of a new extraction chromatography resin 'TK400®' developed by TrisKem International[30]. Further work by Jerome et al. (2018) and

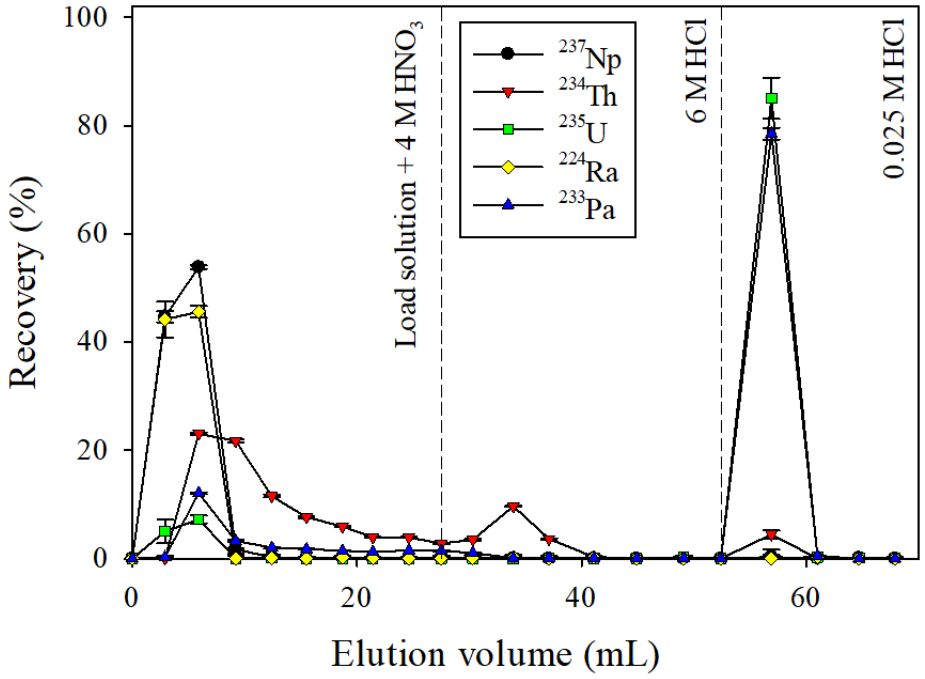

Figure 3-13 Recovery of isotopes ^{233}Pa, ^{237}Np, ^{224}Ra, ^{234}Th and ^{235}U from UTEVA® resin. For several measurements the measurement uncertainty is smaller than the symbol.

Süfke et al. (2018) using this resin for separation of Pa from several elements and actual samples (sediments) showed the effectiveness of TK400® resin for separation of Pa from sample matrices and from Np, U and Th. Süfke et al. (2018) also tested different particle sizes of TK400® resin, 50–100 µm and 100–150 µm, with the latter having superior yields. A series of experiments were undertaken to assess the applicability and reliability of the TK400® resin for the separation of Pa from environmental (biological) samples for this thesis and these are described in the next section.

Section 3.9 Separation of Pa from environmental samples with TK400® resin: Method verification tests

Süfke et al. (2018) reported a method for separation of Pa directly from standard reference materials[31] with a combination of DOWEX® AG 1-X8 and TK400® resins. During ion chromatographic separation, high matrix loads can reduce or prevent retention of the target

[30] www.triskem-international.com

[31] UREM-11, a uranium bearing mineral (Hansen and Ring, 1983) and NIST 2702, a marine sediment (NIST, 2019).

analyte on the resin, reducing chemical recovery from separation. If not adequately separated, the matrix can also cause substantial isobaric interferences with mass spectrometric techniques. The experimental work of Süfke et al. (2018) showed that U and Th are effectively separated from Pa using TK400® resin with decontamination factors in the order of 10^3, however, it was only applied to a limited mass (100 mg) and range of environmental samples (two CRMs). Given that the atomic weight of Th and U are close to that of Pa, separation is critical for any MS measurement as there will be isobars with atomic weights very close to those of ^{231}Pa and ^{233}Pa. In particular, ^{233}U will not be distinguishable from ^{233}Pa (see Section 3.2), and accordingly several tests to verify the method for separation of Pa from U and Th were undertaken (see Section 3.9.1). These tests initially used just ^{233}Pa tracer solution, then biological samples were tested to assess the impact of the sample matrix (freshwater mussel and prawn flesh samples were used as generally representative of a biological sample matrix).

Süfke et al. (2018) also demonstrated that TK400® resin is sensitive to a high matrix load and employed a DOWEX® AG 1-X8 resin separation step to remove the bulk sample matrix which, for this thesis, was achieved using an initial coprecipitation step. For AMS, interference from other elements with the same mass/charge ratio were also of concern (e.g., $^{138}Ba^{3+}$ could be problematic for measurements of $^{231}Pa^{5+}$, and $^{186}W^{4+}$ for $^{233}Pa^{5+}$). Jerome et al. (2018) showed effective separation from Ba using TK400® resin, however, this was not applied to environmental samples. No specific tests were undertaken to verify removal of specific stable elements for this thesis, though potential interferences were assessed during AMS measurement (Section 3.11, see also Medley et al., 2019).

3.9.1 Separation of Pa from Th and U with TK400® resin

The Süfke et al. (2018) method essentially has three steps, with the sample loaded to the resin in 10 M HCl solution, interfering elements including Th and U are then eluted with additional 10 M HCl, and elution of Pa with 1 M HCl is the final step. These three steps were the starting point for testing Pa separation with TK400® resin with slight modifications made to the published preconditioning steps (see method in Appendix F, Section F-2).

3.9.1.1 Test method: Tracer level verification of Pa, Th and U separation with TK400® resin

Two tracer level tests (Test A and B) were undertaken to verify and improve the effectiveness of separation of Pa, Th and U based on the Süfke et al. (2018) method.

In these tests, initial separation was undertaken using the Süfke et al. (2018) method, whereby Th and U are eluted in 10 M HCl, with ^{233}Pa subsequently eluted in 1 M HCl. The relative

chemical recovery of ^{233}Pa in both fractions was determined with HRGS (Appendix H). To measure Th and U using alpha spectrometry, a second separation was required. Uranium-238 and ^{229}Th tracers were added to both eluant fractions to determine chemical recovery and correct for losses in the second separation which used an in-house method based on Horwitz et al. (1992). A $Nd(OH)_3$ coprecipitation method based on Kurosaki et al. (2017) was performed to prepare Th and U for alpha spectrometry (methods in Appendix F, Section F-5).

For the first test (Test A) four samples were prepared with aliquots from solutions of ^{233}Pa (4.4 Bq ^{233}Pa per sample) and ^{232}U tracer (0.24 Bq ^{232}U per sample, in equilibrium with ^{228}Th). A fifth sample was prepared with only ^{233}Pa (8.8 Bq; Table 3-7). Recovery of ^{233}Pa was high (94±7%), however, breakthrough of ^{232}U in the ^{233}Pa fraction was higher than desired (1.9±1.0% of ^{232}U activity added). This is much higher than the of 0.1–0.15% breakthrough observed by Süfke et al. (2018). Breakthrough of Th was relatively low with 0.8±0.7% of the added ^{228}Th activity measured in the ^{233}Pa fraction.

In the second test (Test B), five samples were prepared as per Test A. However, the volume of 10 M HCl used to elute Th and U was increased from 20 mL to 30 mL (i.e., 40 mL total including the load solution). This led to improved separation, with ^{232}U in the ^{233}Pa fraction (1 M HCl) decreasing to 0.6±0.6% (see Table 3-7, only results for ^{232}U in 1 M HCl for Test B are shown). It was expected that the additional 10 M HCl also reduced Th breakthrough.

Table 3-7 Results for Test method: TK400® separation of ^{233}Pa from Th and U tracer solutions.

Sample ID	**Recovery (%) Test A**				**Recovery (%) Test B: with 40 mL 10 M HCl**
	30 mL 10 M HCl	**10 mL 1 M HCl**			**10 mL 1 M HCl**
	^{233}Pa	**^{233}Pa**	**^{228}Th**	**^{232}U**	**^{232}U**
1	3±1	92±3	0.5±0.4	1.7±0.4	0.5±0.2
2	4±1	93±7	0.5±0.3	1.2±0.4	0.5±0.2
3	4±1	92±7	1.0±0.5	2.0±0.4	1.1±0.4
4	2±1	96±6	1.1±0.6	2.5±0.5	0.4±0.2
5[a]	3±1	100±6			
Average	3±1	94±7	0.8±0.7	1.9±1.0	0.6±0.6

[a] This sample was only spiked with ^{233}Pa and used as an analytical blank for ^{228}Th and ^{232}U measurement using alpha spectrometry.

3.9.1.2 Test method: TK400® separation after preconcentration with MnO_2 coprecipitation (mussel flesh samples)

The next test was aimed at verifying the Süfke et al. (2018) method for biological samples, where additional interferences are present in the sample matrix. Five freshwater mussel samples were used, with TK400® resin separation of Pa following microwave-assisted wet acid digestion and preconcentration with MnO_2 coprecipitation (methods in Appendix E and Appendix F). An additional 10 mL 10 M HCl was used to improve Th and U separation from the TK400® resin. As per the tracer level tests above, ^{233}Pa and ^{232}U tracer solutions were added to samples and chemical recovery of ^{233}Pa and ^{232}U was determined using HRGS and alpha spectrometry respectively. Several pieces of equipment used for the test were also measured with HRGS to assess potential losses of Pa throughout the procedure (HRGS methods in Appendix H). Results are shown in Table 3-8.

Table 3-8 Fractional recovery of ^{233}Pa from microwave-assisted digestion of freshwater mussel samples followed by MnO_2 coprecipitation and TK400® resin separation.

Sample ID	^{233}Pa recovery[a] (%)					^{232}U in 1 M HCl
	Digest vessel	PES Filter	TK400® column	10 M HCl	1 M HCl	
Mussel 1	0.010±0.006	0.50±0.05	1.4±0.1	0.27±0.02	99±7	0.67±0.41
Mussel 2	0.012±0.007	0.11±0.02	1.1±0.1	0.66±0.06	97±7	<0.33
Mussel 3	0.059±0.015	1.6±0.1	1.0±0.1	0.66±0.06	96±7	<0.20
Mussel 4	0.034±0.006	0.25±0.03	1.6±0.1	0.44±0.04	98±7	<0.17
Mussel 5	0.009±0.008	0.38±0.03	1.9±0.1	0.18±0.03	97±7	0.44±0.37
Average	0.02±0.04	0.6±1.2	1.4±0.8	0.4±0.4	97±3	0.28±0.54

[a] Results for ^{233}Pa recovery from sample decomposition and MnO_2 coprecipitation for these specific samples are given in an earlier section when testing those methods (Section 3.7.1, Table 3-6). Note that ^{233}Pa chemical recovery values may exceed the chemical recovery recorded for an earlier step, however, values are within the stated measurement uncertainty.

A high ^{233}Pa recovery (97±3%) showed that the method was highly suitable for Pa analysis in biological samples. Results from alpha spectrometry indicate relatively low breakthrough of U (0.28±0.54%), with values lower than the tracer level tests above (Test B, Table 3-7).

The effectiveness of chemical separation can be partly illustrated with images of the TK400® resin column throughout the procedure shown in Figure 3-14. The dark black colour in the 10 M HCl load solution is indicative of Mn which was washed from the column with 10 M HCl. This fraction will contain much of the sample matrix, including Th and U, while Fe is retained. The Fe was then eluted with Pa in the 1 M HCl fraction, this is relevant as the presence of Fe in some samples analysed by AMS was problematic (see Chapter 5, Section 5.1) and led to the next test, aiming to remove Fe at the coprecipitation stage.

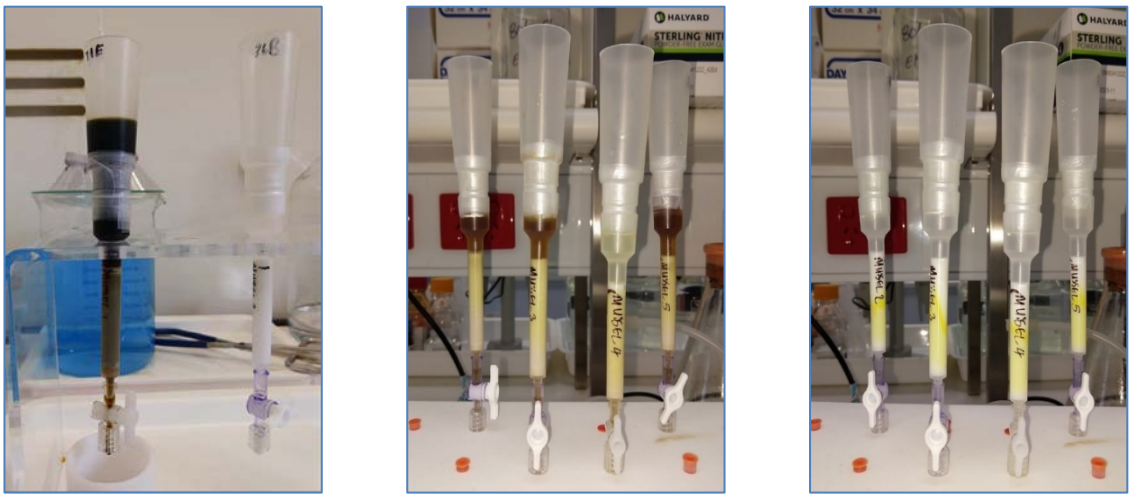

Figure 3-14 Load solution in TK400® resin for mussel 1 (left). Final several mL of 10 M HCl wash for mussels 2–5 (middle). First few mL of 1 M HCl fraction for mussels 2–5 (right).

3.9.1.3 Test method: TK400® separation following preconcentration with $PbSO_4$ coprecipitation (prawn flesh samples)

The effectiveness of $PbSO_4$ coprecipitation for preconcentration of Pa from solution was assessed. The primary aim was to remove Fe shown to be present in the ^{233}Pa fraction from TK400® resin separation for freshwater mussel samples above (Figure 3-14). Coprecipitation with $PbSO_4$ (method described in Appendix E, Section E-9) was used to preconcentrate metals in solution from four prawn tissue samples after sample decomposition with wet acid microwave assisted digestion (Section E-6), with a fifth sample spiked with ^{233}Pa tracer solution as a blank.

The TK400® separation method with increased 10 M HCl (Appendix F, Section F-2) was used to separate Pa from the dissolved $PbSO_4$. No visible yellow Fe colour was apparent on the resin, indicating effective removal of Fe. Results for recovery of ^{233}Pa are shown in Table 3-9.

The recovery of Pa (57–91%) is lower and more variable than achieved for tracer solutions (92–100%; Section 3.9.1.1) and dried freshwater mussel samples using MnO_2 coprecipitation

(96–99%; Section 3.9.1.2), indicating some potential losses of Pa with the $PbSO_4$ coprecipitation technique. Although the chemical recovery may have been somewhat reduced, the $PbSO_4$ coprecipitation method was used for subsequent samples because of its superior ability to remove Fe (Section 3.9.1.3).

Table 3-9 Chemical recovery of ^{233}Pa for prawn flesh samples precipitated from microwave assisted digest solutions using $PbSO_4$ coprecipitation followed by TK400® resin separation. Chemical recovery is corrected for losses from microwave assisted digestion

Sample ID[a]	Average	Prawn 1	Prawn 2	Prawn 3	Prawn 4	Spiked Blank
Recovery (%)	77±26	72±11	91±9	78±11	57±8	85±8

[a] Results for chemical recovery for sample decomposition for these specific samples are in Table 3-6 (Prawn tissues ~2.3 g).

Section 3.10 The 14UD AMS system

This section provides a description of the 14UD AMS system, with details of tests undertaken to optimise methods to prepare the Pa extracted for AMS following this in Section 3.11. Detailed discussion of accelerator mass spectrometry can be found in (Fifield, 1999) and references therein with specific application to the actinides also in (Fifield, 2008).

Here the specific system used for this thesis, the 14UD tandem pelletron accelerator at ANU (Figure 3-15) is described, with discussion relevant to application for measurement of ^{231}Pa in

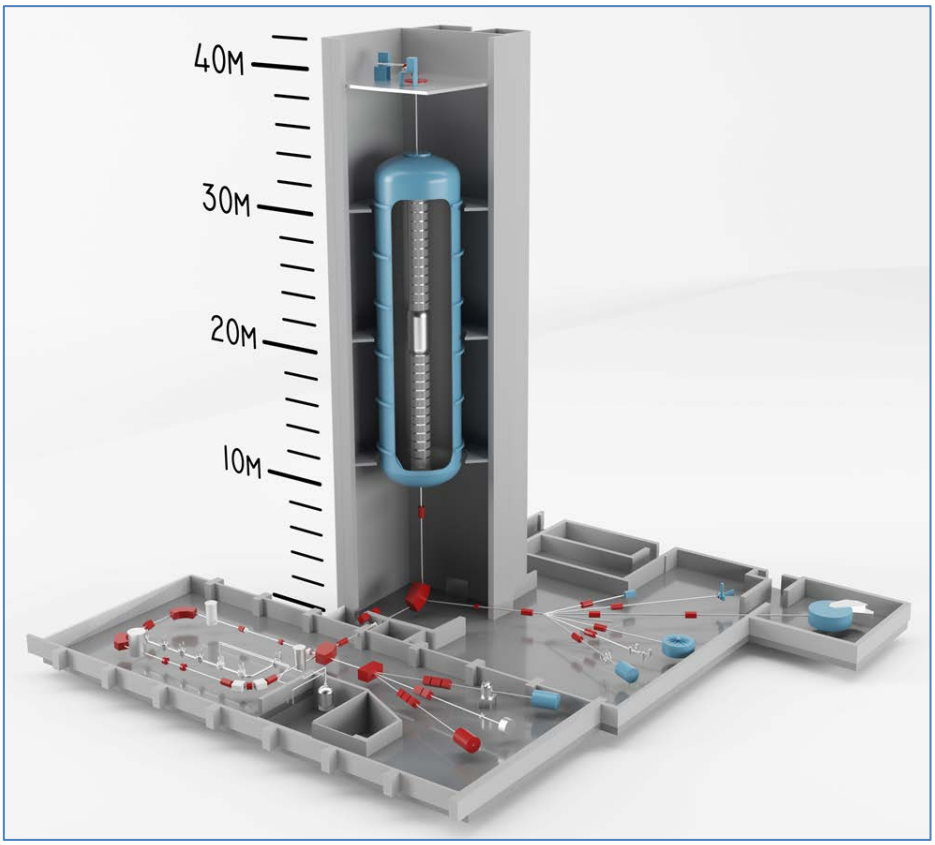

Figure 3-15 The 14UD pelletron tandem accelerator at ANU and associated infrastructure. Image courtesy of Thomas Tunningley (ANU).

environmental samples. Additional detailed information on recent developments for the 14UD AMS system at ANU can be found in De Cesare et al. (2015), Koll (2023), Kuwae et al. (2023), Martschini et al. (2019), Pavetich et al. (2019), and Wallner et al. (2023).

Figure 3-15 depicts the Heavy Ion Accelerator Facility at ANU, of which the AMS is a part. As configured for Pa measurements, the major components of the system comprise a 32 sample 'Multi Cathode Source of Negative Ions by Caesium Sputtering' (MC-SNICS) ion source, the (low energy) injection magnet, the 14UD tandem accelerator, the (high energy) analysing magnet, a velocity selector, and a 6 m long Time-of Flight (TOF) detection system immediately upstream of a compact split-anode ionisation chamber. These aspects of the system are illustrated with a schematic view in Figure 3-16, and are described in more detail below.

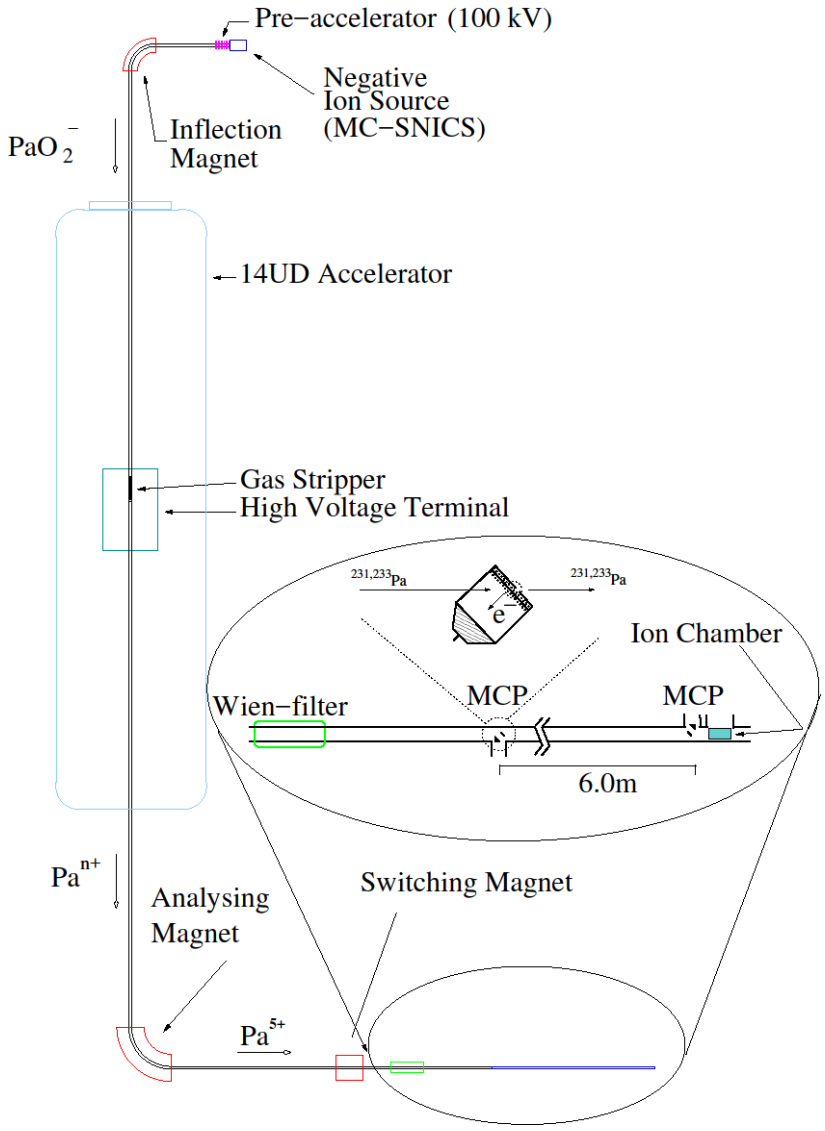

Figure 3-16 Schematic view of the AMS measurement system used in ^{231}Pa analysis for this thesis. Image courtesy of Stephen Tims, ANU.

3.10.1 The MC-SNICS Ion Source

An ion source is an essential part of any MS system (Han et al., 2007), with a modified NEC MC-SNICS providing a source of negative ions to the 14UD tandem accelerator MS at ANU (Weisser et al. 2002). A cut-out diagram of the MC-SNICS is shown in Figure 3-17.

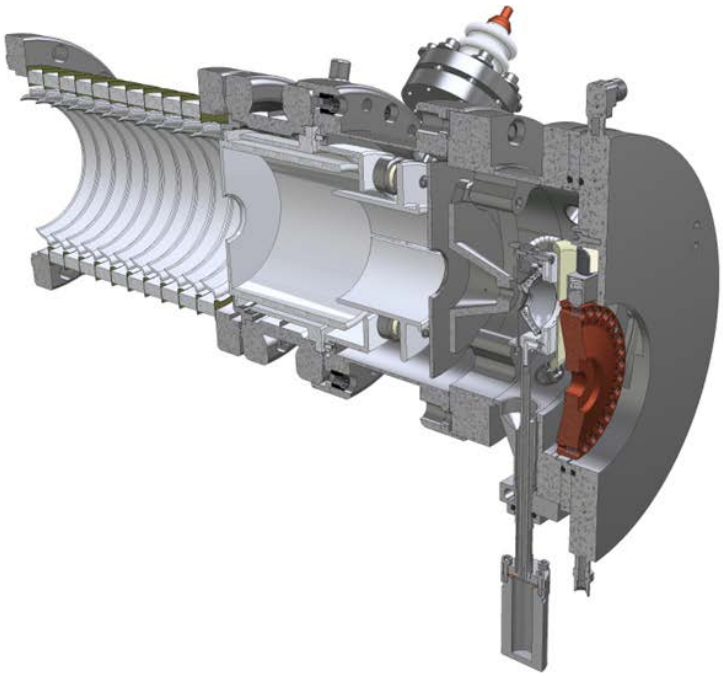

Figure 3-17 Cut-out diagram of the MC-SNICS ion source. The sample holder is highlighted (copper coloured). Image courtesy of Thomas Tunningley (ANU).

Caesium is almost exclusively used in sputtering for AMS for the production of negative ions (Han et al., 2007), this is because it is relatively easy to produce a Cs vapour. The high atomic mass also leads to a relatively high kinetic energy and efficient sputtering of ions from the sample material. The low electronegativity makes it a ready donor of electrons which increases the chance of producing Cs^+ ions on contact with the ioniser and provides a source of electrons to assist negative ion production of the isotope(s) being sputtered from the sample. The ANU ioniser has a spherical profile, which gives a better ion source efficiency and negative ion beam quality than systems using conical profiles (Southon and Santos, 2007).

Operation of the MC-SNICS starts with generation of Cs vapour by heating high purity Cs metal in the oven to approximately 90°C, this temperature determines the Cs flow rate and therefore impacts the Cs ion beam intensity. A pressure differential leads to Cs vapour flowing into the low vacuum sample chamber (~10^{-7} Torr) containing the sample and the ioniser; on contact with the ioniser Cs^+ ions are produced by surface ionisation. The Cs^+ ions are accelerated towards the cathode, containing the sample, which is held at 5 kV with respect to the ioniser, with the spherical shape of the ioniser helping to focus the Cs^+ ions onto the sample. Between the ioniser and the sample is an 'immersion lens', the Cs^+ ions pass through the central hole in this lens which reduces radiant heat on the sample wheel and shields samples adjacent to the one being sputtered by the Cs^+ beam. An independent bias voltage can be applied to the immersion lens helping to focus the Cs ions.

The Cs^+ ions striking the sample cause sputtering and lead to the formation of negative ions, which is enhanced by condensation of Cs vapour in the chamber on to the sample and by the presence of nearby neutral Cs vapour (Brown, 2006; Middleton, 1989). Negative ion formation is also improved by mixing the sample material with a low work function powdered metal. For example, Al was the preferred choice for Pa measurement, with mixing after precipitation as an iron hydroxide and heating at high temperature to remove oxygen (Medley et al., 2019).

The negative ions produced are accelerated back through the immersion lens and a circular gap in the centre of the ioniser by the same electric field used to accelerate the Cs^+ ions onto the sample. The emerging ion beam is focussed with an Einzel lens with the downstream part of the lens electrically connected to the 100 kV pre-accelerator. The Einzel lens used at ANU uniquely acts to decelerate and focus the ions between the F1 and F2 components of the lens but has no overall impact on the ion energy. A detailed description of the lens setup and function is given in Weisser et al. (2002).

The use of elemental ions in tandem accelerators is often preferred as molecular ions beams suffer from Coulomb explosion owing to the intense release of energy by the breaking of molecular bonds in the stripper (Middleton, 1989), potentially leading to significant transmission losses. Although a number of elements form stable negative ions, many do not, and furthermore for many elements the efficiency for the production of molecular ions greatly exceeds that of the atomic ions, and hence molecular ions are often used (Middleton, 1989). The impact of using molecular ions on beam quality can be lessened through selecting lighter molecules but these may not always be easy to produce. For actinides molecular ions, rather than atomic ions, such as (UO^-) are selected as they typically have a higher yield from the ion source (Middleton, 1989).

3.10.2 The injection magnet, accelerator and analysing magnet

The ion beam from the pre-accelerator is directed into the injection magnet which is set to select for the ion of interest and deflect the ion beam through a 90° angle and into the 14UD tandem accelerator. The accelerator is housed in a ~500 m^3 tank, filled with high-pressure (~700 kPa) SF_6 to electrically isolate the high voltage terminal.

Entering the accelerator at 105 keV the negatively charged PaO_2^- ions are further accelerated towards the positively charged high voltage terminal operated at ~4 MV. In the centre of the high voltage terminal is a stripper assembly, consisting of an 8 mm diameter × 852 mm long tube which can be ‘filled’ with low pressure gas, and a cassette holding thin carbon foils

(Fifield, 1999). The stripper gas used at ANU is N_2, though Ar, He, SF_6 and Xe have been investigated for heavy ions at other facilities, with SF_6 showing the potential for increased ion yield for heavy ions Th and U (Hotchkis et al., 2013a; Hotchkis et al., 2013b). Turbo pumps minimise entry of N_2 in the stripper tube to the body of the accelerator. In the work reported here the gas stripper was operated at ~0.004 mbar and a blank (i.e., no foil) position was selected on the foil cassette.

Collisions between the negative ions and gas molecules in the stripper act to dissociate negative molecular ions into their component atoms and remove electrons from these atoms to create positive charge states (Fifield, 1999). For lighter elements this occurs through a series of collisions leading to higher charge states, with variations in the charge state distribution dependent on gas thickness and type. Hotchkis et al. (2013b) however, showed that the charge state distribution for some heavy ions is independent on the gas type and thickness and demonstrated that for several heavy ion species there exists a high probability of single collisions resulting in multiple electron losses, indicating that high charge state formation and molecular break-up can occur simultaneously. Routine actinide measurements with the 14UD tandem accelerator at ANU, use a sufficient density of stripper gas in the stripper tube to give a reproducible distribution of charge states for the actinide elements. While molecular ions with a charge state of 2^+ can survive the stripping process, Coulomb explosion removes higher charge state molecular ions after the charge exchange process in the stripper (Buraglio, 2000). In the present work the 5^+ charge state was used as this provides the optimal trade-off between beam stability, charge state yield and transmission efficiency (Fifield, 2008), and consequently minimised the potential for molecular species giving rise to interference in the detection system.

The positively charged atoms created in the stripper are then accelerated away from the positive high voltage terminal towards the analysing magnet which selects ions of constant ME/q^2 (M: mass; E: energy; q: charge). Total transmission of a given charge state is dependent on gas thickness, with more gas the ion-gas interactions increase, thereby increasing the effectiveness of the stripper.

The yield of the positive charge state selected for analysis is the dominant influence on particle transmission through the accelerator after the initial negative ion formation (Hotchkis et al., 2013b). To optimise the transmission, however, as indicated above the selected charge state may not be the most probable one as this choice is limited by other factors, such as the magnetic rigidity of the analysing magnet and the possible presence of interfering molecular fragments or ions (such as where there is a high probability of a potentially abundant ion having the same

mass/charge ratio as the isotope being measured). The 90° analysing magnet of the 14UD tandem accelerator at ANU can deflect ions with ME/q^2 up to 220 MeV-amu, this provides a limiting factor in the choice of terminal voltage and charge state for actinides owing to the high relative atomic mass. The optimum transmission for actinides through the 14UD tandem accelerator of ~3% is reached by selecting the 5^+ charge state with the analysing magnet and using a terminal voltage of ~4 MeV (Fifield, 2008).

3.10.3 The velocity selector and detection system

After passing through the analysing magnet there is still a significant potential source of background in the ion beam from lighter elements at lower charge states, and isotopes relatively close in mass. Therefore, further steps are required to reduce background to allow reliable measurements of low abundance isotopes. The cause of the potentially high background can be owing to insufficient resolution of the various deflecting magnets or the incomplete radiochemical separation leading to injection of exotic species. For example, $^{109}Ag^{140}Ce^{16}O^-$ and $^{93}Nb^{140}Ce^{16}O_2$ would be of the same injection mass as ^{231}Pa and ^{233}Pa respectively (Medley et al., 2019). Selection for charge states of +3 or higher with the analysing magnet, will remove molecular interference passing through the stripper (Hellborg and Skog, 2008). However, collisions with residual gas in the acceleration tube may lead to the formation of new molecular fragments which may have the correct energy needed to pass through the analysing magnet into the beam line. These fragments can lead to interference in the detector, which is one of the reasons that, after the analysing magnet, the beam passes through a velocity selector, also known as a ‘Wien’ filter.

The Wien filter applies perpendicular electric ($\leq$ 40 kV cm^{-1}) and magnetic fields ($\leq$ 0.26 T), leading to a magnetic force in an opposite direction to the electric force, both acting at 90° to the beam line. Only ions where these opposing forces cancel out will pass through the filter in a straight line, this effectively allows only ions with the same velocity or mass to charge ratio (M/q) to pass without deflection (Fifield, 2008). As the analysing magnet is acting on ions with constant ME/q^2, lighter ions that have passed through the analysing magnet to reach the Wien filter due to a lower charge state will be moving at a higher velocity and so be deflected. The transverse displacement of ions with identical mass-energy product but different mass and energy divided by the primary beam width at the defining aperture for the beam line is 131 ($\Delta M/M$). Hence, the Wien filter is capable of rejecting backgrounds differing by 2 mass units near mass 230.

Insufficient resolution of the Wien filter, for the ultra-low abundance isotope ^{231}Pa, can still lead to background from lighter elements at lower charge states. To discriminate counts from lighter elements an energy measurement is incorporated into the detection system in the form of an ionisation chamber (Martschini et al., 2019).

Neither the Wien filter nor the ionisation chamber are capable of removing or discriminating isotopes which are close in mass to the isotope being measured as they will have a similar velocity and energy after the analysing magnet. For example, the energy difference between ^{231}Pa and ^{232}Th is only ~0.43%, whereas the energy resolution of the ionisation chamber for ^{232}Th is ~4% at full-width-half-maximum (FWHM; Martschini et al., 2019). A high-resolution velocity measurement across the 6 m flight path of the time-of-flight (TOF) detection system immediately upstream of the ionisation chamber allows identification of the mass of each ion, which combined with the energy measurement, provides excellent discrimination between masses close to those of the isotope being measured.

3.10.3.1 The ionisation chamber

Ionisation chambers use the measurement of differential energy loss to discriminate between different particles (Döbeli et al., 2004). The ionisation chamber consists of parallel conducting plates with a single cathode and two anodes inside a gas-filled, gas-tight housing with a constant potential applied between the plates. The standard detector gas for the ionisation chamber used for this thesis was isobutane[32] at ~55 mbar (Martschini et al., 2019) which is flowed through the chamber during operation. Ions enter the ionisation chamber through a 0.7 µm mylar window to prevent the gas leaking into the low-pressure beam line. The Pa ions at 24 MeV will lose about 3 MeV of their energy passing through the mylar window. Ions then lose energy by interaction with the gas which ionises molecules making the gas in the chamber partially conductive. The electrons produced drift towards the anode and the positive ions drift towards the cathode, generating an induced signal at both electrodes. The number of electrons produced is proportional to the energy lost in that part of the chamber by ions interacting with the gas. The gas pressure inside the ionisation chamber is set so that ions stop before reaching the back of the detector. As such, a measure of the total energy lost in the ionisation chamber (ΔE_{Tot}) relative to the total energy lost as measured by the second anode (ΔE_2) provides discrimination

[32] Alternative gases may be used, e.g., both isobutane (at 44 mbar) and propane (at 64 mbar) were used for this thesis (Martschini et al., 2019). The flow rate is minimal and prevents the gas reacting if left too long in the detector, which can affect detector resolution.

between ions of different mass. Circuit diagrams of the TOF system and ionisation chamber used for this thesis are shown in Figure 3-18. Detailed discussion of the "*compact ionisation chamber for actinide detection"* used for this thesis can be found in (Martschini et al., 2019).

3.10.3.2 The TOF system

The Time-of-Flight (TOF) detection system consists of start and stop detectors and discriminates ions close in mass by the time taken to travel between these detectors (Fifield, 2008). The system used in the present work has a 6 m separation between detectors, which yields a resolution of 1.7 ns for actinide beams (Fifield et al., 2013), whereas typical differences in flight times are more than three times this (e.g., the difference between ^{231}Pa and ^{232}Th is ~5.8 ns). The TOF system is based on that described by Gladkis (2008).

The detectors in TOF systems must transmit the ion beam, and therefore minimising losses is an important consideration. Start detectors typically consist of a thin carbon foil (potentially as low as 0.5 µg cm^{-2}) that will emit electrons when ions pass through (Hellborg and Skog, 2008). The electrons emitted are then accelerated towards a microchannel plate (MCP) by a potential difference between the foil and an acceleration grid. A 1 kV potential is used for the ANU TOF system (Gladkis, 2008). A second carbon foil is used as the stop detector with the (downstream) compact ionisation chamber described above (Section 3.10.3.1), used for the energy measurement. The ultra-thin carbon foils prevent major reductions in transmission efficiency through scattering (Fifield, 2008), however, the efficiency is still reduced to ~50% compared to just the use of the ionisation chamber. This is largely due to scattering of ions from a copper mesh support for the ultra-thin carbon foil, which has a transparency of ~75%, and to scattering from the carbon foil itself (Fifield, 2008). The ion beam passing through the start/stop detectors will create an angular spread of ions which will also have a changed charge state distribution. A quadrupole lens located mid-way between the start and stop detectors refocuses the divergent beam to minimise scattering losses.

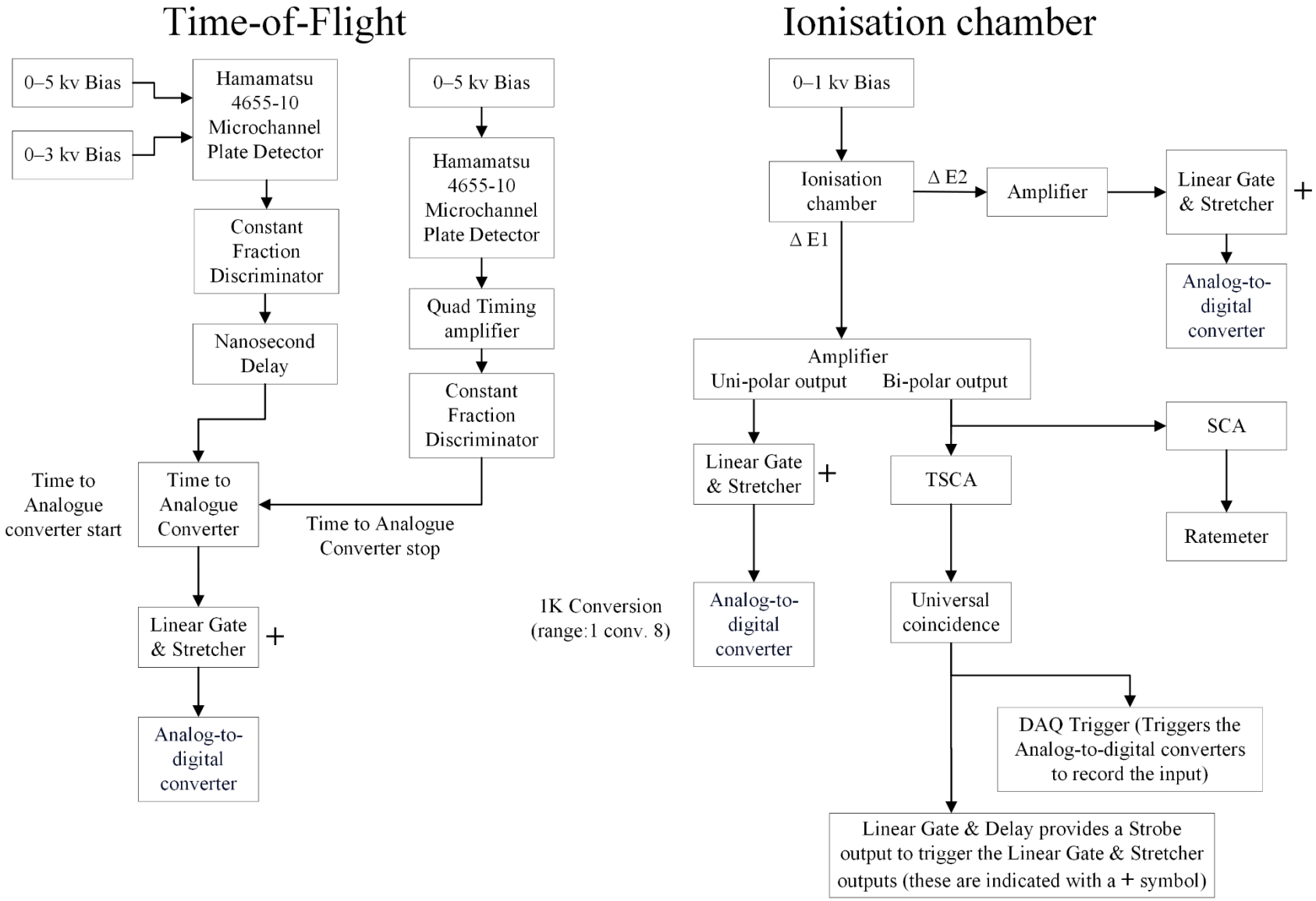

Figure 3-18 Circuit diagrams of the Time-of-Flight and Ionisation chamber used for this thesis.

Section 3.11 Sample preparation for AMS

3.11.1 Preliminary testing of the AMS for Pa analysis

To prepare Pa extracts from TK400® resin separation for AMS they must be prepared in a suitable form for sputtering and creation of negative ions in the MC-SNICS ion source. Injection as an oxide is commonly used for actinides as negative ion yields are superior to atomic ions, with Fe often used to 'bulk' the sample and embed the actinide in an Fe_2O_3 matrix (Fifield, 2008). A low work function 'binding' material is mixed with the oxide to improve negative ion formation then pressed into an AMS cathode. The choice of binding material and cathode can influence the species distribution of sputtered ions produced in the AMS ion source. Injection as the PaO^- species was used for the first measurement of ^{231}Pa with AMS by Christl et al. (2007), however, other oxide species may have superior negative ion yields.

To optimise Pa extraction in the ion source for the 14UD tandem accelerator at the ANU and assess contributions to background, a range of binding materials (Ag, Al and Nb) and cathodes (Al and Cu) were assessed (Medley et al., 2019). The relative negative ion yields of various Pa-oxide molecules (Pa monoxide to pentoxide) were also investigated.

Test samples were prepared by dispersing approximately ~2–4 pg of ^{231}Pa into an $Fe(NO_3)_3$ solution containing ~1.2 mg of Fe. These samples were evaporated to dryness and combusted at 800°C, yielding Pa oxide dispersed in an Fe_2O_3 matrix which was then mixed with binding material and pressed into cathodes for AMS measurement (Medley et al., 2019). The AMS measurement is described in Medley et al. (2019), and results showing the relative negative ion yields of the various oxides tested, normalised to dioxide as the highest yielding, are given in Table 3-10.

Table 3-10 Relative count rates of Pa oxides with the 14UD tandem accelerator at the ANU. An estimate of UO_2^- values at mass 233 relative to PaO_2^- is given to note the potential interference from ^{233}U in the ^{233}Pa spectrum.

AMS settings	**PaO^-**	**PaO_2^-**	**PaO_3^-**	**PaO_4^-**	**PaO_5^-**	**UO_2^-**
Relative count rates						
PaO_x^-/PaO_2^- ratio	0.272	1	0.184	0.001	Negligible	0.039

The PaO_2^- ion had a substantially higher intensity than all other Pa oxide ions tested, with an intensity 3.7, 5.4 and over 1,000 times higher than for PaO^-, PaO_3^- and PaO_4^- respectively; the measured intensity from PaO_5^- was negligible.

An estimate of the UO_2^- was also made, as measurement of the ^{233}Pa spike may be hindered by the presence of ^{233}U (e.g., Christl et al., 2007 where the negative ion yield for $^{233}UO^-$ for their sputter source was about twice that of $^{233}PaO^-$). In the ion source at ANU the negative ion yield for $^{233}UO_2^-$ is a factor of ~7 lower than that for $^{233}UO^-$ (Fifield et al., 1997). Hence, selecting the dioxide rather than the monoxide for injection led to an estimated overall suppression in the ^{233}U count rate in the detector of a factor ~26 (relative to the ^{233}Pa count rate; Table 3-10).

Sample results from the different combinations of binding material and cathode showed the greatest PaO_2^- negative ion output was from Nb with a Cu cathode, followed by Nb with an Al cathode. Similar count rates were observed for Ag and Al binding materials with Cu and Al cathodes respectively, though only ~35% of the count rate from Nb with a Cu cathode. The lowest count rate was for an Ag binding material with Al cathode[33] (Medley et al., 2019).

When measuring at mass 233 high transmission of $^{140}Ce^{3+}$ was observed with Ag and Nb binding materials and likewise for $^{93}Nb^{2+}$ with Nb binding material (likely injected as $^{93}Nb^{140}Ce^{16}O_2^-$ with the same injection mass as $^{233}Pa^{16}O_2^-$). The presence of Ce in the Ag binding material is known (S. Tims, pers. comm., 28 April 2016) and, similarly with the $^{109}Ag^{140}Ce^{16}O^-$ ion being of the same injection mass as the $^{233}Pa^{16}O_2^-$ ions, it is the likely source of Ce (Medley et al., 2019).

The count rates attributable to $^{140}Ce^{3+}$ were considered low enough that the detection system was not impacted significantly. As such, the first test of the AMS system using environmental samples (freshwater mussels: for a detailed description of this test see Medley et al., 2019) proceeded with Nb binding material and a Cu cathode. While the Ce was readily resolved from ^{233}Pa in the ionisation chamber, the high Ce count rate and increased dead time impacted the quality of the data for these first measurements (Medley et al., 2019). As a similar issue would likely always arise with the Ag binding material, the Al/Al binding material/cathode combination which had the next highest count rate, was adopted for the re-analysis of the mussel samples (Medley et al., 2019) and subsequent sample analysis. It is worth noting that the final binding material/cathode combination used (Al/Al) is essentially identical to that used by Christl et al. (2007).

[33] Ceramic and quartz crucibles were tested with the Ag/Al binding material and cathode combination and showed a potential loss of ~40% of the protactinium on the walls of the quartz crucible. This was attributed to the high affinity of Pa for Si (Mendes et al., 2013). Accordingly, ceramic crucibles were used for all subsequent sample preparations.

Section 3.12 Sample analysis

3.12.1 Overview of analytical procedure for ^{231}Pa AMS measurement

An overview of the analytical procedure developed for ^{231}Pa AMS measurement is shown in the flowchart below (Figure 3-19). Tests undertaken to develop suitable methods for sample preconcentration, coprecipitation, and separation of Pa from the sample matrix with ion chromatography were described in Section 3.7 to Section 3.9, and Section 3.11 above.

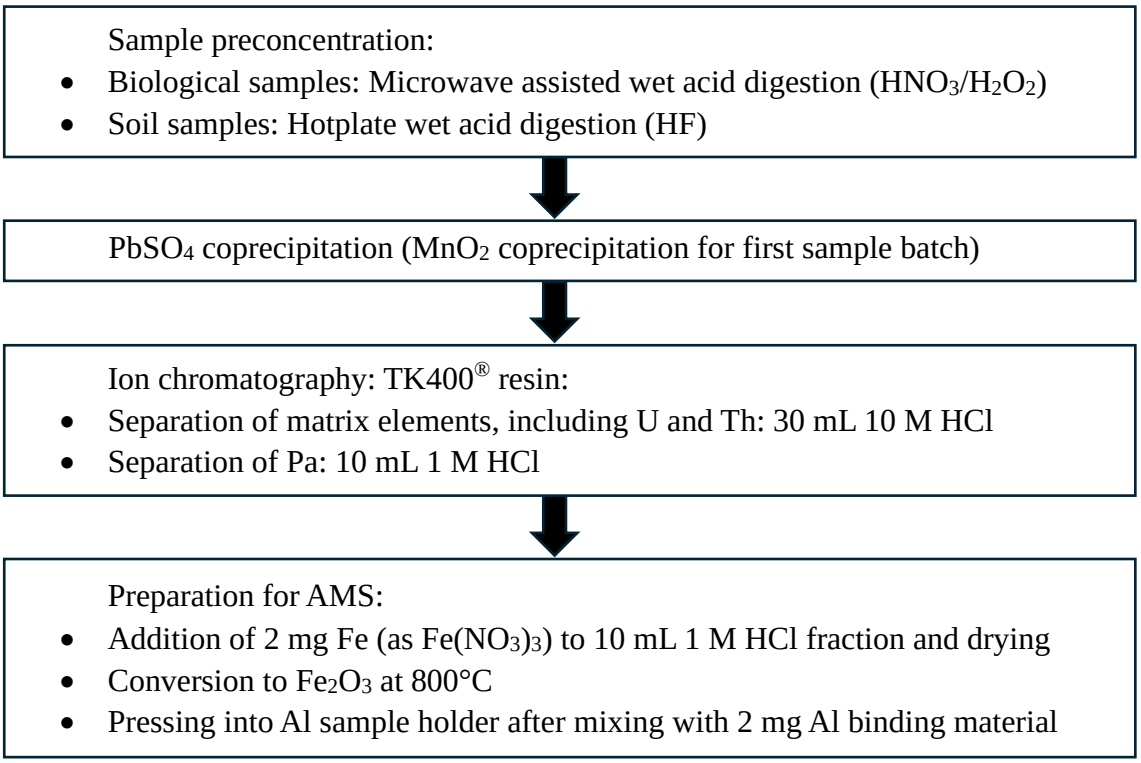

Figure 3-19 Flowchart of analytical procedure for ^{231}Pa AMS measurement (MnO_2 coprecipitation used with samples spiked with ^{233}Pa tracer milked 858 days after preparation of the ANU ^{237}Np cow (see Table 3-5).

Samples for this thesis were measured using four purified ^{233}Pa tracer solutions milked from the ANU ^{237}Np cow (see Table 3-5). Eight batches of 8–11 samples were processed, where a 'batch' is defined as a group of samples, including blanks, processed concurrently; for each milked ^{233}Pa tracer solution, two batches were processed.

Equations use to calculate results for ^{231}Pa are in Appendix A, Section A-2, with results from measurement of ^{231}Pa in samples are in Appendix B, Section B-1 and discussed in Chapter 5.

3.12.2 AMS spectral analysis and fast-cycling

A spectrum for the spiked blank with the highest 231 blank count rate is used below to illustrate ROI setting for the ionisation chamber and ToF, as well as potential interferences. The spiked blank was from Batch 2 for the ^{233}Pa tracer milked 1501 days after preparation of the ANU

^{237}Np Cow (see Appendix J, Section J-1.3). The ToF spectrum when selecting for mass 233 is shown in Figure 3-20 and is from combined data acquisition periods with a total acquisition time of 2,100 s. A pulser was used to monitor dead-time in the electronics and data acquisition system. Dead time corrections were typically less than 1%.

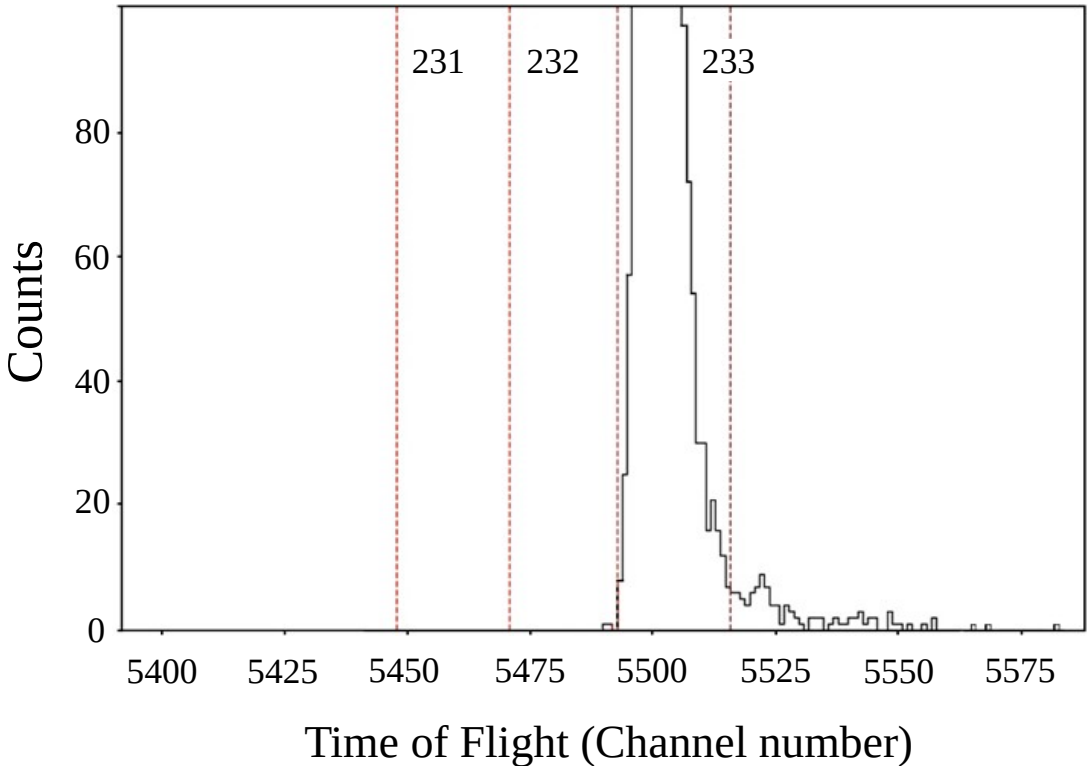

Figure 3-20 One-dimensional projection of the ToF spectrum when selecting for mass 233 showing counts that fell within the energy window around the mass range relevant for Pa measurement. ROI used for masses 231–233 are displayed.

A total of 1.37×10^{10} ^{233}Pa atoms and 6.32×10^{9} ^{233}U atoms were present in the sample at the measurement time for the spectrum in Figure 3-20 (based on measured separation effectiveness and ingrowth from ^{233}Pa between Pa/U separation and AMS measurement; see Section 6.6, Section A-2 for further details). The pressed sample mass was 2.0 mg of Fe_2O_3 with 1.9 mg Al powder. Total counts in the ToF spectrum were 2,818, with 2,732 in the ROI for mass 233. The raw data from the ionisation chamber for the same combined acquisition period is shown in Figure 3-21. The data suggest the presence of more than one species is captured in the ROI.

The ROI ('Energy gate' in Figure 3-21) was set using a tuning sample containing ^{231}Pa and ^{233}Pa (see next section for further details), with the AMS system selecting for mass 231. The ROI contains 3,823 ion events out of a total of 3,904 in the spectrum, with the difference being the straight line of counts below the ROI. This line is an artefact caused by the software when summing counts from both electrodes in the ionisation chamber to determine ΔE_{Total}.

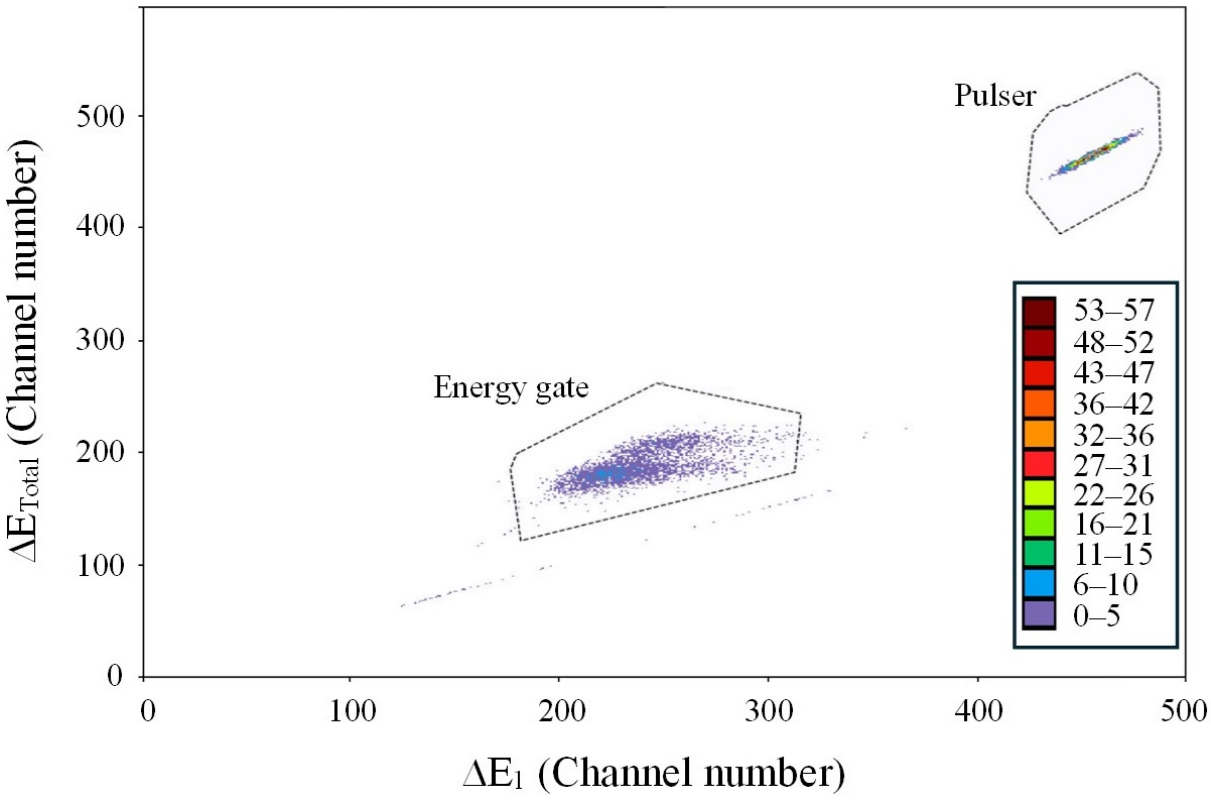

Figure 3-21 Two-dimensional plot of the total energy loss (ΔE_{Total}) versus the energy loss under the first (ΔE_1) electrode from the ANU ionisation chamber when selecting for mass 233. ROI includes counts in the 'Energy gate' with the same mass to charge ratio as 233^{5+} ions.

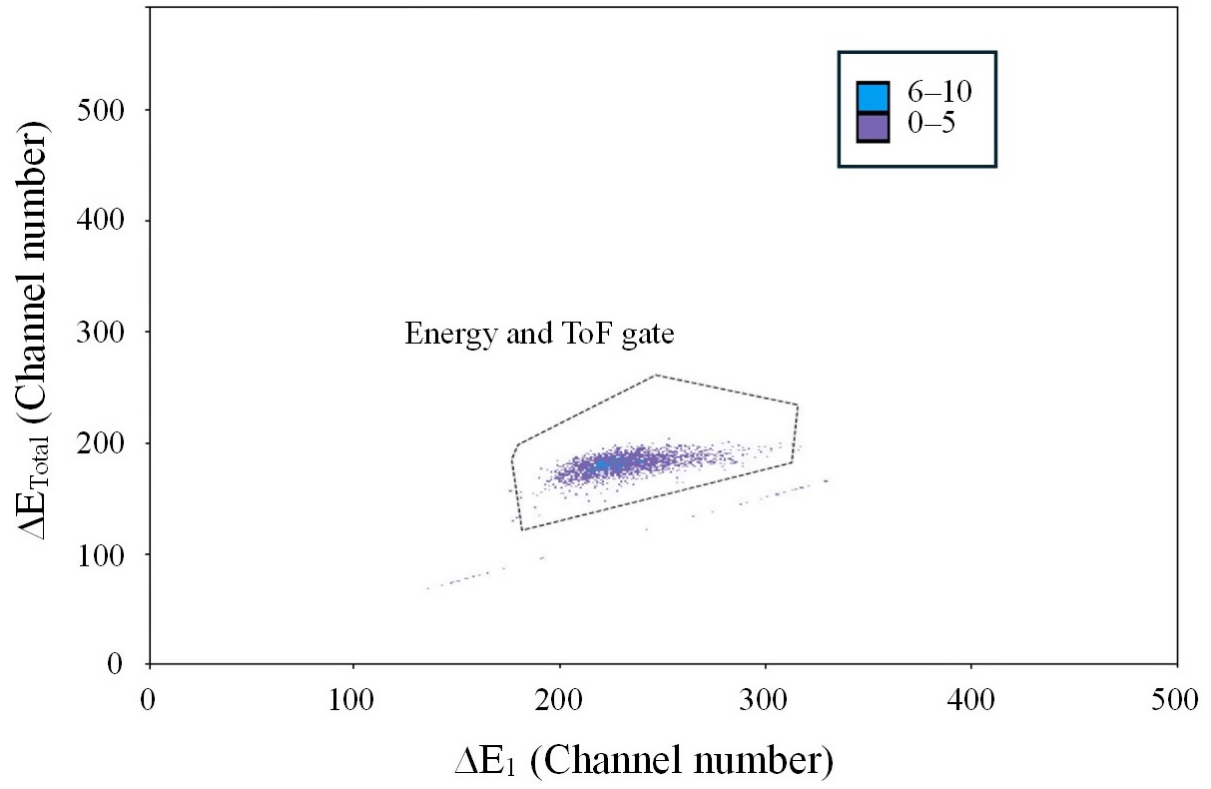

Figure 3-22 Two-dimensional plot of the total energy loss (ΔE_{Total}) versus the energy loss under the first (ΔE_1) electrode from the ANU ionisation chamber as shown in Figure 3-21 with a gate applied to remove counts outside of the ToF ROI for mass 233 shown in Figure 3-20.

Applying the ROI around the 233 peak in Figure 3-20 as a gate to the ungated spectrum from the ionisation chamber (Figure 3-21) yields the gated spectrum shown in Figure 3-22. This removes the unwanted species of a lower charge state present in the spectrum shown in Figure 3-21, which have the same mass to charge ratio as 233^{5+} ions.

Similar gating criteria were applied when measuring at mass 231. Spectra from the ToF and the ionisation chamber (gated) are shown in Figure 3-23 and Figure 3-24, the combined acquisition time when selecting for mass 231 was 1,500 s.

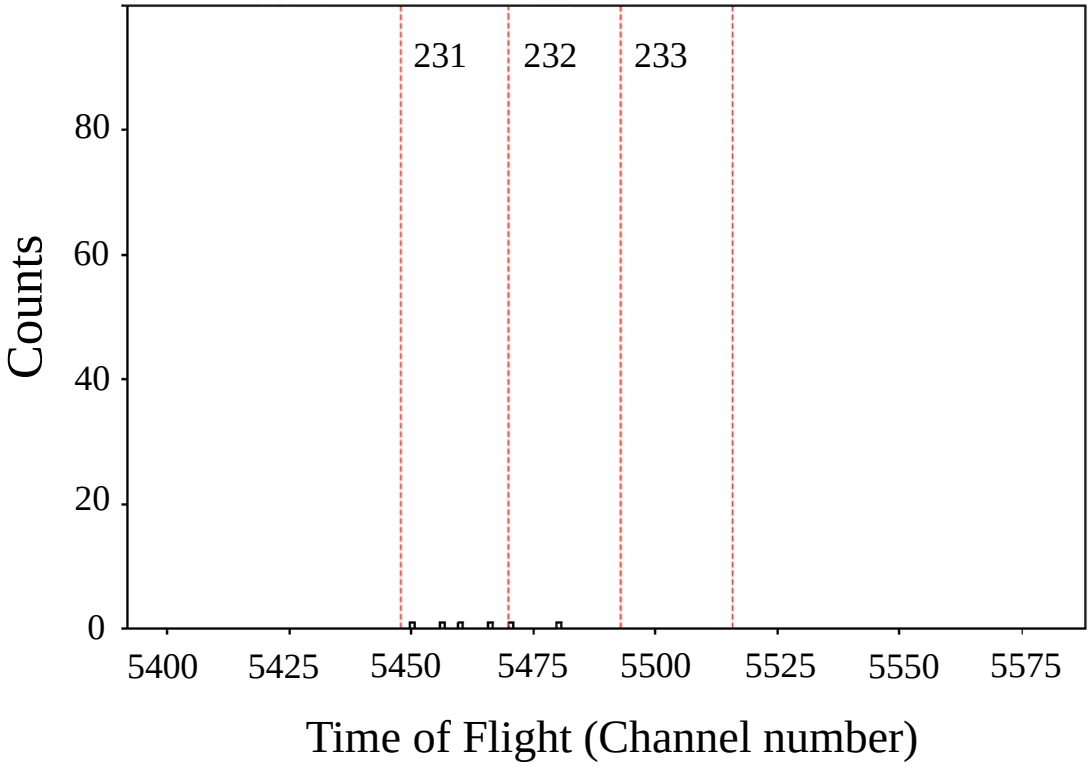

Figure 3-23 One-dimensional projection of the ToF spectrum when selecting for mass 231 showing counts that fell within the energy window around the mass range relevant for Pa measurement. ROI used for masses 231–233 are displayed.

Of the six counts in the ToF spectrum of Figure 3-23, two counts can be attributed to mass 232 (i.e., ^{232}Th) and four to mass 231. One of the 231 counts in the ToF spectrum was a software artefact as described above (Figure 3-24).

The ToF spectrum when measuring at mass 231 for sample RM07011 is shown in Figure 3-25, total acquisition time was 600 s. This sample had the highest number of counts at mass 232 for any sample or blank.

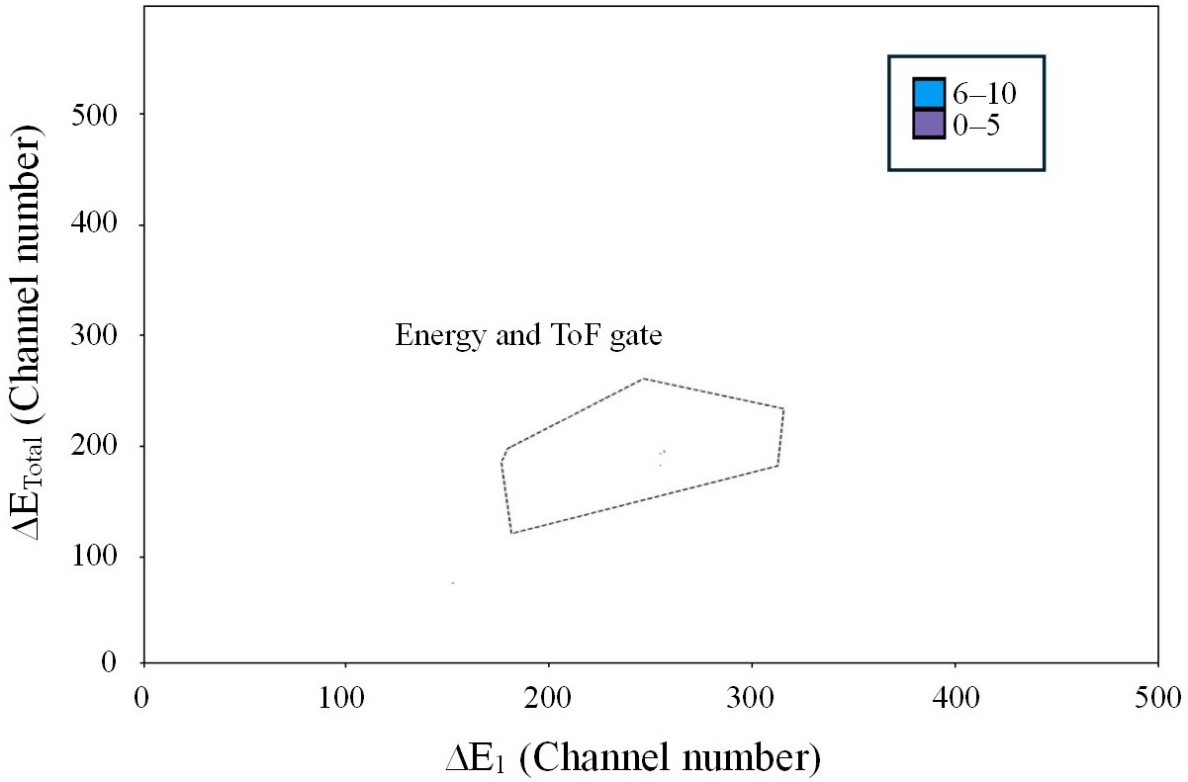

Figure 3-24 Two-dimensional plot of the total energy loss (E_{Total}) versus the energy loss under the first (ΔE_1) electrode from the ANU ionisation chamber when selecting for mass 231 with a gate applied to remove counts outside of the ToF ROI for mass 231 shown in Figure 3-23.

With counts recorded at mass 232 for samples and blanks, the use of a ToF system in this thesis for measurement of ^{231}Pa at environmental concentrations demonstrates an improvement in the sensitivity of ^{231}Pa measurement using AMS compared to other published methods.

A small number of samples were counted without the use of the ToF system (Appendix B, Section B-1, Table B-1). However, the count rate at mass 232 observed for all samples when using the ToF system was low and in a range close to the MDL value for ^{231}Pa. Potential interference from ^{232}Th will therefore be of little significance for dose assessment in this thesis.

For the final batch of samples, a fast-cycling counting system was in place, based on the injection voltage bouncing system described for Pu isotopes given in the supplementary information of Kuwae et al. (2023). This system substantially reduces the time taken to switch between measurement of ^{231}Pa and the ^{233}Pa tracer. Thus, the impact of variations in transmission during data acquisition was reduced, leading to improved precision.

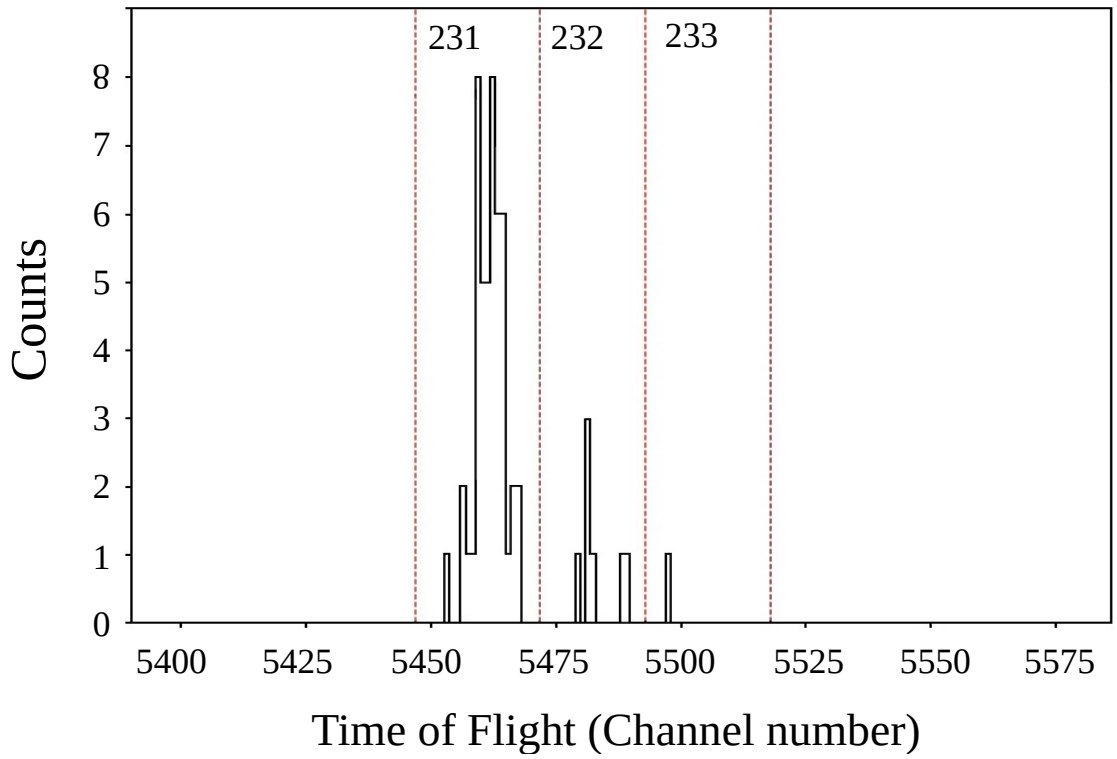

Figure 3-25 One-dimensional projection of the ToF spectrum when selecting for mass 231 for sample RM07011 showing counts that fell within the energy window around the mass range relevant for Pa measurement. ROI used for masses 231–233 are displayed.

3.12.3 ^{233}U relative ion counting efficiency and correction of ^{233}Pa counts

As noted above in Section 3.2.1, ^{233}Pa and its longer-lived isobar (^{233}U) will have different ion counting efficiencies in AMS measurement, which must be accounted for. At the TANDY AMS facility the increased negative ion yield when selecting for the monoxide led to an 'enhancement factor' of two or more for UO^- compared to PaO^- (i.e., a relative efficiency > 2:1 for U:Pa; Christl et al., 2007). For the AMS measurements in this thesis however, a higher negative ion yield was obtained for Pa with the dioxide compared to the monoxide. Thus, determination of the relative efficiency of UO_2^- compared to PaO_2^- was required.

A ^{231}Pa spiked sample was prepared using the ^{233}Pa tracer solution milked 1501 days after preparation of the ANU ^{237}Np cow (Table 3-5) to determine the enhancement factor which was calculated to be 0.104±0.078 (i.e., the ^{233}U count rate is ~10% of the ^{233}Pa count rate). A discussion of the procedure used to determine the enhancement factor and associated calculations are in Section 6.6, Section A-2.1.

The enhancement factor and the ingrowth time between chemical separation and AMS measurement were used to determine the proportion of mass 233 counts attributable to ^{233}U (and ^{233}Pa), as described in Section 6.6, Section A-2. The proportion of ^{233}U counts so determined was typically 3–5% and never exceeded 7.8% of the total mass 233 counts observed.

3.12.4 Losses of Pa during analytical procedures

To understand where losses of Pa may have occurred throughout the analytical procedure, and to adapt the method to minimise losses, HRGS measurements of almost all labware that came in contact with samples throughout the analytical process after addition of the ^{233}Pa tracer solution were made. Also measured by HRGS were the solutions generated from processing samples, including the supernatant from coprecipitation, and the 1 M HCl and 10 M HCl eluant fractions from TK400® resin separation. The results and detailed discussion of this process is detailed in Appendix J, Section J-2. High losses occurred with the PES filters used to filter the sample digest solutions (9±37%, range of 0–80%, n=66) and in the supernatant from coprecipitation. The loss of ^{233}Pa on the PES filters could generally be attributed to the presence of undigested particulate matter. For samples coprecipitated using $PbSO_4$, ^{233}Pa losses in the supernatant for soils were generally higher (36±20%, range of 22–50%, n=7) than for all other samples (7±13%, range of 0–28%, n=43). For the fewer number of samples where MnO_2 coprecipitation was used, losses were much lower (0.3±0.6%, range of 0–1%, n=15). Where the presence of Fe in samples is low (<1.5 mg Fe in the total sample used for analysis), the use of MnO_2 coprecipitation for sample preconcentration may yield superior results. However, the differences may potentially be attributed to the sample type and possibly the larger number of samples which used the $PbSO_4$ method. Losses for whole organism and bone samples which were dry-ashed prior to analysis (19±10%, range of 13–23%, n=4) were the highest for biological samples and all were coprecipitated using $PbSO_4$.

It is noteworthy, however, that the highest losses of ^{233}Pa were observed initially on the 20 mL PFA vials that were used to collect and then evaporate the 10 mL of 1 M HCl solution used to extract Pa from the TK400® resin. High losses were also observed on the 25 mL PTFE beakers acquired to replace the PFA vials. The 1 M HCl solution was evaporated to enable safe air transport from the radiochemistry laboratory in Brisbane to the AMS facility in Canberra. Redissolution in concentrated HCl with the addition of Fe in solution followed by the evaporation to form an Fe_2O_3 powder was used to prepare samples for AMS (see method in Appendix F, Section F-2). For the final batch of samples, the Fe solution was added directly to the 10 mL of 1 M HCl before evaporation in the 25 mL PTFE beakers which led to a substantial reduction in the overall losses (5±3%, range 1–11%, n=18) compared to evaporation without Fe (35±24%, range 4–100%, n=33). This practice should be adopted in future where samples need to be dried for transport prior to AMS measurement.

Chapter 4 : Chemistry of ^{227}Ac and radioanalytical method development

Section 4.1 Chemistry of ^{227}Ac

There are 32 known isotopes of Ac (Morgan and Donnelly, 2021), all of which are radioactive and only six of which have half-lives greater than 10 minutes (Fry and Thoennessen, 2013). Although the discovery and naming of Ac is generally traced to two papers published in 1899 and 1900, it has been argued that it was first truly discovered in 1902 and initially called 'emanium' (Fry and Thoennessen, 2013). Actinium is a homologue of Ln (Stevenson and Nervik, 1961) and, although not formally an actinide, it is often included in discussions regarding the actinides (Hübener, 2003).

Owing to its short half-life, Ac is extremely rare in the environment with an abundance in the earth's crust of approximately 5.5×10^{-10} parts per million (Hübener, 2003). The largest amount ever obtained from a natural supply is 7 µg (Hübener, 2003), while the most feasible method of production through neutron irradiation of ^{226}Ra still only gives yields in mg amounts (Hatcher-Lamarre et al., 2021). Production solely for the purpose of studying the chemistry is rare owing to the difficulties and costs of obtaining it (Deblonde et al., 2021). There are only 12 Ac compounds synthesised for which measured lattice parameters have been published and no single crystal structure has ever been solved for an Ac compound (Deblonde et al., 2021). The information on Ac compounds is derived from studies of the longest-lived known isotope of Ac, ^{227}Ac which has a half-life of 21.77 years and therefore a high specific activity (2.7 TBq g^{-1}). A detailed review of the structural data available on Ac compounds, suggests the data may have been impacted by impurities (e.g., ^{226}Ra, Ba or Pb), as impurities are difficult to detect owing to the high specific activity and low working mass of ^{227}Ac (Deblonde et al., 2021). This leads to the conclusion that even the size of the Ac^{3+} ionic radius is likely to have been overestimated. Given that fundamental properties of the Ac ion and compounds of Ac are still in debate or unknown, there is still a substantial amount of work to be done to fully understand the chemistry of Ac.

Despite the challenges noted above, the chemistry of Ac can be relatively simple compared to elements with multiple oxidation states (Deblonde et al., 2021) as it only exists in the +3 oxidation state in solution. The extremely limited supply, high specific activity and relatively simple chemistry has led to much of the chemistry of this element being inferred from lanthanides and actinides that commonly exist in the +3 oxidation state (Ferrier et al., 2016).

4.1.1 Environmental Chemistry

Environmental analysis of ^{227}Ac has been primarily focussed on ocean water movement and mixing (e.g., Geibert et al., 2008; Geibert and Vöge, 2008; Nozaki, 1984, 1997), or dating geological materials (e.g., Dulaiova et al., 2013; Gascoyne, 1985; Shen, 1996). More recently there has been interest in ^{227}Ac extraction from industrial resources or waste products as a means of producing ^{223}Ra for nuclear medicine applications (Al-Masri et al., 2020; Tang et al., 2014). Outside of the marine environment, the 'environmental chemistry' has therefore been generally focussed on the radiochemistry of extraction from environmental materials, rather than movement within the environment.

Studies in the marine environment show that the higher solubility of ^{227}Ac leads to diffusion from marine sediment to seawater as ^{231}Pa accumulates in sediments (Nozaki et al., 1990). Bioturbation of the sediment and subsequent release of ^{227}Ac from sediment particulates also plays a key role in the movement of ^{227}Ac from sediment to seawater (Nozaki et al., 1990). These processes lead to an excess of ^{227}Ac relative to ^{231}Pa in deep marine waters giving rise to use as a tracer of deep ocean circulation.

There are some studies in which the behaviour of Ac has been studied in terrestrial or freshwater aquatic environments. Many of these were related to former U mines, e.g., Köhler et al. (2000b) measured ^{227}Ac in six mine pit water samples, and Niese (1996) measured ^{227}Ac in stockpile, pit, and river water samples from former U mines to investigate environmental transport processes. However, little can be inferred from these studies other than that ^{227}Ac can be mobilised in such waters. Percival and Martin (1974) measured ^{227}Ac (and ^{231}Pa) in U milling process wastes, similarly little can be inferred from this study other than it is present in such wastes. Other studies investigated general environmental processes, e.g., Megumi (1979) measured ^{235}U series disequilibrium in soils to assess soil age and formation through weathering, with an assumption that ^{227}Ac is indicative of ^{231}Pa activity concentration and that higher activities are found in smaller particles. Whereas Lieser et al. (1991) investigated the movement of actinides in groundwater and "*showed cation exchange reaction to be important at low pH and chemi-sorption reaction at neutral pH*" for ^{227}Ac.

Measurement of Ac in environmental biota samples is limited to several studies investigating transfer to plants from contaminated sites. Köhler et al. (2000a) investigated uptake of ^{227}Ac in tomato plants, publishing CRs for roots, stalk, and fruits. For all parts, CR values were similar for ^{227}Ac, ^{210}Pb, ^{226}Ra and ^{238}U, except for fruits, where ^{238}U CRs were substantially lower. A limitation of this study is that uncertainties were quite high (e.g., 50% or greater for averaged

^{227}Ac results from three soils). Summerton (1992b) measured a range of naturally occurring radionuclides in tidal saltmarsh sediments impacted by a legacy U and monazite treatment plant and showed organic residues from vegetal decay play an important role in incorporation of radionuclides, including ^{227}Ac into sediments. This is consistent with the known ability of Ac to form organic complexes (a property exploited to prepare ^{225}Ac for use in nuclear medicine, Deblonde et al., 2021). Further work measured ^{227}Ac, ^{228}Th, ^{230}Th, ^{232}Th and a range of rare earth elements in an Australian salt tolerant shrub, samphire (*Halosarcia halocnemoides*), growing in an evaporation pond of a former treatment plant (Summerton, 1992a). Their results indicated that Th and La have similar CRs to Ac and an important finding from this study was that higher uptake of rare earths was correlated with lower atomic mass.

As noted in Chapter 1, Section 1.2.3, a previous study measured ^{227}Ac in 13 bush food items and four surface water samples from the study region for human dose assessment. These samples were collected from uncontaminated areas and all results were effectively below the limit of detection (Martin et al., 1998; Martin, 2000).

4.1.2 Biochemistry

There are only a few studies reporting the Ac biochemistry, and fewer still in human subjects, as such, ICRP DCs are typically based on analogues (e.g., ICRP, 1993, 2019).

The ICRP (1993) reviewed Ac biokinetics, though a scarce number of studies were available. These studies are limited to investigating toxicology and internal distribution of Ac in rats by direct injection (Campbell et al., 1956; Langham and Storer, 1952; Taylor, 1970), with the exception of the study by Hamilton (1948), who also investigated oral uptake and skin absorption. The Campbell et al. (1956) study investigated retention of ^{227}Ac and progeny, showing that ^{227}Ac was retained predominantly in the skeleton, where equilibrium with progeny was reached, and the liver, where progeny were redistributed and no equilibrium was attained. Systemic uptake and retention of ^{227}Ac was assessed by Newton and Brown (1974) in a male exposed to these isotopes via a puncture wound. A biological half-life of ~125 years was determined with deposition initially occurring in bone and the liver (3 years) with long-term translocation almost exclusively in bone (9 years). In this publication, Ac was noted as behaving in a similar way to Th, and this is essentially the basis of the justification used by the ICRP (1993) for modelling Ac biokinetics from ingestion for members of the public on the behaviour of Th. This differs from the approach for occupationally exposed workers, where the absorption from the gastrointestinal tract after ingestion is based on a generic value for actinides and systemic biokinetics (with minor modifications) are based on that of Am (ICRP, 2019).

The mode in which ^{227}Ac is introduced into the body in the studies referenced by the ICRP (1993), however, does not necessarily translate to typical exposure from environmental or industrial pathways (e.g., inhalation of dust or aerosols generated from mining or ingestion of food). This leads to an additional level of uncertainty in assessing the relative dose contribution from ^{227}Ac. Dose assessment and distribution of ^{227}Ac in the body has received much attention in recent years, owing to it being a radioimpurity in ^{225}Ac ($t_{½}$ = 10.0 d) used in nuclear medicine (Sgouros et al., 2021). However, these studies have the same limitations when applied to environmental sources owing to the different pathways of exposure.

The assumed biokinetics of Ac and associated DCs for ^{227}Ac also include a contribution from progeny and an assumption that progeny are in equilibrium with ^{227}Ac deposited in bone (ICRP, 1993, 2019). This contributes to a relatively high DC (ICRP, 1995). Without further research into Ac uptake and biokinetics, the assumptions of the ICRP are the best estimates available and the DCs for members of the public, with the incumbent assumptions regarding progeny have been used in this thesis.

For environmental doses, limitations of the generic CR approach and the approach for calculation of dose from ^{227}Ac and progeny were noted in Chapter 2, Section 2.7.2.

4.1.3 Radiochemistry

The similarity of Ac chemistry to that of the REEs is helpful, as e.g., Ac can be ‘carried’ by REEs in chemical reactions such as coprecipitation (Stevenson and Nervik, 1961). It also presents a challenge as Ac often needs to be separated from the REEs for measurement (see e.g., Grench and Buchanan, 1973; Kosynkin et al., 1995; Rychkov et al., 2018). Coprecipitation with $PbSO_4$ is a commonly employed technique for preconcentration of Ac with other metals in solution prior to radiochemical separation. The low pH and high SO_4^{2-} concentration remove competition from most complexing agents, though Ce and La are also coprecipitated (Percival and Martin, 1974). Major anions (Cl^-, PO_4^{3-}, SO_4^{2-}) and cations (Ca^{2+}, Fe^{2+}, K^+, Mg^{2+}, Na^+) are effectively removed with most cations with a charge greater than two and an ionic radius larger than 1 Å coprecipitated (Rogers and Watrous, 1955). Where Bi or lanthanides are present this can lead to a reduction in recovery for some elements, including Ac, with a greater impact from Bi and the lighter rare earths (several mg can have an impact; Sill and Willis, 1964).

Sample preparation of biological samples for Ac analysis has been performed with dry-ashing to prepare samples for gamma analysis (Köhler et al., 2000a; Taylor, 1970) and oven-drying

followed by HNO_3/HF wet-acid digestion to prepare samples for radiochemical separation and alpha spectrometry (Martin et al., 1998).

Further radiochemistry of Ac and associated detection techniques relevant to this thesis is discussed in the sections below. A comprehensive discussion of the radiochemistry of Ac is out of scope in this thesis and comprehensive reviews of the available published data and methods can be found in Deblonde et al. (2021) and Stevenson and Nervik (1961).

4.1.4 Actinium separation methods

There are a variety of published methods for Ac separation, some with a focus on separation of ^{227}Ac in environmental samples (Dulaiova et al., 2013; Guérin et al., 2022; ISO, 2023; Martin et al., 1995), while others are aimed at separation of ^{225}Ac as a medical isotope (Aliev et al., 2014; Ostapenko et al., 2015). Of these, the five most recently published methods all use DGA® ion chromatography resin[34], with TRU® resin after an initial DGA® separation used to remove REEs in the Ostapenko et al. (2015) and Aliev et al. (2014) methods. The Dulaiova et al. (2013) method was selected for this thesis as a relatively rapid and straightforward method that had been applied to environmental samples.

Section 4.2 Detection Techniques

Decay counting techniques are commonly employed for a range of environmental radionuclides, particularly where the half-life is shorter than a few thousand years. Although significant advances have been made in recent years[35] using mass spectrometric techniques for measurement of shorter-lived radioisotopes, decay counting techniques often have advantages over traditional chemical analysis techniques for several reasons. Gamma spectrometry, for example, allows non-destructive testing of samples or reference materials and has often been used to assess the efficiency of chemical testing techniques for this reason. Gamma spectrometry has also been used for analysis of ^{227}Ac in environmental samples (e.g., Alharbi and Akber, 2017; Rekha et al., 2006). However, the minimum detection limits (MDL) are relatively high, and may often be unsuitable for the required purpose, e.g., testing for compliance with the IAEA recommended exemption limit of an activity concentration of 0.1 Bq g^{-1} for ^{227}Ac (IAEA, 2014c). Actinium-227 is often measured indirectly using alpha

[34] Note that the ISO (2023) method appears to be based on the Guérin et al. (2022) technique for radiochemical separation.

[35] e.g., estimated MDL for MC-ICP-MS for ^{227}Ac measurement is ~0.3 mBq g^{-1} (Kayzar and Williams, 2015; Rolison et al., 2017).

spectrometry of the alpha emitting progeny (Geibert and Vöge, 2008; ISO, 2023; Martin et al., 1995), although scintillation counting, and mass spectrometric techniques have also been used. For example, the activity concentration of ^{227}Ac has been inferred from that of ^{223}Ra, after measurement of ^{223}Ra progeny using a ZnS scintillation detector connected to a delayed coincidence counting system (Geibert et al., 2008; Moore and Arnold, 1996). Liquid Scintillation Counting (LSC), with alpha/beta discrimination, has also been used for measurement of ^{227}Ac (Eriksen et al., 2012; Kossert et al., 2015), however, these studies were not focussed on environmental samples and no tracer was used. LSC has been suggested as a technique capable of achieving an MDL comparable to alpha spectrometry for direct measurement of ^{227}Ac (Douglas et al., 2016). In addition, mass spectrometric techniques have also been used to measure ^{227}Ac (e.g., MC-ICP-MS by Kayzar and Williams, 2015). Aside from Martin et al. (1998) who used alpha spectrometry, all references to the ^{227}Ac measurements in biological materials by other authors cited in this thesis refer to evaluations based on gamma spectrometry determination, with limited sample preparation (Campbell et al., 1956; Köhler et al., 2000a; Newton and Brown, 1974; Summerton, 1992a; Taylor, 1970).

Alpha spectrometry, beta counting, mass spectrometry, and LSC require destruction of the sample and chemical separation of the radionuclide of interest. The main advantage of alpha spectrometry and LSC are that they can achieve MDLs far below those of other techniques for isotopes with short half-lives (see Chapter 3, Section 3.2.1). Although the MDL for mass spectrometric techniques (e.g., Kayzar and Williams, 2015) is similar to those achievable using decay counting methods, such methods are often substantially more expensive. Martin et al. (1998) estimated a detection limit of 1 mBq kg^{-1} wet weight for flesh of various animal species is required to measure ^{227}Ac CRs reliably in the ARR[36]. LSC (alpha and beta counting) and alpha spectrometry are the only two possible decay counting techniques that could potentially achieve measurements at this level.

As with measurement of ^{231}Pa, selection of an appropriate tracer isotope is important. For Ac there are only six isotopes with a half-life greater than a few minutes (Table 4-1) and the availability, half-life and decay properties make the alpha emitting isotope ^{225}Ac the optimal

[36] In the same paper it was also estimated that an MDL of 0.05 mBq L^{-1} would be needed for freshwater samples in the study region.

choice as a tracer isotope for ^{227}Ac studies. For samples where preconcentration, separation of Ac and preparation of an Ac 'source' [37] takes days to weeks, ^{225}Ac is the only practical choice.

Table 4-1 Isotopes of Ac with t½ >10 minutes.

Isotope[a]	^{224}Ac	^{225}Ac	^{226}Ac	^{227}Ac	^{228}Ac	^{229}Ac
t½	2.78 hr	10.0 d	29.4 hr	21.8 yr	6.15 hr	62.7 min

[a] ^{224}Ac, ^{226}Ac and ^{229}Ac data taken from (Fry and Thoennessen, 2013).

The tracer isotope used can have implications in how different measurement techniques can perform as the tracer may require a different radiation counting method and can introduce radioactive progeny that need to be taken into consideration.

In alpha decay, alpha particles are emitted with discrete energies, the energy resolution of the measurement technique will determine how effective chemical separation of radioactive isotopes, both in the sample matrix and added with the tracer, need to be. High-resolution alpha spectrometry provides better discrimination based on alpha energy, potentially allowing for less complete separation of alpha-emitting radioisotopes compared to LSC, if the emission energy is sufficiently different (usually >100 keV) from the analyte of interest.

Unlike alpha decay, the electrons emitted in beta decay have a continuous energy spectrum up to a maximum energy. As such, resolving a spectrum with multiple beta energies is quite challenging. With a maximum energy from ^{227}Ac beta decay of 44.8 keV, interference in the spectrum from radionuclides with higher maximum energy beta emissions is virtually guaranteed, this makes good separation from other beta emitting isotopes essential for any beta counting technique for ^{227}Ac (e.g., LSC).

The most suitable tracer isotope for ^{227}Ac analysis, ^{225}Ac, has a complex decay chain (Figure 1-4). Owing to rapid ingrowth of ^{225}Ac progeny which have overlapping alpha and beta spectra to ^{227}Ac and progeny, decay of ^{225}Ac and progeny to a negligible activity, after measurement for chemical recovery, is therefore necessary for low-level analysis of ^{227}Ac by alpha or beta counting. For this thesis, LSC (Section 4.2.1) and alpha spectrometry with adaption of a micro-precipitation technique for source preparation (Section 4.3) were investigated as potential techniques for measurement of ^{227}Ac at the ultra-low levels anticipated.

[37] Sample extracts prepared for analysis using decay counting techniques, including alpha spectrometry, are commonly referred to as a 'source', and this terminology is used throughout this chapter.

4.2.1 Liquid Scintillation counting

Compared to alpha spectrometry, LSC has the advantages that both alpha and beta events can be measured simultaneously on the same sample and with faster preparation time for counting (e.g., Jia and Jia, 2012). Advances in background reduction and pulse processing for LSC have seen it approaching parity with alpha spectrometry in achieving low detection limits in recent years (L'Annunziata, 2012; L'Annunziata and Kessler, 2012). LSC was investigated as a possible detection technique for ^{227}Ac as the high counting efficiency of LSC (up to 100% for alpha decays) can provide a significant advantage over that for alpha spectrometry measurements (L'Annunziata, 2012; L'Annunziata and Kessler, 2012). Thus, with the five short-lived alpha emitting progeny of ^{227}Ac this can potentially be 500%. (Kossert et al., 2015). An increased counting efficiency may be achieved by including the beta decays in the decay chain (^{223}Fr, ^{211}Bi and ^{207}Tl), however, the substantially higher background in the beta spectrum can also lead to an overall increase on the limit of detection.

4.2.2 Alpha spectrometry

Alpha spectrometry is a decay counting technique that involves the counting of alpha particles. There are several types of detectors used in alpha spectrometry, with the most prevalent being ion-implanted silicon surface semi-conductor detectors. This is because semi-conductor detectors have a low intrinsic background (10^{-5} – 10^{-6} counts per second), a high resolution enabling differentiation of alpha particles from different radionuclides at relatively low energy differences (typically 30–40 keV at FWHM), and a low sensitivity to beta and gamma radiation (Vajda et al., 2012). The inherent counting efficiency of semi-conductor detectors is 100%, however, in practice this is dictated by the counting geometry of sources prepared for alpha spectrometry. The energy of an alpha particle is converted to a voltage pulse, digitised through an analogue-to-digital (ADC) converter and an alpha particle spectrum can be realised by a multi-channel analyser (MCA). Resolution of the alpha peaks in the alpha particle spectrum is influenced by self-absorption within a prepared source and by interactions with particles between the alpha source and the detector. Full-Width-Half-Maximum (FWHM), representing the energy range of an alpha peak's full energy width at half the maximum height is typically used to assess resolution of an alpha spectrum. To minimise self-absorption complex radiochemical separation procedures are generally required for alpha spectrometry, with the sample prepared as a thin layer of the purified element (the source) and mounted immediately in front of the detector for counting.

The primary methods for preparing sources for alpha spectrometry are electrodeposition and micro-precipitation. Electrodeposition involves deposition of radionuclides onto a metal planchet from an electrolytic solution (Sawant et al., 2019). In micro-precipitation radionuclides are precipitated from solution, usually with a carrier, and the precipitate mounted on a membrane filter (e.g., Kurosaki et al., 2017; Sill and Williams, 1981). The recently published standard for measurement of ^{227}Ac in water (ISO, 2023) details the electrodeposition (based on Talvitie, 1972) and coprecipitation methods for source preparation.

Electrodeposition can be prone to problems that lead to low recovery (Luskus, 1998) and can be quite complex (Ko, 2020; Krmpotić et al., 2018). The electrodeposition method cited in ISO (2023) is based on a method that was developed for actinides (Am, Pu, Th and U; Talvitie, 1972). Using a similar method for Ac gives recoveries of ~30%, however, replacing the $(NH_4)_2SO_4$ electrolyte with a dilute HNO_3/propanol mix can yield recoveries of ~100% (Bojanowski et al., 1987). Micro-precipitation methods are frequently preferred over electrodeposition as they are often less time-consuming, require simpler equipment and show better reproducibility (Kurosaki et al., 2017; Sawant et al., 2019). Micro-precipitation has been used for preparation of ^{227}Ac sources for alpha spectrometry, however, these methods have employed coprecipitation with lanthanide fluorides which requires the use of conc. HF (e.g., Dulaiova et al., 2013; Groska et al., 2016; Guérin et al., 2022; ISO, 2023). An aim of this thesis was to avoid using HF where possible for safety considerations.

4.2.3 Separation chemistry with DGA® resin

The selected method was adopted from Dulaiova et al. (2013) and is detailed in Appendix F, Section F-4. To summarise, the method involves sample preconcentration using $PbSO_4$ coprecipitation, followed by ion chromatography with DGA® resin (50–100 µm particle size). Major anions and cations remain in solution while most other metals, including Ac, coprecipitate with $PbSO_4$. The $PbSO_4$ precipitate is dissolved in 4 M HCl and Fe added to aid retention of Ac on the resin. Actinides and Fe are retained (Dulaiova et al., 2013; Horwitz et al., 2005). An additional 4 M HCl rinse is followed by a 3 M HNO_3 rinse to remove Fe and traces of alkaline earth elements, then Ac is eluted in 2 M HCl. Actinides and Th are retained on the resin throughout the procedure.

The effectiveness of the dry-ashing and $PbSO_4$ coprecipitation and preconcentration techniques at removing the bulk sample matrix has been detailed in previous sections (see Chapter 3, Section 3.6.1, and Section 4.1.3 for dry-ashing and $PbSO_4$ coprecipitation, respectively). Horwitz et al. (2005) demonstrated the effectiveness of the DGA® resin at separating a range

of trace metals (including Pb, and therefore ^{210}Pb) and radioactive elements (including Ra, Th and U) from spiked solutions. In addition, the effectiveness of the DGA® resin at separation of Ac from alpha emitting isotopes of ^{226}Ra, ^{228}Th, and progeny, and ^{210}Po in geological samples was assessed (Dulaiova et al., 2013).

Given the demonstrated effectiveness of the $PbSO_4$ coprecipitation and the DGA® resin at removing major anions and cations, and trace metals, separation of ^{227}Ac from stable elements was not of concern. Despite similar evidence supporting the separation of Ac from radioactive isotopes, further investigation of the degree of separation for key radionuclides was considered necessary. This was owing to the requirement to separate low activities of ^{227}Ac from a large sample mass. Up to 100 g dry weight was estimated to be required for biota samples depending on sample type. Activity concentrations of other radionuclides measured in similar samples were expected to be orders of magnitude higher than ^{227}Ac (Doering and Bollhöfer, 2016a; Martin et al., 1998). Therefore, higher decontamination factors than had been demonstrated with the Dulaiova et al. (2013) method were likely to be needed.

As noted above for beta counting by LSC, the low energy beta emission of ^{227}Ac almost guarantees other beta emitting radioisotopes present will cause interference (Section 4.2). Better resolution can be achieved with LSC for alpha emissions and substantially better with alpha spectrometry. As such spectra of relevant isotopes including ^{225}Ac, ^{227}Ac, ^{226}Ra, ^{228}Th and progeny were modelled to assess potential overlapping peaks in alpha spectra and to identify the key radionuclides requiring a high degree of separation. The tracer isotope, ^{225}Ac was included as well as NORM isotopes ^{226}Ra and ^{228}Th. These latter two radionuclides will be present in the sample matrix and could cause interference for ^{227}Ac analysis owing to their relatively long half-lives, compared to ^{227}Ac, and short-lived progeny.

Spectra of ^{225}Ac, ^{227}Ac, and potential interferences from ^{226}Ra, and ^{228}Th and progeny were modelled using the method of García-Toraño (2003). Modelled spectra are shown in Figure 4-1, with Figure 4-2 showing a segment of the spectrum which includes alpha emission from isotopes ^{223}Ra and ^{227}Th used for determining ^{227}Ac activity concentration. The peak fitting parameters were derived from a ^{209}Po spectrum, prepared using lanthanide hydroxide coprecipitation, with no interferences from other alpha emitting isotopes and a peak resolution at FWHM of 32 keV (as an approximate estimate of what could be achieved for ^{227}Ac).

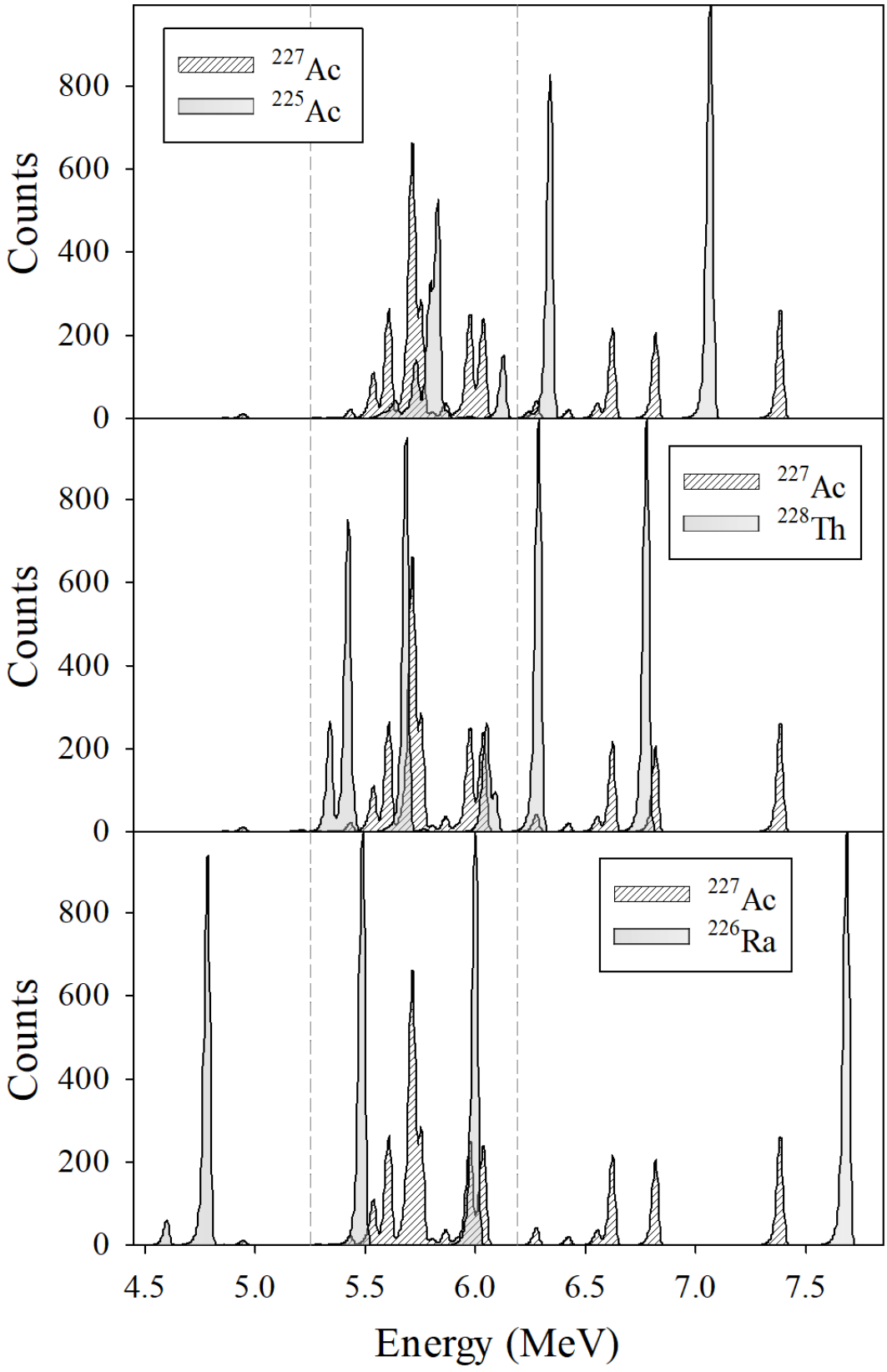

Figure 4-1 Modelled spectra of ^{227}Ac and progeny compared with ^{225}Ac, ^{226}Ra, ^{228}Th and progeny of all isotopes. Alpha emissions from ^{223}Ra and ^{227}Th are bounded by the dotted lines Figure 4-2. A 26% retention of ^{219}Rn was assumed based on ^{215}Po results from Test 4 (see Table 4-4 in optimisation tests below – Section 4.3.2.2.3), whereas retention of ^{222}Rn was assumed to be 100%. As the behaviour may be different owing to the different half-lives of these two isotopes this conservatively reflects the maximum potential interference.

Note that the energy calibration method sets the alpha emission energy at the channel with the highest counts not the upper bound. Many isotopes have not been included in the modelled spectra as they pose no risk of interference (e.g., the maximum alpha emission energy of ^{229}Th is <5.1 MeV).

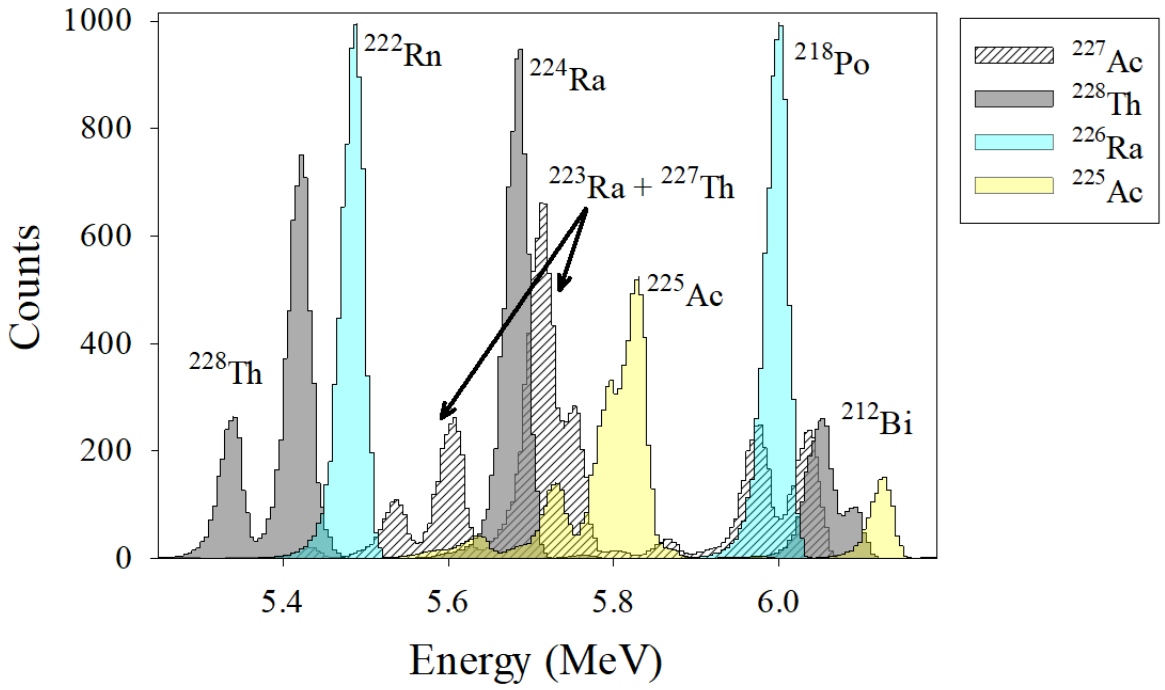

Figure 4-2 Focussed window of modelled spectra showing possible alpha emitting progeny of ^{225}Ac, ^{226}Ra and ^{228}Th in the ^{227}Ac progeny (^{223}Ra and ^{227}Th) region. Labels correspond to the parent isotopes responsible for each peak.

Figures 4-1 and 4-2 show that separation of ^{226}Ra and ^{228}Th is important for analysis of very low-levels of ^{227}Ac, as alpha peaks from decay of their progeny (^{222}Rn and ^{224}Ra) overlap with those of the alpha-emitting progeny of ^{227}Ac (also ^{228}Ra as the parent isotope of ^{228}Th is relevant given the long wait periods require for ingrowth of ^{227}Ac progeny for best detection limits). The figures also show that the decay of ^{225}Ac to negligible levels is required. At low counts, it will be difficult to attribute counts to ^{227}Ac progeny or interfering isotopes owing to the inability to perform peak fitting which makes effective separation particularly important.

Although source preparation for alpha spectrometry can provide additional chemical separation (e.g., Medley et al., 2025; Sill, 1987), Ra may, and Th will, coprecipitate with lanthanide hydroxides which was the method planned for alpha source preparation. Testing of the Dulaiova et al. (2013) method for effectiveness of separation of Ac from Ra and Th was therefore undertaken. Although the primary isotopes of interest were ^{226}Ra and ^{228}Th, using a ^{229}Th standard solution in the tests allowed ^{229}Th and ^{225}Ra to be used as proxies, with ^{225}Ac present

as a tracer for Ac chemistry. Separation of Ac was therefore undertaken on a ^{229}Th standard solution and ^{225}Ra and ^{229}Th activity concentrations relative to that in the initial solution were measured in the Ac fraction. Alpha spectrometry was used for ^{229}Th analysis after spiking with ^{232}U (in equilibrium with ^{228}Th), radiochemical separation with UTEVA® resin, and electrodeposition using a method based on Horwitz et al. (1992) (Appendix F, Section F-3). Breakthrough of Th was determined to be 0.06±0.02% of the ^{229}Th in the initial solution.

The ^{225}Ra activity in the Ac fraction was determined using the method of Medley et al. (2005). This method uses a $BaSO_4$ coprecipitation step to separate Ra from other radionuclides, however, ^{225}Ac was not completely separated. To determine the ^{225}Ra activity concentration, a series of nine measurements of the source prepared for alpha spectrometry were undertaken from 1–41 days after Ra separation. This allowed determination of the upper limit for ^{225}Ra activity breakthrough, based on the differential rates of decay for ^{225}Ra and ^{225}Ac after accounting for ingrowth of ^{225}Ac from ^{225}Ra. Results indicated the Dulaiova et al. (2013) method leads to Ra breakthrough of <0.025%. Actual Ra breakthrough will likely be substantially lower than this, as Ra and other alkaline elements are not expected to be retained on the DGA® resin in the 4 M HCl load solution and any remaining traces would be largely removed with the 3 M HNO_3 rinse (Dulaiova et al., 2013).

4.2.3.1 ^{225}Ac tracer preparation

In some methods for measurement of ^{227}Ac using ^{225}Ac as a tracer for samples are spiked directly with a solution of ^{229}Th in equilibrium with ^{225}Ac (e.g., Geibert and Vöge, 2008; Kayzar and Williams, 2015; Martin et al., 1995). However, for this thesis, the tracer solutions of ^{225}Ac used for sample analysis were chemically separated from ^{229}Th prior to spiking with samples which has also been done in other studies (e.g., Bojanowski et al., 1987). This was done because most samples analysed were expected to have very low activity concentrations of ^{227}Acand thus traces of ^{229}Th were removed as they could potentially interfere with the ^{227}Ac measurement. Based on Th breakthrough of 0.06±0.02% (see above), two stacked DGA® resin cartridges were used for the ^{225}Ac tracer preparation to reduce ^{229}Th to negligible levels for the final measurement of ^{227}Ac in samples. Samples were spiked with the ^{225}Ac tracer solution after weighing and, where possible, prior to any sample preparation being undertaken. Combined sample preparation and radiochemical separation times were long, up to several weeks. This provided another important reason for preparation of purified ^{225}Ac tracer solutions prior to spiking, which was to allow any losses of Ac to be accounted for, and that additional ^{225}Ac produced from decay of ^{229}Th during sample preparation was reduced to negligible levels.

A relatively high activity of ^{225}Ac was needed to ensure that sufficient activity remained after sample preparation for a high precision measurement of the chemical recovery. Actual spike activities ranged from 0.42–8.48 Bq per sample at the time of spiking, leading to a range of 0.23–1.12 Bq ^{225}Ac per sample at the time of Ac separation[38].

As ^{229}Th is retained on the DGA® column after ^{225}Ac separation, an attempt to reuse a column for repeated extraction was made by storing a DGA® column (capped) in 4 M HCl after an initial extraction of ^{225}Ac. After 305 days, ^{225}Ac was extracted again and although recovery was poor (14.6%±0.6%), sufficient activity was extracted for use with a batch of samples. A third extraction of ^{225}Ac was attempted after a further 226 days, however, recovery was negligible and no further attempt to reuse DGA® columns for tracer preparation were made. Excluding the solutions from repeated extraction noted above, five ^{225}Ac tracer solutions were made, with recoveries ranging from 60–100% with an average of 88%.

Chemical recovery of ^{225}Ac tracer solutions was determined using HRGS after allowing secular equilibrium with progeny to be reached (~ 4 hours; Figure 4-3; HRGS method in Appendix H).

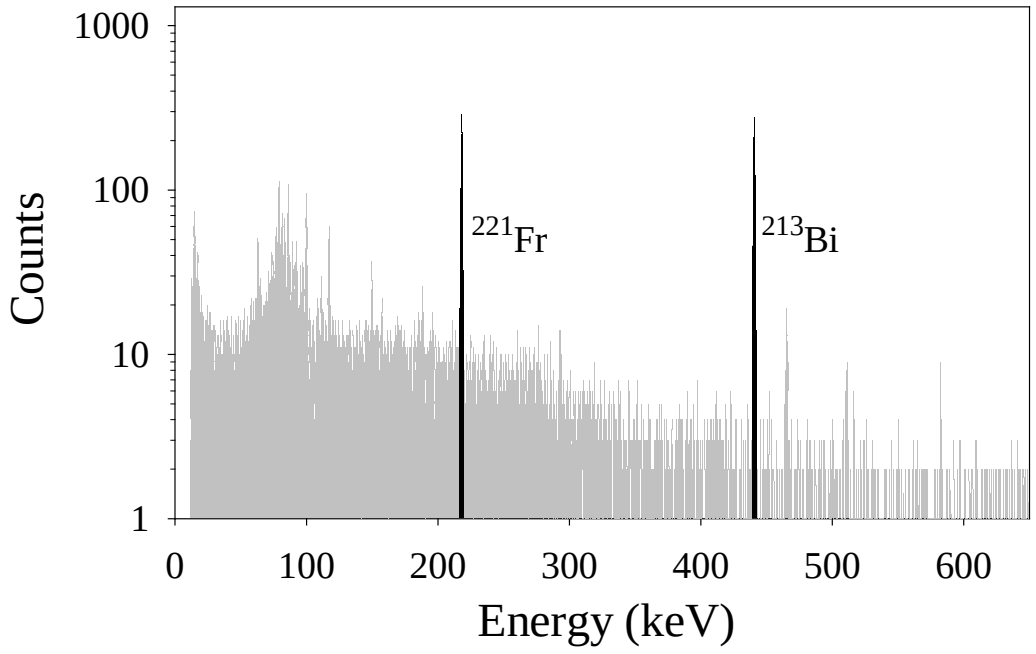

Figure 4-3 Typical HRGS spectrum of ^{225}Ac and progeny in secular equilibrium. The gamma emissions used for activity determination are highlighted (440 keV for ^{213}Bi and 218 keV for ^{221}Fr).

[38] The variation in spike activities is quite large, this is for two reasons: Samples with expected higher activity concentrations of ^{227}Ac (e.g., soils) were spiked with higher activities of ^{225}Ac to prevent ingrowth of ^{227}Ac progeny influencing the recovery determination. There was also some variation in the chemical recovery for tracer preparation, with ^{225}Ac extracted from a higher than typically required activity of ^{229}Th to ensure sufficient activity for the batch size planned if tracer recovery was low.

Section 4.3 Experimental work

4.3.1 Liquid Scintillation Counting

Preliminary assessment of LSC was undertaken to determine the suitability of LSC for low-level measurement of ^{227}Ac. Counting conditions were optimised from counting blanks and standards spiked with surrogate alpha- (^{241}Am) and beta- (^{90}Sr) emitting radioisotopes. Standards were prepared in HDPE vials in varying scintillation cocktail/acid combinations and counted with a Tri-Carb® 3100TR LSC instrument. Blank samples were prepared in both glass and HDPE vials, and repeated measurements were made over 93 days to assess the background count rate and potential variations over time. Blank measurement showed alpha count rates increased over time in HDPE vials making them unsuitable for low-level measurement where long ingrowth periods are required (likely owing to Rn infiltration, e.g., Sanchez-Cabeza and Pujol, 1995). Standards prepared to assess peak resolution of the LSC spectra and approximate MDLs therefore used glass vials. Aliquots of a ^{227}Ac solution in equilibrium with progeny were mixed with Ultima Gold AB™ and Optiphase HiSafe 3™ scintillation cocktails to prepare these standards, with MDLs of 0.1 mBq and 6 mBq determined for a one-day count period for alpha and beta activity, respectively. The alpha spectrum resolution was better than the beta spectrum for the ^{227}Ac standards, but it was not possible to effectively resolve all individual peaks from the decay chain. Where any of the radionuclides identified above as potential interferences (Section 4.2.3) may be present in the scintillation cocktail they may not be resolved, and it may not even be possible to determine that they are present.

4.3.2 Alpha spectrometry – Source preparation and alpha counting

Source preparation for alpha spectrometry was adapted from a micro-precipitation technique for actinides using $Ce(OH)_3$ coprecipitation and collection of the precipitate on PP filters (Kurosaki et al., 2017). This method required actinides to be chemically separated prior to precipitation with notable necessary features being a robustness to variations in solutions suitable for micro-precipitation, and that HF was not required. This method was tested and refined to optimise it for preparation of sources for alpha spectrometry measurement of ^{227}Ac (see Section 4.3.2.2 below).

4.3.2.1 Alpha spectrometry counting system and efficiency calibration

Alpha spectrometry was carried out with a Canberra Alpha Analyst chamber using Passivated Implanted Planar Silicon (PIPS) detectors (PIPS detector active surface areas were 450 mm^2). Knowledge of the efficiency of the alpha-particle detection system was required to determine the chemical recovery of samples and was determined using a NIST traceable standard disc

(Eckert & Zeigler Analytics) with known activities of ^{238}U, ^{234}U, ^{239}Pu and ^{241}Am. To account for differences in the counting geometries of the standard disc and the filters prepared from micro-precipitation, correction factors were used and determined as per Gascón and Muñoz (2003)[39] and Ruby (1994), assuming an effective filtration area of 2.9 cm^2, with a diameter of 19.2 mm, specified for the polysulfone funnel used to constrain the deposition area on the filters. Alpha counting was undertaken with source-to-detector distances ranging from approximately 5.2 to 9.3 mm, for which counting efficiencies of 17–26% were determined. To minimise absorption of alpha particles between the source and detector, while also limiting alpha recoil contamination of the detector, the counting chamber was pressure regulated (with 12 µg cm^{-2} air absorber) as recommended by Sill and Olson (1970). A 6 V negative potential was also applied to the rear surface of the filter holders to attract positively charged recoil atoms back to the filter (Sill and Olson, 1970). All alpha spectrometry results (from five tests assessing a range of optimisation factors detailed in the following section) were blank corrected with blank signals contributing less than 0.1% of measured activities. The NIST traceable standard disc noted above was also used for energy calibration of the alpha spectrometers.

4.3.2.2 Experimental $Nd(OH)_3$ coprecipitation

Micro-precipitation can be affected by variations in procedural factors such as the mass of the carrier, and volume and temperature of the precipitation solution (Sawant et al., 2019). Accordingly, several tests were conducted to evaluate the sensitivity of the Kurosaki et al. (2017) method to variations and to optimise chemical recovery and peak resolution for ^{227}Ac measurement via alpha spectrometry. The method is summarised in Table 4-2, followed by a description of the optimisation test factors assessed. Two minor adjustments to the Kurosaki et al. (2017) method were made, with the addition of 30% H_2O_2 considered an unnecessary step and removed. An additional wash step was included prior to the 80% ethanol wash to remove traces of alkali soluble interferences. The optimised method is presented following discussion of optimisation tests (Section 4.3.3) and a detailed procedure is in Appendix F, Section F-5.

The seven optimisation test factors (A–G) of the Kurosaki et al. (2017) method assessed were:

A. Solution volume: The solution volume may have an influence on the formation of the precipitate and the size of particles that are formed.

[39] I would like to acknowledge Dr. Stephen Long of ARPANSA for deriving an appropriate mathematical approach to determine the correction factors, and for creating and providing a spreadsheet tool to apply the correction factors used here.

Table 4-2 Kurosaki et al. (2017) method for micro-precipitation of actinides for alpha spectrometry with an optimised version for ^{227}Ac developed for this thesis.

Step		Procedure: Kurosaki et al. (2017)
1	Precipitation solution	Various solutions containing actinides of: U – 20 mL 1 M HCl, Th –20 mL 9 M HCl, Np and Pu – 20 mL of Rongalite[a] solution, Am – 15 mL 4 M HCl
2	Preparation for micro-precipitation	Add 50 µg Ce as $CeCl_3.7H_2O$ solution Add indicator solution: Np, Pu, Th and U – bromocresol purple (pH 5.2–6.8), Am – thymol blue (pH 8.0–9.6) Add[b] 2 mL 30% H_2O_2
3	Micro-precipitation	Add conc. (25–30%) NH_4OH dropwise to colour change
4	Source deposition	Vacuum filter through 0.1 µm pore size PP filter Wash filter with 80% ethanol and air dry

[a] Rongalite solution: 0.04 M sodium formaldehyde sulfoxylate + 0.05 M KF + 0.15 M HCl.

[b] H_2O_2 was added (for most actinides) in the Kurosaki et al. (2017) to make the precipitate visible as it produced a yellow colour. The H_2O_2 was also added for U analysis to convert U(VI) to U(IV).

B. Neutralising agent type: A stronger neutralising agent will reduce the solution volume and therefore speed up the filtration process.

C. pH endpoint for precipitation (by indicator type): Kurosaki et al. (2017) showed that optimal chemical recovery from micro-precipitation varied with the pH endpoint for different radionuclides.

D. The use of a substrate: Although not in the Kurosaki et al. (2017) method, a Ce suspension substrate was employed by Sill (1987) to coprecipitate actinides with lanthanide hydroxides from EDTA solution for alpha spectrometry. Substrate use in that study improved retention of the active precipitate at the filter surface by reducing the rate of filtration, yielding superior recovery and peak resolution.

E. Mass of lanthanide carrier used: An excess mass of lanthanide carrier can impact the resolution, whereas insufficient mass may reduce the chemical recovery.

F. Appropriate peaks for recovery determination using ^{225}Ac as a tracer and to quantify ^{227}Ac with progeny using alpha spectrometry.

G. Distribution of precipitate on the filter: This was not investigated previously, however, uneven distribution of the precipitate on the filter may lead to variations in counting efficiency (Pommé, 2015).

The chemical recovery and alpha peak resolution at FWHM were used to optimise the ^{227}Ac yield. Alpha peak resolution was determined using the peak fitting model of García-Toraño (2003), with one standard deviation assumed to be one channel (or ~3.0–3.5 keV as the channel width for the spectrum energy calibration depended on the detector used).

A total of five tests were conducted to optimise and assess the micro-precipitation technique for preparation of ^{227}Ac for alpha spectrometry, with some tests aimed at optimising several factors. These tests involved varying parameters of the Kurosaki et al. (2017) method, spectral analysis of the alpha peaks and relative recovery of ^{225}Ac, ^{227}Ac and progeny, and autoradiography of prepared filter papers. Owing to the relatively short half-life, two tracer solutions of ^{225}Ac (^{225}Ac-A and ^{225}Ac-B) were prepared fresh for these optimisation and assessment tests using the DGA® radiochemical separation (see Section 4.2.3.1 above; note that one DGA® resin cartridges was used for ^{225}Ac-A but two stacked cartridges were used for ^{225}Ac-B). A tabulated summary of the five tests is shown in Section 4.3.2.2.6 below.

4.3.2.2.1 Test 1: Conditions for coprecipitation of Ac

Test 1 was conducted using Tracer solution ^{225}Ac-A to evaluate variations in several conditions of the coprecipitation step of the method. These were (optimisation test factors A–D):

A. Precipitation solution volume: 1, 2, 5, 10 and 20 mL of 2 M HCl.

B. Neutralising agents – either 28% NH_4OH or 10 M NaOH.

C. pH endpoint for precipitation,

    a. Bromocresol purple (pH 5.2–6.8) or,

    b. Thymol blue (pH 8.0–9.6).

D. Use of a Ce substrate.

The Ce substrate was a suspension of $Ce(OH)_3$ and was prepared as per Sill (1987). The carrier solution for Test 1 was a $Ce(NO_3)_3$ solution and 0.1 mL of solution (50 µg Ce) was used per sample. Evidence of ^{210}Po contamination was identified in the $Ce(NO_3)_3$ used in Test 1 and

$Nd(NO_3)_3$ was used as the carrier solution for subsequent tests. Results from Test 1 are shown in Figure 4-4.

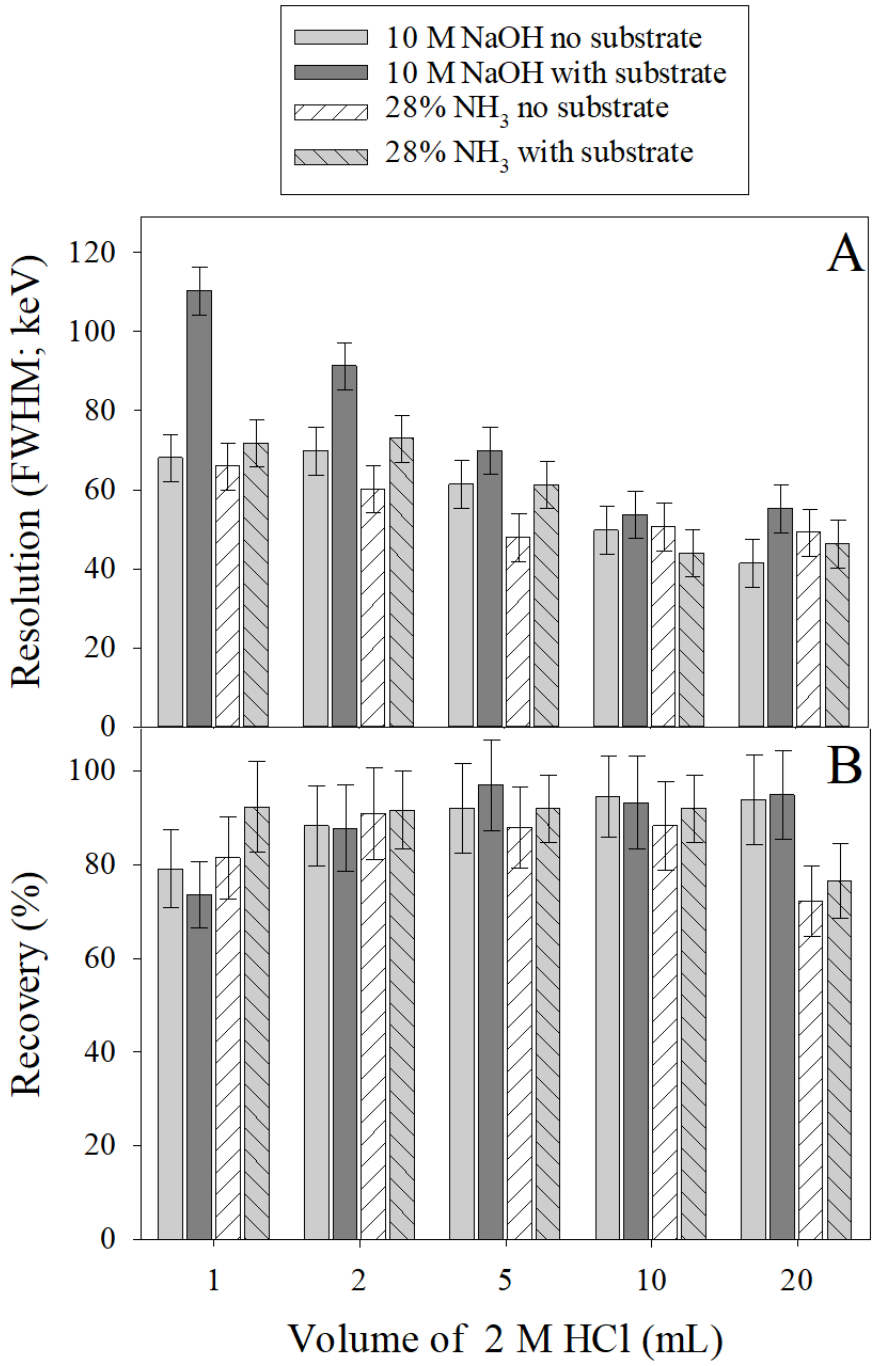

Figure 4-4 Results from Test 1 showing variations in factors affecting the ^{225}Ac alpha-particle spectrum from coprecipitation of ^{225}Ac with $Ce(OH)_3$. Resolution (A) and recovery (B) of filters prepared with varying sample volume, neutralising agent and with or without the use of a substrate. Recovery and resolution were determined using the progeny ^{217}At.

When using 10 M NaOH, all volumes, except for the 1 mL solution, gave chemical recoveries of ~90%. Notably, the 20 mL solution volume using 28% NH_4OH resulted in markedly lower recovery (Figure 4-5). The higher total solution volume, owing to the high volume of

28% NH_4OH required, inhibited the ability to mix the solution without spillage, which may have reduced the efficiency of coprecipitation for this sample. There was little variation in the resultant resolution for samples neutralised with 10 or 20 mL 10 M NaOH or 28% NH_4OH, with or without the use of a Ce substrate. Peak resolution at FWHM decreases with increasing volume of the precipitation solution. The best resolution was obtained from the solution using 10 M NaOH as a neutralising agent, precipitating from 20 mL 2 M HCl and without the use of a substrate. No differences in recovery or resolution were observed for the different pH endpoints. Bromocresol purple indicator, which has the lower pH range of pH 5.2–6.8, was used for subsequent tests to reduce the overall volume of the precipitation solution.

4.3.2.2.2 Test 2: Mass of Nd carrier

Following optimisation of the factors assessed in Test 1, Test 2 used Tracer solution ^{225}Ac-B to determine the optimum mass of the carrier for micro-precipitation (optimisation test factor E). The mass of added Nd was varied from 12.5–75 µg and showed the optimum mass of Nd was 40 µg where resolution was low, and recovery was high (80–100%; see Figure 4-5).

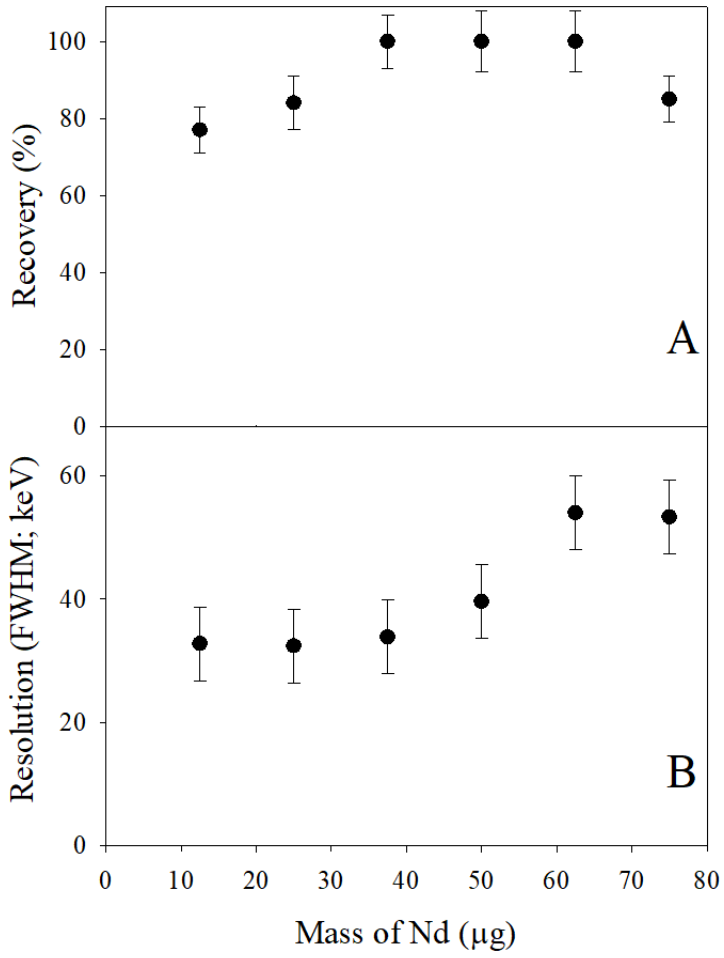

Figure 4-5 Results from Test 2. Chemical recovery (A) and resolution (FWHM) (B) for the ^{225}Ac alpha particle spectrum relative to the mass of Nd used as a carrier for coprecipitation. The ^{217}At peak was used to determine the resolution.

4.3.2.2.3 Test 3: Accuracy of ^{217}At peak for ^{225}Ac recovery determination

Unlike ^{225}Ac, ^{217}Ac yields essentially a single energy peak at 7067 keV that is unaffected by other radionuclides (Figure 4-6).

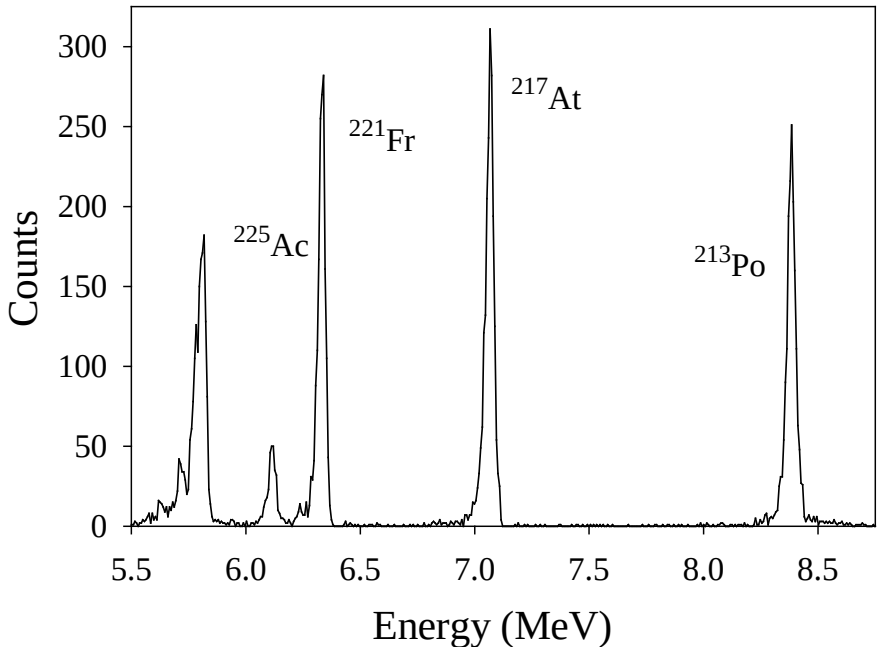

Figure 4-6 The alpha spectrum for ^{225}Ac showing alpha particles that arise from the decay of progeny ^{221}Fr, ^{217}At and ^{213}Po. The 7067 keV peak resolution at FWHM is 37±6 keV. Labels correspond to the parent isotopes responsible for each peak.

Test 3 assessed the reproducibility of the method parameters optimised from Test 1 and 2 and was used to confirm the accuracy of using ^{217}At for recovery determination (optimisation test factor F). To this end, six micro-precipitated filters were prepared from Tracer solution ^{225}Ac-B. The relative activity of ^{221}Fr, ^{217}At and ^{213}Po compared to ^{225}Ac activity was determined from the alpha spectra; these data are shown in Table 4-3. Two measurement uncertainty parameters are given in Table 4-3, one is based on counting statistics only which removes uncertainty components common to each isotope (e.g., uncertainty for tracer activity concentration and detector counting efficiency). This allows direct comparison of the relative activities of the four isotopes as determined from each spectrum. The larger measurement uncertainty values correspond to a combined expanded uncertainty calculation as described in (Kragten, 1994). These larger values are based on all relevant uncertainty parameters (such as recovery of Ac from DGA® separation of the stock solution) and give an indication of the reproducibility of the micro-precipitation technique, with an average chemical recovery of 83±10%. There were no differences (within uncertainty) in the measured activities of ^{225}Ac and progeny on the six filters used to determine the chemical recovery, indicating use of the alpha peak from decay of ^{217}At is suitable for chemical recovery determination of ^{225}Ac.

Table 4-3 Recovery of ^{225}Ac and activity ratios of progeny to ^{225}Ac. Measurement uncertainties are based on counting statistics alone (with all uncertainty components common to each isotope on the filter paper removed) or a full measurement uncertainty where all relevant uncertainty components are included (e.g., recovery of Ac from DGA® separation of the stock solution).

Sample ID	Count time (ks)	^{225}Ac recovery[a] (%; uncertainty based on counting statistics)	^{225}Ac recovery[a] (%; expanded combined uncertainty)	Activity[b] relative to ^{225}Ac: ^{221}Fr	Activity[b] relative to ^{225}Ac: ^{217}At	Activity[b] relative to ^{225}Ac: ^{213}Po
1	15.0	96±4	96±13	1.07±0.06	1.05±0.06	0.96±0.06
2	8.0	88±6	88±14	0.99±0.08	0.95±0.08	0.90±0.08
3	13.2	64±4	64±10	0.99±0.06	0.92±0.06	0.92±0.06
4	11.1	83±5	83±13	1.03±0.07	1.03±0.07	1.04±0.07
5	10.9	83±5	83±13	0.98±0.07	1.00±0.07	0.95±0.07
6	20.0	85±4	83±13	1.06±0.05	0.99±0.05	0.99±0.05
Average				1.02±0.06	0.99±0.09	0.96±0.09

[a] ^{225}Ac recovery has been corrected for alpha decay of ^{213}Bi assuming equilibrium with ^{217}At, and that 1.9% of all ^{213}Bi decays contribute to the peak corresponding to ^{225}Ac.

[b] uncertainty based on counting statistics only.

Based on these results, chemical recovery, and peak resolution were estimated using the alpha peak from decay of ^{217}At for further tests; these results also validated results for optimised parameters from Tests 1 and 2.

4.3.2.2.4 Test 4: Suitability of alpha peaks from decay of ^{227}Ac progeny for ^{227}Ac activity determination

Test 4 was undertaken to determine the typical MDL that could be achieved for measurement of ^{227}Ac through assessing optimum peaks to quantify ^{227}Ac with progeny using alpha spectrometry (also optimisation test factor F). Although the MDL is a function of the uncertainty of the blank signal (Currie, 1968) and therefore independent of the sample measurement, when converted to an activity concentration the MDL will vary with each sample. With the optimised method for Ac measurement by alpha spectrometry using an ^{225}Ac tracer, the MDL expressed as an activity concentration is affected by:

- Background counts and count time (influencing the counts and thus uncertainty of the blank signal),
- Alpha detector efficiency,
- Chemical recovery,
- Activity of ^{225}Ac tracer added to the sample corrected to the time of measurement, and
- Relative ingrowth of ^{227}Ac progeny at the time of measurement.

Using the optimised method from the previous tests and after separation of ^{227}Ac from progeny using the Dulaiova et al. (2013) method, 12 micro-precipitated filters were prepared (no ^{225}Ac tracer solution was added). These filters were counted after allowing sufficient time for ingrowth of ^{227}Ac progeny to achieve a measurement uncertainty <2.5% on counting statistics for each peak with a count time of 15 ks (after approximately 20 days ingrowth time; the expected activity of each isotope was determined using the Bateman equations). A typical ^{227}Ac spectrum is shown in Figure 4-7.

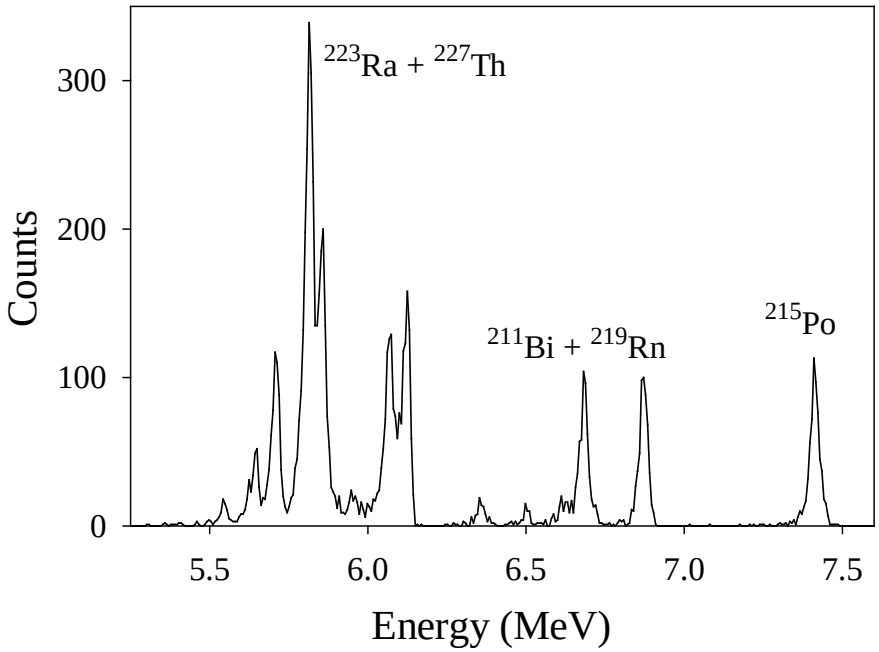

Figure 4-7 An ^{227}Ac alpha-particle spectrum showing alpha-particles that arise from the decay of progeny ^{227}Th, ^{223}Ra, ^{219}Rn, ^{211}Bi and ^{215}Po. The 7067 keV peak of ^{217}At was used to determine resolution for this sample from an earlier count (see Figure 4-6) and was 33±6 keV FWHM. Labels correspond to the isotopes responsible for each peak.

The ^{227}Ac recovery was determined separately from the yields of ^{227}Th and ^{223}Ra combined[40], ^{211}Bi and ^{219}Rn combined[40] and ^{215}Po, using the alpha detector counting efficiency, peak counts and calculated activity from ingrowth after ^{227}Ac separation (Table 4-4).

Table 4-4 Recovery of ^{227}Ac as determined by ^{223}Ra and ^{227}Th (combined) and expected activity versus measured activity of ^{223}Ra progeny ^{211}Bi and ^{219}Rn (combined), and ^{215}Po.

Sample ID (counting statistics only)	Count time (ks)	Recovery for ^{223}Ra and ^{227}Th combined (%)		Actual:Expected activity	
		(uncertainty based on counting statistics only)	(expanded combined uncertainty)	^{211}Bi and ^{219}Rn combined	^{215}Po
1	11.9	74±2	74±9	0.31±0.02	0.32±0.03
2	12.2	100±2	100±12	0.36±0.02	0.33±0.02
3	60.0	99±1	99±12	0.25±0.01	0.23±0.01
4	10.5	85±2	85±10	0.22±0.02	0.22±0.02
5	14.9	100±2	100±12	0.25±0.01	0.20±0.02
6	15.0	86±2	86±10	0.29±0.01	0.23±0.02
Average ± two standard deviations			0.91±0.21	0.28±0.10	0.26±0.10

The actual activities of ^{211}Bi and ^{219}Rn combined and ^{215}Po measured were approximately three times lower than expected based on the Ac recoveries determined from the combined peak counts of ^{227}Th and ^{223}Ra. The lower activities for radionuclides below ^{223}Ra in the decay chain suggest that there is a high loss of ^{219}Rn from the filters. This is far greater than the loss of 2±3% of Rn Geibert and Vöge (2008) from electroplated sources determined by Geibert and Vöge (2008). Although not directly measured, the spectra shown in Martin et al. (1995) and Bojanowski et al. (1987) also suggest much lower loss of ^{219}Rn from electroplated sources than from the micro-precipitated filters used for this study. This highlights that only the alpha peaks from decay of ^{227}Th and ^{223}Ra can be reliably used to determine the activity of ^{227}Ac with this method. Maximum ingrowth of ^{227}Th and ^{223}Ra is achieved 178 days after Ac separation with

[40] The counts were combined for recovery determination as it was not possible to resolve individual peaks sufficiently in the alpha-particle spectrum.

activities equivalent to 98.6% (^{227}Th) and 98.5% (^{223}Ra and progeny) of the ^{227}Ac activity determined using the Bateman equations.

The MDL is calculated using Equation A-3 (Section 6.6, Section A-1) and setting the net count rate of ^{227}Th and ^{223}Ra (N_{TR}) to the uncertainty of the blank signal multiplied by a constant '*k*', which for the 'paired-observation' method used throughout this thesis was equal to 4.65 (Currie, 1968). In this way, the MDL as a function of the uncertainty of the blank signal is converted to an activity concentration and is unique to each sample measurement. For a detailed discussion of MDL determination for both alpha spectrometry and AMS used for sample analysis in this thesis refer to Section 6.6, Section A-3.

To estimate a typical MDL for alpha spectrometry of ^{227}Ac, several assumptions were applied, i.e., 80% chemical recovery, an ingrowth period of 178 days, and that ^{225}Ac has decayed to negligible levels. Only the ^{227}Th and ^{223}Ra peaks were used with a blank count rate of 10 counts per day[41] in the ROI and a detection efficiency[42] of 17% giving a MDL of 0.6 mBq for a one--day count. The MDL for a one-week count period reduces to 0.1 mBq.

4.3.2.2.5 Test 5: Uniformity of $Nd(OH)_3$ precipitate deposition on filters

The radionuclide activity distribution on sources prepared for alpha spectrometry can lead to differences in the counting efficiency for alpha counting (e.g., if concentrated in the centre or on the edges; Pommé, 2015). Test 5 involved the use of autoradiography[43] to assess the uniformity of the lateral/horizontal distribution[44] of Ac on the filters to determine if additional

[41] Based on results from the average of analytical blank samples prepared and measured for this thesis.

[42] This refers to the most common configuration of the alpha spectrometry system used for the present measurements at the Queensland Health Radiation and Nuclear Science laboratory. See Section 4.3.2.1 above for details of the system.

[43] I am indebted to Mr. N. Howell who carried out the autoradiography measurements at the Australian Nuclear Science and Technology Organisation Laboratories. Briefly, filters were affixed to a flexible plastic substrate and then sealed under a layer of Mylar film (2.5 mg cm^{-2}) as a surface barrier to protect the screen from contamination. The samples were placed into an X-ray cassette (GE Healthcare) along with an imaging phosphor (IP) plate (BAS-SR 2025, Fuji Photo Film Co.) and allowed to expose for 168 hours. A multi-modal laser scanner (FLA7000, GE Lifesciences) was used to read the events that had accumulated on the IP plate. A radial profile was created for each filter, using the Radial Profile Plot plugin (Baggethun, 2009) for the ImageJ image processing program (Rasband, 1997-2018), by plotting the integrated intensities around concentric circles as a function of their radius from the centre of the filter. The profiles for each filter were normalised to a percentage of the maximum intensity and averaged to create an integrated profile to demonstrate the distribution of Ac and progeny across a filter.

[44] Note that the peak resolution can be used as a proxy to determine the vertical Ac activity distribution or penetration depth of $Ac/Nd(OH)_3$ on the filters.

uncertainty contributions needed to be taken into consideration for determining the chemical recovery of sources prepared for alpha counting (optimisation test factor G).

Autoradiography images are shown for six of the filters prepared from the ^{227}Ac tracer solution in Figure 4-8. The combined integrated radial profile of the autoradiography images of the six samples is shown in Figure 4-9. For the counting geometry used there was a difference in the counting efficiency of 5.3% determined for a point source (i.e., radius set to 0 mm) compared with a radius of 11 mm (the estimated maximum possible edge of the active surface area). The gradual and small decline in relative emission intensity as a function of radius as shown in Figure 4-9 is therefore expected to have a minimal impact on the counting efficiency for this method. Consequently, additional uncertainty corrections to determine the chemical recovery of sources prepared for alpha counting using this method were not deemed necessary.

4.3.3 Results of method development and conclusions from experimental work

Conclusions from the optimisation tests were:

- The 20 mL 2 M HCl directly from ^{227}Ac separation using the Dulaiova et al. (2013) DGA® resin separation method was a suitable precipitation solution,
- 10 NaOH was suitable for pH adjustment and reduced overall sample volume, leading to faster filtration,
- There were no differences in method performance with pH endpoint. Bromocresol purple was deemed superior as the lower pH at colour change requires a lower volume for pH adjustment and will allow faster filtration.
- The alpha peak from decay of ^{217}At was suitable for recovery determination using ^{225}Ac,
- Only alpha peaks from decay of ^{223}Ra and ^{227}Th were suitable for activity determination of ^{227}Ac, other progeny were not suitable, and
- The distribution of precipitate on the filter paper was sufficiently uniform such that no additional uncertainty contributions were required.

The optimised method is shown in Table 4-6.

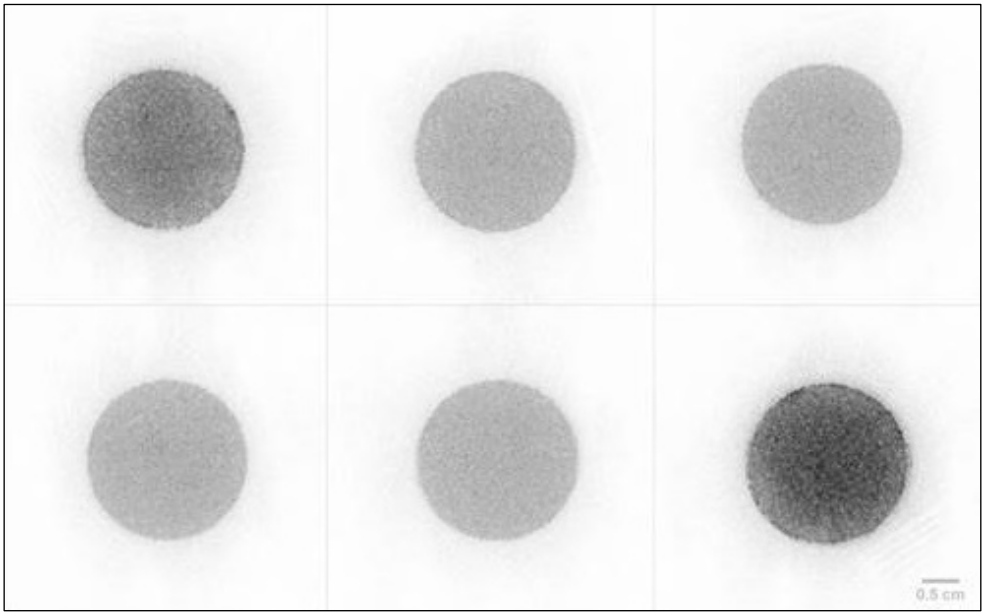

Figure 4-8 The spatial distribution of ^{227}Ac coprecipitated with 50 µg Nd as $Nd(OH)_3$ on six 0.1 µm pore size filters as measured by autoradiography. Samples were exposed to an imaging phosphor plate for 168 hours and exposure was started 55 days after radiochemical separation.

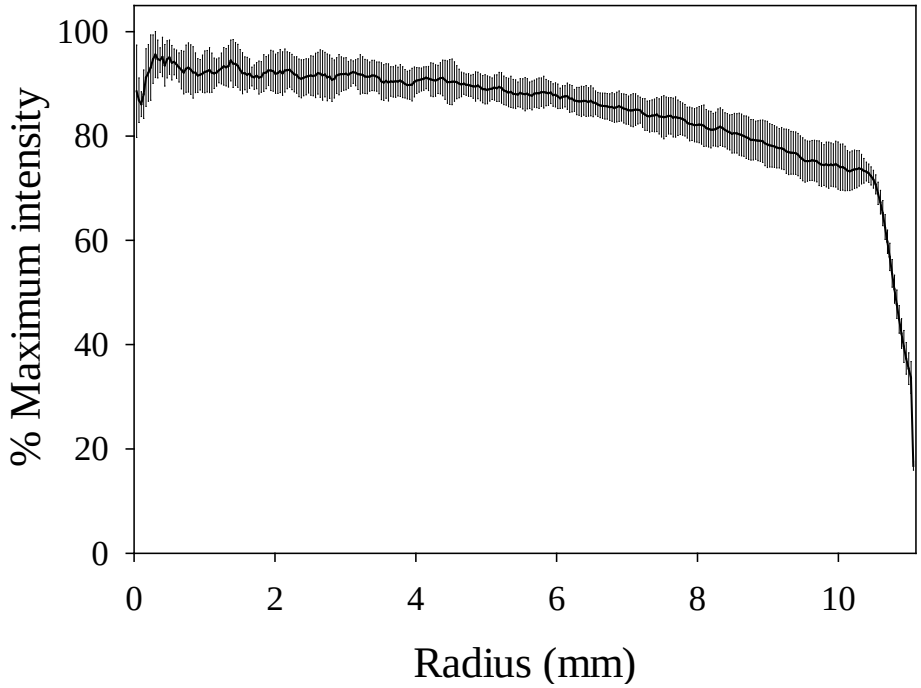

Figure 4-9 Plot of integrated radial intensities as a function of the radius of the filter for the emissions from radioactive decay of ^{227}Ac and progeny as measured by autoradiography. Samples were coprecipitated with 50 µg Nd as $Nd(OH)_3$ on 0.1 µm pore size (polypropylene) filters. Intensities have been normalised to a percentage of the maximum intensity and sample measurements combined to better illustrate the distribution of ^{227}Ac precipitate across the filters. Data presented as mean and one standard deviation (n=6). Samples were exposed to an imaging phosphor plate for 168 hours and exposure was started 55 days after radiochemical separation of ^{227}Ac.

4.3.3.1.1 Summary of optimisation tests

Table 4-5 Summary of tests conducted for optimisation assessment of ^{227}Ac separation and analysis using alpha spectrometry.

Test ID	Tracer type[a]	Purpose of test	Test/procedure description	Test outcome and conclusions
1	^{225}Ac (Tracer ^{225}Ac-A)	Assess conditions for coprecipitation of Ac with lanthanide hydroxide for optimal chemical recovery and peak resolution	50 µg Ce carrier used Parameters varied were: Precipitation solution volume 1, 2, 5, 10 and 20 mL 2 M HCl Neutralising agents – either 28% NH_4OH or 10 M NaOH pH endpoint for precipitation – Bromocresol purple (pH 5.2–6.8) or thymol blue (pH 8.0–9.6) With and without the use of a Ce substrate	$Ce(NO_3)_3$ used to prepare Ce solution contaminated with ^{210}Po, use Nd for future tests. Peak resolution and chemical recovery comparison used to indicate optimum parameters i.e., 20 mL 2 M HCl, 10 M NaOH neutralising agent, bromocresol purple indicator without the use of a substrate.
2	^{225}Ac (Tracer ^{225}Ac-B)	Determine optimum mass of Nd carrier	Various masses of Nd carrier (12.5–75 µg) were tested	Optimum mass of Nd carrier was 40 µg (determined from peak resolution and chemical recovery comparison).
3	^{225}Ac (Tracer ^{225}Ac-B)	Accuracy of alpha peak from decay of	Determination of chemical recovery using ^{225}Ac and progeny to assess	Decay of ^{217}At was suitable for determining chemical recovery of ^{225}Ac.

Test ID	Tracer type[a]	Purpose of test	Test/procedure description	Test outcome and conclusions
		^{217}At for recovery determination and reproducibility of the method	reproducibility and accuracy of ^{217}At alpha peak for recovery determination.	Typical chemical recoveries averaged 83% with a standard deviation of 10%.
4	^{227}Ac	Determine suitable alpha particle emissions for ^{227}Ac analysis and MDL for ^{227}Ac	Assessment of the optimised method to determine reliability of peaks to analyse for alpha spectrometry and estimate MDL for ^{227}Ac	A combination of ^{223}Ra and ^{227}Th peaks were optimal for analysis of ^{227}Ac. Alpha particle emissions of ^{223}Ra progeny were unsuitable, likely owing to high, and variable, radon (^{219}Rn) emanation, with counts from progeny only 26% of expected counts (based on ^{215}Po results).
5	^{227}Ac	Assessment of lateral distribution of Ac on the filters	Autoradiography of ^{227}Ac filters	Lateral distribution was nearly uniform, with decreased activity concentration at the edges. Minor irregularities in lateral distribution will have a negligible effect on efficiency determination.

[a] ^{227}Ac solution calibrated in-house using high-resolution gamma spectrometry, with NIST traceable calibration standards.

Table 4-6 Kurosaki et al. (2017) method for micro-precipitation of actinides for alpha spectrometry with an optimised version for ^{227}Ac developed for this thesis.

Step		Procedure: Optimised for ^{227}Ac in this thesis
1	Precipitation solution	Precipitation solution of 20 mL 2 M HCl directly from DGA® resin separation
2	Preparation for micro-precipitation	Add 40 µg Nd – 0.1 mL of 400 µg Nd mL^{-1} as $Nd(NO_3)_3$ solution Add 2–3 drops of <0.25% bromocresol purple solution
3	Micro-precipitation	Add 10 M NaOH solution dropwise to colour change, swirling gently to prevent compaction of precipitate
4	Source deposition	Vacuum filter through 0.1 µm pore size PP filter Rinse beaker with 4 mL 0.2 M NaOH used for precipitation then add rinse to the filter to remove alkali soluble salts Repeat the beaker rinse with 80% ethanol then add to the filter to remove organic material and the indicator Air dry the filter

Alpha spectrometry was selected as the preferred method over LSC for measurement of ^{227}Ac in samples for this thesis. This was because of the better discrimination of alpha energies for assessing potential contaminant radionuclides that may not be fully separated during radiochemical separation. With reliable separation chemistry, LSC may be a suitable alternative to alpha spectrometry methods.

For alpha spectrometry measurement of ^{227}Ac, using ^{225}Ac as a tracer, recovery determination was performed within one week following radiochemical separation of Ac to minimise the potential for ^{227}Ac progeny to influence the recovery determination. Actinium-225 must then be allowed to decay while allowing for ingrowth of ^{227}Ac progeny ^{227}Th and ^{223}Ra. The best MDL for determination of ^{227}Ac activity concentrations in samples is based on decay of ^{225}Ac and progeny and ingrowth of ^{227}Th and ^{223}Ra, yielding a value of 178 days after Ac separation (See Section 4.3.2.2.4 for details). At this point (after 18 half-lives) the ^{225}Ac tracer and progeny will have decayed to negligible activities and make a negligible contribution to the alpha-particle spectrum. Shorter wait times may be used, however, the potential for contribution to ^{227}Th and ^{223}Ra counts from ^{225}Ac and progeny must be considered.

Section 4.4 Sample preparation for ^{227}Ac analysis

A broader discussion of considerations in sample preparation techniques is in Chapter 3, Section 3.6.1, application specifically for analysis of ^{227}Ac is discussed here.

No specific preliminary tests were undertaken for preconcentration and digestion techniques for Ac (as they were for Pa) for two reasons: Known issues with the chemistry of Pa (e.g., tendency to hydrolyse, formation of insoluble oxides and affinity for Si – see Chapter 3, Section 3.1) are not known to affect Ac. There are no tracer isotopes for Ac suitable for relatively rapid gamma counting with HPGe detectors that have long enough half-lives to be relevant for the sample processing time of days to weeks (whereas ^{233}Pa was ideal for Pa testing at every stage of the sample preparation and the chemical separation process). As such, techniques suitable for analysis of ^{227}Ac in large sample volumes were identified and applied to samples directly, these are described in detail below.

4.4.1 Sample preparation

4.4.1.1 Water sample

Owing to the remoteness of the sampling location and the large volume (~65 L), only one water sample was collected for this thesis. Evaporation was done in a glass beaker and the sample was therefore not considered suitable for analysis of ^{231}Pa due to the high potential for loss of ^{231}Pa during evaporation. Complete details of the preparation steps are in Appendix E, Section E-3. As a summary the unfiltered water was evaporated at 80°C to a volume of < 1 L then transferred into a HPDE bottle for transport and storage. The sample was then stored for six months prior to Ac separation. These initial sample preparation steps were prior to addition of ^{225}Ac. For Ac analysis, ^{225}Ac tracer was added and the sample was evaporated to dryness. Particulate matter was digested with conc. HNO_3 followed by a conc. HNO_3/30% H_2O_2 digestion and the sample was filtered through 0.45 µm to remove undigested particulate material then diluted with high purity water prior to $PbSO_4$ coprecipitation. The method is consistent with low-level analysis of the similarly low-level radionuclide, ^{226}Ra, in the same catchment as per methods used for Magela and Gulungul creeks in (Supervising Scientist, 2015).

4.4.1.2 Biological samples

For biological samples, the microwave-assisted digestion technique used for Pa analysis, was not considered suitable as the sample mass that can be used for this technique is too low. Furthermore, the chemistry of Ac is such that heating to high temperatures with dry-ashing techniques was not considered likely to pose a risk to -subsequent- dissolution of Ac for

radiochemical separation[45]. The dry-ashing technique was based on the USTUR method 100 (USTUR, 1995) and involves incrementally heating samples to 500°C to combust organic material. The rate of temperature increase is limited to prevent significant loss of material by generation of particulates (i.e., smoke). A yield tracer (^{225}Ac) was added prior to ashing to ensure that potential losses of Ac were accounted for. Dry-ashing at up to 500°C did not completely remove all C, therefore a wet-ashing step after dry-ashing was used to remove excess C and dissolve samples for radiochemical separation. The applied technique allowed for up to 50 g dry weight, or around 250 g wet weight of sample to be digested while still achieving relatively high recovery for Ac (full method is in Appendix E, Section E-4).

Although increasing the sample mass may be possible. There were several factors that limited the total mass used for each sample. The amount of material available for individual samples, the size of the Pt crucibles available and the trade-off between the length of time it takes to ash the sample fractions (i.e., where multiple ashing steps are required) and the half-life of the tracer. As ion chromatography columns can become saturated with high loads of ions, there was also a limit to the amount of sample that can be used before recovery is affected.

4.4.1.3 Soil/sediment samples

As for Pa, microwave-assisted HF digestion was undertaken by an external laboratory[46] for ^{227}Ac analysis.

4.4.2 Sample preconcentration, radiochemical separation and source preparation for alpha spectrometry

For this thesis seven batches of samples for ^{227}Ac measurement comprising 8–11 samples, including blanks and quality control samples, were processed. Sample preconcentration was done by $PbSO_4$ coprecipitation from the digest solutions for water, biological and soil/sediment samples according to the procedure detailed in Section 4.1.4) which is based on that in Dulaiova et al. (2013) (the full method is in Appendix E, Section E-9 with some minor modification also detailed).

Radiochemical separation using the DGA® resin cartridges was undertaken using the procedure described in Dulaiova et al. (2013), with the full method in Appendix F, Section F-4.2.

---

[45] ^{225}Ac tracer was still added to the sample prior to the dry-ashing process to ensure that any losses, such as adhesion to the crucible walls or being bound in refractory oxides were accounted for.

[46] The Inorganics chemistry laboratory at Forensic and Scientific Services, Queensland Health.

After radiochemical separation, Ac sources were prepared for alpha spectrometry using the optimised method described in Section 4.3 above. No issues were encountered with this stage of the process for samples. Samples were counted by alpha spectrometry twice, initially for ^{225}Ac measurement and chemical recovery determination, followed by a period of ingrowth. The second measurement was for ^{227}Ac determination via ^{223}Ra and ^{227}Th progeny. Analysis was undertaken as described in Section 4.3 above. Equations use to calculate results for ^{227}Ac are in Appendix A, Section A-1, with results from measurement of samples in Table B-1, Appendix B, Section B-1 and discussed in Chapter 5.

Chapter 5 : Results and discussion

Section 5.1 ^{227}Ac and ^{231}Pa activity concentrations in biota

Activity concentrations of ^{227}Ac and ^{231}Pa for all samples measured for this project are given in Appendix B, Table B-1. Activity concentrations of ^{227}Ac are corrected to the sample collection date and to account for ingrowth from ^{231}Pa present in the sample at the time of collection. Where ^{231}Pa results were unavailable for a sample, no correction for ingrowth of ^{227}Ac has been applied. The actual correction applied to account for ingrowth is low, with the maximum correction applied being 0.74% of the reported ^{227}Ac activity concentration and an average correction of 0.05±0.14%. Results for ^{232}Th and ^{238}U series radionuclides and elemental concentrations for the same samples, where available, are also presented in Appendix B, Table B-2 and Table B-3.

Activity concentrations of ^{227}Ac in tissues and whole organisms (wet weight) ranged from <0.11 to 550 mBq kg^{-1} for animals and 0.33 to 17 mBq kg^{-1} for plants. For ^{231}Pa, equivalent ranges were <0.42 to 78 mBq kg^{-1} for animals and 0.66 to 12 mBq kg^{-1} for plants. For individual tissues, activity concentrations of ^{227}Ac in freshwater mussel flesh was an order of magnitude higher than the next highest value for all samples. Bone, liver, and yam flesh represented the next highest values for both ^{227}Ac and ^{231}Pa. Magpie goose flesh had an unexpectedly high activity concentration of ^{231}Pa when compared to other animal flesh results and was the second highest value for all samples.

A linear regression of freshwater mussel ^{227}Ac activity concentrations (Bq kg^{-1}) with age (years), showed a linear correlation with an R^2=0.55 and higher values in older mussels (data in Table B-1). This is similar to the trend observed for ^{226}Ra (Bollhöfer et al., 2011) and may indicate a potential for strong bioaccumulation of ^{227}Ac in this species (*Velesunio angasi*). Mussel results for ^{231}Pa had relatively high MDLs, owing to high Fe breakthrough in the separation chemistry leading to a large mass of Fe_2O_3 as a final AMS target. This led to a ‘dilution’ of the sample for AMS measurement (by a factor of approximately 2.5–4.5 for the four samples analysed). This issue was resolved by replacing the preconcentration by MnO_2 coprecipitation step, with $PbSO_4$ coprecipitation. However, no additional freshwater mussel samples were analysed using the $PbSO_4$ coprecipitation method.

Relatively high values of ^{227}Ac and ^{231}Pa were expected in bone samples compared to other tissues as human studies showed high fractional concentrations of these isotopes deposited in the skeleton from blood (e.g., Campbell et al., 1956; Newton and Brown, 1974; see also Chapter 3, Sections 3.1.2 and Chapter 4, Section 4.1.2). This may be reflected in the relatively high activity concentrations of ^{227}Ac and ^{231}Pa in whole organisms, which has a contribution from bones, compared to most other tissues. Actual activity concentrations were still, however, quite low for bone samples compared to radionuclides from the ^{238}U series, in particular ^{226}Ra (Appendix B, Section B-1, Table B-1 and Section B-2, Table B-2; Doering et al., 2018).

The relatively high activity concentrations of ^{227}Ac and ^{231}Pa in liver samples for animals, and yams in plants, compared to other tissues or foods reflects a similar pattern to the ^{238}U series. However, values for the ^{235}U series radionuclides are orders of magnitude lower (results in Appendix B and also relative to ^{238}U series results from Doering and Bollhöfer, 2016a).

Direct comparison of ^{227}Ac results presented in this thesis with those previously measured in the ARR (Martin et al., 1998) are hindered by the relatively large measurement uncertainty associated with earlier results. However, the values reported here are in the range expected based on those earlier measurements.

Section 5.2 Concentration ratios

As noted in Chapter 2, Section 2.4, CRs in the present work are derived to undertake a prospective dose assessment for people and the environment in the RPA study area, and have been used to predict the uptake or transfer of a radionuclide from environmental media to flora and fauna. Thus, radionuclide activity concentrations in plants and animals on contaminated sites, such as the RPA, can be estimated using data from unimpacted areas. This section details how environmental media activity concentrations of ^{227}Ac and ^{231}Pa were determined and the subsequent derivation of CRs. The CRs derived include those for edible tissues and whole organisms for use in human and environmental dose assessment respectively.

Despite the substantial differences in the biochemistry and environmental chemistry of ^{227}Ac and ^{231}Pa, and radionuclides in the ^{238}U series, the highest CRs occur in the same organisms. The overall results presented here are broadly similar to those published in

Doering et al. (2017) for the ^{238}U series. The measured CRs were typically higher for fruit, yams and pig flesh from the ^{238}U series and both ^{227}Ac and ^{231}Pa compared to other terrestrial foods. The CRs of ^{227}Ac, ^{210}Pb, ^{210}Po and ^{226}Ra for freshwater mussels trended higher with the other radionuclide CRs measured being substantially lower. The notable exception was the high CR for ^{231}Pa in magpie goose flesh.

5.2.1 Derivation of concentration ratios for ^{227}Ac and ^{231}Pa

A database of ^{238}U decay series radionuclide activity concentrations measured in the ARR has been published (the 'CR Database'; Doering and Bollhöfer, 2016a). This database has been updated to include ^{227}Ac and ^{231}Pa activity concentrations measured or derived in this thesis. Soil and water activity concentrations from the ^{238}U series in the CR Database were used to derive ^{227}Ac and ^{231}Pa activity concentrations to increase the available media data for these isotopes (see below). Some soil values in the original CR Database were removed to provide a more consistent and relevant database (see Section 5.2.1.2) from which to derive CRs for the ARR. A tool (the 'CR Tool'), developed to query the CR Database to derive CRs based on a range of criteria, was then used to derive ^{227}Ac and ^{231}Pa CRs for reference organisms and bush foods (Doering and Bollhöfer, 2016c).

The CR Tool uses the geometric mean (GM) for soil and water activity concentrations (as a more appropriate measure of central tendency for lognormally distributed datasets; Wood et al., 2013).

5.2.1.1 Water activity concentrations – ^{227}Ac and ^{231}Pa

For the freshwater environment, only ^{227}Ac was measured in surface water to derive $CR_{WO\text{-}Media}$ values. This sample was from Mudginberri billabong (Chapter 2, Figure 2-4), where long term monitoring of ^{226}Ra continues. Unfiltered water samples were used to determine ^{227}Ac activity concentrations because freshwater mussels are filter feeders. As such, radionuclide transfer is from both metals dissolved in water and particles suspended in the water column (Humphrey and Simpson, 1985). A comparison of the ^{227}Ac and ^{226}Ra activity concentrations in the unfiltered water from Mudginberri billabong is shown in Table 5-1.

Table 5-1 ^{227}Ac and ^{226}Ra activity concentration in water from Mudginberri billabong.

Radionuclide	Sample[a]	Activity concentration (mBq L^{-1})	*n*[b]

		Average	Range	
^{226}Ra[c]	Unfiltered	2.0±1.1	1.0–5.1	15
	Filtered	1.25±0.69	0.62–3.2	15
^{227}Ac (predicted[d])	Unfiltered	0.093	0.047–0.24	
^{227}Ac (measured)	Unfiltered	0.019±0.007		1

[a] The 'unfiltered' sample is referred to as the 'Total' sample in the cited references. Filtered activity concentrations of ^{226}Ra were calculated using an unfiltered:filtered ratio of 1.6 (Bollhöfer et al., 2016).

[b] *n* = Number of samples

[c] Doering and Bollhöfer (2017).

[d] Assuming activity ratio of ^{227}Ac:^{226}Ra = ^{235}U:^{238}U activity ratio of 0.0466:1.

The measured activity concentration of ^{227}Ac is less than a quarter of the predicted value if the ^{227}Ac:^{226}Ra activity ratio is assumed equal to the ^{235}U:^{238}U activity ratio. This is consistent with ^{227}Ac being less environmentally mobile than ^{226}Ra, which is expected based on the chemistry of Ac (i.e., +3 oxidation state for Ac, see Chapter 4, Section 4.1.1). A ratio of 0.0095 for ^{227}Ac:^{226}Ra unfiltered water activity concentration was calculated using the measured value of ^{227}Ac and the average for ^{226}Ra (Table 5-1). This ^{227}Ac:^{226}Ra activity ratio and the unfiltered:filtered ratio of ^{226}Ra (Table 5-1) were used to derive unfiltered and filtered ^{227}Ac activity concentrations for water samples in the CR Database where a ^{226}Ra activity concentration was available. Activity concentrations of ^{231}Pa were assumed[47] to be equal to ^{227}Ac.

Activity concentrations in unfiltered water samples were used to determine CRs for ingestion dose assessment, whereas filtered water was used for environmental dose assessment. The use of filtered water allows comparison with regional $CR_{WO\text{-}Media}$ values (Doering et al., 2019a) and international datasets (e.g., Copplestone et al., 2013).

5.2.1.2 Soil activity concentrations – ^{227}Ac and ^{231}Pa

Soil activity concentrations of ^{227}Ac and ^{231}Pa were measured in several soil samples using the methods described in this thesis (variously described within Appendix E to Appendix J). Uranium-235 activity concentrations were also determined using both HRGS and ICP-MS (assuming the natural activity ratio of 0.0466:1 for ^{235}U:^{238}U).

[47] Although there is no data to support this, it has been assumed as a conservative estimate. An alternative was to use the ^{235}U value as an upper limit, however, this was not considered a realistic assumption.

Results for all isotopes and measurement techniques are shown in Table 5-2. The site 'Status' shown refers to 'perturbed' and 'unperturbed' sites. The perturbed sites are those impacted by mining operations, or other human activities, and may include mine tailings and areas where mining wastewaters were used for irrigation. Unperturbed sites are considered as those not significantly impacted by human activities.

The measured activity concentrations of ^{235}U from ICP-MS are consistently lower (57±16%) than those from HRGS. As HRGS is a non-destructive test, whereas ICP-MS requires sample dissolution through a digestion process (in this case a HF digest), this difference is likely owing to chemical recovery from HF digestion being less than 100%. No yield tracer is added for U analysis by ICP-MS, whereas a tracer is added for both ^{227}Ac and ^{231}Pa prior to commencement of the wet-acid digestion process.

The chemical recovery for ^{227}Ac and ^{231}Pa from analysis of soil samples averaged 94±6% and 31±19% respectively[48]. Relative to the ^{235}U values measured using HRGS, the measured activity concentrations of ^{227}Ac and ^{231}Pa in soils were still low after correction for the chemical recovery (77±26% and 42±13% of the measured ^{235}U values respectively). If equilibrium is assumed for the ^{235}U series this indicates that some of the ^{227}Ac and ^{231}Pa was not released from the sample matrix during HF digestion. Losses of Ac and Pa may have occurred with HF digestion and at other steps during the chemical separation procedure. Given the chemistry of Pa, and affinity for Si, it is not unexpected that it had the lowest overall recovery, both from the chemical separation procedure and in release from the sample matrix through HF digestion. Negre et al. (2009) report variations in chemical recovery similar to those observed in this project (~50% for Pa and ~70% for U in sediment samples; unfortunately, ^{227}Ac was not measured).

Megumi (1979) measured activity concentrations of ^{235}U in soils, after acid digestion, that were lower than those of ^{227}Ac and ^{231}Pa (using ^{227}Th as an analogue). It was suggested that this was from release of ^{227}Ac and ^{231}Pa from minerals in the soil matrix followed by rapid adsorption to the outer surface of soil particles, leading to an increased acid-extractability. The activity concentration ratios of ^{227}Ac:^{235}U and

[48] Excluding one sample for ^{231}Pa analysis that had a chemical recovery of 1%.

^{231}Pa:^{235}U measured for this project were at or slightly below unity, suggesting that if such processes are occurring at the collection sites, they represent a very small fraction of the total activity in the samples.

Comparison of ^{238}U data from the CR Database where results were available from both HRGS and ICP-MS measurement showed consistently higher values with HRGS for perturbed and unperturbed sites (Figures 5-1 and 5-2; note that 15 additional soil sample results have been added to the current CR Database since initial publication and were included in this analysis).

Table 5-2 Activity concentrations of ^{227}Ac, ^{231}Pa, ^{226}Ra, ^{235}U (HRGS and ICP-MS) and ^{238}U in soil samples (uncertainty is σ=1 for HRGS and reported as 10% for ICP-MS.

Sample ID	Sample type	Collection date[a]	Status	Activity concentration (Bq kg^{-1}; Dry weight)					
				^{227}Ac	^{231}Pa	^{235}U (HRGS)	^{235}U (ICP-MS[b])	^{226}Ra (HRGS)	^{238}U (HRGS)
2021-218	Soil	15/07/2021	Unperturbed	1.61 ± 0.06			1.2		
2021-221	Soil	29/07/2021	Perturbed	2.88 ± 0.10	1.36 ± 0.10	3.4 ± 1.2	2.2	67 ± 5	73 ± 26
2021-222	Soil	19/07/2021	Unperturbed	0.34 ± 0.02	0.22 ± 0.02	0.56 ± 0.60	0.28	27 ± 2	12 ± 13
2021-224	Soil	29/07/2021	Unperturbed	1.61 ± 0.06	0.78 ± 0.05	1.6 ± 1.1	1.0	26 ± 2	35 ± 2
2021-225	Soil	16/07/2021	Unperturbed	0.57 ± 0.03	0.34 ± 0.03	1.5 ± 1.0	0.48	18 ± 2	32 ± 22
2021-228	Soil	19/07/2021	Unperturbed	0.92 ± 0.03	0.59 ± 0.03	1.0 ± 1.0	0.75	34 ± 3	22 ± 22

[a] Date format is 'Day/Month/Year'.

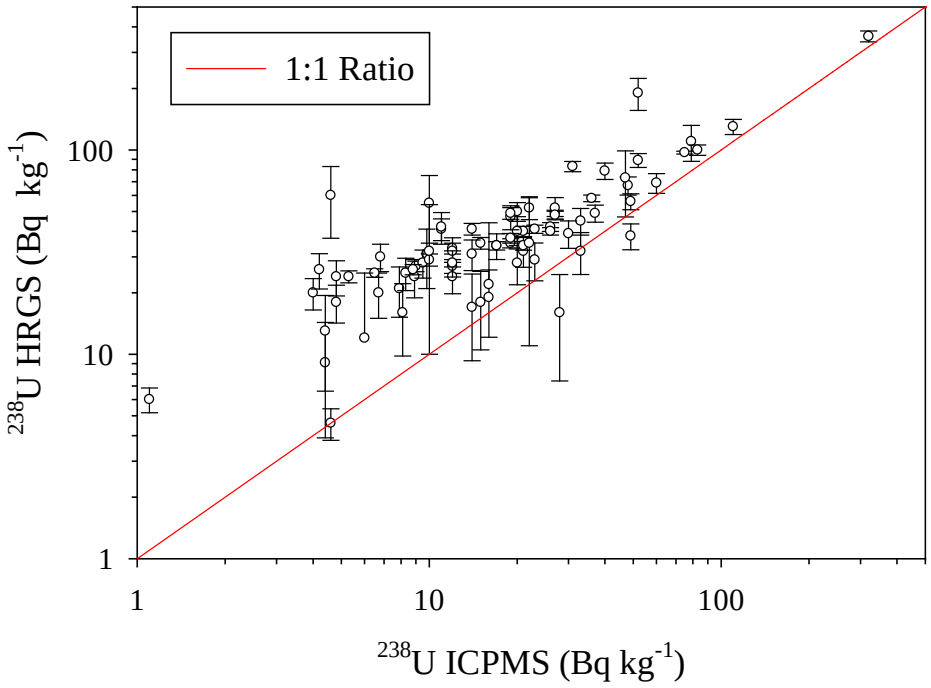

Figure 5-1 Comparison of ^{238}U activity concentrations from the CR Database (Doering and Bollhöfer, 2016a) where results were available from both HRGS and ICP-MS for unperturbed sites. Results from ICP-MS are reported in mg kg^{-1} converted to Bq kg^{-1} assuming a specific activity of 12.346 Bq mg^{-1} for ^{238}U.

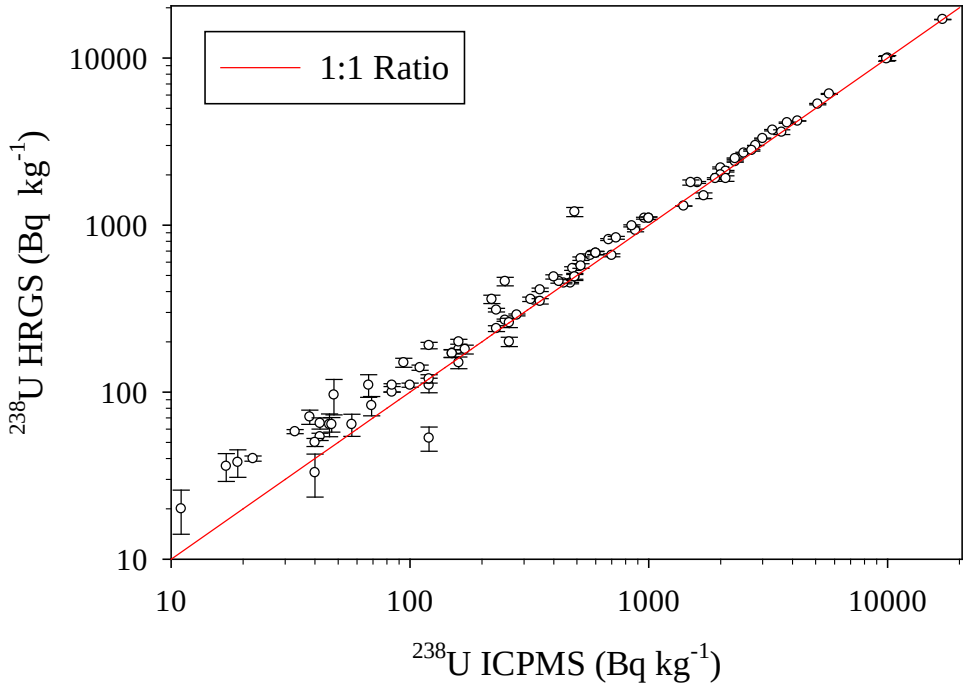

Figure 5-2 Comparison of ^{238}U activity concentrations from the CR Database (Doering and Bollhöfer, 2016a) where results were available from both HRGS and ICP-MS for perturbed sites. Results from ICP-MS are reported in mg kg^{-1} converted to Bq kg^{-1} assuming a specific activity of 12.346 Bq mg^{-1} for ^{238}U.

Comparative analysis using a Student's t-test showed that the measured activity concentrations of ^{238}U from ICP-MS were significantly lower, relative to HRGS, for natural (unperturbed mean = 0.52±0.50) sites compared to perturbed sites (mean = 0.85±0.42) with $t(166) = 9.18$, and p = <.0001. This difference supports the proposition of differential recoveries from wet-acid digestion, with the perturbed sites more likely to have a significant radionuclide component that is surface-bound and therefore more readily extractable (see e.g., Willett and Bond, 1995).

Based on the comparison of results from HRGS and ICP-MS highlighting that ICP-MS values for U are likely to be underestimates, only soil U results where data was available from HRGS measurement were retained in the CR Database adapted for use in this project. A total of 154 values were removed with 653 results remaining, of these ^{238}U activity concentrations were derived for 32 samples by assuming equilibrium with ^{226}Ra (also measured by HRGS).

Measured values for ^{227}Ac and ^{231}Pa in soils were also included in the CR Database and used where spatial matching criteria were met (see Section 5.2.2). For most soils in the database, measured soil activity concentrations of ^{227}Ac and ^{231}Pa were not available and for these the soil activity concentrations were assumed to be in equilibrium with ^{235}U (derived assuming the natural activity ratio of ^{235}U:^{238}U of 0.0466:1)[49]. These data were then used to derive CRs.

5.2.1.3 Spatial and temporal criteria for $CR_{WO\text{-}Media}$ values

Spatial and temporal criteria are used to provide an estimate of average exposure conditions for an organism. These are set such that they are reasonably reflective of the lifetime and foraging range of an organism. The CR tool uses only environmental media activity concentrations of samples collected within the specified criteria (radius in m for spatial; time in days for temporal) to derive CRs.

Foraging ranges for various animals in the ARR were used to determine spatial matching criteria, with some variations used for the same animal in previous studies in the ARR (e.g., Doering, 2019b; Doering et al., 2017; Doering et al., 2018). There are also differences in reported foraging ranges from other ecological studies. For example, Doering (2019b) used a 6 km range for Flying fox (*Pteropus* sp.) based on the work of Palmer et al. (2000), although

[49] For one sample (2021-218; Appendix B), no ^{238}U series and no ^{231}Pa values were available, however, ^{227}Ac was measured and the activity concentration of ^{231}Pa was assumed to be equal to ^{227}Ac.

20 km is reported by Tidemann et al. (1999). A 1 km foraging range (i.e., 3.1 km^2) for the Agile wallaby (*Macropus agilis*) was used in Doering et al. (2017), whereas (Doering, 2019b) reported a 'home range' of 0.11–0.25 km^2 for Agile wallaby, which gives a maximum radius of only 160 m. This is based on a maximum range of 38.2 ha for male wallabies (200 m radius) reported by Stirrat (2003). A 10 km radius for water buffalo (*Bubalus bubalis*) was used in Doering et al. (2017), and 25–50 km^2 in Doering (2019b), both studies cite Tulloch (1969) as the source.

A 5 km radius was used for feral pig (*Sus scrofa*) from Doering et al. (2017). A 400 m radius (5 km^2 range; Todd and Nowakowski, 2021) is relevant for green tree snake (*Dendrelaphis punctulatus*), however, for this project, only one soil sample was collected and analysed within this range. For birds, freshwater and terrestrial, the home ranges may be extensive, however, detailed analysis for these is out of scope for this thesis. A spatial matching criterion of 10 km was set for terrestrial birds as per Doering (2019b).

The foraging ranges of freshwater species such as fish and crocodiles are generally limited to the home waterbody, though foraging may extend further during the wet season as waterbodies become more interconnected. For freshwater species a 365-day temporal matching criterion with water collected from the same waterbody (i.e., spatial matching criterion = 0 m) was used by Doering et al. (2019a) for all organisms except birds, where data from all billabongs was used. Such restrictions for freshwater biota samples were not possible owing to limited environmental media ^{227}Ac and ^{231}Pa data for the desired collection time or location. Therefore, spatial matching criteria were set greater than foraging ranges or typical life spans where no media activity concentrations were available for ^{227}Ac or ^{231}Pa in the desired range to ensure matching was possible.

5.2.1.4 Tissue:Whole-organism conversion factors: Analogue elements

Whole organism activity concentrations of ^{227}Ac and ^{231}Pa were derived for several organisms from Tissue:Whole-organism conversion factors from a range of analogue elements (see Appendix C, Section C-2). Activity concentrations in whole organisms are calculated by multiplying the tissue-specific activity concentration by the Tissue:Whole organism conversion factor. As a conservative approach for the environmental dose assessment for RUM, the highest activity concentration estimated from the different chemical analogues was used to derive $CR_{WO\text{-}Media}$ values. These were calculated using:

- The highest value of a reported Tissue:Whole-organism conversion factor, and
- MDL values where results were <MDL, or
- the 95% upper confidence limit of the highest measured value for a tissue type.

Consequently, all whole organism activity concentration and associated CRs derived using Tissue:Whole-organism conversion factors are effectively upper confidence limit values (see Section 5.2.3).

Differences in radionuclide transfer, and therefore derived CRs, often exist between contaminated and uncontaminated sites (e.g., Medley et al., 2013; Thomas, 2000b). The perturbed sites included in this study have all been impacted to some degree by U mining and/or milling activities (i.e., they are potentially contaminated sites). As indicated above, the perturbed sites were shown to have differences in acid-extractable U compared to unperturbed sites which may reflect differences in availability for uptake (Section 5.2.1.2). Therefore, CRs were derived using only soil or water activity concentrations with the same site status as the sample (i.e., perturbed or unperturbed; see Section 5.2.3 below).

5.2.1.5 Tissue:Whole-organism conversion factors: ^{227}Ac and ^{231}Pa measurements

Sufficient individual tissue activity concentrations of ^{227}Ac and ^{231}Pa were available to derive Tissue:Whole-organism conversion factors for some reference organisms from unperturbed sites. Conversion factors were derived for the ‘mammal’ reference organism from results for the Northern brown bandicoot (*Isoodon macrourus*; see Appendix C, Section C-2.4) and for the ‘freshwater bivalve’ reference organism from results for the freshwater mussel (*Velesunio angasi*). Note that, Tissue:Whole-organism conversion factors are calculated by dividing the whole organism activity concentration by the tissue-specific activity concentration (as opposed to the application of Tissue:Whole-organism conversion factors being used to calculated whole organism activity concentrations as in Section 5.2.1.4 above).

For the ‘mammal’ reference organism the Tissue:Whole-organism conversion factor derived from muscle tissue for ^{227}Ac was 11.8, this compares to a range for mean values of 1.1–34 for the different chemical analogues with the highest value derived from Ce (Table C-3, Appendix C, Section C-2.1). For ^{231}Pa the Tissue:Whole-organism conversion factor derived from muscle tissue was 10.5 and from bone was 2.06, which compares to ranges for mean values of 1.1–13 and 0.13–0.83 respectively for the different chemical analogues, with the

highest values for both tissue types being from Am (Table C-3 and Table C-4, Appendix C, Section C-2.1). It is noteworthy that for bandicoot, the activity concentration of ^{231}Pa measured in the gastrointestinal tract was at least an order of magnitude higher compared to other tissues. Also, substantially higher in this tissue were Fe, Mn, and U concentrations, potentially indicating the presence of soil or mineralised material in the gastrointestinal tract. A potential reason for high variation in $CR_{WO\text{-}Media}$ values reported in global studies may be related to variations in contents of the gastrointestinal tract rather than actual uptake. This suggests that reporting of $CR_{WO\text{-}Media}$ values should include information regarding whether animals were 'purged' of gastrointestinal contents, or whether digestive system contents were otherwise taken into account.

For the 'freshwater bivalve' reference organism, the ^{227}Ac Tissue:Whole-organism conversion factor derived from soft tissue was 1.07 and from shell was 15.9, which compares to ranges of 0.46–10 and 0.63–4.9 respectively when based on the different chemical analogues, with the highest values being from the rare earth elements Lu, for soft tissue, and La for shell.

The conversion factors derived for the Northern brown bandicoot and the freshwater mussel from measured values of ^{227}Ac and ^{231}Pa were all within the range of mean values for relevant chemical analogues. The values for the individual chemical analogue and tissue combinations typically vary by an order of magnitude or more, thus, measured values falling within this range provides support for the use of chemical analogues for ^{227}Ac and ^{231}Pa in environmental dose assessment where direct measurement is not achievable. Although lanthanide elements have often been used as an analogue for ^{227}Ac, they tend to provide comparatively higher CR values for ^{227}Ac than other chemical analogues such as Th and U (Medley et al., 2024).

The activity concentrations of ^{231}Pa measured in the Northern brown bandicoot offer insight into the relative significance of estimated doses and the validity of whole organism measurements for dose assessment. Results for ^{231}Pa were available for bone, flesh, carcass and the gastrointestinal tract (including contents). The 'carcass', representing 78% of the whole organism mass, was the remaining tissues after removing the heart, kidney, liver, testicles, the gastrointestinal tract and a sub-sample of bone (equivalent to 1.2% of the total organism mass). Bone activity concentrations of ^{231}Pa were 5.1 times higher than muscle tissue, and the carcass,

which included the remainder of bone[50] tissue, was 2.8 times higher. Notably, the gastrointestinal tract had an activity concentration 17 times that of bone and, though only 10% of the total body mass, accounted for 78% of the whole organism activity. Given the low relative flesh activity concentrations, it is likely that the contents of the gastrointestinal tract contributed the bulk of the activity which may be attributed to soil particles consumed in the diet. This may lead to an over-estimation of internal dose with high energy loss from alpha and beta particles in the gastrointestinal tract contents. The use of a wet-acid digestion technique, without the use of HF or similar agent to breakdown the mineral matrix may also have led to an underestimation of the total activity in the gastrointestinal tract fraction but may be more representative of surface adsorbed material. An alternative explanation is that there are higher activity concentrations of ^{227}Ac and ^{231}Pa at lower trophic levels, organisms for which values are not currently available.

5.2.2 Concentration ratios for bush foods

Freshwater and terrestrial CRs for bush foods used for dose assessment are shown in Figures 5-3 and 5-4 (further details are in Appendix C, Section C-3, Table C-13 andTable **C-14**).

For bush foods, as is typical for $CR_{Tissue\text{-}Media}$ values, variations for the same radionuclide/tissue combination often span several orders of magnitude. It is therefore difficult to compare the $CR_{Tissue\text{-}Media}$ values determined for ^{227}Ac and ^{231}Pa from a limited number of samples to those for other radionuclides. Nevertheless, broad trends can be seen, with ^{227}Ac and ^{231}Pa $CR_{Tissue\text{-}Media}$ values generally being of similar magnitude and relatively low compared to the ^{238}U series radionuclides ^{210}Pb, ^{210}Po, and ^{226}Ra which are generally the highest contributors to dose from that series (6.6.3Appendix CAppendix C, Section C-6, Table C-18). Actinium-227 and ^{231}Pa have $CR_{Tissue\text{-}Media}$ values close to those of Th and U, while also similar to Ra values for some organisms, but broadly trending lower than Pb and Po.

[50] The bones are roughly estimated to be about 10% of total body mass based on ratios derived for kangaroos from Tribe and Peel (1963).

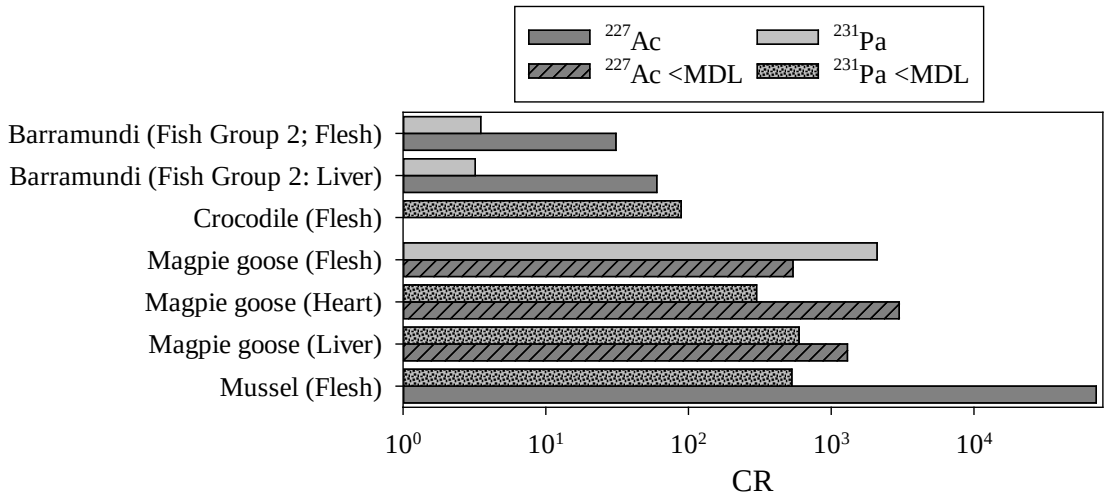

Figure 5-3 ^{227}Ac and ^{231}Pa CRs for freshwater bush food items from the ARR.

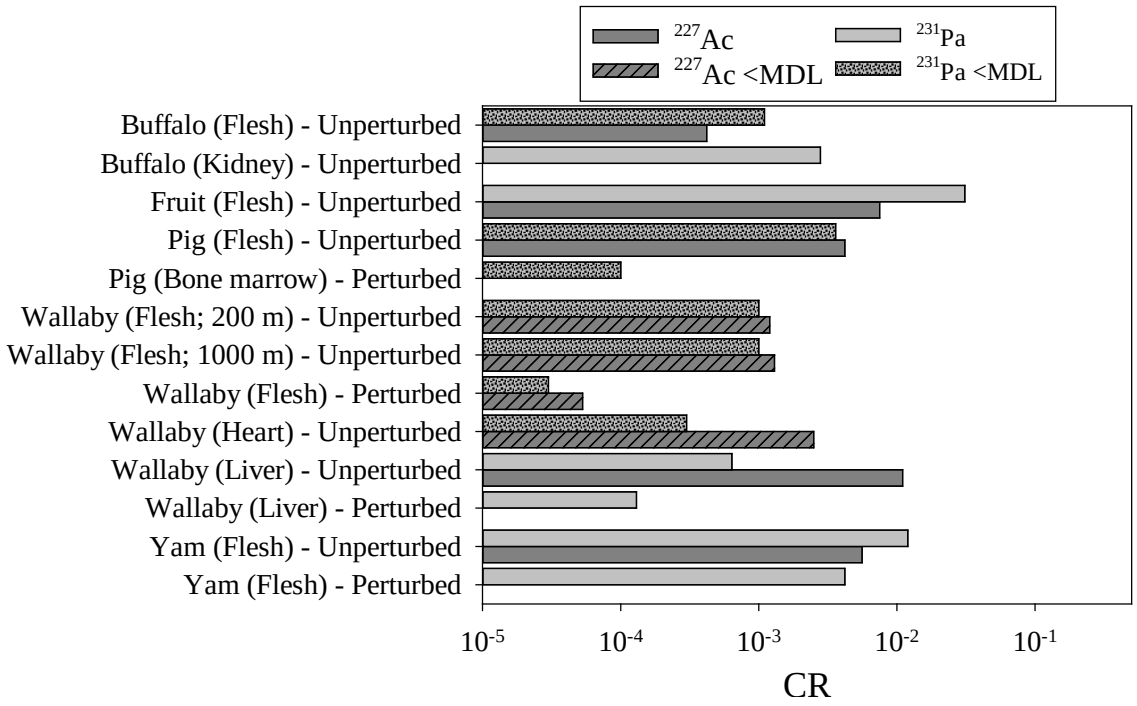

Figure 5-4 ^{227}Ac and ^{231}Pa CRs for terrestrial bush food items from the ARR.

There are some notable exceptions, with the $CR_{Tissue\text{-}Media}$ of ^{231}Pa being the highest reported value of any other radionuclide for magpie goose flesh for example (Figure 5-3 and Table C-18, Appendix C, Section C-6). The ^{227}Ac $CR_{Tissue\text{-}Media}$ in freshwater mussel flesh was high and of a similar magnitude to Ra, which is known to strongly bioaccumulate in those tissues. The value was also similar to Pb and Po, with high $CR_{Tissue\text{-}Media}$ values for both elements in freshwater mussel flesh. There was a slight trend upward with increasing age for ^{227}Ac, but this is confounded by being of a similar magnitude to the measurement uncertainty (6.6.3Appendix CAppendix C, Section C-6, Table C-19). Investigating whether ^{227}Ac activity concentrations

increase in freshwater mussels as they age, or if they reach a steady-state value will improve accuracy in related dose estimates.

The similarity of both ^{227}Ac and ^{231}Pa $CR_{Tissue\text{-}Media}$ values to those for both Th and U suggests the previous use of these elements as chemical analogues in human dose assessment in the ARR was appropriate[51].

More than one foraging range was used for Agile Wallaby and Flying fox to compare ^{227}Ac and ^{231}Pa CRs derived under different assumptions. For Agile Wallaby flesh, the difference in CRs calculated was low for ranges with 200 m and 1 km radius (5% and 2% for ^{227}Ac and ^{231}Pa respectively; Figure 5-4). Whereas for Agile wallaby whole organism values the CR for ^{227}Ac and ^{231}Pa were ~20% lower with the increased range (Figure 5-6). Changing the foraging range from 6 km to 20 km for Flying fox led to a ~50% increase in the CR for ^{227}Ac and ^{231}Pa (see Section 5.2.3 below, Figure 5-6). All variation in CRs were attributable to differences in the soil activity concentrations used to derive GM values.

For fruits, where results were available for up to six samples for ^{227}Ac and ^{231}Pa, a more complex comparison of variations in spatial and temporal criteria was undertaken (Appendix C, Section C-3). Although CR values varied in some cases up to an order of magnitude, the GM (a better measure of central tendency) varied by less than 50% when varying spatial and temporal criteria. Given the typical variation in CRs spans several orders of magnitude this is a minor difference and reflects low variability in activity concentrations of NORM in unperturbed sites across the region.

Results >MDL were obtained for ^{227}Ac in fruit and wallaby flesh, and ^{231}Pa in Fruit and Yam flesh from both perturbed and unperturbed sites (Table B-1, Appendix B, Section B-1). This allowed comparison of CRs, which showed that CRs were 1–2 orders of magnitude lower for perturbed sites than those for unperturbed sites (Figure 5-4). This infers lower transfer at higher soil concentrations for ^{227}Ac and ^{231}Pa, a pattern that is compatible with a non-linear model for soil uptake (e.g., Medley and Bollhöfer, 2016; Sheppard and Sheppard, 1985). This suggests it is likely that modelling transfer on a contaminated site, such as the final landform, may over-estimate uptake and associated ingestion doses from consumption of bush foods.

[51] The Ac CR was assumed to be the same as Th, and Pa the same as U in bush foods in Doering et al. (2017).

5.2.3 Concentration ratios for whole organisms

Freshwater and terrestrial $CR_{WO\text{-}Media}$ values used for dose assessment are shown in Figures 5-5 and 5-6 (further details are in Appendix C, Section C-4, Tables C-15 and C-16).

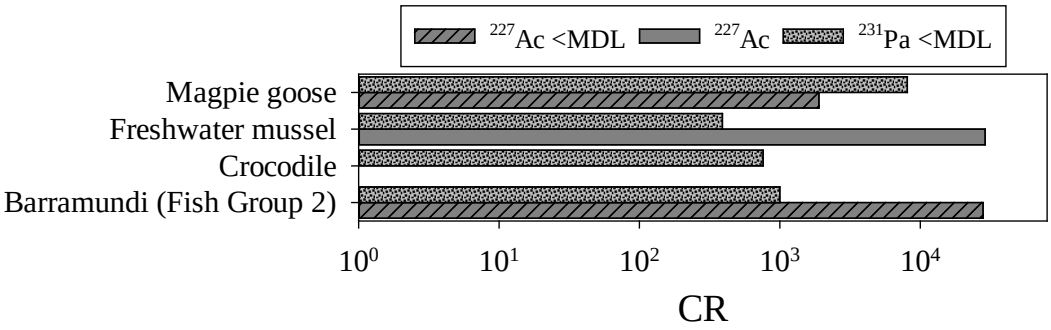

Figure 5-5 $CR_{WO\text{-}Media}$ values for the freshwater environment used for ERICA environmental dose assessment. Results are from unperturbed sites, except for Barramundi which is from a perturbed site.

The $CR_{WO\text{-}Media}$ values derived from direct measurement of ^{227}Ac and ^{231}Pa activity concentrations or from Tissue:Whole-organism conversion factors (see Section 5.2.1.5) for terrestrial organisms are lower than the default $CR_{WO\text{-}Media}$ values, but similar to those derived using Th, and U, in the ERICA tool (see Table C-20, Appendix C, Section C-7). Comparison of the ERICA tool $CR_{WO\text{-}Media}$ values and those reported in (Doering et al., 2017), indicates that use of Th and U as chemical analogues for Ac and Pa to determine uptake in the ARR is likely to provide a reasonable upper estimate for terrestrial environmental dose assessment.

For freshwater organisms, the ERICA default ^{227}Ac and ^{231}Pa $CR_{WO\text{-}Media}$ values are similar to those derived in the present work and generally higher than those for Th and U. Indicating that use of Th and U as chemical analogues for Ac and Pa to determine uptake in the ARR is likely to provide an underestimate for freshwater environmental dose assessment. This must, however, be considered in the context that many values in Figures 5-5 and 5-6 are less than the MDL.

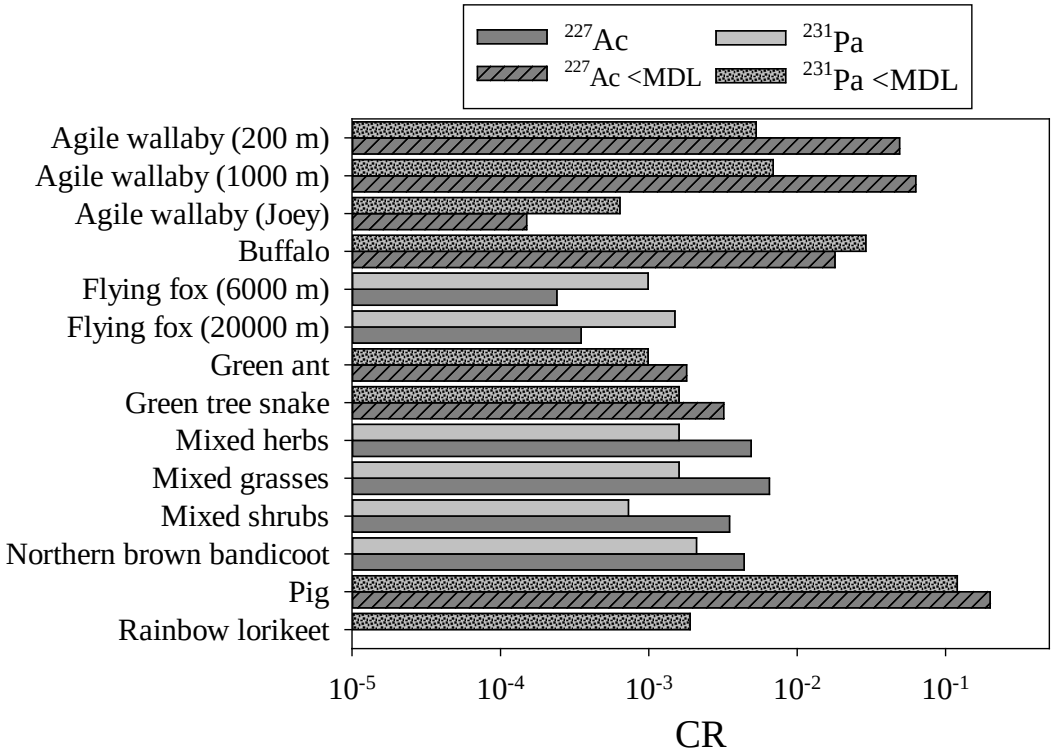

Figure 5-6 $CR_{WO\text{-}Media}$ values for the terrestrial environment used for ERICA environmental dose assessment of the RPA. Results are from unperturbed sites.

Section 5.3 Dose assessment

To estimate the above background doses to people and the environment from the RPA (see Chapter 2, Section 2.6.2), background media concentrations of soil and water were required.

5.3.1 Above background activity concentration of ^{235}U series in soil

The pre-mining background activity concentration of ^{238}U series radionuclides across the 8 km^2 final landform area was determined to be 260 Bq kg^{-1}, with an average of 110 Bq kg^{-1} across the remainder of the 79 km^2 RPA (based on data reported in Bollhöfer et al., 2014). This yields an area weighted average of 125 Bq kg^{-1} for the ^{238}U series, equivalent to 5.84 Bq kg^{-1} for the ^{235}U series (based on the ^{235}U:^{238}U activity ratio of 0.0466:1). Current estimates of the activity concentrations of the waste rock capping material for the final landform is <0.007% U_3O_8 or 728 Bq kg^{-1} ^{238}U (ERA, 2023), with the remainder of the RPA to have the equivalent of the pre-mining background ^{238}U activity concentration. This leads to a maximum for the average above background activity concentration of 47.3 Bq kg^{-1} for ^{238}U series radionuclides and 2.21 Bq kg^{-1} for ^{235}U series radionuclides across the entire RPA, which has been used to determine an above background dose from ^{227}Ac and ^{231}Pa associated with soils in this thesis.

Different occupation scenarios were reported by ERA (2023) to assess ingestion doses and results for ^{227}Ac and ^{231}Pa for two of these scenarios are reported in this thesis. The most conservative scenario assumes 100% of annual bush food intake is sourced from the RPA, whereas the alternative assumes a proportional consumption based on the relative time estimated to be spent on the RPA (i.e., 1040 hours per year or 11.9%).

5.3.2 Above background activity concentration of ^{227}Ac and ^{231}Pa in water

To allow achievement of the Primary Environmental objectives (Commonwealth of Australia, 1999) for mine closure at RUM, a management goal is that:

"*Mine derived analytes from surface or ground waters discharged to surface waters off the RPA do not cause detrimental impact to the ecosystem health, and that there will be no detrimental environmental impact off the RPA from tailings contaminants for at least 10,000 years.*" (ERA, 2023)

This requires complex hydrogeological modelling, an assessment of the impacts of acid sulphate soils, and other considerations as part of probabilistic estimates of contaminant transport (ERA, 2023). Although a detailed discussion of these topics is out of scope for this thesis, an assessment based on radiological water quality guideline values during the operational phase of the mine has been undertaken to provide an indication of the relative risk posed by the ^{235}U series via the aquatic pathway.

Owing to the bioaccumulation of ^{226}Ra in freshwater mussels, this food source was determined to be the largest contributor to radiological dose from a traditional diet (Supervising Scientist, 2023). A guideline value of 3 mBq L^{-1} above background for ^{226}Ra in the receiving water (unfiltered, see Section 5.2.1.1) of Mudginberri billabong was set accordingly. This would result in a mine origin ingestion dose from ^{226}Ra bioaccumulated in mussels of about 0.2 mSv, if 2 kg of mussels were ingested by a 10-year-old child (Turner et al., 2019). The guideline value is an annual geometric mean encompassing the wet season (i.e., when water is flowing) and, to put this into context, the average background activity concentration is 2.0±1.1 mBq L^{-1} (Table 5-1, Section 5.2.1.1). The long-term annual geometric mean above background concentration during operation of RUM from 2002–2023 was close to zero (Supervising Scientist, 2023). Applying the activity ratio of ^{227}Ac:^{226}Ra for Total water of 0.0095 (determined above in Section 5.2.1.1) to the guideline value of 3 mBq L^{-1} above background

for ^{226}Ra, yields an above background activity concentration of 0.029 mBq L^{-1} for ^{227}Ac. This value was used here for dose assessment for the freshwater environment ingestion pathway.

For environmental dose assessment, an above background activity concentration in the receiving water (filtered, see Section 5.2.1.1) of Mudginberri billabong for ^{226}Ra of 14 mBq L^{-1} was used. This is the guideline value appropriate for RUM rehabilitation (ERA, 2023) and is based on an ERICA assessment where estimated ^{226}Ra activity concentrations determined 'Mollusc – bivalve' to be the limiting organism for the freshwater ecosystem (i.e, the reference organism with the highest dose rate, see Chapter 2, Section 2.3.1; Doering et al., 2019a). Although this value is higher than the guideline value for radiation protection of people, it is used here to allow comparison of environmental dose estimates from the ^{235}U and ^{238}U series from the study area.

5.3.3 Annual ingestion doses

Above background annual ingestion doses from ^{227}Ac and ^{231}Pa are shown for the freshwater and terrestrial pathways in Figure 5-7 (data tables are in Appendix C, Section C-8). The dose from each pathway is shown in Table 5-3. Several different assumptions were made to choose an alternative CR when including annual ingestion doses for organisms not measured for ^{227}Ac and ^{231}Pa. Where an alternative CR was used, it was selected from potential values in this order: the Ac CR is set equal to that of the Pa CR for the same organism or tissue (and vice versa), the CR for Whole organism is used for edible tissues from the same organism, the CR is set equal to the Ac or Pa CR for a similar organism or tissue type, the CR is set equal to the highest geometric mean CR from reported CRs of Th and U for the same organism/tissue.

The calculated annual ingestion doses are considered a 'Worst case scenario' because:

- Where measured activity concentrations of ^{227}Ac and ^{231}Pa were <MDL, 'less than' values have been used as potential maximum values to calculate dose,
- 100% of the traditional diet is assumed to be collected from the RPA (see Section 5.3.1)
- A guideline value has been used to determine above background activity concentrations of ^{227}Ac and ^{231}Pa in water (i.e., a specified upper limit value), and
- The highest measured CR value for a bush food type was used (i.e., fruit, mussel, and pig flesh), when more than one result was available.

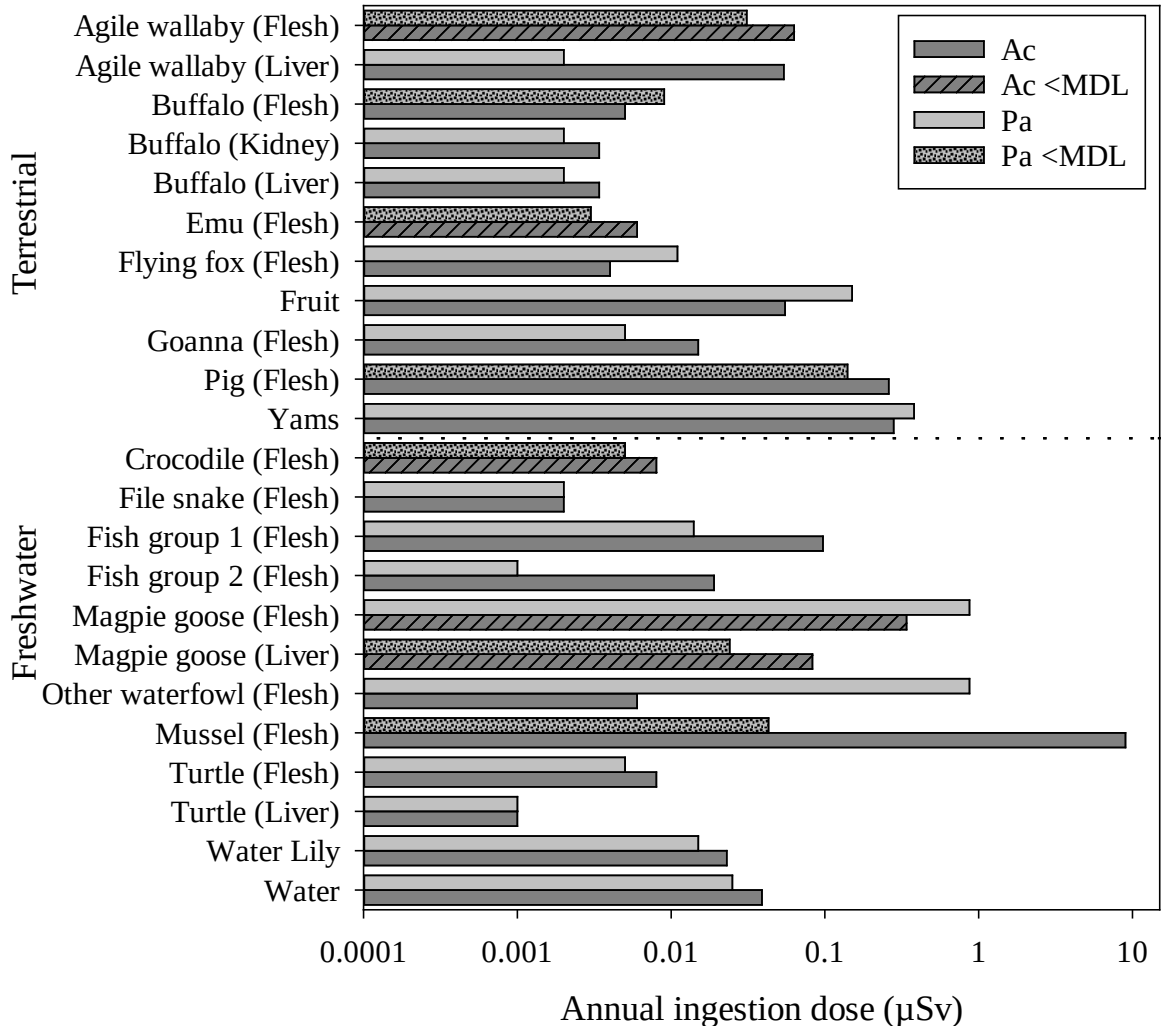

Figure 5-7 Above background annual ingestion doses from ^{227}Ac and ^{231}Pa – Worst case scenario.

Table 5-3 Above background annual ingestion doses from ^{227}Ac and ^{231}Pa – Worst case scenario.

Food item	**kg per person**	**Bq consumed**		**Annual ingestion dose (µSv)**	
		^{227}Ac	**^{231}Pa**	**^{227}Ac**	**^{231}Pa**
Terrestrial total	83	0.63	1.0	0.69	0.73
Freshwater total	72	8.7	2.6	9.6	1.8
Total	155	9.3	3.7	10.3	2.6

The total above background annual ingestion dose from ^{227}Ac and ^{231}Pa is <13.0 µSv year^{-1} under this scenario. In the scenario based on current occupancy estimates for Aboriginal people on the RPA (11.9% of bush foods consumed are derived from the RPA) this is <1.6 µSv year^{-1}. Although several assumptions have been made to include all food items in the traditional diet,

measurements made in this thesis are representative of 78% of total consumption in the model diet (see Chapter 2, Section 2.7.1.2). The freshwater component of the diet is by far the largest contribution in this assessment, partly owing to it being a more conservative approach with a guideline value being used to determine the above background activity concentrations of ^{227}Ac and ^{231}Pa in water. However, CRs for the freshwater bush foods also include the highest values for each isotope.

The highest potential dose contribution from the ^{235}U series is from ^{227}Ac in freshwater mussels, with a potential dose an order of magnitude higher than the next highest contribution (Figure 5-7). To put this into context with the dose from the ^{238}U series, we can compare the relative dose to a 10-year-old child in relation to the guideline value of 3 mBq L^{-1} for ^{226}Ra in water (Total). Under the modelled scenario (see Section 5.2.3 above), ^{227}Ac would contribute 3.1% of the dose relative to ^{226}Ra using the maximum measured CR for ^{227}Ac. Using instead the geometric mean CR for ^{227}Ac in freshwater mussels, the dose equivalent is only 1.5% of that from ^{226}Ra.

The next highest potential contributor to annual ingestion dose from freshwater bush foods was 0.87 µSv year^{-1} from ^{231}Pa in the flesh of magpie goose and other waterfowl. The highest potential contributor to dose from terrestrial bush foods is from yams, with >40% of the estimated terrestrial dose from ^{227}Ac and ^{231}Pa attributed to this food item. The next highest value is for pig flesh, however, the ^{231}Pa activity concentration used was equal to the MDL.

Activity concentrations and potential dose for magpie goose and wallaby liver are reported here but not used in the annual ingestion dose assessment as, although consumption of organs is noted in the diet, the specific organs and the amount consumed is not reported. Were magpie or wallaby liver to be incorporated it would lead to a potentially higher annual ingestion dose estimate, with the $CR_{Tissue\text{-}Media}$ values for liver about one order of magnitude higher than for flesh.

The DCs for ^{227}Ac include decay products which, owing to their short half-lives, are unlikely to bioaccumulate to significant levels independently of the parent isotope. As such, the annual ingestion dose estimates here cover all ^{235}U series radionuclides except ^{235}U itself. Annual ingestion doses from ^{235}U only (i.e., without decay products) were calculated, using the $CR_{Tissue\text{-}Media}$ values for U reported in Doering et al. (2017) and the DC for adults from ICRP (2019), for traditional diet items assuming 100% of the traditional diet is collected from the

RPA (Table 5-3). An assumption was made that the $CR_{Tissue\text{-}Media}$ value for emu was the same as for wallaby and all waterfowl CRs were the same as magpie goose. An additional U $CR_{WO\text{-}Media}$ value for Flying fox of 9.61×10^{-4} was calculated from the CR Database and used as the $CR_{Tissue\text{-}Media}$ value for flesh (using spatial and temporal criteria of 20,000 m and 365 days respectively). The guideline value in freshwater of 2.8 µg L^{-1} for U was used to determine ^{235}U activity concentrations in water[52]. Annual ingestion doses from ^{235}U for freshwater and terrestrial bush foods were only 0.21 and 0.020 µSv $year^{-1}$ respectively.

An annual background radiation dose to Aboriginal people living in the region around the Ranger Uranium mine from ingestion of bush food items has previously been determined to be 0.84 mSv $year^{-1}$ (Ryan et al., 2009). This dose reflects the natural state of the environment, unimpacted by mining activities. Although there are slight variations in the diet used to calculate the background dose rate, which are discussed in Chapter 2, Section 2.7.1.2, it is not likely to have a substantial impact on calculated background doses (ERA, 2023). Thus, the potential above background annual ingestion doses for the ^{235}U series, estimated at less than 13.0 µSv, are rather low in comparison to the total natural background dose.

A substantial increase in activity concentrations in soil or water from those anticipated for the RPA and surrounding waterbodies would be required for ^{235}U series radionuclides to make a significant contribution to dose from the ingestion pathway.

5.3.3.1 Doses to people from all pathways

Total estimated doses from the ^{235}U series to people occupying the rehabilitated RPA from all pathways are shown in Table 5-4, with a comparison of doses from several pathways for the ^{238}U series. Ingestion dose estimates from the ^{238}U series were not included as they have not been completed for the updated diet model and the revised above background activity concentrations of soil on the rehabilitated RPA.

Table 5-4 Annual dose estimates from occupancy of the rehabilitated RPA (excluding the ingestion pathway for ^{238}U series).

Source	Dust[a]	External gamma[a]	Ingestion	Radon[a]	Total
Dose (µSv $year^{-1}$) – 100% occupancy on rehabilitated RPA[b]					

[52] As per the approximately equivalent guideline value for ^{226}Ra. Note that, as opposed to ^{226}Ra, the U guideline value is lower for human health protection than for ecosystem protection and U guideline values are set as absolute values and not above background values. The natural activity ratio of ^{235}U:^{238}U of 0.0466:1 was assumed.

^{235}U series	1.1	4.0	13		18
^{238}U series	3.6	300		96[b]	400
Dose (µSv year^{-1}) – Estimated occupancy scenario (11.9%)					
^{235}U series	0.13	0.48	1.6		2.1
^{238}U series	0.42	35		11	47

[a] Dose estimates for dust and radon inhalation, and for external exposure previously reported (Doering, 2019a; Doering et al., 2019b, 2022) have been corrected to account for the revised above background activity concentration in soil on the rehabilitated RPA (see Section 5.3.1 above). Contribution to dose from inhalation of dust for the ^{235}U series was determined to be 23.5% of total dust inhalation dose with a negligible contribution to Rn inhalation dose from ^{219}Rn and decay products owing to the very short half-life (see Chapter 2, Section 2.5.1.2).

[b] The 100% occupancy scenario for radon represents a position 1 km WNW of the landform centroid during the dry season and at the centroid during the wet season (Doering et al., 2022); for external gamma it assumes equal occupancy averaged over the RPA; for ingestion it assumes all bush food and drinking water is sourced from the RPA.

The ^{235}U series makes a significant contribution (23.5%) to total exposure from inhalation of dust which represents approximately 6% of the total dose from the ^{235}U series for all pathways. External gamma contributes about 22% for the ^{235}U series total, but only 1.3% of the total (i.e., ^{235}U and ^{238}U series radionuclides) external dose.

Given that the total dose from the ^{235}U series is slightly less than 5% of the ^{238}U series before inclusion of the ingestion pathway for the ^{238}U series, the relative dose to people from the ^{235}U series occupying the rehabilitated RPA will be a minor component of the total dose.

5.3.4 Environmental doses: ERICA assessment

The ERICA tool was used to undertake environmental dose assessment for ^{227}Ac and ^{231}Pa for the freshwater and terrestrial environments at RUM. This assessment included determination of dose rates for region-specific organisms where results were available. Default reference organisms and $CR_{WO\text{-}Media}$ values for Ac and Pa from the ERICA tool were used to determine dose rates for the remaining reference organisms (see Chapter 2, Section 2.3.1 for more information).

An environmental dose assessment using the ERICA default Th and U $CR_{WO\text{-}Media}$ values for region-specific and ERICA reference organisms was also undertaken to compare doses when using Th and U as chemical analogues of both Ac and Pa.

The RUM mine closure plan specifies benchmark dose rates of 100 µGy hr^{-1} for the most highly exposed terrestrial plants and animals, and 400 µGy hr^{-1} for aquatic plants and animals (ERA,

2023). It is important to note that the 'most highly exposed' terrestrial plants and animals in this context refers to individuals and not to a population (see Chapter 2, Section 2.7.2 and also UNSCEAR, 2008).

Using site-specific data for the ^{238}U series, the limiting organisms for the freshwater and terrestrial environment for the RUM rehabilitation were determined from ERICA Tier 3 (probabilistic) dose assessments using the 95th percentile of the output probability distribution to represent the most highly exposed individuals in the population. In both freshwater and terrestrial environments, the highest dose rates or lowest corresponding water or soil activity concentrations were associated with ^{226}Ra. Based on these assessments the limiting organisms for ^{226}Ra were determined to be the 'Mollusc – bivalve' reference organism for the freshwater environment (Doering et al., 2019a) and 'Reptile' for the terrestrial environment (Doering and Bollhöfer, 2016b).

The relative dose contribution from ^{238}U for reference organisms in the freshwater and terrestrial environment for the RUM rehabilitation were low (Doering et al., 2019a; Doering and Bollhöfer, 2016b), as such the contribution from ^{235}U to total dose can be considered negligible. As the DCCs interpolated for ^{227}Ac in the ERICA tool to determine the dose from ^{227}Ac include progeny, the environmental dose determined for ^{227}Ac and ^{231}Pa covers all remaining radionuclides in the ^{235}U series. Conclusions drawn from these results can therefore be considered to include the entire ^{235}U series.

5.3.4.1 Region-specific organism geometries

Region-specific organism data were used to define several new representative organisms in the ERICA assessment tool in place of default reference organisms (e.g., the generic 'Large mammal' was replaced with Agile wallaby). Details of these and comparison of region-specific and default organism geometries are shown in Appendix C, Section C-1. The ERICA tool interpolated new DCCs for the region-specific organism ellipsoids from the DCCs of the ERICA reference organism ellipsoids. A comparison of the DCCs for ERICA default reference organisms and region-specific terrestrial organisms is included in Table C-2, Appendix C, Section C-1 and indicates that reference organism size has little impact on the determined dose. This is particularly true where the internal dose is the dominant pathway, as is the case for ^{227}Ac and ^{231}Pa. A similar comparison for freshwater organisms leads to essentially the same conclusions. Despite size variations in organism geometries having a low impact on calculated

dose rates, use of region-specific organism geometries was considered important for communication of results to Traditional Owners.

5.3.4.2 Terrestrial environment dose assessment

Results from a Tier 2 ERICA environmental dose assessment for the terrestrial environment, assuming occupancy of the rehabilitated RPA only, are shown in Figure 5-8 for ^{227}Ac and ^{231}Pa (data tables are in Appendix C, Section C-9, Table C-22).

The above background activity concentration of ^{235}U series radionuclides averaged across the RPA was 2.21 Bq kg^{-1} (see Section 5.3.1 above). Dose rate estimates derived from ^{227}Ac and ^{231}Pa $CR_{WO\text{-}Media}$ values for ERICA reference, and region-specific, organisms are shown in Figure 5-8. Comparative dose rate estimates for the ERICA default Th and U $CR_{WO\text{-}Media}$ values are also shown in Figure 5-8. The highest dose rate for region-specific organisms is to the Agile wallaby using ^{227}Ac and ^{231}Pa $CR_{WO\text{-}Media}$ values derived from direct measurement of whole organism activity concentrations or derivation of whole organism activity concentrations from Tissue:Whole-organism conversion factors. The reference organism with the highest dose rate for the ^{227}Ac and ^{231}Pa combined dose rate, using the ERICA default ^{227}Ac and ^{231}Pa $CR_{WO\text{-}Media}$ values, was the ERICA reference organism 'Lichen and Bryophytes'.

Internal dose rates for ERICA reference organisms accounted for >98% of the total dose rate, whereas it contributed a lower percentage for region-specific organisms at 81% and 85% for ^{227}Ac and ^{231}Pa respectively (Figure 5-8, see also Appendix C, Section C-9 Table C-22). Flying fox was somewhat of an outlier with the internal dose from ^{227}Ac contributing only 44% of the total dose from ^{227}Ac owing to the very low $CR_{WO\text{-}Media}$ relative to other organisms (Appendix C, Section C-9 Table C-22). The internal dose rate predicted for ^{227}Ac is the largest contributor to the total dose from ^{227}Ac and ^{231}Pa combined. For region-specific organisms, the calculated dose rates from ^{227}Ac and ^{231}Pa combined were similar to those using the ERICA default $CR_{WO\text{-}Media}$ values for Th or U, but 1–2 orders of magnitude lower than the equivalent ERICA default reference organism using the ERICA default chemical analogue $CR_{WO\text{-}Media}$ values provided for Ac and Pa. Agile wallaby was the only exception being ~50% higher than the ERICA default, owing to the increased dose rate attributable to ^{227}Ac.

The ERICA Tier 3 assessment which determined Reptile to be the limiting organism for the ^{238}U series, showed that ^{226}Ra accounted for 94.9% of the total dose (Doering and Bollhöfer, 2016b). The limited data set reported here is not sufficient to perform a Tier 3 ERICA

assessment for ^{227}Ac and ^{231}Pa to allow direct comparison of dose from the ^{235}U and ^{238}U series to the most highly exposed individuals of the limiting organism. Therefore, a simpler Tier 2 assessment was undertaken for the Reptile ERICA reference organism using the ^{226}Ra $CR_{WO\text{-}Media}$ arithmetic mean from Doering and Bollhöfer (2016b) and the ^{227}Ac and ^{231}Pa $CR_{WO\text{-}Media}$ values determined in this thesis. This allowed direct comparison of dose to the limiting organism from the ^{235}U and ^{238}U series and showed the total dose from ^{227}Ac and ^{231}Pa to be less than 0.06% of the dose attributable to ^{226}Ra.

It is important to note that there are likely to be differences in uptake for the species of reptile for which data in this thesis was obtained (Green tree snake, *Dendrelaphis punctulatus*) and the limiting organism from Doering and Bollhöfer (2016b) (Goanna, *Varanus* spp.). Using radionuclide activity concentrations measured in the green tree snake sample, the relative dose from ^{227}Ac and ^{231}Pa is higher at 0.54% of the dose attributable to ^{226}Ra. Whichever approach is taken, it can still be concluded that there is a negligible internal dose contribution from ^{235}U series radionuclides to the limiting organism in the terrestrial environment for RUM. As such, the above background activity concentrations of ^{238}U series radionuclides for soil remain the primary determinant in assessing whether the RUM rehabilitation meets the specified closure criteria dose rate of 100 μGy hr^{-1} to the most highly exposed terrestrial plants and animals (Doering and Bollhöfer, 2016b; ERA, 2023).

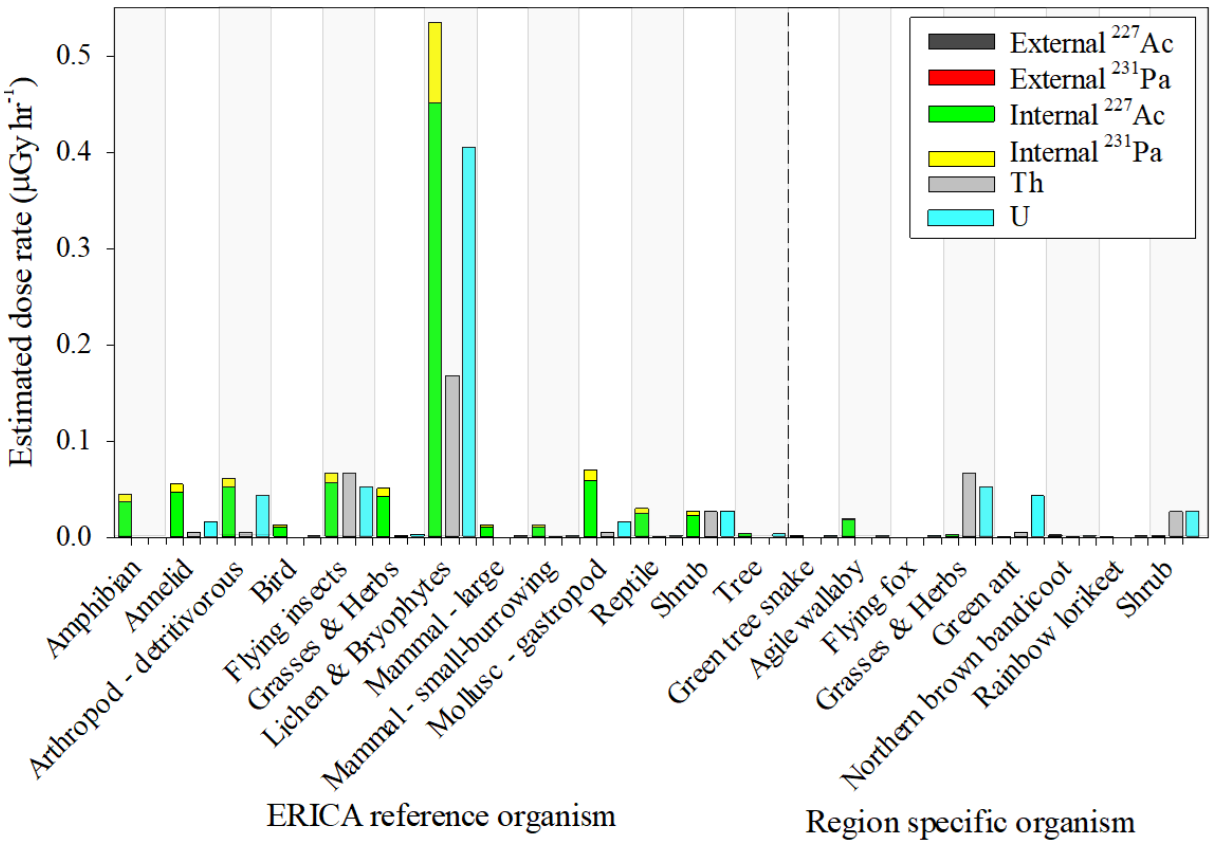

Figure 5-8 Above background terrestrial dose rates on the RPA. For region-specific organisms ^{227}Ac and ^{231}Pa $CR_{WO\text{-}Media}$ values are derived from direct measurement of whole organism activity concentrations or derivation of whole organism activity concentrations from Tissue:Whole-organism conversion factors. For ERICA reference organisms, ERICA default $CR_{WO\text{-}Media}$ values are used for ^{227}Ac and ^{231}Pa. Dose rates derived using $CR_{WO\text{-}Media}$ values for Th and U (dose rates from ^{232}Th and ^{238}U only) are shown for comparison. Shaded bars group data from each reference organism. Where not displayed (e.g., 'External ^{231}Pa) values are too low to be visible at a linear scale (data tabulated in Appendix C, Section C-9 Table C-22).

5.3.4.3 Freshwater environmental dose assessment

Results from a Tier 2 ERICA environmental dose assessment for the freshwater environment are shown in Figure 5-9 for ^{227}Ac and ^{231}Pa (data tables are in Appendix C, Section C-9, Table C-23). The above background activity concentration of ^{227}Ac in filtered water used for this assessment was 0.133 mBq L^{-1}. This was based on an ^{227}Ac:^{226}Ra activity ratio in unfiltered water of 0.0095 (see Section 5.2.1.1) and the 14 mBq L^{-1} guideline value of ^{226}Ra in filtered water for environmental protection (Doering et al., 2019a). The guideline value is the specified closure criteria for RUM (ERA, 2023) and is used as an upper limit because the above background activity concentration of radionuclides in water after rehabilitation of RUM is unknown (Section 5.2.3) and may vary over time. The above background activity concentration of ^{231}Pa in filtered water was assumed equal to that of ^{227}Ac (see footnote 47).

Dose rate estimates derived from ^{227}Ac and ^{231}Pa $CR_{WO\text{-}Media}$ values for ERICA reference, and region-specific, organisms are shown in Figure 5-9. Comparative dose rate estimates for the ERICA default Th and U $CR_{WO\text{-}Media}$ values are also shown in Figure 5-9. The highest dose rate for region-specific organisms is to the freshwater mussel.

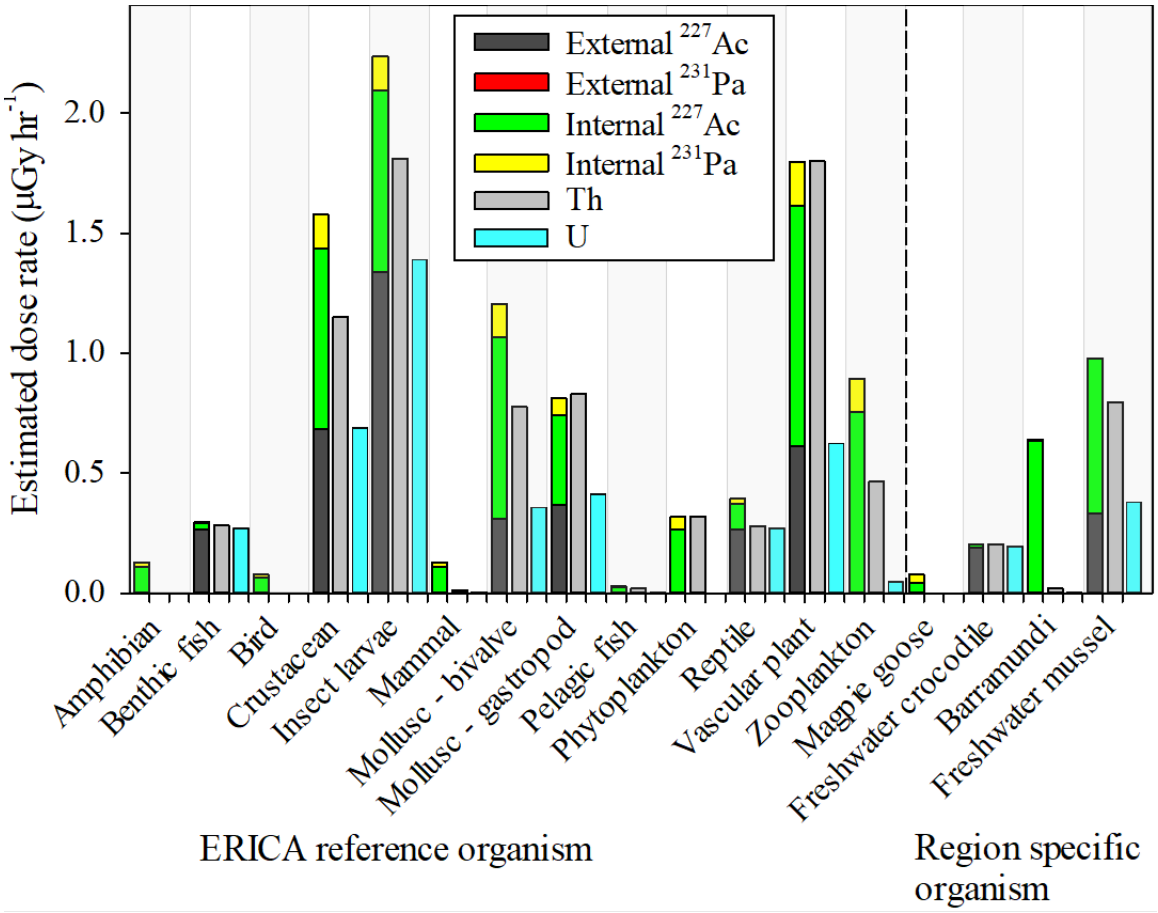

Figure 5-9 Above background freshwater dose rates from the RPA. For region-specific organisms ^{227}Ac and ^{231}Pa $CR_{WO\text{-}Media}$ values are derived from direct measurement of whole organism activity concentrations or derivation of whole organism activity concentrations from Tissue:Whole-organism conversion factors. For ERICA reference organisms, ERICA default $CR_{WO\text{-}Media}$ values are used for ^{227}Ac and ^{231}Pa. Dose rates derived using $CR_{WO\text{-}Media}$ values for Th and U (dose rates from ^{232}Th and ^{238}U only) are shown for comparison. Shaded bars group data from each reference organism. Where not displayed (e.g., 'External ^{231}Pa) values are too low to be visible at a linear scale (data tabulated in Appendix C, Section C-9 Table C-23).

The reference organism with the highest dose rate for the ^{227}Ac and ^{231}Pa combined dose rates was the ERICA default reference organism 'Insect larvae'.

Compared to the terrestrial environment reference organisms where internal dose accounted for the majority of dose, the external dose rate makes a substantially higher relative contribution in the freshwater environment for organisms with occupancy 'in Sediment' or at the 'Sediment-

surface' (Freshwater crocodile and freshwater mussel for region-specific organisms; Benthic fish, Crustacean, Insect larvae, Mollusc – bivalve, Mollusc – gastropod, Reptile and Vascular plant for ERICA reference organisms). This difference can primarily be attributed to the default K_d value for ^{227}Ac. This leads to a predicted sediment activity concentration of 2,660 Bq kg^{-1} for ^{227}Ac, compared to 3.6 Bq kg^{-1} for Pa (and Th, which provides the default K_d for Pa) and 7.0 Bq kg^{-1} for ^{238}U.

The K_d value of 2.0 ×10^7 L kg^{-1} for ^{227}Ac in the ERICA tool is cited from IAEA (2001), which reports a K_d value for Ac in saltwater of 2.0 × 10^6 L kg^{-1} but provides no K_d value for freshwater. Of two alternative references for the table where this value is reported, a revised version of the first (IAEA, 2004) provides the same saltwater K_d value for ^{227}Ac (2.0 × 10^6 L kg^{-1}), which is derived from a "*periodically adjacent element*" (unspecified but presumably Am). The very high predicted ^{227}Ac concentration in sediment highlights that an improved estimate of the K_d value for ^{227}Ac in freshwater and marine environments is necessary for meaningful environmental dose assessments for the ^{235}U series in these ecosystems.

Calculated dose rates using the ERICA default $CR_{WO\text{-}Media}$ values for Th or U, and region-specific values for ^{227}Ac and ^{231}Pa combined, were similar for both freshwater crocodile and freshwater mussel (Figure 5-9). They were also similar to the dose rates for the equivalent ERICA default reference organisms, 'Reptile' and 'Mollusc – bivalve' respectively, using the ERICA default chemical analogue $CR_{WO\text{-}Media}$ values provided for Ac and Pa. Calculated dose rates using ERICA default $CR_{WO\text{-}Media}$ values for Th or U, however, were much lower than for region-specific ^{227}Ac and ^{231}Pa values, for both magpie goose and barramundi. Calculated dose rates for the ERICA default reference organisms equivalent to magpie goose and barramundi, 'Bird' and 'Benthic fish' respectively, were similar using the ERICA default and region-specific $CR_{WO\text{-}Media}$ values for Ac and Pa. However, the majority of the ^{227}Ac dose for barramundi was from the internal component when using region specific $CR_{WO\text{-}Media}$ values, while external dose was much higher using the ERICA default value.

The Tier 3 ERICA assessment that determined 'Mollusc – bivalve' to be the limiting organism for the ^{238}U series in the freshwater environment showed 66% of the total dose was attributable to ^{226}Ra (Doering et al., 2019a). As for the terrestrial environment above, a Tier 3 ERICA assessment for the ^{235}U series was not possible and a comparison was undertaken with a Tier 2 ERICA assessment to compare the contribution to dose from the ^{235}U and ^{238}U series. This

assessment used the ^{226}Ra $CR_{WO\text{-}Media}$ arithmetic mean from Doering et al. (2019a) and the ^{227}Ac and ^{231}Pa $CR_{WO\text{-}Media}$ values determined in this thesis. This showed the total dose from ^{227}Ac and ^{231}Pa to be less than 0.9% of the dose attributable to ^{226}Ra. This is despite the previously identified issue of the high K_d value for ^{227}Ac which leads to an implausible 22 times higher activity concentration of ^{227}Ac in sediment compared to that predicted for ^{226}Ra using the ERICA default K_d value (8.5×10^3 L kg^{-1}).

Rather than using the predicted activity concentrations of ^{227}Ac and ^{226}Ra to compare the relative dose, the measured activity concentrations in freshwater mussel samples can be used for a comparative dose assessment. To this end, ^{226}Ra activity concentrations in Mudginberri Billabong sediment of 26 Bq kg^{-1} (Bollhöfer et al., 2011) were used, with ^{227}Ac activity concentrations in sediment calculated using the natural activity ratio of ^{235}U:^{238}U (0.0466:1). This assessment showed the relative dose from ^{227}Ac and ^{231}Pa is slightly higher than predicted using the ERICA tool at 1.2% of the dose attributable to ^{226}Ra. Whichever approach is taken, it can still be concluded that there is a negligible dose contribution from ^{235}U series radionuclides to the limiting organism in the freshwater environment for RUM. As such, current recommendations for environmental dose guideline values for water are still relevant.

Chapter 6 : Conclusions

There has been a general assumption that the ^{235}U series contribution to radiological dose in the context of U mining is low. To confirm or refute this assumption, the former RUM was chosen with the focus on ^{227}Ac and ^{231}Pa, being part of the ^{235}U series.

Such confirmation through direct measurement of ^{235}U series radionuclides is an important aspect for communication of the rehabilitation success for the RUM site. Such direct measurements are unique in global dose assessment and can help to provide confidence for Indigenous peoples that reconnecting with country and with places of cultural significance on the site can be done safely.

Equally important is the contribution to demonstrating successful mine rehabilitation for RUM, which can provide the global community with assurances that the internationally significant and world heritage listed KNP is, and will remain, protected from the impacts of U mining.

Novel methods for chemical separation of ^{227}Ac and ^{231}Pa from environmental samples with the capability of achieving the desired detection limits for the sample matrices were developed. This included methods for preparation of the yield tracers ^{225}Ac and ^{233}Pa, necessary to assess losses of Ac and Pa throughout the sample preparation and chemical separation processes. A technique was developed to prepare a ^{233}Pa generator (a ^{237}Np cow) for regular extraction of ^{233}Pa from the parent radionuclide ^{237}Np using ion chromatography. A published technique for separation of ^{227}Ac was adapted for extraction of ^{225}Ac from the parent radionuclide ^{229}Th to be used as a tracer. Novel methods were designed for sample preparation and separation of Pa from biological sample matrices using microwave-assisted wet-acid digestion followed by ion chromatography. Verification of the suitability of dry-ashing and published ion chromatography methods for separation of ultra-low levels of ^{227}Ac (<1 mBq kg^{-1} fresh weight) in high sample masses (up to 250 g wet weight) was also undertaken. A $Nd(OH)_3$ coprecipitation technique for actinides from a published method was adapted and optimised to produce Ac sources for alpha spectrometry.

Accelerator Mass Spectrometry (AMS) with the 14UD tandem accelerator at the Australian National University was used for the ^{231}Pa measurement after radiochemical separation where equally low detection limits were achieved (<1 mBq kg^{-1} fresh weight) with a smaller mass (<10 g wet weight).

The primary conclusion of this thesis is that estimated doses to people and the environment from ^{235}U series radionuclides for the RUM rehabilitated site are low and negligible compared to ^{238}U series radionuclides. The highest contributors to ingestion and environmental doses for rehabilitation of RUM remain ^{210}Pb, ^{210}Po and ^{226}Ra.

Section 6.1 ^{227}Ac method development

Dry-ashing of relatively high sample masses of biota (potentially >250 g wet weight) followed by $PbSO_4$ coprecipitation for Ac analysis was effective at removing the bulk sample matrix. Chemical separation of Ac from biota, soil and water using DGA® resin cartridges was generally effective at removing alpha emitting interferences from NORM. Breakthrough of Th was determined to be 0.06±0.02% and less than 0.025% for Ra in tracer studies. Measured Ra breakthrough was higher in freshwater mussels at 0.47±0.17% (n=6), however, it was only 0.022% for a bone sample. Where activity concentrations of ^{228}Ra are several orders of magnitude higher than ^{227}Ac, significant interference from progeny (^{224}Ra) may occur.

Preparation of ^{225}Ac tracer solutions by separation from ^{229}Th with two stacked DGA® resin cartridges showed negligible levels of ^{229}Th were present for the final measurement of ^{227}Ac in samples.

Coprecipitation of Ac with $Nd(OH)_3$ from the 20 mL 2 M HCl eluant directly after DGA® resin separation is a suitable method for preparation of Ac for alpha spectrometry, with 10 M NaOH suitable for pH adjustment and use of Bromocresol purple indicator to determine the pH endpoint. The distribution of precipitate on the filter paper was sufficiently uniform such that no additional uncertainty contributions needed to be considered for this counting geometry.

The alpha peak from ^{217}At decay is suitable for recovery determination using ^{225}Ac, though only alpha peaks from decay of ^{223}Ra and ^{227}Th can be used for activity determination of ^{227}Ac. Other progeny cannot be used owing to loss of ^{219}Rn from the precipitate. The retention of ^{222}Rn in the $Nd(OH)_3$ was negligible such that, even where activity concentrations of ^{226}Ra are several orders of magnitude higher than ^{227}Ac, there is no observable interference from ^{226}Ra progeny.

The best MDL for determination of ^{227}Ac activity concentrations in samples is reached 178 days after Ac separation, based on decay of ^{225}Ac and progeny and ingrowth of ^{227}Th and ^{223}Ra.

Section 6.2 ^{231}Pa method development

Preparation of a ^{233}Pa generator (a '^{237}Np cow') on TEVA® resin without the use of HF and allowing extraction of ^{233}Pa, also without HF, was possible and was stable for over four years.

The ^{233}Pa solutions prepared from the ^{237}Np cow can be stabilised by treatment with H_2O_2 to prevent loss of ^{233}Pa from aqueous solution. Uranium-233 is extracted with ^{233}Pa, however, purification of ^{233}U in ^{233}Pa solutions generated and subsequent quantification allows accurate estimation of isobaric interference from ^{233}U when measuring ^{233}Pa with AMS.

Several coprecipitation test methods for preconcentration of metals in solution were shown to be effective at precipitating Pa with high chemical recovery (>90%), including $Fe(OH)_3$, MnO_2 and $PbSO_4$ coprecipitation. Although the chemical recovery of Pa with $PbSO_4$ coprecipitation is potentially lower than the other methods, it has a superior ability to remove Fe, which may impact measurement of Pa by AMS where Fe_2O_3 is used to bulk the sample mass.

Wet acid digestion techniques on a hotplate were shown to be unsuitable for Pa, as was borate fusion for preconcentration of Pa from soil samples. The high temperature and pressure achievable with microwave-assisted digestion was required for relatively complete decomposition of biological samples, and to minimize losses of Pa bound to undigested particulate matter. The use of HF was required for digestion of soil samples.

The UTEVA® resin was not suitable for separation of Pa from U, however, TK400® resin showed reproducible separation of Pa from environmental (biological) samples with adaptions to a previously published method required to improve separation of U. Although no particular tests were undertaken to verify removal of specific stable elements for this thesis, no significant interferences were observed in the detection system using ToF during AMS measurement. Evaporation of the 1 M HCl eluant from TK400® resin separation of Pa showed the potential for very high loss of Pa to PFA and PTFE surfaces. However, the addition of a small amount of Fe in solution can substantially reduce the loss of Pa.

The PaO_2^- ion exhibited a substantially higher intensity than all other Pa oxide ions tested from the Cs ion source of the 14UD tandem accelerator at the ANU, with an intensity 3.7, 5.4 and over 1000 times higher than for PaO^-, PaO_3^- and PaO_4^-, respectively; the measured intensity from PaO_5^- was negligible. An Al/Al binding material/cathode combination was optimal as it had the highest count rate in combination with the lowest interference from contaminants in the binding material when measuring $^{231,233}Pa^{5+}$ with the 14UD accelerator. The relative ion counting efficiency of ^{233}U compared to ^{233}Pa was calculated to be 0.104±0.078.

Section 6.3 Results and discussion

In biota samples from the ARR, activity concentrations of ^{227}Ac in tissues and whole organisms (wet weight) ranged from less than 0.11 to 550 mBq kg^{-1} for animals and from 0.33 to

17 mBq kg^{-1} for plants. For ^{231}Pa, equivalent ranges were less than 0.42 to 78 mBq kg^{-1} for animals and from 0.66 to 12 mBq kg^{-1} for plants. The maximum activity concentration of ^{227}Ac observed was in freshwater mussel flesh and was an order of magnitude higher than the next highest value observed in the other samples. Magpie goose (*Anseranas semipalmata*) flesh had the highest activity concentration of ^{231}Pa when compared to other animal flesh results. A linear regression of freshwater mussel (*Velesunio angasi*) ^{227}Ac activity concentrations (Bq kg^{-1}) versus age (years), showed a linear correlation with R^2=0.55 and higher activity concentrations in older mussels, similar to what is observed for Ra in mussels. The activity concentration of ^{231}Pa measured in the gastrointestinal tract of the Northern brown bandicoot was at least an order of magnitude higher compared to other tissues. Also, substantially higher in this tissue were Fe, Mn, and U concentrations, potentially indicating the presence of soil or mineralised material in the gastrointestinal tract.

The very low activity concentrations measured highlights the importance of using ultra-sensitive measurement techniques, such as AMS, and/or advanced sample preparation methods where accurate quantitation of the analyte is needed.

Although activity concentrations for different sample types spans several orders of magnitude, the relatively high activity concentrations of ^{227}Ac and ^{231}Pa in liver samples for animals and yams for plant species compared to other tissues or foods reflects a similar pattern to the ^{238}U series. Activity concentrations for the ^{235}U series radionuclides are orders of magnitude lower than the ^{238}U series, reflecting a higher environmental mobility of ^{238}U series radionuclides.

The measured CRs were generally higher for fruit, yams and pig flesh from members of the ^{238}U series and both ^{227}Ac and ^{231}Pa of the ^{235}U series compared to all other terrestrial foods. For freshwater mussels, measured CRs were high for ^{227}Ac, ^{210}Pb, ^{210}Po and ^{226}Ra, and substantially lower for all other radionuclides. The notable exception was the high $CR_{Tissue\text{-}Media}$ for ^{231}Pa in magpie goose flesh, which was the highest reported value of any other radionuclide for magpie goose flesh. The ^{227}Ac $CR_{Tissue\text{-}Media}$ in freshwater mussel flesh was high and of a similar magnitude to those for other NORM radionuclides of Pb, Po and Ra.

The CRs determined for terrestrial bush foods on sites impacted by U mining and/or milling activities were 1–2 orders of magnitude lower than those for natural sites, inferring lower transfer at higher soil concentrations for ^{227}Ac and ^{231}Pa. Hence, it is possible that modelling transfer on contaminated sites may over-estimate uptake and associated ingestion doses from consumption of bush foods.

The measured ^{227}Ac and ^{231}Pa $CR_{Tissue\text{-}Media}$ values were similar in magnitude, and relatively low compared to the ^{238}U series radionuclides ^{210}Pb, ^{210}Po, and ^{226}Ra, which are generally the highest contributors to dose from that series. Both ^{227}Ac and ^{231}Pa have $CR_{Tissue\text{-}Media}$ values close to those of Th and U, while also similar to Ra values for several organisms, but trending lower than Pb and Po.

Measurements of ^{227}Ac and ^{231}Pa in whole organisms were used to derive site-specific $CR_{WO\text{-}Media}$ values using species local to the ARR. Tissue:Whole-organism conversion factors from chemical analogues were used to derive $CR_{WO\text{-}Media}$ values for additional reference organisms from ^{227}Ac and ^{231}Pa measurements of individual tissues. The data generated for both ^{227}Ac and ^{231}Pa is by far the largest dataset of values for both isotopes and provides some of the only CR values globally for these two isotopes. This will allow improvement in the knowledge available for, and reliability of, environmental and human health dose assessments for the ^{235}U series globally.

Tissue:Whole-organism conversion factors for the 'mammal' reference organism were calculated from results for the Northern brown bandicoot (*Isoodon macrourus*) and for the 'freshwater bivalve' reference organism from results for the freshwater mussel (*Velesunio angasi*). For the 'mammal' reference organism the value derived from muscle tissue for ^{227}Ac was within the range of mean values for the different chemical analogues. This was also the case for the ^{231}Pa conversion factor derived from muscle tissue, however, the value for bone was higher.

For the 'freshwater bivalve' reference organism, the ^{227}Ac Tissue:Whole-organism conversion factor derived from soft tissue was within the mean range of values deduced from the different chemical analogues, though for shell it was higher. The conversion factors derived for the Northern brown bandicoot and freshwater mussel from measured values of ^{227}Ac and ^{231}Pa fall within the range of conversion factor values for relevant chemical analogues. Thus, providing support for use of conversion factors from chemical analogues to estimate ^{227}Ac and ^{231}Pa activity concentrations in environmental dose assessment where direct measurement is not achievable.

For terrestrial organisms, the $CR_{WO\text{-}Media}$ values derived from direct measurement of ^{227}Ac and ^{231}Pa activity concentrations or using Tissue:Whole-organism conversion factors were generally lower by an order of magnitude or more than the default $CR_{WO\text{-}Media}$ values from the ERICA tool. However, they were generally similar to those for Th and U in the ERICA tool.

For freshwater organisms the derived $CR_{WO\text{-}Media}$ values for ^{227}Ac and ^{231}Pa were generally of a similar magnitude to the default $CR_{WO\text{-}Media}$ values from the ERICA tool but an order of magnitude higher than those for Th and U in the ERICA tool. There were notable exceptions, with the ^{227}Ac and ^{231}Pa $CR_{WO\text{-}Media}$ values for Barramundi 1–2 orders of magnitude higher than the default $CR_{WO\text{-}Media}$ values, including those for Th and U, from the ERICA tool. The Agile wallaby $CR_{WO\text{-}Media}$ for ^{227}Ac was also an order of magnitude higher than the commonly used default $CR_{WO\text{-}Media}$ values for Th and U. This highlights the importance of undertaking site- or region-specific measurements for high-risk scenarios or where dose rates from screening assessments using default parameters exceed the prescribed benchmark dose rates.

Section 6.4 Dose assessment – Human exposure

The estimated annual ingestion dose above background for ^{227}Ac and ^{231}Pa from the consumption of bush foods derived from the RPA for the representative person is less than 1.6 µSv $year^{-1}$. This estimate is based on current occupancy estimates where 11.9% of bush foods consumed are derived from the RPA. However, if it is conservatively assumed that all bush foods consumed are derived from the RPA, this estimate remains below 13.0 µSv $year^{-1}$. With 9.6 and 1.8 µSv $year^{-1}$ (freshwater bush foods), and 0.69 and 0.73 µSv $year^{-1}$ (terrestrial bush foods) attributed to ^{227}Ac and ^{231}Pa respectively.

The highest potential contribution from the ^{235}U series to ingestion dose for freshwater bush foods is from ^{227}Ac in freshwater mussels, with a potential dose of up to 9.0 µSv $year^{-1}$. Under the dose assessment scenario from which the guideline value of 3 mBq L^{-1} for ^{226}Ra in water (Total) is derived, ^{227}Ac is estimated to contribute 1.5% of the dose relative to ^{226}Ra using the geometric mean CR for ^{227}Ac in soft tissues of freshwater mussels. The next highest potential contributor to annual ingestion dose from freshwater bush foods was only 0.87 µSv $year^{-1}$ from ^{231}Pa in the flesh of magpie goose and other waterfowl. The highest potential contributor to dose from terrestrial bush foods is from yams, with >45% of the estimated terrestrial dose from ^{227}Ac and ^{231}Pa attributed to this food item.

Annual ingestion doses from ^{235}U (excluding progeny) for freshwater and terrestrial bush foods were 0.21 and 0.020 µSv $year^{-1}$ respectively, which is low compared to ^{227}Ac and ^{231}Pa, highlighting that these two isotopes are the main contributors to dose from the ^{235}U series.

The ^{235}U series makes a significant contribution (23.5%) to total exposure from inhalation of dust, which represents approximately 6% of the total dose from the ^{235}U series for all pathways. Conversely, while the ^{235}U series contributes only 1.3% of the total (i.e., ^{235}U and ^{238}U series

radonuclides) external gamma dose, this represents about 22% of the total dose from the ^{235}U series for all pathways.

The total dose from the ^{235}U series is therefore expected to be a minor component of the total dose from the rehabilitated RUM site and ^{227}Ac and ^{231}Pa are not materially important to the bush food dose pathway.

Section 6.5 Dose assessment – Exposure to the environment

Region-specific organism data were used to define several new region-specific 'representative' organisms in the ERICA assessment tool in place of default reference organisms. A comparison of the DCCs for ERICA default reference organisms and region-specific terrestrial organisms shows that reference organism size has little impact on the determined dose.

6.5.1 Terrestrial environment

The highest dose rate from ^{227}Ac and ^{231}Pa combined determined for region-specific organisms in the terrestrial environment is to the Agile wallaby. However, the reference organism with the highest dose rate for the ^{227}Ac and ^{231}Pa combined dose rates was the ERICA default reference organism 'Lichen and Bryophytes'.

Comparison of dose to the limiting organism determined for the ^{238}U series (Reptile) showed the total dose from ^{227}Ac and ^{231}Pa to be less than 0.06% of the dose attributable to ^{226}Ra, which accounts for 94.9% of the dose from the ^{238}U series.

Internal dose rates for ERICA reference organisms from ^{227}Ac and ^{231}Pa combined accounted for more than 98% of the total dose, whereas it contributed a lower percentage for region-specific organisms at 81% and 85% for ^{227}Ac and ^{231}Pa respectively.

For region-specific organisms, the calculated dose rates from ^{227}Ac and ^{231}Pa combined were similar to those using the ERICA default $CR_{WO\text{-}Media}$ values for Th or U, but 1–2 orders of magnitude lower than the equivalent ERICA default reference organism using the ERICA default chemical analogue $CR_{WO\text{-}Media}$ values provided for Ac and Pa. Agile wallaby was the only exception being ~50% higher than the ERICA default, owing to the increased dose rate attributable to ^{227}Ac.

6.5.2 Freshwater environment

The highest dose rate determined for region-specific organisms in the freshwater environment is to the freshwater mussel. However, the reference organism with the highest dose rate for the ^{227}Ac and ^{231}Pa combined dose rates was the ERICA default reference organism 'Insect larvae'.

Comparison of dose to the limiting organism determined for the ^{238}U series (Mollusc - Bivalve) showed the total dose from ^{227}Ac and ^{231}Pa to be less than 0.9% of the dose attributable to ^{226}Ra, which accounts for 66% of the dose from the ^{238}U series radionuclides.

External dose makes a substantially higher relative contribution in the freshwater environment compared to the terrestrial environment, with a 30% contribution for ERICA reference organisms and 32% for region-specific organisms. This is attributable to the high default K_d value for ^{227}Ac, an improved estimate for which is necessary for more meaningful environmental dose assessments for the ^{235}U series in freshwater and marine environments.

Section 6.6 Concluding remarks: Implications, opportunities, and outlook

Rehabilitation planning of mine sites requires comprehensive and defensible scientific decisions. It is also important for those decisions to be communicated effectively, particularly where failure to do so can lead to greater social and business risks, such as has occurred on traditional lands in many parts of the world associated with U mining. Effective communication is equally necessary where the success of mine rehabilitation concerns protection of internationally significant places such as world heritage areas. There has been a general assumption that the ^{235}U series contribution to radiological dose in the context of U mining is low. However, without direct measurement of ^{235}U series radionuclides in environments associated with U mining, this assumption has remained untested.

Here, activity concentrations of ^{227}Ac and ^{231}Pa were measured in environmental media, local plants and animals important for a traditional diet and for ecosystem function, essential for Traditional Owners and their cultural relationship with the land. Samples were collected in a region with a sub-tropical monsoonal climate and a long association with U mining. Samples were relevant to a traditional diet for local Aboriginal people to enable dose assessment for the ingestion pathway post rehabilitation of the RUM. Local plants and animals have been modelled for input into the ERICA assessment tool to estimate doses in a practical manner for environmental dose assessment and reporting.

Estimated doses to people and the environment from the major radionuclides in the ^{235}U series (^{227}Ac and ^{231}Pa) are low and negligible compared to doses from the ^{238}U series radionuclides. The highest contributors to ingestion and environmental doses for rehabilitation of RUM remain ^{210}Pb, ^{210}Po and ^{226}Ra.

Regional datasets used to estimate doses from the ^{235}U series at RUM, and global datasets produced by the IAEA, ICRP or used in environmental dose models such as the ERICA integrated approach currently rely on the use of chemical analogues. The values reported here provide relevant data where none currently exists and will facilitate improved dose estimates for the ^{235}U series globally.

6.6.1 Implications for radiological doses from ^{235}U series radionuclides globally

Where inhalation doses from dust may be significant, even at equilibrium the ^{235}U series makes a significant contribution to dose. The ^{235}U series radionuclides are likely to be the dominant dose contributor from inhalation of dusts where higher activity concentrations of ^{235}U decay products, relative to the ^{238}U series, may occur (e.g., handling of REE concentrates). Nevertheless, if ^{226}Ra is present in relatively high activity concentrations, the dose from ^{222}Rn and progeny is likely to be the dominant contributor to dose from the inhalation pathway.

The ^{235}U series is unlikely to make a significant contribution to external gamma doses where ^{238}U series radionuclides are present as the gamma dose from ^{235}U and decay products is almost four times lower than if the relative dose is assumed using the ^{235}U:^{238}U natural activity ratio.

The dose assessments conducted in this thesis are likely to be highly ‘conservative’, with upper limit values for CRs being used in many instances when biota measurements were below the MDL. There is also the potential for lower uptake of radionuclides on contaminated sites and therefore CRs based on environmental measurements used predominantly for this thesis may have overestimated doses to people and wildlife.

6.6.2 Opportunities

With results from ^{227}Ac and ^{231}Pa presented in this thesis accounting for more than three quarters of consumption in the traditional diet model for the region, additional sample collection targeting the remaining food items will enable the full diet to be assessed. Region-specific whole organism data for ^{227}Ac and ^{231}Pa presented in this thesis also included more than half, and about one third, of the terrestrial and freshwater reference organisms represented in the ERICA assessment tool, respectively. There is no absolute need to cover all default reference organisms of the ERICA tool as not all may inhabit a given site or perform a significant ecological role. However, there remains an opportunity to enhance the coverage and relevance of the environmental dose assessment for RUM by targeting the remaining ecologically relevant reference organisms, some of which also lack region-specific information for the ^{238}U series radionuclides.

Improving the reliability, and traceability, of the K_d value for ^{227}Ac presents an opportunity for further work to be conducted both in the marine and freshwater environments, not only for dose assessment but to better understand environmental transport processes.

The CRs presented here could be further refined with additional measurements of ^{227}Ac and ^{231}Pa in environmental media, where measurements in soils may lend further support to the assumption of secular equilibrium in the ^{235}U decay series. Measurement of ^{231}Pa in water samples will also improve knowledge of mobility within freshwater ecosystems and there are opportunities to develop sample collection and preconcentration techniques that take into account the unique chemistry of Pa. Additional measurements of edible tissues and whole organism can also further understanding of the variability in CRs for ^{227}Ac and ^{231}Pa, in particular in those items that exhibited activity concentrations <MDL.

Results have shown that there is a low potential for significant environmental and ingestion doses from the ^{235}U series associated with U mining activities in a sub-tropical monsoonal environment. There is, however, scarce information to assess ingestion doses in other areas such as coastal, arid, and marine environments where radionuclide migration and biological uptake will differ substantially. Cooking and other food preparation techniques and the potential variations in radionuclide content that may be associated with those techniques were considered (e.g., unpeeled yams). Results were presented for some commercially available food products (e.g., water buffalo and pig flesh), the results presented in this thesis were only from wild caught animals. Further research involving measurement of ^{227}Ac and ^{231}Pa in farmed plants, animals, and foods, including analysis of variations in radionuclide content with different food preparation techniques, will improve understanding of the broader contribution from these radionuclides to dose to people and the environment.

6.6.3 Outlook: Where does or could this work lead?

The radiochemical methods developed for this thesis provide useful tools for further assessment of the potential impacts of U mining (and other mining activities) and doses associated with the ^{235}U series to people and the environment.

Outside the application of the analytical methods to research in U mining, relevant for this thesis, measurement of ^{231}Pa is primarily undertaken in oceanography studies and for radiometric dating techniques. It is important to note that the methods developed for this thesis for measurement of ^{231}Pa provide safer methods for analysis by removal of HF from chemical separation processes for other such areas of research. The use of AMS for measurement of ^{231}Pa

was applied for the first time at the 14UD pelletron accelerator and improvements were made to the measurement of ^{231}Pa using AMS. These improvements included reducing isobaric interference from ^{233}U by injection of PaO_2^-, increasing sensitivity with a ToF system, and enhancing precision through use of a fast-cycling system to more rapidly switch between measurement at mass 231 and 233. In conjunction with the preparation of a ^{237}Np cow for ^{233}Pa tracer production undertaken for this thesis, this facilitates the ability to measure large numbers of samples making a broad range of new studies feasible.

Targeted alpha therapy (TAT) is an emerging field in cancer therapy and the measurement of ^{227}Ac is required for assessment as an impurity in both ^{225}Ac and ^{223}Ra based TAT radiopharmaceuticals. Actinium-227 is also a primary contaminant in REE concentrates, which are critical minerals for a global technology and energy transition. The methods developed for this thesis will improve rapid analysis for ^{227}Ac (i.e., rapid alpha source preparation) and provide valuable information for environmental impact assessments in mineral resource processing. The alpha source preparation technique using micro-precipitation is also less prone to difficulties experienced with electrodeposition methods, making analysis more reliable. The methods developed for ^{227}Ac measurement in biological samples demonstrated exceptionally low limits of detection, increasing the range of laboratories that will be capable of quantifying ^{227}Ac at environmental levels.

The data generated for both ^{227}Ac and ^{231}Pa is by far the largest dataset of values for both isotopes and provides some of the only CR values globally for these two isotopes. This will allow improvement in the knowledge available for, and reliability of, environmental and human health dose assessments for the ^{235}U series globally.

Despite a substantial number of values for the environmental dose assessment being presented in this thesis, the data available to conduct such assessment is still comparatively sparse. Half of the terrestrial and under a third of the freshwater reference organisms in the ERICA integrated approach were covered in this thesis. In addition, values for a sub-tropical climate were presented which may differ in other areas such as coastal, arid, and marine environments. The methods developed in this thesis are highly suitable for application to ^{227}Ac and ^{231}Pa measurement of the remaining reference organisms for which no current data exists.

The data presented in this thesis in particular allows for human dose assessment in a regional context and covers most components of the traditional diet consumed in the region. Most of the foodstuffs analysed, however, are not relevant for the Australian typical diet and agricultural

produce (e.g., farmed food) was not represented. Further measurements of a range of dietary items, including assessing potential variations with food preparation and cooking techniques is needed to better understand the contribution to dose from ^{235}U series radionuclides for different diets around the world.

Bibliography

Agarande, M., Schmidt, S., Neiva-Marques, A.M., Bouisset, P., 2005. Plutonium, protactinium, uranium and thorium isotopes determination in environmental samples by SF ICP-MS. Radioprotection 40, S727-S731.

Aggarwal, S.K., 2018. A review on the mass spectrometric studies of americium: Present status and future perspective. Mass Spectrom. Rev. 37, 43-56.

Akber, R., Lu, P., Bollhöfer, A., Gellert, C., 2011. Radioactivity in Land Application Areas estimated from historic water monitoring data. Report prepared for Energy Resources of Australia Ltd.

Akovali, Y.A., 1996. Nuclear Data Sheets for A = 226. NDS 77, 433-470.

Al-Farsi, A., 2008. Radiological aspects of petroleum exploration and production in the sultanate of Oman. PhD thesis. Queensland University of Technology.

Al-Masri, M.S., Al Abdullah, J., Amin, Y., Al-Khateeb, Y., Al-Masri, W., Hassan, M., Nashawati, A., Al-Howary, M.A., 2020. Separation of actinium-227 and its daughter radium-223 from phosphogypsum. J. Radioanal. Nucl. Chem. 325, 463-470.

Alharbi, S.H., Akber, R.A., 2017. Broad-energy germanium detector for routine and rapid analysis of naturally occurring radioactive materials. J. Radioanal. Nucl. Chem. 311, 59-75.

Aliev, R.A., Ermolaev, S.V., Vasiliev, A.N., Ostapenko, V.S., Lapshina, E.V., Zhuikov, B.L., Zakharov, N.V., Pozdeev, V.V., Kokhanyuk, V.M., Myasoedov, B.F., Kalmykov, S.N., 2014. Isolation of Medicine-Applicable Actinium-225 from Thorium Targets Irradiated by Medium-Energy Protons. Solvent Extr. Ion Exch. 32, 468-477.

Altman, J., 1984. The dietary utilisation of flora and fauna by contemporary hunter-gatherers at Momega Outstation, north-central Arnhem Land. Aboriginal Studies Press.

Anderson, R.F., Bacon, M.P., Brewer, P.G., 1983a. Removal of ^{230}Th and ^{231}Pa at ocean margins. Earth. Planet. Sci. Lett. 66, 73-90.

Anderson, R.F., Bacon, M.P., Brewer, P.G., 1983b. Removal of ^{230}Th and ^{231}Pa from the open ocean. Earth. Planet. Sci. Lett. 62, 7-23.

Andersson, P., Garnier-Laplace, J., Beresford, N.A., Copplestone, D., Howard, B.J., Howe, P., Oughton, D., Whitehouse, P., 2009. Protection of the environment from ionising radiation in a

regulatory context (protect): proposed numerical benchmark values. J. Environ. Radioact. 100, 1100-1108.

ARPANSA, 2008. Safety Guide for the Management of Naturally Occurring Radioactive Material (NORM). www.arpansa.gov.au/regulation-and-licensing/regulatory-publications/radiation-protection-series/guides-and-recommendations/rps15 Accessed 17 July 2023

ARPANSA (Australian Radiation Protection and Nuclear Safety Agency), 2020a. Code for Radiation Protection in Planned Exposure Situations. Australian Radiation Protection and Nuclear Safety Agency. www.arpansa.gov.au/regulation-and-licensing/regulatory-publications/radiation-protection-series/codes-and-standards/rpsc-1 Accessed 26 August 2024

ARPANSA (Australian Radiation Protection and Nuclear Safety Agency), 2020b. Ionising radiation in our everyday environment. www.arpansa.gov.au/sites/default/files/2021_ionising_radiation_and_health.pdf Accessed 26 August 2024

ASNO (Australian Safeguards and Non-Proliferation Office), 2021. Australian Safeguards and Non-Proliferation Office Annual Report 2020–2021. www.dfat.gov.au/sites/default/files/asno-annual-report-2020-21.pdf Accessed 22 February 2024

Baes, C.F., III, Sharp, R.D., Sjoreen, A.L., Shor, R.W., 1984. Review and analysis of parameters for assessing transport of environmentally released radionuclides through agriculture. United States. www.nrc.gov/docs/ML1015/ML101590306.pdf Accessed 26 August 2024

Baggethun, P., 2009. https://imagej.nih.gov/ij/plugins/radial-profile.html Accessed 25 June 2010.

Barnes, R.M., Júnior, D.S., Krug, F.J., 2014. Chapter 1 - Introduction to Sample Preparation for Trace Element Determination, In: Microwave-Assisted Sample Preparation for Trace Element Analysis. (Ed.) Flores, É.M.d.M. Elsevier, Amsterdam, pp. 1-58.

Barry, A., Thomson, S., Dimayuga, I., Chaudhuri, A., Do, T., 2022. Isotope ratio method: state-of-the-art of forensic applications to CBRNE materials. Canadian Society of Forensic Science Journal 55, 115-141.

Beaugelin-Seiller, K., Goulet, R., Mihok, S., Beresford, N.A., 2016. Should we ignore U-235 series contribution to dose? J. Environ. Radioact. 151, Part 1, 114-125.

Belli, M., Indovina, L., 2020. The Response of Living Organisms to Low Radiation Environment and Its Implications in Radiation Protection. Front. Public Health 8, 601711.

Berry, J.A., Hobley, J., Lane, S.A., Littleboy, A.K., Nash, M.J., Oliver, P., Smith-Briggs, J.L., Williams, S.J., 1989. Solubility and sorption of protactinium in the near-field and far-field environments of a radioactive waste repository. Analyst 114, 339-347.

Birdlife Australia, 2023. HANZAB Volume 4 Parrots to Dollarbird. [Text before updates sourced from: Marchant, S. et al (eds) 1990-2006 Handbook of Australian, New Zealand and Antarctic Birds.Volume 1 to 7.]. Birdlife Australia. https://hanzab.birdlife.org.au/hanzab/hanzab-volume-4-parrots-to-dollarbird/ Accessed 9 November 2024

Bojanowski, R., Holm, E., Whitehead, N.E., 1987. Determination of ^{227}Ac in environmental samples by ion-exchange and alpha spectrometry. J. Radioanal. Nucl. Chem. 115, 23-37.

Bollhoefer, A., Ryan, B., Pfitzner, K., Martin, P., 2002. A radiation dose estimate for visitors of the South Alligator River Valley from remnants of uranium mining and milling activities. Supervising Scientist, Darwin.

Bollhöfer, A., Beraldo, A., Pfitzner, K., Esparon, A., Doering, C., 2014. Determining a pre-mining radiological baseline from historic airborne gamma surveys: A case study. Sci. Total Environ. 468-469, 764-773.

Bollhöfer, A., Brazier, J., Humphrey, C., Ryan, B., Esparon, A., 2011. A study of radium bioaccumulation in freshwater mussels, *Velesunio angasi*, in the Magela Creek catchment, Northern Territory, Australia. J. Environ. Radioact. 102, 964-974.

Bollhöfer, A., Doering, C., Fox, G., Pfitzner, J., Medley, P., 2012. Assessment of the radiological exposure pathways at Rum Jungle Creek South (Rum Jungle Lake Reserve) - Batchelor. Report prepared by the Environmental Research Institute of the Supervising Scientist, Darwin, N.T.

Bollhöfer, A., Doering, C., Medley, P., 2016. A revised operational limit for the water ^{226}Ra activity concentration downstream of Ranger mine. Internal Report 643, Darwin, N.T. www.dcceew.gov.au/sites/default/files/documents/ir643.pdf Accessed 6 May 2024

Boretti, A., 2023. There is no reason to persist in the linear no-threshold (LNT) assumption. J. Environ. Radioact. 266-267, 107239.

Brady, C., Christophersen, P., O'Brien, J., 2021. Incorporating Indigenous knowledge in mine closure: Ranger Uranium Mine. Proc. R. Soc. Vic. 133, 18-22.

Braysher, E., Russell, B., Woods, S., García-Miranda, M., Ivanov, P., Bouchard, B., Read, D., 2019. Complete dissolution of solid matrices using automated borate fusion in support of

nuclear decommissioning and production of reference materials. J. Radioanal. Nucl. Chem. 321, 183-196.

Bréchignac, F., 2016. Assessing Ecological Risk from Radiation Requires an Ecosystem Approach, In: Genetics, Evolution and Radiation: Crossing Borders, The Interdisciplinary Legacy of Nikolay W. Timofeeff-Ressovsky. (Eds.) Korogodina, V.L., Mothersill, C.E., Inge-Vechtomov, S.G., Seymour, C.B. Springer International Publishing, Cham, pp. 207-223. https://doi.org/10.1007/978-3-319-48838-7_18

Bréchignac, F., Oughton, D., Mays, C., Barnthouse, L., Beasley, J.C., Bonisoli-Alquati, A., Bradshaw, C., Brown, J., Dray, S., Geras'kin, S., Glenn, T., Higley, K., Ishida, K., Kapustka, L., Kautsky, U., Kuhne, W., Lynch, M., Mappes, T., Mihok, S., Møller, A.P., Mothersill, C., Mousseau, T.A., Otaki, J.M., Pryakhin, E., Rhodes Jr, O.E., Salbu, B., Strand, P., Tsukada, H., 2016. Addressing ecological effects of radiation on populations and ecosystems to improve protection of the environment against radiation: Agreed statements from a Consensus Symposium. J. Environ. Radioact. 158–159, 21-29.

Brenner, D.J., 2012. We can do better than effective dose for estimating or comparing low-dose radiation risks. Ann. ICRP 41, 124-128.

Brown, D., Maddock, A.G., 1963. Protactinium. Q. Rev. Chem. Soc. 17, 289-341.

Brown, I.G., 2006. The Physics and Technology of Ion Sources. Wiley, United States.

Brown, J.E., Alfonso, B., Avila, R., Beresford, N.A., Copplestone, D., Hosseini, A., 2016. A new version of the ERICA tool to facilitate impact assessments of radioactivity on wild plants and animals. J. Environ. Radioact. 153, 141-148.

Brown, T.A., Marchetti, A.A., Martinelli, R.E., Cox, C.C., Knezovich, J.P., Hamilton, T.F., 2004. Actinide measurements by accelerator mass spectrometry at Lawrence Livermore National Laboratory. Nucl. Instrum. Methods Phys. Res. B 223–224, 788-795.

Browne, E., 2002. Nuclear Data Sheets for A=223, NDS 93, 763 (2001) - E. Browne. NDS 96, 391.

Bruland, Ø.S., Nilsson, S., Fisher, D.R., Larsen, R.H., 2006. High-Linear Energy Transfer Irradiation Targeted to Skeletal Metastases by the α-Emitter ^{223}Ra: Adjuvant or Alternative to Conventional Modalities? Clin. Cancer. Res. 12, 6250s-6257s.

Buraglio, N., 2000. Accelerator Mass Spectrometry of ^{129}I and Its Applications in Natural Water Systems. PhD thesis. Uppsala University.

Burney, G.A., Harbour, R.M., 1974. Radiochemistry of neptunium. www.osti.gov/servlets/purl/4242713 Accessed 26 August 2024

Caffrey, E.A., Rood, A.S., Grogan, H.A., Mangini, C., Till, J.E., 2023. Comparison of Doses from Disposals of Technologically Enhanced Naturally Occurring Radioactive Materials in Kentucky and Oregon. Health Phys. 124, 441-450.

Campbell, J.E., Robajdek, E.S., Anthony, D.S., 1956. The Metabolism of Ac^{227} and Its Daughters Th^{227} and Ra^{223} by Rats. Radiat. Res. 4, 294-302.

Carvalho, F.P., 2012. Environmental Radioactive Impact Associated to Uranium Production. Am. J. Environ. Sci. 7 (6), 547-553.

Chao, T.T., Sanzolone, R.F., 1992. Decomposition techniques. J. Geochem. Explor. 44, 65-106.

Chapman, W.H., Fisher, H.L., Pratt, M.W., 1968. Concentration Factors of Chemical Elements in Edible Aquatic Organisms. United States. https://ntrl.ntis.gov/NTRL/dashboard/searchResults/titleDetail/UCRL50564REV1.xhtml Accessed 26 August 2024

Chapuisat, M., Keller, L., 2002. Division of Labour Influences the Rate of Ageing in Weaver Ant Workers. PBioS 269, 909-913.

Christl, M., Wacker, L., Lippold, J., Synal, H.-A., Suter, M., 2007. Protactinium-231: A new radionuclide for AMS. Nucl. Instrum. Methods Phys. Res. B 262, 379-384.

Commonwealth of Australia, 1999. Environmental Requirements of the Commonwealth of Australia for the Operation of Ranger Uranium Mine.

Commonwealth of Australia, 2016. Kakadu National Park Management Plan 2016-2026.

Copplestone, D., Beresford, N.A., Brown, J.E., Yankovich, T., 2013. An international database of radionuclide concentration ratios for wildlife: development and uses. J. Environ. Radioact. 126, 288-298.

Ćujić, M., Dragović, S., 2018. Assessment of dose rate to terrestrial biota in the area around coal fired power plant applying ERICA tool and RESRAD BIOTA code. J. Environ. Radioact. 188, 108-114.

Currie, L.A., 1968. Limits for qualitative detection and quantitative determination. Application to radiochemistry. Anal. Chem. 40, 586-593.

Currie, L.A., 1995. Nomenclature in evaluation of analytical methods including detection and quantification capabilities (IUPAC Recommendations 1995). Pure Appl. Chem. 67, 1699-1723.

Dalvi, A.A., Remya Devi, P.S., Singh, V., Tewari, R., Verma, R., Swain, K.K., 2021. Characterization of siliceous cake for the beneficiation of ^{231}Pa. Prog. Nucl. Energy 134, 103675.

Darling, P., Society for Mining, M., Exploration, 2011. SME Mining Engineering Handbook, Third Edition. Society for Mining, Metallurgy, and Exploration.

Davis, T., 1982. Maturity and sexuality in Barramundi, *Lates calcarifer* (Bloch), in the Northern Territory and south-eastern Gulf of Carpentaria. Mar. Freshwat. Res. 33, 529-545.

DCEEW (Department of Climate Change, Energy, the Environment and Water), 2021. www.dcceew.gov.au/parks-heritage/national-parks/kakadu-national-park/culture-and-history/traditional-owners-bininjmungguy#clans-and-kinship Accessed 22 February 2024.

De Cesare, M., Fifield, L.K., Weisser, D.C., Tsifakis, D., Cooper, A., Lobanov, N.R., Tunningley, T.B., Tims, S.G., Wallner, A., 2015. A new fast-cycling system for AMS at ANU. Nucl. Instrum. Methods Phys. Res. B 361, 475-482.

Deblonde, G.J.P., Zavarin, M., Kersting, A.B., 2021. The coordination properties and ionic radius of actinium: A 120-year-old enigma. Coord. Chem. Rev. 446, 214130.

Dennerlein, K., Kiesewetter, F., Kilo, S., Jäger, T., Göen, T., Korinth, G., Drexler, H., 2016. Dermal absorption and skin damage following hydrofluoric acid exposure in an ex vivo human skin model. Toxicol. Lett. 248, 25-33.

Döbeli, M., Kottler, C., Stocker, M., Weinmann, S., Synal, H.A., Grajcar, M., Suter, M., 2004. Gas ionization chambers with silicon nitride windows for the detection and identification of low energy ions. Nucl. Instrum. Methods Phys. Res. B 219-220, 415-419.

Doering, C., 2018. Radiation doses to Aboriginal people living near Ranger uranium mine Internal Report 655. Supervising Scientist, Darwin.

Doering, C., 2019a. Public exposure to external gamma radiation on a mine landform covered by low uranium grade waste rock. Radiat. Prot. Dosimetry 188, 123-128.

Doering, C., 2019b. Whole organism concentration ratios of radionuclides and metals in terrestrial vertebrates of an Australian tropical savanna environment. J. Environ. Radioact. 207, 7-14.

Doering, C., Bollhöfer, A., 2016a. A database of radionuclide activity and metal concentrations for the Alligator Rivers Region uranium province. J. Environ. Radioact. 162–163, 154-159.

Doering, C., Bollhöfer, A., 2016b. A soil radiological quality guideline value for wildlife-based protection in uranium mine rehabilitation. J. Environ. Radioact. 151, Part 3, 522-529.

Doering, C., Bollhöfer, A., 2016c. A tool for calculating concentration ratios from large environmental datasets. J. Environ. Radioact. 165, 32-34.

Doering, C., Bollhöfer, A., 2017. Water hardness determines ^{226}Ra uptake in the tropical freshwater mussel. J. Environ. Radioact. 172, 96-105.

Doering, C., Bollhöfer, A., Medley, P., 2017. Estimating doses from Aboriginal bush foods post-remediation of a uranium mine. J. Environ. Radioact. 172, 74-80.

Doering, C., Carpenter, J., Orr, B., Urban, D., 2019a. Whole organism concentration ratios in freshwater wildlife from an Australian tropical U mining environment and the derivation of a water radiological quality guideline value. J. Environ. Radioact. 198, 27-35.

Doering, C., McMaster, S.A., Johansen, M.P., 2019b. Modelling the dispersion of radionuclides in dust from a landform covered by low uranium grade waste rock. J. Environ. Radioact. 202, 51-58.

Doering, C., McMaster, S.A., Johansen, M.P., 2022. Corrigendum to “Modelling the dispersion of radon-222 from a landform covered by low uranium grade waste rock” [J. Environ. Radioact. 192 (2018) 498–504]. J. Environ. Radioact. 250, 106911.

Doering, C., Medley, P., Orr, B., Urban, D., 2018. Whole organism to tissue concentration ratios derived from an Australian tropical dataset. J. Environ. Radioact. 189, 31-39.

Douglas, M., Bernacki, B.E., Erchinger, J.L., Finn, E.C., Fuller, E.S., Hoppe, E.W., Keillor, M.E., Morley, S.M., Mullen, C.A., Orrell, J.L., Panisko, M.E., Warren, G.A., Wright, M.E., 2016. Liquid scintillation counting of environmental radionuclides: a review of the impact of background reduction. J. Radioanal. Nucl. Chem. 307, 2495-2504.

Dowie, M., 2009. Nuclear Caribou: on the front lines of the new uranium rush with the Inuit of Nunavut., Orion Mag.

Doyle, J., 2019. Nuclear Safeguards, Security, and Nonproliferation : Achieving Security with Technology and Policy. Elsevier Science & Technology, Saint Louis, United States.

Dulaiova, H., Sims, K.W., Charette, M., Prytulak, J., Blusztajn, J., 2013. A new method for the determination of low-level actinium-227 in geological samples. J. Radioanal. Nucl. Chem. 296, 279-283.

Dulieu, C., Kellett, M.A., Mougeot, X., 2017. Dissemination and visualisation of reference decay data from Decay Data Evaluation Project (DDEP). EPJ Web Conf. 146, 07004.

Edwards, G.P., Webb, G.J., Manolis, S.C., Mazanov, A., 2017. Morphometric analysis of the Australian freshwater crocodile (*Crocodylus johnstoni*). Aust. J. Zool. 65, 97-111.

Edwards, R.L., Cheng, H., Murrell, M.T., Goldstein, S.J., 1997. Protactinium-231 Dating of Carbonates by Thermal Ionization Mass Spectrometry: Implications for Quaternary Climate Change. Sci 276, 782-786.

Ehlken, S., Kirchner, G., 2002. Environmental processes affecting plant root uptake of radioactive trace elements and variability of transfer factor data: a review. J. Environ. Radioact. 58, 97-112.

Eichrom Technologies Inc., 2005. ACW08: Thorium and Neptunium in Water. Revision 1.7.

Eichrom Technologies Inc., 2006. ACW16 (VBS): Americium, Neptunium, Plutonium, Thorium, Curium and Uranium in Water (with Vacuum Box System). Revision 1.0.

Eichrom Technologies Inc., 2014. ACS07: Uranium in soil. Revision 1.6. www.eichrom.com/wp-content/uploads/2018/02/acs07-16_uranium-in-soil.pdf

Eppich, G.R., Williams, R.W., Gaffney, A.M., Schorzman, K.C., 2013. ^{235}U-^{231}Pa age dating of uranium materials for nuclear forensic investigations. J. Anal. At. Spectrom. 28, 666-674.

ERA, 2023. 2023 Ranger Mine Closure Plan. Revision 1.23.1. www.energyres.com.au/ranger-rehabilitation/mine-closure-plan/ Accessed 26 August 2024

Eriksen, D.O., Ryningen, B., Schoultz, B., Salberg, G., Larsen, R.H., 2012. Liquid Scintillation Spectroscopy of ^{227}Ac and Daughters. J. anal. sci. methods instrum. 2, 4.

Essex, R.M., Mann, J.L., Collé, R., Laureano-Perez, L., Bennett, M.E., Dion, H., Fitzgerald, R., Gaffney, A.M., Gourgiotis, A., Hubert, A., Inn, K.G.W., Kinman, W.S., Lamont, S.P., Steiner, R., Williams, R.W., 2018. New determination of the 229Th half-life. J. Radioanal. Nucl. Chem. 318, 515-525.

Ettenhuber, E., 2002. Investigations and radiological assessments of mining residues in Germany. Int. congr. ser. 1225, 103-110.

Feldman, A., Meiri, S., 2012. Length–mass allometry in snakes. Biol. J. Linn. Soc. 108, 161-172.

Ferguson, J., Goleby, A., 1980. Uranium in the Pine Creek Geosyncline. International Atomic Energy Agency, Vienna.

Ferrier, M.G., Batista, E.R., Berg, J.M., Birnbaum, E.R., Cross, J.N., Engle, J.W., La Pierre, H.S., Kozimor, S.A., Lezama Pacheco, J.S., Stein, B.W., Stieber, S.C.E., Wilson, J.J., 2016. Spectroscopic and computational investigation of actinium coordination chemistry. Nat. Commun. 7, 12312.

Fietzke, J., Bollhöfer, A., Frank, N., Mangini, A., 1999. Protactinium determination in manganese crust VA13/2 by thermal ionization mass spectrometry (TIMS). Nucl. Instrum. Methods Phys. Res. B 149, 353-360.

Fifield, L.K., 1999. Accelerator mass spectrometry and its applications. Rep. Prog. Phys. 62, 1223-1274.

Fifield, L.K., 2008. Accelerator mass spectrometry of the actinides. Quat. Geochronol. 3, 276-290.

Fifield, L.K., Clacher, A.P., Morris, K., King, S.J., Cresswell, R.G., Day, J.P., Livens, F.R., 1997. Accelerator mass spectrometry of the planetary elements. Nucl. Instrum. Methods Phys. Res. B 123, 400-404.

Fifield, L.K., Tims, S.G., Stone, J.O., Argento, D.C., De Cesare, M., 2013. Ultra-sensitive measurements of ^{36}Cl and ^{236}U at the Australian National University. Nucl. Instrum. Methods Phys. Res. B 294, 126-131.

Fowler, S.W., 2011. ^{210}Po in the marine environment with emphasis on its behaviour within the biosphere. J. Environ. Radioact. 102, 448-461.

Frantellizzi, V., Cosma, L., Brunotti, G., Pani, A., Spanu, A., Nuvoli, S., De Cristofaro, F., Civitelli, L., De Vincentis, G., 2020. Targeted Alpha Therapy with Thorium-227. Cancer Biother. Radiopharm. 35, 437-445.

Frith, H., Davies, S., 1961. Ecology of the Magpie Goose, *Anseranas semipalmata* Latham (Anatidae). Wildl. Res. 6, 91-141.

Fry, C., Thoennessen, M., 2013. Discovery of actinium, thorium, protactinium, and uranium isotopes. At. Data Nucl. Data Tables 99, 345-364.

Fuller, N., Ford, A.T., Nagorskaya, L.L., Gudkov, D.I., Smith, J.T., 2018. Reproduction in the freshwater crustacean Asellus aquaticus along a gradient of radionuclide contamination at Chernobyl. Sci. Total Environ. 628-629, 11-17.

García-Toraño, E., 2003. A model shape for the analysis of alpha-particle spectra. Nucl. Instrum. Methods Phys. Res. A 498, 289-291.

Garnier-Laplace, J., Copplestone, D., Gilbin, R., Alonzo, F., Ciffroy, P., Gilek, M., Agüero, A., Björk, M., Oughton, D.H., Jaworska, A., Larsson, C.M., Hingston, J.L., 2008. Issues and practices in the use of effects data from FREDERICA in the ERICA Integrated Approach. J. Environ. Radioact. 99, 1474-1483.

Garnier-Laplace, J., Della-Vedova, C., Andersson, P., Copplestone, D., Cailes, C., Beresford, N.A., Howard, B.J., Howe, P., Whitehouse, P., 2010. A multi-criteria weight of evidence approach for deriving ecological benchmarks for radioactive substances. J. Radiol. Prot. 30, 215.

Gascón, J.L., Muñoz, A., 2003. Optimization of the parameters affecting the solid state detector efficiency in alpha-spectrometry. J. Radioanal. Nucl. Chem. 257, 371-374.

Gascoyne, M., 1985. Application of the $^{227}Th^{230}Th$ method to dating Pleistocene carbonates and comparison with other dating methods. Geochim. Cosmochim. Acta 49, 1165-1171.

Gdaniec, S., Roy-Barman, M., Foliot, L., Thil, F., Dapoigny, A., Burckel, P., Garcia-Orellana, J., Masqué, P., Mörth, C.-M., Andersson, P.S., 2018. Thorium and protactinium isotopes as tracers of marine particle fluxes and deep water circulation in the Mediterranean Sea. Mar. Chem. 199, 12-23.

Geibert, W., Charette, M., Kim, G., Moore, W.S., Street, J., Young, M., Paytan, A., 2008. The release of dissolved actinium to the ocean: A global comparison of different end-members. Mar. Chem. 109, 409-420.

Geibert, W., Vöge, I., 2008. Progress in the determination of ^{227}Ac in sea water. Mar. Chem. 109, 238-249.

Gellermann, R., Caplin, H., Chambers, N., Dongen, O.v., Grandia, F., Hondros, J., Kunze, C., Michalik, B., Pepin, S., Rovenska, K.N., Trevisi, R., 2023. Experience with NORM waste disposal in different European countries. Radiat. Prot. Dosimetry 199, 835-842.

Geras'kin, S.A., 2016. Ecological effects of exposure to enhanced levels of ionizing radiation. J. Environ. Radioact. 162-163, 347-357.

Geras'kin, S.A., Alexakhin, R.M., Oudalova, A.A., 2016. Effects of Ionizing Radiation on Populations and Ecosystems, In: Genetics, Evolution and Radiation: Crossing Borders, The Interdisciplinary Legacy of Nikolay W. Timofeeff-Ressovsky. (Eds.) Korogodina, V.L., Mothersill, C.E., Inge-Vechtomov, S.G., Seymour, C.B. Springer International Publishing, Cham, pp. 237-250. https://doi.org/10.1007/978-3-319-48838-7_20

Gherardi, J.-M., Labeyrie, L., Nave, S., Francois, R., McManus, J.F., Cortijo, E., 2009. Glacial-interglacial circulation changes inferred from $^{231}Pa/^{230}Th$ sedimentary record in the North Atlantic region. Paleoceanogr. 24.

Gies, R.A., Ballou, J.E., Case, A.C., Ryan, J.L., 1984. Method for determining protactinium-231 in biological samples. Health Phys. 46, 5.

Gillberg-Wickman, M., 1983. The geochemical behavior of protactinium 231 and its chosen geochemical analogue thorium in the biosphere. Sweden. http://inis.iaea.org/search/search.aspx?orig_q=RN:16039428 Accessed 26 August 2024

Gilmore, G.R., 2008. Spectrometer Calibration, In: Practical Gamma-Ray Spectrometry. (Ed.) Gilmore, G.R., pp. 143-163. https://onlinelibrary.wiley.com/doi/abs/10.1002/9780470861981.ch7

Gladkis, L., 2008. Development of AMS techniques for ^{53}Mn and ^{236}U. PhD thesis. Australian National University.

Golian, C., Nightingale, T., Airey, P.L., 1984. Protactinium-231 measurement and application to a uranium series transport model. Nucl. Instrum. Methods Phys. Res. 223, 577-581.

Goulet, R.R., Newsome, L., Vandenhove, H., Keum, D.-K., Horyna, J., Kamboj, S., Brown, J., Johansen, M.P., Twining, J., Wood, M.D., Černe, M., Beaugelin-Seiller, K., Beresford, N.A., 2022. Best practices for predictions of radionuclide activity concentrations and total absorbed dose rates to freshwater organisms exposed to uranium mining/milling. J. Environ. Radioact. 244-245, 106826.

Graetz, G., 2014. Uranium mining and First Peoples: the nuclear renaissance confronts historical legacies. J. Clean. Prod. 84, 339-347.

Graetz, G., Manning, H., 2011. The Politics of Uranium Mining in Australia, In: Australia's Uranium Trade : The Domestic and Foreign Policy Challenges of a Contentious Export. (Eds.) Frühling, S., Clarke, M., O'Neill, A. Taylor & Francis Group, London, UNITED KINGDOM, pp. 137-163. http://ebookcentral.proquest.com/lib/anu/detail.action?docID=4501166 Accessed 13 February 2024

Grench, H.A., Buchanan, R.A., 1973. Determination of natural radioactivity in rare earth materials. NucIM 112, 415-421.

Groska, J., Vajda, N., Molnár, Z., Bokori, E., Szeredy, P., Zagyvai, M., 2016. Determination of actinides in radioactive waste after separation on a single DGA resin column. J. Radioanal. Nucl. Chem. 309, 1145-1158.

Grossmann, R., Maier, H.J., Szerypo, J., Friebel, H.U., 2008. Preparation of ^{231}Pa targets. Nucl. Instrum. Methods Phys. Res. A 590, 122-125.

Grün, R., 2006. Direct dating of human fossils. American Journal of Physical Anthropology 131, 2-48.

Grün, R., Aubert, M., Hellstrom, J., Duval, M., 2010. The challenge of direct dating old human fossils. Quat. Int. 223-224, 87-93.

Guérin, N., Fabian, X., Leppinen, J., Gagné, A., 2022. Determination of ^{227}Ac in water by alpha spectrometry after purification with titanium phosphate and DGA resin. J. Radioanal. Nucl. Chem. 331, 5781-5788.

Hain, K., Steier, P., Froehlich, M.B., Golser, R., Hou, X., Lachner, J., Nomura, T., Qiao, J., Quinto, F., Sakaguchi, A., 2020. ^{233}U/^{236}U signature allows to distinguish environmental emissions of civil nuclear industry from weapons fallout. Nat. Commun. 11, 1275.

Hamilton, J.G., 1948. The Metabolic Properties of the Fission Products and Actinide Elements. Rev. Mod. Phys 20, 718-728.

Han, B.X., Southon, J.R., Roberts, M.L., von Reden, K.F., 2007. Computer simulation of MC-SNICS for performance improvements. Nucl. Instrum. Methods Phys. Res. B 261, 588-593.

Hanfi, M.Y., Yarmoshenko, I.V., Zhukovsky, M.V., 2021. Assessment of radiation dose from inhalation of outdoor dust containing natural radionuclides. Radiat. Prot. Dosimetry 196, 184-189.

Hansen, R.G., Ring, E.J. (Council for Mineral Technology), 1983. The preparation and certification of a uranium reference material. https://inis.iaea.org/collection/NCLCollectionStore/_Public/14/785/14785946.pdf Accessed 26 August 2024

Harrison, J., Day, P., 2008. Radiation doses and risks from internal emitters. J. Radiol. Prot. 28, 137.

Harrison, J.D., Stather, J.W., 1981. The Gastrointestinal Absorption of Protactinium, Uranium, and Neptunium in the Hamster. Radiat. Res. 88, 47-55.

Harvey, B.R., Lovett, M.B., 1984. The use of yield tracers for the determination of alpha-emitting actinides in the marine environment. Nucl. Instrum. Methods Phys. Res. 223, 224-234.

Hatcher-Lamarre, J.L., Sanders, V.A., Rahman, M., Cutler, C.S., Francesconi, L.C., 2021. Alpha emitting nuclides for targeted therapy. Nucl. Med. Biol. 92, 228-240.

Hayes, C.T., Anderson, R.F., Fleisher, M.Q., Vivancos, S.M., Lam, P.J., Ohnemus, D.C., Huang, K.-F., Robinson, L.F., Lu, Y., Cheng, H., Edwards, R.L., Moran, S.B., 2015. Intensity of Th and Pa scavenging partitioned by particle chemistry in the North Atlantic Ocean. Mar. Chem. 170, 49-60.

Hellborg, R., Skog, G., 2008. Accelerator mass spectrometry. Mass Spectrom. Rev. 27, 398-427.

Higley, K.A., Bytwerk, D.P., 2007. Generic approaches to transfer. J. Environ. Radioact. 98, 4-23.

Hirth, G., 2014. A review of existing Australian radionuclide activity concentration data in non-human biota inhabiting uranium mining environments, Technical Report Series No. 167. www.arpansa.gov.au/sites/default/files/legacy/pubs/technicalreports/tr167.pdf Accessed 30 July 2023

Hirth, G.A., Grzechnik, M., Tinker, R., Larsson, C.M., 2018. Australia's proactive approach to radiation protection of the environment: how integrated is it with radiation protection of humans? Ann. ICRP 47, 313-326.

Hirth, G.A., Johansen, M.P., Carpenter, J.G., Bollhöfer, A., Beresford, N.A., 2017. Whole-organism concentration ratios in wildlife inhabiting Australian uranium mining environments. J. Environ. Radioact. 178-179, 385-393.

Hoenig, M., 2001. Preparation steps in environmental trace element analysis — facts and traps. Talanta 54, 1021-1038.

Horwitz, E.P., Dietz, M.L., Chiarizia, R., Diamond, H., Essling, A.M., Graczyk, D., 1992. Separation and preconcentration of uranium from acidic media by extraction chromatography. Anal. Chim. Acta 266, 25-37.

Horwitz, E.P., Dietz, M.L., Chiarizia, R., Diamond, H., Maxwell Iii, S.L., Nelson, M.R., 1995. Separation and preconcentration of actinides by extraction chromatography using a supported liquid anion exchanger: application to the characterization of high-level nuclear waste solutions. Anal. Chim. Acta 310, 63-78.

Horwitz, E.P., McAlister, D.R., Bond, A.H., Barrans, R.E., 2005. Novel Extraction of Chromatographic Resins Based on Tetraalkyldiglycolamides: Characterization and Potential Applications. Solvent Extr. Ion Exch. 23, 319-344.

Hosseini, A., Beresford, N.A., Brown, J.E., Jones, D.G., Phaneuf, M., Thørring, H., Yankovich, T., 2010. Background dose-rates to reference animals and plants arising from exposure to naturally occurring radionuclides in aquatic environments. J. Radiol. Prot. 30, 235.

Hotchkis, M.A.C., Child, D., Fink, D., Garton, D., Levchenko, V., Wilcken, K., 2013a. Sulphur hexafluoride as a stripper gas for tandem accelerators. Nucl. Instrum. Methods Phys. Res. B 302, 14-18.

Hotchkis, M.A.C., Child, D., Fink, D., Levchenko, V., Wallner, A., 2013b. Investigation of gas stripping at 4.1 MeV for high mass negative ions. Nucl. Instrum. Methods Phys. Res. B 294, 387-391.

Howard, B.J., Wells, C., Beresford, N.A., Copplestone, D., 2013. Exploring methods to prioritise concentration ratios when estimating weighted absorbed dose rates to terrestrial Reference Animals and Plants. J. Environ. Radioact. 126, 326-337.

Hübener, S., 2003. Actinide Elements, In: Encyclopedia of Physical Science and Technology (Third Edition). (Ed.) Meyers, R.A. Academic Press, New York, pp. 211-236. www.sciencedirect.com/science/article/pii/B0122274105000119 Accessed 10 March 2023

Humphrey, C.L., Simpson, R.D., 1985. The biology and ecology of Velesunio angasi (Bivalvia: Hyriidae) in the Magela Creek, Northern Territory. Supervising Scientist for the Alligator Rivers Region. https://www.dcceew.gov.au/sites/default/files/documents/ofr038.pdf Accessed 19/07/2023

IAEA, 1980. Biological Implications of Radionuclides Released from Nuclear Industries (Vienna, 26-30 March 1979). International Atomic Energy Agency, Vienna.

IAEA (International Atomic Energy Agency), 2001. Generic Models for Use in Assessing the Impact of Discharges of Radioactive Substances to the Environment, Safety Reports Series No. 19. IAEA, Vienna. https://www-pub.iaea.org/MTCD/Publications/PDF/Pub1103_scr.pdf Accessed 29 July 2023

IAEA (International Atomic Energy Agency), 2004. Sediment Distribution Coefficients and Concentration Factors for Biota in the Marine Environment, Technical Reports Series No. 422.

IAEA, Vienna. www.iaea.org/publications/6855/sediment-distribution-coefficients-and-concentration-factors-for-biota-in-the-marine-environment Accessed 19 July 2023

IAEA (International Atomic Energy Agency), 2010. Handbook of Parameter Values for the Prediction of Radionuclide Transfer in Terrestrial and Freshwater Environments, Technical Reports Series No. 472. IAEA, Vienna. https://www-pub.iaea.org/MTCD/Publications/PDF/trs472_web.pdf Accessed 19 July 2023

IAEA (International Atomic Energy Agency), 2014a. The Environmental Behaviour of Radium: Revised Edition, Technical Reports Series No. 476. IAEA, Vienna. https://www-pub.iaea.org/MTCD/Publications/PDF/trs476web-45482131.pdf Accessed 19 July 2023

IAEA (International Atomic Energy Agency), 2014b. Handbook of Parameter Values for the Prediction of Radionuclide Transfer to Wildlife, Technical Reports Series No. 479. IAEA, Vienna. https://www-pub.iaea.org/MTCD/Publications/PDF/Trs479_web.pdf Accessed 19 July 2023

IAEA (International Atomic Energy Agency), 2014c. Radiation Protection and Safety of Radiation Sources: International Basic Safety Standards, IAEA Safety Standards Series No. GSR Part 3. IAEA, Vienna. https://www-pub.iaea.org/MTCD/Publications/PDF/Pub1578_web-57265295.pdf Accessed 19 July 2023

IAEA (International Atomic Energy Agency), 2017. The Environmental Behaviour of Polonium, Technical Reports Series No. 484. IAEA, Vienna. https://www-pub.iaea.org/MTCD/Publications/PDF/D484_web.pdf Accessed 19 July 2023

IAEA (International Atomic Energy Agency), 2022. Exposure due to Radionuclides in Food other than during a Nuclear or Radiological Emergency, Part 2: Considerations in Implementing Requirement 51 of IAEA General Safety Requirements Part 3 (International Basic Safety Standards). IAEA, Vienna. https://www-pub.iaea.org/MTCD/publications/PDF/TE-2011web.pdf Accessed 19 July 2023

IAEA (International Atomic Energy Agency), 2023. The Environmental Behaviour of Uranium, Technical Reports Series No. 488. IAEA, Vienna. www.iaea.org/publications/14688/the-environmental-behaviour-of-uranium Accessed 29 November 2023

ICRP, 1977. Recommendations of the International Commission on Radiological Protection. ICRP Publication 26. Ann. ICRP 1 (3).

ICRP, 1981. Metabolic data for protactinium. Ann. ICRP 6, 108-110.

ICRP, 1991. 1990 Recommendations of the International Commission on Radiological Protection. ICRP Publication 60. Ann. ICRP 21 (1-3).

ICRP, 1993. Age-dependent Doses to Members of the Public from Intake of Radionuclides - Part 2 Ingestion Dose Coefficients. ICRP Publication 67. Ann. ICRP 23.

ICRP, 1995. Age-dependent Doses to Members of the Public from Intake of Radionuclides - Part 4 Inhalation Dose Coefficients. ICRP Publication 71. Ann. ICRP 25 (3-4).

ICRP, 2003. A Framework for Assessing the Impact of Ionising Radiation on Non-human Species. ICRP Publication 91. Ann. ICRP 33 (3).

ICRP, 2006. Assessing Dose of the Representative Person for the Purpose of the Radiation Protection of the Public. ICRP Publication 101a. Ann. ICRP 36 (3).

ICRP, 2007. The 2007 Recommendations of the International Commission on Radiological Protection. ICRP Publication 103. Ann. ICRP 37 (2-4).

ICRP, 2008a. Environmental Protection - the Concept and Use of Reference Animals and Plants. ICRP Publication 108. Ann. ICRP 38.

ICRP, 2008b. Nuclear Decay Data for Dosimetric Calculations. ICRP Publication 107. Ann. ICRP 38.

ICRP, 2009. Environmental Protection: Transfer Parameters for Reference Animals and Plants. ICRP Publication 114. Ann. ICRP 39 (6).

ICRP, 2012. Compendium of Dose Coefficients based on ICRP Publication 60. ICRP Publication 119. Ann. ICRP 41(Suppl.).

ICRP, 2017. Dose Coefficients for Non-human Biota Environmentally Exposed to Radiation. ICRP Publication 136. Ann. ICRP 46 (2).

ICRP, 2019. Occupational intakes of radionuclides: Part 4. ICRP Publication 141. Ann. ICRP 48 (2/3).

ICRP, 2020. ICRP Publication 144: Dose Coefficients for External Exposures to Environmental Sources. Ann. ICRP 49, 11-145.

Ingleby, S., 2024. https://australian.museum/learn/animals/mammals/northern-brown-bandicoot/ Accessed 11th May 2024.

ISO, 2023. Water quality — Actinium-227 — Test method using alpha-spectrometry (ISO Standard No. ISO 4723:2023).

JCGM, 2008. Evaluation of measurement data - Guide to the expression of uncertainty in measurement. Joint Committee for Guides in Metrology, J. www.bipm.org/documents/20126/2071204/JCGM_100_2008_E.pdf/cb0ef43f-baa5-11cf-3f85-4dcd86f77bd6

Jerome, S.M., Collins, S.M., Happel, S., Ivanov, P., Russell, B.C., 2018. Isolation and purification of protactinium-231. Appl. Radiat. Isot. 134, 18-22.

Jia, G., Jia, J., 2012. Determination of radium isotopes in environmental samples by gamma spectrometry, liquid scintillation counting and alpha spectrometry: a review of analytical methodology. J. Environ. Radioact. 106, 98-119.

Johansen, M.P., Carpenter, J.G., Charmasson, S., Gwynn, J.P., Mc Ginnity, P., Mori, A., Orr, B., Simon-Cornu, M., Osvath, I., 2023. Seafood dose parameters: Updating ^{210}Po retention factors for cooking, decay loss and mariculture. J. Environ. Radioact. 268-269, 107243.

Johansen, M.P., Child, D.P., Hotchkis, M.A.C., Johansen, A., Thiruvoth, S., Whiting, S.D., 2020. Radionuclides in sea turtles at the Montebello Islands former nuclear test sites: Current and historical dose rates for adults and embryos. Mar. Pollut. Bull. 158, 111390.

Johansen, M.P., Twining, J.R., 2010. Radionuclide concentration ratios in Australian terrestrial wildlife and livestock: data compilation and analysis. Radiat. Environ. Biophys. 49, 603-611.

Johnston, A., 1987. Radiation exposure of members of the public resulting from operations of the Ranger Uranium Mine. Technical Memorandum 20. Supervising Scientist for the Alligator Rivers Region. AGPS, Canberra. www.dcceew.gov.au/sites/default/files/documents/tm20.pdf Accessed 6 June 2024

Kayzar, T.M., Williams, R.W., 2015. Developing ^{226}Ra and ^{227}Ac age-dating techniques for nuclear forensics to gain insight from concordant and non-concordant radiochronometers. J. Radioanal. Nucl. Chem. 307, 2061-2068.

Kim, C.S., Kim, C.K., Lee, K.J., 2004. Simultaneous analysis of 237Np and Pu isotopes in environmental samples by ICP-SF-MS coupled with automated sequential injection system. J. Anal. At. Spectrom. 19, 743-750.

Kim, E.-H., Chung, D.-Y., Park, J.-H., Yoo, J.-H., 2000. Dissolution of Oxalate Precipitate and Destruction of Oxalate Ion by Hydrogen Peroxide in Nitric Acid Solution. J. Nucl. Sci. Technol. 37, 601-607.

Kirby, H.W., 1959. The Radiochemistry of Protactinium. United States. www.osti.gov/servlets/purl/4106339

Kitatsuji, Y., Kimura, T., Kihara, S., 2010. Reduction behavior of neptunium(V) at a gold or platinum electrode during controlled potential electrolysis and procedures for electrochemical preparations of neptunium(IV) and (III). J. Electroanal. Chem. 641, 83-89.

Kleinschmidt, R., 2017. Reference natural radionuclide concentrations in Australian soils and derived terrestrial air kerma rate. J. Environ. Radioact. 172, 160-162.

Knibbs, L.D., Sly, P.D., 2014. Indigenous health and environmental risk factors: an Australian problem with global analogues? Global Health Action 7, 23766-23766.

Knight, A., Nelson, A., Eitrheim, E., Forbes, T., Schultz, M., 2016. A chromatographic separation of neptunium and protactinium using 1-octanol impregnated onto a solid phase support. J. Radioanal. Nucl. Chem. 307, 59-67.

Knight, A.W., Eitrheim, E.S., Nelson, A.W., Nelson, S., Schultz, M.K., 2014. A simple-rapid method to separate uranium, thorium, and protactinium for U-series age-dating of materials. J. Environ. Radioact. 134, 66-74.

Ko, Y.G., 2020. Preparation and characterization of electrodeposited layers as alpha sources for alpha-particle spectrometry. J. Radioanal. Nucl. Chem. 326, 861-877.

Köhler, M., Gleisberg, B., Niese, S., 2000a. Investigation of the soil–plant transfer of primordial radionuclides in tomatoes by low-level γ-ray spectrometry. Appl. Radiat. Isot. 53, 203-208.

Köhler, M., Niese, S., Gleisberg, B., Jenk, U., Nindel, K., 2000b. Simultaneous determination of Ra and Th nuclides, ^{238}U and ^{227}Ac in uranium mining waters by γ-ray spectrometry. Appl. Radiat. Isot. 52, 717-723.

Kolb, W.A., Wojcik, M., 1985. Enhanced radioactivity due to natural oil and gas production and related radiological problems. Sci. Total Environ. 45, 77-84.

Koll, D., 2023. A 10-million year time profile of interstellar influx to Earth mapped through supernova ^{60}Fe and *r*-process ^{244}Pu. thesis. Australian National University and Technische Universität Dresden.

Koppel, D.J., Cresswell, T., MacIntosh, A., von Hellfeld, R., Hastings, A., Higgins, S., 2023. Threshold values for the protection of marine ecosystems from NORM in subsea oil and gas infrastructure. J. Environ. Radioact. 258, 107093.

Kossert, K., Bokeloh, K., Dersch, R., Nähle, O., 2015. Activity determination of ^{227}Ac and ^{223}Ra by means of liquid scintillation counting and determination of nuclear decay data. Appl. Radiat. Isot. 95, 143-152.

Kosynkin, V.D., Moiseev, S.D., Vdovichev, V.S., 1995. Cleaning rare earth elements from actinium. J. Alloys Compd. 225, 320-323.

Kragten, J., 1994. Tutorial review. Calculating standard deviations and confidence intervals with a universally applicable spreadsheet technique. Analyst 119, 2161-2165.

Krmpotić, M., Rožmarić, M., Benedik, L., 2018. Investigation of key factors in preparation of alpha sources by electrodeposition. Appl. Radiat. Isot. 136, 37-44.

Kurosaki, H., Mueller, R.J., Lambert, S.B., Rao, G.R., 2017. Alternate method of source preparation for alpha spectrometry: no electrodeposition, no hydrofluoric acid. J. Radioanal. Nucl. Chem. 311, 323-329.

Kuwae, M., Finney, B.P., Shi, Z., Sakaguchi, A., Tsugeki, N., Omori, T., Agusa, T., Suzuki, Y., Yokoyama, Y., Hinata, H., Hatada, Y., Inoue, J., Matsuoka, K., Shimada, M., Takahara, H., Takahashi, S., Ueno, D., Amano, A., Tsutsumi, J., Yamamoto, M., Takemura, K., Yamada, K., Ikehara, K., Haraguchi, T., Tims, S., Froehlich, M., Fifield, L.K., Aze, T., Sasa, K., Takahashi, T., Matsumura, M., Tani, Y., Leavitt, P.R., Doi, H., Irino, T., Moriya, K., Hayashida, A., Hirose, K., Suzuki, H., Saito, Y., 2023. Beppu Bay, Japan, as a candidate Global boundary Stratotype Section and Point for the Anthropocene series. The Anthropocene Review 10, 49-86.

Kyser, E., 2009. Dissolution of neptunium oxide residues. University of North Texas Libraries, U.D.L., Aiken, South Carolina. https://digital.library.unt.edu/ark:/67531/metadc900517/ Accessed 26 July 2020

L'Annunziata, M.F., 2012. Handbook of Radioactivity Analysis (Third Edition). Elsevier, Amsterdam.

L'Annunziata, M.F., Kessler, M.J., 2012. Chapter 7 - Liquid Scintillation Analysis: Principles and Practice, In: Handbook of Radioactivity Analysis (Third Edition). (Ed.) L'Annunziata, M.F. Elsevier, Amsterdam, pp. 423-573.

Lamble, K.J., Hill, S.J., 1998. Microwave digestion procedures for environmental matrices. Critical Review. Analyst 123, 103R-133R.

Lamontagne, S., Le Gal La Salle, C., Hancock, G.J., Webster, I.T., Simmons, C.T., Love, A.J., James-Smith, J., Smith, A.J., Kämpf, J., Fallowfield, H.J., 2008. Radium and radon

radioisotopes in regional groundwater, intertidal groundwater, and seawater in the Adelaide Coastal Waters Study area: Implications for the evaluation of submarine groundwater discharge. Mar. Chem. 109, 318-336.

Landa, E.R., Gray, J.R., 1995. US Geological Survey research on the environmental fate of uranium mining and milling wastes. Environ. Geol. 26, 19-31.

Langham, W., Storer, J., 1952. Toxicology of actinium equilibrium mixture, Atomic Energy Commission Report AECD 3365. www.osti.gov/biblio/4406766/ Accessed 26 August 2024

Larsson, C.-M., 2008. An overview of the ERICA Integrated Approach to the assessment and management of environmental risks from ionising contaminants. J. Environ. Radioact. 99, 1364-1370.

Lawrence, C.E., Akber, R.A., Bollhöfer, A., Martin, P., 2009. Radon-222 exhalation from open ground on and around a uranium mine in the wet-dry tropics. J. Environ. Radioact. 100, 1-8.

Lawrence, R., O'Faircheallaigh, C., 2022. Ignorance as strategy: 'Shadow places' and the social impacts of the ranger uranium mine. Environ. Impact Assess. Rev. 93, 106723.

Leger, L., Fisk, G., 2016. Kakadu – vulnerability to climate change impacts, Case Study for CoastAdapt, National Climate Change Adaptation Research Facility. https://nccarf.edu.au/wp-content/uploads/2019/05/CS07_Kakadu_NP.pdf Accessed 22 February 2024.

Leggett, R.W., 2001. Reliability of the ICRP's dose coefficients for members of the public. 1. Sources of uncertainty in the biokinetic models. Radiat Prot Dosimetry 95, 199-213.

Lieser, K.H., Hill, R., Mühlenweg, U., Singh, R.N., Shu-De, T., Steinkoff, T., 1991. Actinides in the environment. J. Radioanal. Nucl. Chem. 147, 117-131.

Lieser, K.H., Mühlenweg, U., Sipos-Galiba, I., 1985. Dissolution of Neptunium Dioxide in Aqueous Solutions under Various Conditions. Radiochim. Acta 39, 35.

Linsalata, P., Morse, R., Ford, H., Eisenbud, M., Franca, E.P., de Castro, M.B., Lobao, N., Sachett, I., Carlos, M. 1989. Transport pathways of Th, U, Ra and La from soil to cattle tissues. J. Environ. Radioact. 10, 115-140.

Linsalata, P., Morse, R., Ford, H., Eisenbud, M., Franca, E.P., de Castro, M.B., Lobao, N., Sachett, I., Carlos, M. 1991. Th, U, Ra and rare earth element distribution in farm animal tissues from an elevated natural radiation background environment. J. Environ. Radioact. 14, 233-257.

Lowe, L.M., 1997. Impact of the ^{235}U Series on Doses from Intakes of Natural Uranium and Decay Progeny. Health Phys. 73, 694-695.

Luskus, C.A., 1998. Electroplating versus microprecipitation of the actinides in alpha-spectroscopic analysis. J. Radioanal. Nucl. Chem. 234, 287-292.

MacIntosh, A., Koppel, D.J., Johansen, M.P., Beresford, N.A., Copplestone, D., Penrose, B., Cresswell, T., 2022. Radiological risk assessment to marine biota from exposure to NORM from a decommissioned offshore oil and gas pipeline. J. Environ. Radioact. 251-252, 106979.

Martin, P., Akber, R.A., 1996. Groundwater seepage from the Ranger uranium mine tailings dam: Radioisotopes of radium, thorium and actinium. Supervising Scientist, Darwin, N.T. www.dcceew.gov.au/sites/default/files/documents/ssr106.pdf Accessed 16 June 2023

Martin, P., Hancock, G., 2004. Routine analysis of naturally occurring radionuclides in environmental samples by alpha-particle spectrometry. www.dcceew.gov.au/sites/default/files/documents/ssr180.pdf Accessed 1 July 2024

Martin, P., Hancock, G.J., Johnston, A., Murray, A.S., 1998. Natural-series radionuclides in traditional North Australian aboriginal foods. J. Environ. Radioact. 40, 37-58.

Martin, P., Hancock, G.J., Paulka, S., Akber, R.A., 1995. Determination of ^{227}Ac by α-particle spectrometry. Appl. Radiat. Isot. 46, 1065-1070.

Martin, P., Ryan, B., 1995. The 1994/1995 Wet Season Application for Release of Ranger RP2 Water: Progress Report. Internal Report 184. Supervising Scientist for the Alligator Rivers Region, Canberra.

Martin, P., Ryan, B., 2004. Natural-Series Radionuclides in Traditional Aboriginal Foods in Tropical Northern Australia: A Review. TheScientificWorldJOURNAL 4, 77-95.

Martin, P.C., 2000. Radiological impact assessment of uranium mining and milling. PhD thesis.

Martschini, M., Fifield, L.K., Froehlich, M.B., Leckenby, G., Pavetich, S., Tims, S.G., Tranter, B., Wallner, A., 2019. New and upgraded ionization chambers for AMS at the Australian National University. Nucl. Instrum. Methods Phys. Res. B 438, 141-147.

Medley, P., Bollhöfer, A., 2016. Influence of group II metals on Radium-226 concentration ratios in the native green plum (*Buchanania obovata*) from the Alligator Rivers Region, Northern Territory, Australia. J. Environ. Radioact. 151, Part 3, 551-557.

Medley, P., Bollhöfer, A., Iles, M., Ryan, B., Martin, P., 2005. Barium sulphate method for radium-226 analysis by alpha spectrometry. Internal Report 501. Supervising Scientist, Darwin. www.dcceew.gov.au/sites/default/files/documents/ir501.pdf Accessed 28 June 2023

Medley, P., Bollhöfer, A., Parry, D., Martin, P., 2013. Radium concentration factors in passionfruit (*Passiflora foetida*) from the Alligator Rivers Region, Northern Territory, Australia. J. Environ. Radioact. 126, 137-146.

Medley, P., Doering, C., Evans, F., Bollhöfer, A., 2017. Natural radionuclides and stable elements in weaver ants (*Oecophylla smaragdina*) from tropical northern Australia. J. Environ. Radioact. 178-179, 404-410.

Medley, P., Doering, C., Froehlich, M.B., 2024. Data for concentration ratios and uptake of ^{227}Ac and ^{231}Pa is reliant on analogue measurements [Manuscript in preparation]. Radiation Sciences, Queensland Health.

Medley, P., Patterson, S., 2022. Determining baseline radiation levels in marine biota – A comparison of SE Queensland commercial species. J. Environ. Radioact. 255, 107032.

Medley, P., Patterson, S., Howell, N., Froehlich, M.B., 2025. Improving ^{210}Po source preparation for alpha spectrometry: Neodymium hydroxide micro-precipitation. Appl. Radiat. Isot. 224, 111890.

Medley, P., Tims, S.G., Froehlich, M.B., Fifield, L.K., Bollhöfer, A., Wallner, A., Pavetich, S., 2019. Development of ^{231}Pa AMS measurements to improve radiological dose assessment from uranium mining and milling. Nucl. Instrum. Methods Phys. Res. B 438, 66-69.

Megumi, K., 1979. Radioactive disequilibrium of uranium and actinium series nuclides in soil. J. Geophys. Res. Solid Earth 84, 3677-3682.

Mendes, M., Aupiais, J., Jutier, C., Pointurier, F., 2013. Determination of weight distribution ratios of Pa(V) and Np(V) with some extraction chromatography resins and the AG1-X8 resin. Anal. Chim. Acta 780, 110-116.

Menzel, H.-G., Harrison, J., 2012. Effective dose: a radiation protection quantity. Ann. ICRP 41, 117-123.

Michel, H., Levent, D., Barci, V., Barci-Funel, G., Hurel, C., 2008. Soil and sediment sample analysis for the sequential determination of natural and anthropogenic radionuclides. Talanta 74, 1527-1533.

Middleton, R., 1989. A negative ion cookbook. University of Pennsylvania, unpublished.

Moore, W.S., Arnold, R., 1996. Measurement of ^{223}Ra and ^{224}Ra in coastal waters using a delayed coincidence counter. J. Geophys. Res. Oceans 101, 1321-1329.

Morgan, K.A., Donnelly, P.S., 2021. Chapter Two - Metallic radionuclides for diagnostic imaging and cancer radiotherapy: The development of theragnostic matched pairs and targeted alpha therapy, In: Adv. Inorg. Chem. (Eds.) Hubbard, C.D., van Eldik, R. Academic Press, pp. 37-63. https://www.sciencedirect.com/science/article/pii/S089888382100026X

Mudd, G.M., Diesendorf, M., 2008. Sustainability of Uranium Mining and Milling: Toward Quantifying Resources and Eco-Efficiency. Environ. Sci. Technol. 42, 2624-2630.

Murchie, M.P., Reid, S.J., 2020. 9 - Uranium conversion and enrichment, In: Advances in Nuclear Fuel Chemistry. (Ed.) Piro, M.H.A. Woodhead Publishing, pp. 331-370. www.sciencedirect.com/science/article/pii/B9780081025710000100 Accessed 22 July 2023

Murray, A.S., Marten, R., Johnston, A., Martin, P., 1987. Analysis for naturally occuring radionuclides at environmental concentrations by gamma spectrometry. J. Radioanal. Nucl. Chem. 115, 263-288.

Myasoedov, B.F., Kirby, H.W., Tananaev, I.G., 2011. Protactinium, In: The Chemistry of the Actinide and Transactinide Elements. (Eds.) Morss, L., Edelstein, N., Fuger, J. Springer Netherlands, pp. 161-252. http://dx.doi.org/10.1007/978-94-007-0211-0_4

NCBI (National Center for Biotechnology Information), 2022. https://pubchem.ncbi.nlm.nih.gov/element/Protactinium. Accessed 10 March 2022.

Negre, C., Thomas, A.L., Mas, J.L., Garcia-Orellana, J., Henderson, G.M., Masqué, P., Zahn, R., 2009. Separation and Measurement of Pa, Th, and U Isotopes in Marine Sediments by Microwave-Assisted Digestion and Multiple Collector Inductively Coupled Plasma Mass Spectrometry. Anal. Chem. 81, 1914-1919.

Newton, D., Brown, D.A., 1974. The Long-term Retention of Systemic Protactinium-231 and Actinium-227. Health Phys. 27, 459-467.

Nichols, A.L., Aldama, D.L., Verpelli, M., 2008. Handbook of Nuclear Data for Safeguards: Database Extensions. https://www-nds.iaea.org/publications/indc/indc-nds-0534.pdf Accessed 26 August 2024

Niese, S., 1996. Application of low-level counting techniques for the investigation of the impact of uranium mining as well as remediation on the environment. Appl. Radiat. Isot. 47, 1109-1112.

NIST (National Institute of Standards & Technology), 2019. Certificate of Analysis, Standard Reference Material 2702: Inorganics in Marine Sediment. https://tsapps.nist.gov/srmext/certificates/2702.pdf Accessed 25 April 2024

Nóbrega, J.A., Pirola, C., Fialho, L.L., Rota, G., de Campos Jordão, C.E.K.M.A., Pollo, F., 2012. Microwave-assisted digestion of organic samples: How simple can it become? Talanta 98, 272-276.

Nozaki, Y., 1984. Excess ^{227}Ac in deep ocean water. Nature 310, 486-488.

Nozaki, Y., 1997. A fresh look at element distribution in the North Pacific Ocean. EOS Trans. Am. Geophys. Union.

Nozaki, Y., Yamada, M., Nikaido, H., 1990. The marine geochemistry of actinium-227: Evidence for its migration through sediment pore water. Geophys. Res. Lett. 17, 1933-1936.

NRC (U.S. Nuclear Regulatory Commission), 2001. Systematic Radiological Assessment of Exemptions for Source and Byproduct Materials, Rep. NUREG-1717. NRC, Wahington, DC. www.nrc.gov/reading-rm/doc-collections/nuregs/staff/sr1717/nureg-1717.pdf Accessed 29 July 2023

O'Faircheallaigh, C., Lawrence, R., 2019. Mine closure and the Aboriginal estate. Aust. Aborig. Stud., 65-81.

Okonkwo, U.C., Ohagwu, C.C., Aronu, M.E., Okafor, C.E., Idumah, C.I., Okokpujie, I.P., Chukwu, N.N., Chukwunyelu, C.E., 2022. Ionizing radiation protection and the linear No-threshold controversy: Extent of support or counter to the prevailing paradigm. J. Environ. Radioact. 253-254, 106984.

Ostapenko, V., Sinenko, I., Arefyeva, E., Lapshina, E., Ermolaev, S., Zhuikov, B., Kalmykov, S., 2017. Sorption of protactinium(V) on extraction chromatographic resins from nitric and hydrochloric solutions. J. Radioanal. Nucl. Chem. 311, 1545-1550.

Ostapenko, V., Vasiliev, A., Lapshina, E., Ermolaev, S., Aliev, R., Totskiy, Y., Zhuikov, B., Kalmykov, S., 2015. Extraction chromatographic behavior of actinium and REE on DGA, Ln and TRU resins in nitric acid solutions. J. Radioanal. Nucl. Chem., 1-5.

Oughton, D.H., Strømman, G., Salbu, B., 2013. Ecological risk assessment of Central Asian mining sites: application of the ERICA assessment tool. J. Environ. Radioact. 123, 90-98.

Palmer, C., Price, O., Bach, C., 2000. Foraging ecology of the black flying fox (*Pteropus alecto*) in the seasonal tropics of the Northern Territory, Australia. Wildl. Res. 27, 169-178.

Paulka, S., Martin, P., Hancock, G., Akber, R.A., 1993. Radionuclide analyses of water from Ranger Uranium Mine retention ponds and tailings dam. Internal report 129. Supervising Scientist for the Alligator Rivers Region, Canberra.

Pavetich, S., Carey, A., Fifield, L.K., Froehlich, M.B., Halfon, S., Kinast, A., Martschini, M., Nelson, D., Paul, M., Shor, A., Sterba, J.H., Tessler, M., Tims, S.G., Weissman, L., Wallner, A., 2019. 93Zr developments at the Heavy Ion Accelerator Facility at ANU. Nucl. Instrum. Methods Phys. Res. B 438, 77-83.

Payne, T.E., Edis, R., Seo, T., 1992. Radionuclide Transport by Groundwater Colloids at the Koongarra Uranium Deposit. MRS Proceedings 257.

Percival, D.R., Martin, D.B., 1974. Sequential determination of radium-226, radium-228, actinium-227, and thorium isotopes in environmental and process waste samples. Anal. Chem. 46, 1742-1749.

Pommé, S., 2015. Typical uncertainties in alpha-particle spectrometry. Metro 52, S146-S155.

Pröhl, G., Brown, J., Gomez-Ros, J.-M., Jones, S., Woodhead, D., Vives, J., Taranenko, V., ThØrring, H. (Swedish Radiation Protection Authority), 2003. Dosimetric models and data for assessing radiation exposure to biota. Deliverable Report 3 to the Project 'FASSET' Framework for the assessment of Environmental Impact, contract No. FIGE-CT-2000-00102.

Raje, N., Swain, K.K., Kumar, S.A., Kayasth, S.R., Parthasarathy, R., Mathur, P.K., 2001. Preconcentration of natural protactinium (^{231}Pa) from monazite on Dowex 1X8 and subsequent determination by gamma-spectrometry. J. Radioanal. Nucl. Chem. 247, 115-120.

Ralph, M.I., Tsurikov, N., Cattani, M., 2020. Impacts of revised dose coefficients for the inhalation of NORM-containing dusts encountered in the Western Australian Mining Industry. J. Radiol. Prot. 40, 1457.

Rasband, W.S., 1997-2018. https://imagej.net/ij/index.html

Rea, M.A.D., Johansen, M.P., Payne, T.E., Hirth, G., Hondros, J., Pandelus, S., Tucker, W., Duff, T., Stopic, A., Green, L., Pring, A., Lenehan, C.E., Popelka-Filcoff, R.S., 2021. Radionuclides

and stable elements in vegetation in Australian arid environments: Concentration ratios and seasonal variation. J. Environ. Radioact. 234, 106627.

Real, A., Garnier-Laplace, J., 2020. The importance of deriving adequate wildlife benchmark values to optimize radiological protection in various environmental exposure situations. J. Environ. Radioact. 211, 105902.

Regelous, M., Turner, S.P., Elliott, T.R., Rostami, K., Hawkesworth, C.J., 2004. Measurement of Femtogram Quantities of Protactinium in Silicate Rock Samples by Multicollector Inductively Coupled Plasma Mass Spectrometry. Anal. Chem. 76, 3584-3589.

Rekha, A.K., Dingankar, M.V., Anilkumar, S., Narayani, K., 2006. Determination of the activity ratios of ^{231}Pa to ^{235}U and ^{227}Th to ^{235}U in ore samples using gamma-spectrometry. J. Radioanal. Nucl. Chem. 268, 453-460.

Ren, X., Zhou, J., Wang, E., Yang, T., Xu, Z., Sisourat, N., Pfeifer, T., Dorn, A., 2022. Ultrafast energy transfer between π-stacked aromatic rings upon inner-valence ionization. Nature Chemistry 14, 232-238.

Rich, B.L., Hinnefeld, S.L., Lagerquist, C.R., Mansfield, W.G., Munson, L.H., Wagner, E.R., 1988. EGG–2530, Health Physics Manual of Good Practices for Uranium Facilities. Idaho National Engineering Laboratory: Idaho Falls, Idaho. www.osti.gov/biblio/6840260 Accessed 29 July 2023

Richter, S., Eykens, R., Kühn, H., Aregbe, Y., Verbruggen, A., Weyer, S., 2010. New average values for the $n(^{238}U)/n(^{235}U)$ isotope ratios of natural uranium standards. Int. J. Mass spectrom. 295, 94-97.

Rock, T., Ingram, J.C., 2020. Traditional Ecological Knowledge Policy Considerations for Abandoned Uranium Mines on Navajo Nation. Hum. Biol. 92, 19-26.

Rogers, N.E., Watrous, R.M., 1955. Radiochemical Separation of Actinium and Its Daughters by Means of Lead Sulfate. Anal. Chem. 27, 2009-2012.

Rolison, J.M., Treinen, K.C., McHugh, K.C., Gaffney, A.M., Williams, R.W., 2017. Application of the ^{226}Ra–^{230}Th–^{234}U and ^{227}Ac–^{231}Pa–^{235}U radiochronometers to uranium certified reference materials. J. Radioanal. Nucl. Chem. 314, 2459-2467.

Ruby, L., 1994. Further comments on the geometrical efficiency of a parallel-disk source and detector system. Nucl. Instrum. Methods Phys. Res. A 337, 531-533.

Russell, D., Garrett, R., 1985. Early life history of barramundi, *Lates calcarifer* (Bloch), in north-eastern Queensland. Mar. Freshwat. Res. 36, 191-201.

Rweyemamu, M., Kim, J., 2020. Potential environmental hazard to the public from the operation of uranium mining and milling facility. Radiat. Prot. Dosimetry 192, 75-88.

Ryan, B., Medley, P., Bollhöfer, A., 2008. Bioaccumulation of radionuclides in terrestrial plants on rehabilitated landforms, In: ERISS research summary 2006-2007. Supervising Scientist Report 196. (Eds.) Jones, D.R., Humphrey, C., van Dam, R., Webb, A. Supervising Scientist, Darwin, NT, pp. 99-103. www.dcceew.gov.au/sites/default/files/documents/ssr196-web.pdf Accessed 26 August 2024

Ryan, B., Medley, P., Bollhöfer, A., 2009. Bioaccumulation of radionuclides in terrestrial plants on rehabilitated landforms, In: eriss research summary 2007-2008, Supervising Scientist Report 200. (Eds.) Jones, D.R., Webb, A. Supervising Scientist, Darwin, NT, pp. 152-159. www.dcceew.gov.au/science-research/supervising-scientist/publications/ssr/eriss-research-summary-2007-2008

Rychkov, V.N., Semenishchev, V.S., Kirillov, E.V., Kirillov, S.V., Ryabukhina, V.G., Smyshlyaev, D.V., Bunkov, G.M., Botalov, M.S., 2018. Radiochemical characterization and decontamination of rare-earth-element concentrate recovered from uranium leach liquors. J. Radioanal. Nucl. Chem. 317, 203-213.

Saïdou, Bochud, F., Laedermann, J.-P., Kwato Njock, M.G., Froidevaux, P., 2008. A comparison of alpha and gamma spectrometry for environmental natural radioactivity surveys. Appl. Radiat. Isot. 66, 215-222.

Saint-Fort, R., 2018. Understanding Sorption Behavior and Properties of Radionuclides in the Environment, In: Principles and Applications in Nuclear Engineering. (Eds.) Rehab, O.A.R., Hosam El-Din, M.S. IntechOpen, Rijeka, p. Ch. 6. https://doi.org/10.5772/intechopen.76215 Accessed 20 April 2023

Sakamoto, Y., Ishii, T., Inagawa, S., Gunji, Y., Takebe, S., Ogawa, H., Sasaki, T., 2002. Sorption Characteristics of Actinium and Protactinium onto Soils. J. Nucl. Sci. Technol. 39, 481-484.

Sanchez-Cabeza, J.A., Pujol, U., 1995. A Rapid Method for the Simultaneous Determination of Gross Alpha and Beta Activities in Water Samples Using a Low Background Liquid Scintillation Counter. Health Phys. 68, 674-682.

Sánchez-Villagra, M.R., 2013. Why are There Fewer Marsupials than Placentals? On the Relevance of Geography and Physiology to Evolutionary Patterns of Mammalian Diversity and Disparity. J. Mamm. Evol. 20, 279-290.

Sarkar, A., Wilton, D.H.C., Fitzgerald, E., Sharma, A., Sharma, A., Sathya, A.J., 2019. Environmental impact assessment of uranium exploration and development on indigenous land in Labrador (Canada): a community-driven initiative. Environ. Geochem. Health 41, 939-949.

Sawant, P.D., Wankhede, S., Kumar, S.A., Chaudhary, S., Prabhu, S.P., 2019. Alpha source preparation of actinides by micro-precipitation. J. Radioanal. Nucl. Chem. 319, 109-113.

Schmitt, A.K., 2007. Ion microprobe analysis of (^{231}Pa)/(^{235}U) and an appraisal of protactinium partitioning in igneous zircon. Am. Mineral. 92, 691-694.

Schultz, R., 2021. Investigating the health impacts of the Ranger uranium mine on Aboriginal people. Med. J. Aust. 215, 157-159.e151.

Sdraulig, S., Orr, B., Urban, D., Tinker, R.A., 2019. Radiation doses from the average Australian diet, Technical Report 181. ARPANSA, Melbourne, Australia.

Sgouros, G., He, B., Ray, N., Ludwig, D.L., Frey, E.C., 2021. Dosimetric impact of Ac-227 in accelerator-produced Ac-225 for alpha-emitter radiopharmaceutical therapy of patients with hematological malignancies: a pharmacokinetic modeling analysis. EJNMMI Phys. 8, 60.

Shen, C.-C., Cheng, H., Edwards, R.L., Moran, S.B., Edmonds, H.N., Hoff, J.A., Thomas, R.B., 2003. Measurement of Attogram Quantities of ^{231}Pa in Dissolved and Particulate Fractions of Seawater by Isotope Dilution Thermal Ionization Mass Spectroscopy. Anal. Chem. 75, 1075-1079.

Shen, G., 1996. ^{227}TH^{230}TH dating method: Methodology and application to Chinese speleothem samples. Quat. Sci. Rev. 15, 699-707.

Sheppard, M.I., Sheppard, S.C., 1985. The Plant Concentration Ratio Concept as Applied to Natural U. Health Phys. 48, 8.

Sheppard, S.C., Herod, M., 2012. Variation in background concentrations and specific activities of ^{36}Cl, ^{129}I and U/Th-series radionuclides in surface waters. J. Environ. Radioact. 106, 27-34.

Shine, R., 1991. Strangers in a Strange Land: Ecology of the Australian Colubrid Snakes. Copeia 1991, 120-131.

Sill, C.W., 1978. Radiochemical determination of protactinium-231 in environmental and biological materials. Anal. Chem. 50, 1559-1571.

Sill, C.W., 1987. Precipitation of actinides as fluorides or hydroxides for high-resolution alpha spectrometry. Nucl. Chem. Waste Manage. 7, 201-215.

Sill, C.W., Olson, D.G., 1970. Sources and prevention of recoil contamination of solid-state alpha detectors. Anal. Chem. 42, 1596-1607.

Sill, C.W., Williams, R.L., 1981. Preparation of actinides for alpha spectrometry without electrodeposition. Anal. Chem. 53, 412-415.

Sill, C.W., Willis, C.P., 1964. Precipitation of Submicrogram Quantities of Thorium by Barium Sulfate and Application to the Fluorometric Determination of Thorium in Mineralogical and Biological Samples. Anal. Chem. 36, 622-630.

Simon, S., Ibrahim, S., 1990. Biological uptake of radium by terrestrial plants, In: The environmental behaviour of radium. IAEA, Vienna.

Simpson, H.P., Schwarcz, J.J., Stringer, C.B., 1998. Neanderthal skeleton from Tabun: U-series data by gamma-ray spectrometry. J. Hum. Evol. 35, 635-645.

Simpson, J.J., Grün, R., 1998. Non-destructive gamma spectrometric U-series dating. Quat. Sci. Rev. 17, 1009-1022.

Skoko, B., Babić, D., Marović, G., Papić, S., 2019. Environmental radiological risk assessment of a coal ash and slag disposal site with the use of the ERICA Tool. J. Environ. Radioact. 208-209, 106018.

Smoak, J.M., Krest, J.M., 2006. Source of radium in a well-water-augmented Florida lake. J. Environ. Radioact. 89, 102-114.

Southon, J., Santos, G.M., 2007. Life with MC-SNICS. Part II: Further ion source development at the Keck carbon cycle AMS facility. Nucl. Instrum. Methods Phys. Res. B 259, 88-93.

Standards Australia, 2003. AS 2706–2003 Numerical values–Rounding and interpretation of limiting values. Sydney: SAI Global Limited.

Stark, K., Goméz-Ros, J.M., Vives i Batlle, J., Lindbo Hansen, E., Beaugelin-Seiller, K., Kapustka, L.A., Wood, M.D., Bradshaw, C., Real, A., McGuire, C., Hinton, T.G., 2017. Dose assessment in environmental radiological protection: State of the art and perspectives. J. Environ. Radioact. 175-176, 105-114.

Staven, L.H., Napier, B.A., Rhoads, K., Strenge, D.L., 2003. A Compendium of Transfer Factors for Agricultural and Animal Products. United States. www.osti.gov/biblio/15010186 Accessed 26 August 2024

Steier, P., Bichler, M., Keith Fifield, L., Golser, R., Kutschera, W., Priller, A., Quinto, F., Richter, S., Srncik, M., Terrasi, P., Wacker, L., Wallner, A., Wallner, G., Wilcken, K.M., Maria Wild, E., 2008. Natural and anthropogenic ^{236}U in environmental samples. Nucl. Instrum. Methods Phys. Res. B 266, 2246-2250.

Stevenson, P.C., Nervik, W.E., 1961. The Radiochemistry of the Rare Earths, Scandium, Yttrium and Actinium. United States. www.osti.gov/biblio/4061656 Accessed 04 June 2023

Stewart, B.T., Santos, I.R., R. Tait, D., Macklin, P.A., Maher, D.T., 2015. Submarine groundwater discharge and associated fluxes of alkalinity and dissolved carbon into Moreton Bay (Australia) estimated via radium isotopes. Mar. Chem. 174, 1-12.

Stirrat, S.C., 2003. Seasonal changes in home-range area and habitat use by the agile wallaby (*Macropus agilis*). Wildl. Res. 30, 593-600.

Süfke, F., Lippold, J., Happel, S., 2018. Improved Separation of Pa from Th and U in Marine Sediments with TK400 Resin. Anal. Chem. 90, 1395-1401.

Sullivan, M.F., Miller, B.M., Ryan, J.L., 1983. Absorption of thorium and protactinium from the gastrointestinal tract in adult mice and rats and neonatal rats. Health Phys. 44, 425-428.

Summerton, A.P., 1992a. Incorporation of natural radionuclides and rare earth elements into a salt tolerant plant. J. Radioanal. Nucl. Chem. 161, 421-428.

Summerton, A.P., 1992b. Natural radionuclides in tidal saltmarsh soils in South Australia—An unusual distribution? J. Radioanal. Nucl. Chem. 161, 475-482.

Supervising Scientist, 2015. ERISS research summary 2013-2014. Supervising Scientist Report 209., Darwin, N.T. www.dcceew.gov.au/sites/default/files/documents/ssr209.pdf Accessed 29 April 2023

Supervising Scientist, 2018a. Environmental Radiation — Rehabilitation Standard for the Ranger uranium mine (version 1), Darwin, NT. www.dcceew.gov.au/science-research/supervising-scientist/publications/ss-rehabilitation-standards Accessed 28 January 2023

Supervising Scientist, 2018b. Public Radiation — Rehabilitation Standard for the Ranger uranium mine (version 1). Darwin, NT. www.dcceew.gov.au/science-research/supervising-scientist/publications/ss-rehabilitation-standards Accessed 16 June 2022

Supervising Scientist, 2022. Radionuclide concentration ratios for understorey vegetation. Technical Advice 052, Darwin, NT.

Supervising Scientist, 2023. Annual Technical Report 2022–23, Darwin, NT. www.dcceew.gov.au/sites/default/files/documents/supervising-scientist-annual-technical-report-2022-23.pdf Accessed 26 August 2024

Sweeck, L., Vives i Batlle, J., Vanhoudt, N., 2024. Assessment of radiation dose to people and wildife inhabiting the Grote Nete catchment in Belgium. J. Environ. Radioact. 273, 107395.

Tagami, K., Twining, J.R., Wasserman, M.A.V., 2012. Chapter 5 - Terrestrial Radioecology in Tropical Systems, In: Radioactivity in the Environment. (Ed.) Twining, J.R. Elsevier, pp. 155-230. www.sciencedirect.com/science/article/pii/B9780080450162000059

Talvitie, N.A., 1972. Electrodeposition of Actinides for Alpha Spectrometric Determination. Anal. Chem. 44, 280-283.

Tang, Q., Qiu, S., Xiao, D., Zhou, Y., An, X., 2014. Extraction and purification of ^{227}Ac and development of solid ^{219}Rn source. Radiochim. Acta 102, 169-174.

Taylor, D.M., 1970. The metabolism of actinium in the rat. Health Phys. 19, 411-418.

Taylor, D.M., Seidel, A., Planas-Bohne, F., Schuppler, U., Neu-Mlüler, M., Wirth, R.E., 1987. Biochemical studies of the interactions of plutonium, neptunium and protactinium with blood and liver cell proteins. Inorg. Chim. Acta 140, 361-363.

Tedman, R., Hall, L., 1985. The Morphology of the Gastrointestinal Tract and Food Transit Time in the Fruit Bats *Pteropus Alecto* and *P. Poliocephalus* (Megachiroptera). Aust. J. Zool. 33, 625-640.

Terning, J.-Å., 1970. Radiochemical analysis of radium, thorium and protactinium in uranium milling process samples. Int. J. Appl. Radiat. Isot. 21, 507-512.

Thiessen, K.M., Thorne, M.C., Maul, P.R., Pröhl, G., Wheater, H.S., 1999. Modelling radionuclide distribution and transport in the environment. Environ. Pollut. 100, 151-177.

Thomas, P.A., 2000a. Radionuclides in the terrestrial ecosystem near a Canadian uranium mill--Part I: Distribution and doses. Health Phys. 78, 614-624.

Thomas, P.A., 2000b. Radionuclides in the terrestrial ecosystem near a Canadian uranium mill--Part II: Small mammal food chains and bioavailability. Health Phys. 78, 625-632.

Tidemann, C.R., Vardon, M.J., Loughland, R.A., Brocklehurst, P.J., 1999. Dry season camps of flying-foxes (*Pteropus* spp.) in Kakadu World Heritage Area, north Australia. J. Zool. 247, 155-163.

Todd, B.D., Nowakowski, A.J., 2021. Ectothermy and the macroecology of home range scaling in snakes. Global Ecol. Biogeogr. 30, 262-276.

Tribe, D., Peel, L., 1963. Body composition of the Kangaroo (Macropus Sp.). Aust. J. Zool. 11, 273-289.

Tucker, A.D., Limpus, C.J., McDonald, K.R., McCallum, H.I., 2007. Growth dynamics of freshwater crocodiles (*Crocodylus johnstoni*) in the Lynd River, Queensland. Aust. J. Zool. 54, 409-415.

Tulloch, D., 1969. Home range in feral water buffalo, Bubalus bubalis Lydekker. Aust. J. Zool. 17, 143-152.

Turcanu, C., Perko, T., Muric, M., Popic, J.M., Geysmans, R., Železnik, N., 2022. Societal aspects of NORM: An overlooked research field. J. Environ. Radioact. 244-245, 106827.

Turner, K., Tayler, K., Tyrrell, J.W.R., Leggett, A., 2019. Revised Ranger Mine Water Quality Objectives for Magela Creek and Gulungul Creek. Supervising Scientist, Darwin, NT. www.dcceew.gov.au/sites/default/files/documents/ir670.pdf

Ulanovsky, A., Pröhl, G., Gómez-Ros, J.M., 2008. Methods for calculating dose conversion coefficients for terrestrial and aquatic biota. J. Environ. Radioact. 99, 1440-1448.

UNSCEAR, 2000. Sources and effects of ionizing radiation : United Nations Scientific Committee on the Effects of Atomic Radiation : UNSCEAR 2000 report to the General Assembly, with scientific annexes. United Nations, New York.

UNSCEAR, 2008. Annex E: Effects of ionizing radiation on non-human biota, In: Sources and Effects of Ionizing Radiation, United Nations Scientific Committee on the Effects of Atomic Radiation (UNSCEAR) 2008 Report, Volume II. United Nations, New York. www.un-ilibrary.org/content/books/9789210544825s001-c003

Uranium in Plants and the Environment, 2020. (Eds.) Dharmendra, K.G., Clemens, W. Springer Charm.

USEPA (United States Environmental Protection Agency), 2019. Federal Guidance Report No. 15 (FGR 15), External Exposure to Radionuclides in Air, Water and Soil. www.epa.gov/radiation/federal-guidance-report-no-15-external-exposure-radionuclides-air-water-and-soil Accessed 5 July 2023

USEPA (United States Environmental Protection Agency), 2024. MARLAP Manual Volume II: Chapter 14, Separation Techniques. www.epa.gov/sites/default/files/2015-05/documents/402-b-04-001b-14-final.pdf Accessed 26 April 2024

USTUR (United States Transuranium and Uranium Registries), 1995. United States Transuranium and Uranium Registries Radiochemical Analytical Procedure Manual, USTUR 100. Washington State University, Pullman, WA. https://s3.wp.wsu.edu/uploads/sites/1058/2016/10/USTUR_100.pdf

Vajda, N., Martin, P., Kim, C.K., 2012. Alpha Spectrometry, In: Handbook of Radioactivity Analysis (Third Edition). (Ed.) L'Annunziata, M.F. Elsevier, Amsterdam.

Vajda, N., Molnar, Z.S., Kabai, E., Zagyvai, P., 2003. Radiochemical Determination Of Long-Lived Radionuclides In Environmental Samples. Springer Netherlands, Dordrecht, pp. 133-146.

van Calsteren, P., Thomas, L., 2012. Quantitation of protactinium, ^{231}Pa in abyssal carbonate. J. Anal. At. Spectrom. 27, 952-956.

van der Heijde, H.B., Klijn, P.-J., Passchier, W.F., 1988. Radiological Impacts of the Disposal of Phosphogypsum. Radiat. Prot. Dosimetry 24, 419-423.

Vandenhove, H., Vives i Batlle, J., Sweeck, L., 2015. Potential radiological impact of the phosphate industry on wildlife. J. Environ. Radioact. 141, 14-23.

Varga, B., Leclerc, E., Zagyvai, P. 2009. The role of analogues in radioecology. J. Environ. Radioact. 100, 802-805.

Vera Tome, F., Blanco Rodrguez, P., Lozano, J.C., 2002. Distribution and mobilization of U, Th and ^{226}Ra in the plant-soil compartments of a mineralized uranium area in. J. Environ. Radioact. 59, 41-60.

Veselovský, F., Ondruš, P., Komínek, J., 1997. History of the Jáchymov (Joachimsthal) ore district. J. Czech Geol. Soc. 42, 127-132.

Vicente, R., Dellamano, J.C., Bellintani, S.A., 1991. Radiological Significance Of ^{227}Ac and ^{231}Pa. Health Phys. 60, 719-720.

Vlastélic, I., Piro, J.l., 2022. Volatilisation of Trace Elements During Evaporation to Dryness of HF-Dissolved Silicates (BHVO-2, AGV-1, BIR-1, UB-N): Open- *Versus* Closed-System Conditions. Geostand. Geoanal. Res. 46, 519-534.

Wallner, A., Fifield, L.K., Froehlich, M.B., Koll, D., Leckenby, G., Martschini, M., Pavetich, S., Tims, S.G., Schumann, D., Slavkovská, Z., 2023. Accelerator mass spectrometry with ANU's 14 million volt accelerator. Nucl. Instrum. Methods Phys. Res. B 534, 48-53.

Weisser, D.C., Lobanov, N.R., Hausladen, P.A., Fifield, L.K., Wallace, H.J., Tims, S.G., Apushkinsky, E.G., 2002. Novel matching lens and spherical ionizer for a cesium sputter ion source. Prama 59, 997-1006.

Willett, I.R., Bond, W.J., 1995. Sorption of Manganese, Uranium, and Radium by Highly Weathered Soils. J. Environ. Qual. 24, 834-845.

Wilson, R., 2012. Peculiar protactinium. Nat Chem 4, 586-586.

Wolf, S.F., 2006. Trace Analysis of Actinides in Geological, Environmental, and Biological Matrices, In: The Chemistry of the Actinide and Transactinide Elements. (Eds.) Morss, L.R., Edelstein, N.M., Fuger, J. Springer Netherlands, Dordrecht, pp. 3273-3338. https://doi.org/10.1007/1-4020-3598-5_30

Wood, M.D., Beresford, N.A., Howard, B.J., Copplestone, D., 2013. Evaluating summarised radionuclide concentration ratio datasets for wildlife. J. Environ. Radioact. 126, 314-325.

Wood, M.D., Beresford, N.A., Semenov, D.V., Yankovich, T.L., Copplestone, D., 2010. Radionuclide transfer to reptiles. Radiat. Environ. Biophys. 49, 509-530.

World Nuclear News, 2021. Ranger mine ends processing operations. www.world-nuclear-news.org/Articles/Processing-ends-at-Ranger-mine Accessed 4 March 2023.

Xu, N., Tandon, L., Gallimore, D., Lujan, E., Porterfield, D.R., Colletti, L., Kuhn, K., 2013. Dissolution and assay of neptunium oxide. J. Radioanal. Nucl. Chem. 296, 245-249.

Yankovich, T.L., Beresford, N.A., Wood, M.D., Aono, T., Andersson, P., Barnett, C.L., Bennett, P., Brown, J.E., Fesenko, S., Fesenko, J., Hosseini, A., Howard, B.J., Johansen, M.P., Phaneuf, M.M., Tagami, K., Takata, H., Twining, J.R., Uchida, S., 2010. Whole-body to tissue

concentration ratios for use in biota dose assessments for animals. Radiat. Environ. Biophys. 49, 549-565.

Appendix A Calculation of ^{227}Ac and ^{231}Pa activity concentrations and associated MDL

A-1 Calculation of ^{227}Ac activity concentrations

The following series of equations were used to determine the ^{227}Ac activity concentration measured in samples, corrected to the fresh weight of the sample at the time of collection. These equations are based on measurement of the integrated ^{227}Th and ^{223}Ra activity after an ingrowth period after Ac separation and corrected for chemical recovery using ^{225}Ac as a yield tracer. These equations are consistent with previous application of alpha spectrometry for proxy measurement of ^{227}Ac (e.g., Bojanowski et al., 1987; Martin et al., 1995). The present work includes several additional components not detailed in the cited articles. A correction for ingrowth of ^{227}Ac from ^{231}Pa present in the sample, between the collection date and the date of Ac separation from the sample is applied. Specific calculations for determining recovery of the yield tracer (^{225}Ac) are given and, owing to the moderately short half-life in comparison to the potential count time, these calculations take into account decay of ^{225}Ac over the counting period. This method is based on preparation of a ^{225}Ac tracer as opposed to spiking samples with ^{229}Th, this reduced the potential interference from ^{229}Th for ultra-low measurement of ^{227}Ac. To this end, calculations are given to correct for decay of the ^{225}Ac tracer between preparation and sample spiking.

Combined measurement uncertainty[53] for ^{227}Ac activity concentration was calculated using the method of Kragten (1994).

$$A_{Ac-227} = (A_{Ac-WW} - C_{Pa}) \times e^{\lambda_{Ac-227} \times t_{Coll}}$$

Equation A-1 Activity concentration of ^{227}Ac in sample at the time of collection.

Where:

$A_{Ac\text{-}227}$ = Activity concentration of ^{227}Ac in sample at the time of collection (wet weight; Bq kg^{-1})

[53] Measurement uncertainty for variables having a negligible effect on the combined measurement uncertainty were excluded (e.g., count time, decay constant, sample mass)

$A_{Ac\text{-}WW}$ = Activity concentration of ^{227}Ac in sample at the time of Ac separation (wet weight; Bq kg^{-1}; Equation A-3)

C_{Pa} = Correction factor for ingrowth of ^{227}Ac, between the collection date and the date of Ac separation from the sample, from ^{231}Pa present in the sample (wet weight; Bq kg^{-1}; Equation A-2)

t_{Coll} = Time between sample collection and separation of Ac (s)

$\lambda_{Ac\text{-}227}$ = The decay constant of ^{227}Ac (s^{-1})

$$A_{Ac-WW} = \frac{D \times N_{TR} \times 1000}{m_{Sample} \times \varepsilon_A \times R_{225} \times C}$$

Equation A-2 Activity concentration of ^{227}Ac in sample at measurement start time.

Where:

m_{Sample} = The sample weight (g; dry weight)

D = Dry weight to wet weight ratio of sample (unitless)

ε_A = The counting efficiency of the alpha spectrometer used for ^{227}Ac determination (counts s^{-1} Bq^{-1})

C = Ingrowth correction factor for ^{223}Ra and ^{227}Th (Equation A-4; see footnote [54]). This is equal to the integrated activity of ^{227}Th and ^{223}Ra relative to the activity of ^{227}Ac at the time of Ac separation (unitless).

N_{TR} = Net count rate of ^{223}Ra and ^{227}Th (counts s^{-1}; Equation A-6)

R_{225} = Chemical recovery of ^{225}Ac (Equation A-7). This value takes into account the decay of ^{225}Ac over the counting period for recovery determination (unitless).

[54] The constant 0.99295 used in Equation A-4 accounts for the branching ratio of ^{227}Ac. Actinium-227 decays via alpha decay to ^{227}Th (98.59%) and to ^{223}Fr (1.41%), the alpha particles produced by decay of ^{227}Ac are well beyond the integrated range of ^{227}Th and ^{223}Ra alpha particle energies and are therefore excluded. Francium-223 has a 22-minute half-life before decaying to ^{223}Ra (98.98%) via beta decay, as such, effectively 100% of ^{227}Ac decays lead to alpha decay of ^{223}Ra. The correction accounts for the lower relative activity of ^{227}Th and is equal to (1 + 0.9859)÷2. This simplified correction is based on a minimum ingrowth period of 124 days (otherwise the relative activity of ^{227}Th is slightly higher).

$$C_{Pa} = \frac{\lambda_{Ac-227}}{\lambda_{Ac-227} - \lambda_{Pa-231}} \times A_{Pa-231} \times \left(e^{-\lambda_{Pa-231} \times t_{Coll}} - e^{-\lambda_{Ac-227} \times t_{Coll}}\right)$$

Equation A-3 Correction factor for ingrowth of ^{227}Ac from ^{231}Pa.

Where:

A_{Pa-231} = Activity concentration of ^{231}Pa in sample at the time of collection (wet weight; Bq kg^{-1})

λ_{Pa-231} = The decay constant of ^{231}Pa (s^{-1})

$$C = 0.99295 \times \left(\frac{\lambda_{Th-227} \times \left(e^{-\lambda_{Ac-227} \times t_{ASep}} - e^{-\lambda_{Th-227} \times t_{ASep}}\right)}{\lambda_{Th-227} - \lambda_{Ac-227}} + \lambda_{Ra-223} \times \lambda_{Th-227}(C_1 + C_2 + C_3) \right)$$

Equation A-4 Ingrowth correction factor for ^{223}Ra and ^{227}Th.

Where:

λ_{Th-227} = The decay constant of ^{227}Th (s^{-1})

λ_{Ra-223} = The decay constant of ^{223}Ra (s^{-1})

t_{ASep} = Time between separation of Ac from the sample and the count start time for ^{227}Ac determination (s)

C_1, C_2, C_3 = These are correction factors forming part of the Bateman equation for calculating ingrowth of ^{227}Th and ^{223}Ra from ^{227}Ac (unit is s^2, i.e., seconds squared)

$$C_1 = \frac{e^{-\lambda_{Ac-227} \times t_{ASep}}}{(\lambda_{Th-227} - \lambda_{Ac-227}) \times (\lambda_{Ra-223} - \lambda_{Ac-227})}$$

$$C_2 = \frac{e^{-\lambda_{Th-227} \times t_{ASep}}}{(\lambda_{Ac-227} - \lambda_{Th-227}) \times (\lambda_{Ra-223} - \lambda_{Th-227})}$$

$$C_3 = \frac{e^{-\lambda_{Ra-223} \times t_{ASep}}}{(\lambda_{Ac-227} - \lambda_{Ra-223}) \times (\lambda_{Th-227} - \lambda_{Ra-223})}$$

Equation A-5 C_1, C_2 and C_3 from Equation A-4.

$$N_{TR} = \frac{S_{At}}{t_{ASample}} - \frac{B_{At}}{t_{ABlank}}$$

Equation A-6 Net count rate of ^{223}Ra and ^{227}Th.

Where:

$t_{ASample}$ = The sample count time for ^{227}Ac determination (s)

t_{ABlank} = The analytical blank count time for ^{227}Ac determination (s)

S_{At} = The gross ^{217}At counts for the sample (counts; assumed to be in secular equilibrium with ^{225}Ac and to therefore decay with the half-life of ^{225}Ac)

B_{At} = The gross ^{217}At counts for the analytical blank (counts)

$$R_{225} = \frac{N_{At} \times \lambda_{Ac-225}}{A_{225} \times e^{-\lambda_{Ac-225} \times t_{RSep}} \times \varepsilon_R \times \left(1 - e^{-\lambda_{Ac-225} \times t_{RSample}}\right)}$$

Equation A-7 Chemical recovery of ^{225}Ac.

Where:

A_{225} = Total activity of ^{225}Ac added to the sample, corrected to the time of Ac separation from the parent isotope ^{229}Th for preparation of the ^{225}Ac tracer solution (Bq)

$\lambda_{Ac\text{-}225}$ = The decay constant of ^{225}Ac (s^{-1})

N_{At} = Net counts of ^{217}At (Equation A-8). This equation takes into account the potential for different count times of the sample and analytical blank for recovery determination (counts)

t_{RSep} = Time between separation of Ac from the sample and the count start time for recovery determination (s)

$$N_{At} = t_{RSample} \times \left(\frac{S_{At}}{t_{RSample}} - \frac{B_{At}}{t_{RBlank}}\right)$$

Equation A-8 Net counts of ^{217}At.

Where:

$t_{RSample}$ = The sample count time for recovery determination (s)

t_{RBlank} = The analytical blank count time for recovery determination (s)

S_{At} = The gross ^{217}At counts for the sample (counts)

B_{At} = The gross ^{217}At counts for the analytical blank (counts)

ε_R = The counting efficiency of the alpha spectrometer used for recovery determination (counts s^{-1} Bq^{-1})

A-2 Calculation of ^{231}Pa activity concentration

The following series of equations were used to determine the ^{231}Pa activity concentration measured in samples, corrected to the sample collection date. Combined measurement uncertainty[55] for ^{231}Pa activity concentration was determined according to the principles of JCGM (2008). The combined measurement uncertainty does not include the systematic error in the AMS measurement process, which is estimated at 4%.

$$A_{Pa-231} = Nc_{Pa-231} \times \lambda_{Pa-231} \times D \times 1000$$

Equation A-9 Activity concentration of ^{231}Pa in sample at collection date.

Where:

$A_{Pa\text{-}231}$ = Activity concentration of ^{231}Pa in sample[56] at collection date (wet weight; Bq kg^{-1})

$\lambda_{Pa\text{-}231}$ = The decay constant of ^{231}Pa (s^{-1})

D = Dry weight to wet weight ratio of sample (unitless)

$Nc_{Pa\text{-}231}$ = Net ^{231}Pa atom concentration measured in sample (dry weight; atoms g^{-1}; Equation A-10)

[55] Measurement uncertainty for variables having a negligible effect on the combined measurement uncertainty were excluded (e.g., count time, decay constant, sample mass). Different techniques (i.e., JCGM, 2008; Kragten, 1994) were used to determine measurement uncertainty for ^{227}Ac and ^{231}Pa as data was provided by different institutions. The calculated measurement uncertainty for the two different techniques is not materially different.

[56] Where multiple measurements were taken of the same sample fraction after chemical separation, these values were averaged to give the final reported value with some exceptions were the 'best' result(s) only were taken (i.e., where measurement(s) had very low ^{233}Pa counts and later measurement(s) were substantially higher, the more precise value(s) were used.

$$Nc_{Pa-231} = \frac{Na_{Pa-231}}{m_{Sample}}$$

Equation A-10 Net ^{231}Pa atom concentration measured in sample.

Where:

$Na_{Pa\text{-}231}$ = Net ^{231}Pa atoms measured in sample (atoms; Equation A-11)

m_{Sample} = The sample weight (g; dry weight)

$$Na_{Pa-231} = At_{Pa-231} - B_{Pa-231}$$

Equation A-11 Net ^{231}Pa atoms measured in sample.

Where:

$At_{Pa\text{-}231}$ = Total ^{231}Pa atoms measured in sample (atoms; Equation A-12)

$B_{Pa\text{-}231}$ = Total ^{231}Pa atoms in analytical blank (atoms)

$$At_{Pa-231} = At_{Pa-233} \times Rc_{Pa-231:Pa-233}$$

Equation A-12 Total ^{233}Pa atoms added to sample at the count time.

Where:

$At_{Pa\text{-}233}$ = Total ^{233}Pa atoms added to sample at the count time (atoms)

$Rc_{Pa\text{-}231:Pa\text{-}233}$ = Corrected ratio of ^{231}Pa to ^{233}Pa atoms measured in the sample (unitless; this requires the measured number of mass 233 counts to be corrected for the ^{233}U atom contribution present in sample at count time)

$$Rc_{Pa-231:Pa-233} = \frac{C_{Pa-231} \times (At_{Pa-233} + At_{U-233} \times \varepsilon_{U-233})}{At_{Pa-233} \times C_{233}}$$

Equation A-13 Corrected ratio of ^{231}Pa to ^{233}Pa atoms measured in the sample.

Where:

$C_{Pa\text{-}231}$ = Normalised ^{231}Pa counts (corrected for dead time as determined from the measured yield of a known number of artificial pulses injected into the detector pre-amplifiers, and then normalised to 233 mass count time to account for longer count times for mass 231) from sample measurement (counts)

C_{233} = Counts for mass 233 (Pulser corrected) from sample measurement (counts)

$At_{U\text{-}233}$ = Total ^{233}U atoms in the sample at the count time (atoms). This is determined using the Bateman equations calculating from the date of Pa separation from the sample. This value was multiplied to 1.0028±0.0054 to account for incomplete separation of Pa from U with the TK400® resin (see Section 3.9.1.2). For all samples the time between separation of Pa from the sample ranged from 12 to 23 days.

$\varepsilon_{U\text{-}233}$ = The relative ion counting efficiency of ^{233}U atoms compared to ^{233}Pa atoms. This was determined by the process described below and was equal to 0.104±0.078 (unitless; Equation A-14).

A-2.1 Determination of ^{233}U relative ion counting efficiency

The relative ion counting efficiency of ^{233}U was determined from a sample spiked with both ^{231}Pa and ^{233}Pa prepared for AMS analysis. Although the concentration of ^{233}Pa atoms in the spiked sample was known, that of ^{231}Pa was not. To determine the relative counting efficiency of Pa to U, this spiked sample was measured soon after radiochemical separation of Pa, after some ingrowth of ^{233}U atoms had occurred and again after ^{233}Pa had effectively decayed completely to ^{233}U. This allowed for a more accurate determination of the UO_2^- counting efficiency relative to PaO_2^-, assuming the counting efficiencies remained similar between both measurements.

$$\varepsilon_{U-233} = \frac{Ru_{Pa-231:Pa-233}}{R_{Pa-231:U-233} \times R_{U-233}}$$

Equation A-14 The relative counting efficiency of ^{233}U atoms compared to ^{233}Pa atoms.

Where:

$Ru_{Pa\text{-}231:Pa\text{-}233}$ = Ratio of ^{231}Pa to ^{233}Pa atoms measured in the sample after correction for ^{233}U atoms present in sample at count the time (unitless). This is essentially the same variable as above, however, the value initially input into this equation is the ratio of mass 231 to mass 233 counts from the first measurement of the standard spiked with ^{231}Pa and ^{233}Pa. This initial ratio is uncorrected for ^{233}U atoms present in the sample at the count time and includes measurement of both ^{233}Pa and ^{233}U atoms. The initial measured ratio was 3.29±0.54. To account for the presence of ^{233}U atoms, it was assumed that no ^{233}U was present to initially determine the relative ion counting efficiency of ^{233}U. This value was

then used to correct the ratio of ^{231}Pa to ^{233}Pa atoms measured in the sample in the first count and the ^{233}U relative counting efficiency ($\varepsilon_{U\text{-}233}$) was recalculated. This process was applied through 100 iterations[57] to determine the final ^{233}U relative counting efficiency, with the final ratio of ^{231}Pa to ^{233}Pa atoms measured after correction for ^{233}U atoms present in sample at count time corrected to 3.15±0.52.

$R_{Pa\text{-}231:U\text{-}233}$ = The ratio of ^{231}Pa atoms measured in the sample to ^{233}U atoms measured in the sample (unitless). This was equal to 21.0±15.3.

$R_{U\text{-}233}$ = The ratio of ^{233}U atoms in the sample at the time of first measurement relative to the second measurement, determined using the Bateman equations calculating from the date of Pa separation from the sample (unitless). This was equal to 1.44±0.03.

The relative transmission efficiency of ^{233}U was determined through measurement of a standard spiked with both ^{231}Pa and ^{233}Pa and separated for Pa using the TK400® resin separation method (Chapter 3, Section 3.12.3). AMS measurement of the separated Pa fraction was conducted both 14–15 days and 474–477 days after initial Pa/U separation. Thus, the ratio of ^{231}Pa atoms to a combination of ^{233}Pa and ^{233}U atoms was measured initially, then, after effectively complete decay of ^{233}Pa, the ratio of ^{231}Pa to ^{233}U atoms was measured. The number of ^{233}Pa atoms added was known through calibration of the solution with HPGe gamma spectrometry and the number of ^{233}U atoms was known at the measurement date by calculating the ingrowth since Pa/U initial separation. The number of ^{231}Pa atoms added was imprecisely known as there was no reliable method available to calibrate this solution. This allowed the transmission efficiency of ^{233}U relative ^{233}Pa atoms to be determined, assuming the injection efficiency of ^{231}Pa remained similar between both measurements. The iterative approach described above for calculating the ^{233}U relative counting efficiency accounts for variations in the counting relative injection efficiencies between PaO_2^- and UO_2^- across the two different measurements.

A-3 MDL calculation for ^{227}Ac and ^{231}Pa

In this thesis 'MDL' is equivalent to the 'L_D' parameter defined by Currie (1968), where the probability of Type I and Type II errors are set at 5%. As such, MDL is the level of the true net signal that, if present, will be assessed as detected with a 95% probability. As noted in Chapter 4 (Section 4.3.2.2.4) the MDL for a measurement process can be calculated as a function of the

[57] Note that the ^{233}U relative counting efficiency is accurate to within 0.2% of the final value after only two iterations.

uncertainty of the blank signal (σ_B) which is multiplied by a constant '*k*'. Currie (1968) defines *k* under two situations, being the 'paired-observation' and 'Well-known blank'. Throughout this thesis blanks were run with each batch of samples which is equivalent to the 'paired-observation' situation where *k* is equal to 4.65. To convert the MDL, determined as a function of σ_B, to an activity concentration, parameters unique to each sample measurement are then taken into consideration.

For ^{227}Ac, σ_B is determined from the analytical blank and the unit is 'counts'. The MDL for each sample measurement is calculated by replacing the parameter N_{TR} (in Equation A-3 above) with '$\sigma_B \times 4.65$' and proceeding to calculate $A_{Ac\text{-}227}$ (in Equation A-1 above) to determine the MDL as an activity concentration of ^{227}Ac in the sample at the collection date.

A problem that may occur with this approach for MDL determination, which is based on statistical modelling and hypothesis testing, is where the measured result is less than twice the standard deviation of the measured value, but above the calculated MDL. This implies a distribution that includes negative values, which cannot be reasonably attributed to an activity concentration.

An alternative and easily calculated approach that incorporates result specific parameters of the experimental result, is to apply the principles used in the statistical models and hypothesis testing directly to the measured value and associated uncertainty. In this case a measurement is considered to have exceeded the MDL when it is greater than twice the standard deviation of the measured value. In statistical terms, this is the point above which there is a greater than 95% probability that a true net signal has been assessed as detected. The MDL can therefore be expressed as the sum of the measured value plus twice the standard deviation, except where the measured value is negative (i.e., where it implies values below zero). In this case, the measured value is assumed to be zero, and the reported value is then twice the standard deviation. In such situations the result specific parameters, the blank signal, and the measurement uncertainty are accounted for appropriately, even though the sample signal is less than the blank signal. The approach for determining the MDL for ^{227}Ac was to use the highest value of either that from Currie (1968) or the measured value plus twice the standard deviation as described above.

For ^{231}Pa, because the transmission efficiency can vary significantly between samples, the blank signal is not defined in absolute terms (e.g., counts) but as an atom ratio (i.e., ^{231}Pa:^{233}Pa). This makes determining the blank signal somewhat more complex than is the case for alpha spectrometry, while also taking into account parameters unique to each sample. For AMS, tracer

atoms (e.g., ^{233}Pa) must be present to measure the atom ratio for the blank, therefore the blank signal is determined using the spiked blank and not the analytical blank. Differences in the relative transmission efficiency between the spiked blank and samples are likely to exist, and the chemical recovery for a sample relative to a spiked blank is also likely to be different. Both cases lead to differences in the number of ^{233}Pa counts which leads to differences in the relative uncertainty specific to each measurement that is not accounted for with independent measurement of the blank. Hence, to account for parameters unique to each sample measurement when determining the MDL for analysis of ^{231}Pa, the approach using the measured value plus twice the standard deviation as described above was used, where twice the standard deviation was larger than the measured result. Where this was not the case, results were reported as above MDL (i.e., an activity concentration and associated measurement uncertainty was reported).

To determine an average MDL for each batch to allow comparison of the general method performance the Currie (1968) method was used. For this, the value used for σ_B was the standard deviation from multiple measurements of the spiked blank run with each batch and was equal to the number atoms of ^{231}Pa measured in the spiked blank. The MDL for each sample measurement was then determined by replacing the parameter $Na_{Pa\text{-}231}$ (in Equation A-10 above) with '$\sigma_B \times 4.65$' then proceeding to calculate $A_{Pa\text{-}231}$ (in Equation A-9 above) to determine the MDL as an activity concentration of ^{231}Pa in the sample at the collection date. Results of this are provided in (Appendix J-1.3).

Appendix B Radionuclide activity concentrations

B-1 Activity concentrations of ^{227}Ac and ^{231}Pa

Table B-1 ^{227}Ac and ^{231}Pa activity concentrations in bush food and wildlife samples from the ARR. The age is included in the 'Sample ID' column for freshwater mussel samples (uncertainty is σ=1).

Sample ID	Common name	Scientific name	Compartment	Collection date[a]	Status[b]	^{227}Ac (mBq kg^{-1}; wet weight)[c]	^{231}Pa (mBq kg^{-1}; wet weight)[d]
JE15006[e]	Northern brown bandicoot	*Isoodon macrourus*	Bone	12/03/2015	Unperturbed		4.7 ± 2.2
JE15008[e]	Northern brown bandicoot	*Isoodon macrourus*	Carcass	12/03/2015	Unperturbed	5.3 ± 0.4	2.5 ± 1.1
JE15007[e]	Northern brown bandicoot	*Isoodon macrourus*	Flesh	12/03/2015	Unperturbed	<1.7	<0.91
JE15009[e]	Northern brown bandicoot	*Isoodon macrourus*	Gastrointestinal tract (including contents)	12/03/2015	Unperturbed		78 ± 25
JT14002[f]	Flying fox	*Pteropus sp.*	Whole organism	05/07/2014	Unperturbed	<0.39	1.6 ± 0.7
DN15008[e]	Rainbow lorikeet	*Trichoglossus moluccanus*	Whole organism	31/07/2015	Unperturbed		<3.6
RM08002[g]	Water buffalo	*Bubalus bubalis*	Flesh	07/10/2007	Unperturbed	1.1 ± 0.4	<3.0
RM08005[g]	Water buffalo	*Bubalus bubalis*	Kidney	07/10/2007	Unperturbed		7.7 ± 2.8

Sample ID	Common name	Scientific name	Compartment	Collection date[a]	Status[b]	^{227}Ac (mBq kg^{-1}; wet weight)[c]	^{231}Pa (mBq kg^{-1}; wet weight)[d]
XX14054	Freshwater crocodile	*Crocodylus johnstoni*	Flesh	01/02/2014	Unperturbed		<2.8
GN14001	Barramundi	*Lates calcarifer*	Flesh	11/06/2014	Perturbed	<6.7	<0.71
GN14002	Barramundi	*Lates calcarifer*	Liver	11/06/2014	Perturbed	12 ± 3	<0.65
RM07011[h]	Passionfruit	*Passiflora foetida*	Flesh	17/01/2007	Unperturbed		2.2 ± 0.5
RJX10059	Fig	*Ficus congesta*	Flesh	30/11/2010	Perturbed	3.6 ± 0.2	
RM07015	White apple	*Syzygium eucalyptoides*	Flesh	17/01/2007	Unperturbed	0.33 ± 0.31	1.8 ± 0.5
RM08046	Cocky apple	*Planchonia careya*	Flesh	11/01/2008	Perturbed		<32
RM08053	Sand palm fruit	*Livistona humilis*	Flesh	11/01/2008	Perturbed	1.5 ± 0.3	0.66 ± 0.17
RM08078[g]	Billygoat plum	*Terminalia ferdinandiana*	Flesh	24/10/2008	Unperturbed	2.8 ± 0.4	<30
RM08080	Billygoat plum	*Terminalia ferdinandiana*	Flesh	20/11/2008	Unperturbed	5.6 ± 0.9	
RM08082	Billygoat plum	*Terminalia ferdinandiana*	Flesh	20/11/2008	Unperturbed		
RM10071	Billygoat plum	*Terminalia ferdinandiana*	Flesh	17/03/2010	Unperturbed	4.5 ± 0.3	

Sample ID	Common name	Scientific name	Compartment	Collection date[a]	Status[b]	^{227}Ac (mBq kg^{-1}; wet weight)[c]	^{231}Pa (mBq kg^{-1}; wet weight)[d]
RM10072	White apple	*Syzygium spp.*	Flesh	16/12/2010	Unperturbed	0.33 ± 0.05	
XX12085[g]	Red apple	*Syzygium fibrosum*	Flesh	13/11/2012	Unperturbed		<1.3
XX12085S[g]	Red apple	*Syzygium fibrosum*	Seed	13/11/2012	Unperturbed	1.9 ± 0.3	<6.7
XX12093	Cluster fig	*Ficus racemosa*	Flesh	13/11/2012	Unperturbed	3.5 ± 0.7	<0.72
XX12051[g]	Magpie goose	*Anseranas semipalmata*	Flesh	18/06/2012	Unperturbed	<9.4	39 ± 16
XX14002	Magpie goose	*Anseranas semipalmata*	Heart	23/08/2012	Unperturbed	<14	<1.4
XX14003[g]	Magpie goose	*Anseranas semipalmata*	Liver	12/08/2012	Unperturbed	<6.2	<2.8
RM09031	Wild boar	*Sus scrofa*	Flesh	04/09/2009	Unperturbed	0.64 ± 0.17	
RM09033	Wild boar	*Sus scrofa*	Flesh	04/09/2009	Unperturbed	<1.4	
RM09034[g]	Wild boar	*Sus scrofa*	Flesh	04/09/2009	Unperturbed	3.5 ± 0.8	<3.0
RM13067[f]	Wild boar	*Sus scrofa*	Bone	16/09/2013	Unperturbed	3.2 ± 0.9	<1.6
RM13066	Wild boar	*Sus scrofa*	Bone marrow	28/09/2013	Perturbed		<2.4
DN15009[g]	Green tree snake	*Dendrelaphis punctulatus*	Whole organism	30/11/2015	Unperturbed	7.4 ± 2.4	<3.8
GL12003	Agile wallaby	*Macropus agilis*	Flesh	11/01/2012	Unperturbed	<3.6	<0.80

Sample ID	Common name	Scientific name	Compartment	Collection date[a]	Status[b]	^{227}Ac (mBq kg^{-1}; wet weight)[c]	^{231}Pa (mBq kg^{-1}; wet weight)[d]
GL12002	Agile wallaby	*Macropus agilis*	Heart	11/01/2012	Unperturbed	<6.9	<0.73
GL12004	Agile wallaby	*Macropus agilis*	Liver	11/01/2012	Unperturbed	31 ± 7	1.6 ± 0.4
RM08021	Agile wallaby	*Macropus agilis*	Liver	09/01/2008	Perturbed		3.4 ± 0.7
RM08018	Agile wallaby	*Macropus agilis*	Flesh	09/01/2008	Perturbed	<1.9	<0.95
RM13078[f]	Agile wallaby	*Macropus agilis*	Bone	05/11/2013	Perturbed	27 ± 7	<8.0
XX14048	Agile wallaby	*Macropus agilis*	Flesh	01/10/2013	Unperturbed		<0.66
XX14053[f]	Agile wallaby	*Macropus agilis*	Joey	01/10/2013	Unperturbed	<0.11	<0.42
RM07001	Bush potato	*Eriosema chinense*	Flesh	03/01/2007	Perturbed		10 ± 4
XX12010	Cheeky yam	*Dioscorea bulbifera*	Flesh	04/05/2012	Unperturbed	5.6 ± 2.1	12 ± 4
2017-390	Freshwater mussel	*Velesunio angasi*	Shell	24/10/2017	Unperturbed	51 ± 19	<10
RM08075	Wild boar	*Sus scrofa*	Flesh	05/11/2008	Unperturbed		<0.80
2021-220[e]	Green Ant	*Oecophylla smaragdina*	Whole organism	15/07/2021	Unperturbed	<2.9	<1.6

Sample ID	Common name	Scientific name	Compartment	Collection date[a]	Status[b]	^{227}Ac (mBq kg^{-1}; wet weight)[c]	^{231}Pa (mBq kg^{-1}; wet weight)[d]
2021-107[e]	Shrub	Mixed shrub species	Whole organism	07/04/2021	Unperturbed	8.8 ± 2	1.9 ± 0.4
2021-109[e]	Grass	Mixed grass species	Whole organism	07/04/2021	Unperturbed	17 ± 2	4.2 ± 0.5
2021-119[e]	Herbs	Mixed herb species	Whole organism	07/04/2021	Unperturbed	5.3 ± 0.9	1.7 ± 0.3
2017-360[i] (3 years)	Freshwater mussel	*Velesunio angasi*	Flesh	24/10/2017	Unperturbed	350 ± 50	<0.53
2018-686[i] (2 years)	Freshwater mussel	*Velesunio angasi*	Flesh	01/10/2018	Unperturbed	450 ± 60	
2018-687[g,i,j] (3 years)	Freshwater mussel	*Velesunio angasi*	Flesh	01/10/2018	Unperturbed	440 ± 60	<2.3
2018-689[i] (5 years)	Freshwater mussel	*Velesunio angasi*	Flesh	01/10/2018	Unperturbed	550 ± 80	
2018-701[g,i] (2 years)	Freshwater mussel	*Velesunio angasi*	Flesh	01/10/2018	Unperturbed	340 ± 50	<1.5
2018-704[g,i] (5 years)	Freshwater mussel	*Velesunio angasi*	Flesh	01/10/2018	Unperturbed		<2.5

[a] Date format is 'Day/Month/Year'.

[b] The perturbed sites are those impacted by mining operations, or other human activities, and may include mine tailings and areas where mining wastewaters were used for irrigation. Unperturbed sites are considered as those not significantly impacted by human activities.

[c] ^{227}Ac activity concentrations corrected to sample collection date and to account for ingrowth from ^{231}Pa present in the sample at the time of collection. Where ^{231}Pa results are unavailable, no correction has been applied. The actual correction is potentially large, with the potential to account for all the measured activity of ^{227}Ac in a sample where ^{231}Pa activity concentrations are close to or higher than ^{227}Ac and the time between sampling and analysis are high relative to the half-life of ^{227}Ac.

[d] For ^{231}Pa analysis by AMS, repeated measurements were made for most samples. For samples where results were <MDL, the measurement with the lowest MDL is reported. This was either when the highest number of ^{233}Pa counts were recorded or the lowest background count rate measurement was made.

[e] These samples were washed prior to analysis. For Northern brown bandicoot, washing involved rinsing the whole animal (fur and outer skin) with high purity water to removed dirt and dust. For grasses, herbs and shrub washing procedures are detailed in (Supervising Scientist, 2022) and for green ant samples in (Medley et al., 2017).

[f] These samples were received as dry-ashed samples (i.e., dry-ashing occurred prior to addition of tracer solution).

[g] The ToF system was not used in AMS measurement for these samples and there may be some counts attributed to ^{232}Th included in ^{231}Pa and ^{233}Pa counts used to determine count rates from AMS analysis for ^{231}Pa (see Section 3.12.2).

[h] This sample was not washed; sample preparation procedures detailed in (Medley et al., 2013).

[i] Samples preparation for freshwater mussels is detailed in (Bollhöfer et al., 2011).

[j] Two replicates of this sample were processed, with all measurements for both replicates <MDL. From repeated measurements, the average MDL was 0.074 mBq kg^{-1} (n=2) for replicate 1 and 0.046 mBq kg^{-1} (n=3) for replicate 2. The lowest MDL value is reported here.

B-2 Activity concentrations of ^{238}U series radionuclides

Table B-2 ^{238}U series activity concentrations in bush food and wildlife samples from the ARR. Data from ERISS unpublished results unless otherwise noted (uncertainty is σ=1).

Sample ID	^{238}U series radionuclide activity concentrations (Bq kg^{-1}; wet weight)						
	Gamma or alpha spectrometry[a]						ICP-MS[b]
	^{238}U	^{234}U	^{230}Th	^{226}Ra	^{210}Pb	^{210}Po	^{238}U
JE15006							0.98
JE15008				2.9 ± 0.2	1.7 ± 0.8		0.37
JE15007							<0.027
JE15009							8.9
JT14002				3.1 ± 0.2	6.6 ± 1.0		0.012

Sample ID	^{238}U series radionuclide activity concentrations (Bq kg^{-1}; wet weight)						
	Gamma or alpha spectrometry[a]						ICP-MS[b]
	^{238}U	^{234}U	^{230}Th	^{226}Ra	^{210}Pb	^{210}Po	^{238}U
DN15008[c]				0.28 ± 0.01	<6.0		<0.041
RM08002	0.0087 ± 0.0034	0.0082 ± 0.0039	<0.015	<0.0061	0.090 ± 0.019		0.035
RM08005	0.022 ± 0.005	0.014 ± 0.005	<0.026	0.30 ± 0.01	0.92 ± 0.10	91 ± 9	<0.0052
XX14054				0.039 ± 0.004			<0.016
GN14001							<0.014
GN14002							
RM07011[d]				2.4 ± 0.1	1.4 ± 0.2	<0.92	0.099
RJX10059[e]				1.6 ± 0.04	0.19 ± 0.03	0.14 ± 0.03	0.16
RM07015				0.30 ± 0.02	0.56 ± 0.12	<0.59	0.052
RM08046				33.0 ± 0.8	6.0 ± 0.8		21
RM08053[c]				0.36 ± 0.06			0.19
RM08078				0.082 ± 0.018	2.7 ± 0.3		0.048
RM08080				0.14 ± 0.02	1.9 ± 0.4	<3.3	0.19
RM08082				2.0 ± 0.1	<1.6	<7.3	0.14
RM10071				0.39 ± 0.02			0.068
RM10072				0.30 ± 0.01			<0.017
XX12085[c]				0.54 ± 0.02	6.0 ± 0.5		0.023
XX12085S				0.43 ± 0.02			<0.014
XX12093[c]				1.90 ± 0.05	0.50 ± 0.34		0.022

Sample ID	^{238}U series radionuclide activity concentrations (Bq kg^{-1}; wet weight)						
	Gamma or alpha spectrometry[a]						ICP-MS[b]
	^{238}U	^{234}U	^{230}Th	^{226}Ra	^{210}Pb	^{210}Po	^{238}U
XX12051							0.0065
XX14002							0.023
XX14003							0.016
RM09031				0.019 ± 0.006	0.077 ± 0.026	0.21 ± 0.05	0.19
RM09033				0.019 ± 0.006	<0.22	4.6 ± 0.5	0.15
RM09034				0.017 ± 0.003	<0.21	0.82 ± 0.3	0.1
RM13067				5.3 ± 0.2	22 ± 1		2
RM13066							0.052
DN15009				1.50 ± 0.05			0.074
GL12003				0.047 ± 0.004	<0.046	0.37 ± 0.02	0.028
GL12002				0.074 ± 0.007	0.37 ± 0.04	0.55 ± 0.03	<0.014
GL12004				0.13 ± 0.008	1.3 ± 0.2	4.4 ± 0.2	0.048
RM08021	0.34 ± 0.04	0.44 ± 0.04	<0.065	0.27 ± 0.05	1.2 ± 0.2	8.5 ± 0.8	0.25
RM08018	0.061 ± 0.009	0.058 ± 0.01	0.016 ± 0.01	0.052 ± 0.004	0.18 ± 0.04	2.5 ± 0.2	0.015
RM13078				160 ± 2	17 ± 2		0.52
XX14048				0.0036 ± 0.0019			<0.015
XX14053				3.0 ± 0.1	1.4 ± 0.4		0.0079
RM07001				7.3 ± 0.2	14 ± 2	<7.9	1.1
XX12010				0.61 ± 0.02	0.29 ± 0.04	1.0 ± 0.2	0.078

Sample ID	^{238}U series radionuclide activity concentrations (Bq kg^{-1}; wet weight)						
	Gamma or alpha spectrometry[a]						ICP-MS[b]
	^{238}U	^{234}U	^{230}Th	^{226}Ra	^{210}Pb	^{210}Po	^{238}U
2017-390				19.8 ± 0.6			1.7
RM08075				0.0087 ± 0.0027	0.28 ± 0.03	<0.19	0.020
2021-220							0.035
2021-107				6.0 ± 0.3	26.3 ± 0.4	5.0 ± 0.5	0.070
2021-109				7.3 ± 0.2	26.0 ± 0.4	11.0 ± 0.5	2.4
2021-119				4.7 ± 0.1	27.1 ± 0.3	5.2 ± 0.4	0.55
2017-360				39.3 ± 0.2	5.7 ± 0.6	18 ± 0.7	0.012
2018-686				36.6 ± 0.3	9.8 ± 0.7	46 ± 2	0.011
2018-687				53.8 ± 0.9	10 ± 1	48 ± 2	0.014
2018-689				59.8 ± 0.7	11 ± 1	41 ± 2	0.011
2018-701				21.1 ± 0.4		34 ± 1	0.007
2018-704				27.5 ± 0.4	14 ± 1		0.0088

[a] Gamma spectrometry methods described in Murray et al. (1987), alpha spectrometry methods described in Martin and Hancock (2004) and Medley et al. (2005).

[b] ICP-MS performed by an external laboratory, measurement uncertainty is estimated at 10%.

[c] ^{226}Ra data for RM08053 and ^{210}Pb data for all other noted samples from Radiation Sciences, Queensland Health, unpublished.

[d] Data taken from Medley et al. (2013).

[e] Data taken from (Bollhöfer et al., 2012).

B-3 Activity concentrations of ^{232}Th series radionuclides

Table B-3 ^{232}Th series activity concentrations in bush food and wildlife samples from the ARR. Data from ERISS unpublished results unless otherwise noted (uncertainty is σ=1).

Sample ID	^{232}Th series radionuclide activity concentrations (Bq kg^{-1}; wet weight)			
	Gamma or alpha spectrometry[a]			ICP-MS[b]
	^{232}Th	^{228}Ra	^{228}Th	^{232}Th
JE15006				<0.025
JE15008		0.45 ± 0.35	0.53 ± 0.15	<0.041
JE15007				<0.0089
JE15009				1.1
JT14002		1.1 ± 0.4	1.4 ± 0.2	
DN15008				0.13
RM08002	0.0046 ± 0.0041			0.49
RM08005	0.012 ± 0.010			0.21
XX14054				<0.053
GN14001				<0.045
GN14002				
RM07011[c]		0.94 ± 0.05		0.023
RJX10059[d]				<0.045
RM07015				0.022
RM08046				0.069
RM08053				0.057
RM08078				0.053
RM08080				1.2
RM08082				0.49
RM10071				<0.057
RM10072				<0.057
XX12085				<0.0077
XX12085S				<0.11
XX12093				<0.0073

Sample ID	^{232}Th series radionuclide activity concentrations (Bq kg^{-1}; wet weight)			
	Gamma or alpha spectrometry[a]			ICP-MS[b]
	^{232}Th	^{228}Ra	^{228}Th	^{232}Th
XX12051				<0.053
XX14002				<0.053
XX14003				<0.053
RM09031				0.03
RM09033				0.39
RM09034				0.25
RM13067		2.2 ± 0.4	1.1 ± 0.1	0.041
RM13066				<0.17
DN15009				0.012
GL12003				<0.0094
GL12002				<0.0094
GL12004				<0.011
RM08021	<0.035			<0.011
RM08018	0.0078 ± 0.0058			0.069
RM13078		31 ± 1	26.0 ± 0.7	<0.069
XX14048				<0.049
XX14053		0.69 ± 0.16	0.46 ± 0.07	
RM07001				0.14
XX12010				0.14
2017-390		5.5 ± 0.9		2.0
RM08075				0.041
2021-220				0.046
2021-107				0.18
2021-109				0.80
2021-119				0.24
2017-360		11.5 ± 0.2	4.4 ± 0.1	0.15
2018-686		10.6 ± 0.3	3.1 ± 0.1	<0.0013

Sample ID	^{232}Th series radionuclide activity concentrations (Bq kg^{-1}; wet weight)			
	Gamma or alpha spectrometry[a]			ICP-MS[b]
	^{232}Th	^{228}Ra	^{228}Th	^{232}Th
2018-687		13.1 ± 0.7	5.3 ± 0.3	<0.0013
2018-689		16.2 ± 0.5	7.6 ± 0.3	<0.0013
2018-701		10.7 ± 0.4	3.3 ± 0.2	0.006
2018-704		13.2 ± 0.5	7.5 ± 0.3	0.041

[a] Gamma spectrometry methods described in Murray et al. (1987), alpha spectrometry methods described in Martin and Hancock (2004) and Medley et al. (2005).

[b] ICP-MS performed by an external laboratory, measurement uncertainty is estimated at 10%.

[c] Data taken from Medley et al. (2013).

[d] Data taken from (Bollhöfer et al., 2012).

B-4 Elemental concentrations

Table B-4 Concentrations of Al, As, Ba, Ca, Cd, Co, Cr, Cu, Fe, Hg, K and Mg in bush food and wildlife samples from the ARR (Measured by ICP-MS, measurement uncertainty is estimated at 10%). Data from ERISS unpublished results unless otherwise noted.

Sample ID	Concentration (mg kg^{-1}; wet weight)											
	Al	**As**	**Ba**	**Ca**	**Cd**	**Co**	**Cr**	**Cu**	**Fe**	**Hg**	**K**	**Mg**
JE15006	12	<0.30	75	120000	<0.03	<0.03	<3.0	0.61	67	<0.03	1800	1800
JE15008	60	<0.50	32	55000	<0.050	0.05	<5.0	3.2	240	0.1	9700	1400
JE15007	<2.2	<0.11	0.033	66	<0.011	<0.011	<1.1	0.71	15	0.044	4000	270
JE15009	1500	<0.50	52	2200	0.15	1.3	45	9.6	2900	0.1	13000	1100
JT14002	6.9	<0.025	0.7	3100	<0.0025	0.0025	<0.25	0.44	16	<0.0025	440	93
DN15008	6.6	<0.17	1.7	13000	<0.017	<0.017	<1.7	2.3	110	<0.017	3800	440
RM08002	6.1	0.015	0.036	32	<0.0024	<0.012	0.048	1.6	30		3300	210
RM08005	6.5	0.021	0.3	78	0.068	0.084	0.063	1.7	53		1800	110
XX14054	0.26	<0.013	0.73	180	<0.0013	<0.013	0.052	0.18	4.9	0.078	3400	190
GN14001	0.21	<0.011	<0.11	120	<0.0013	<0.011	0.4	0.12	3.2	0.15	3800	250
RM07011[a]	2	<0.014	4.4	330	<0.0028	0.2	0.025	2.1	6.5		4000	420
RJX10059[b]	23	<0.0055	0.96	1100	0.012	0.081	0.073	2	8	<0.0055	3500	420
RM07015	3	<0.014	0.64	130	<0.0028	<0.014	0.55	2.3	6.4		1200	250
RM08046	130	0.018	60	390	<0.0028	0.18	13	1.6	160		2800	660
RM08053	<2.8	<0.14	0.028	65	<0.014	<0.014	<1.4	1.2	8.3	<0.014	2300	280
RM08078	3.9	<0.021	0.45	810	0.013	0.034	0.13	1.4	5.6		4300	920
RM08080	52	<0.023	0.35	940	<0.0046	0.14	0.77	2	19		5100	970

Sample ID	Concentration (mg kg^{-1}; wet weight)											
	Al	**As**	**Ba**	**Ca**	**Cd**	**Co**	**Cr**	**Cu**	**Fe**	**Hg**	**K**	**Mg**
RM08082	16	0.015	1.8	910	<0.0029	0.088	0.18	3	5.9		3600	1000
RM10071	33	<0.014	6.6	720	0.017	0.2	5.3	1.7	66	0.0055	3600	580
RM10072	33	<0.014	1.6	300	<0.0014	<0.014	0.44	1.2	7.5	<0.0028	2000	250
XX12085	2.7	0.21	0.84	500	<0.0019	<0.0095	0.11	0.59	3.9	<0.0095	1100	260
XX12085S	0.53	<0.027	1.3	450	0.0053	<0.027	0.21	1.3	7.4		2900	590
XX12093	1.1	<0.0091	8.1	1200	<0.0018	<0.0091	0.27	0.85	6.5	<0.0091	2700	470
XX12051	0.53	0.024	<0.13	29	<0.0013	<0.013	0.11	4.5	59		3200	250
XX14002	1.3	<0.013	<0.13	35	<0.0013	<0.013	0.17	2.9	53	<0.0027	1700	170
XX14003	2.1	0.027	<0.13	64	0.016	0.027	4	2.1	560	0.0053	1700	150
RM09031	2.4	<0.12	0.024	45	<0.012	<0.012	<1.2	0.97	11	<0.012	3000	210
RM09033	4.8	<0.12	0.048	40	<0.012	<0.012	<1.2	0.92	11	<0.012	3400	230
RM09034	<2.4	<0.12	0.036	39	<0.012	<0.012	<1.2	0.9	13	<0.012	3000	190
RM13067	17	<0.10	27	84000	<0.01	0.021	<1.0	1.1	19	<0.010	680	1200
RM13066	1.7	<0.042	<0.42	550	<0.0042	<0.042	<0.042	0.42	11	<0.0084	120	23
DN15009	15	<0.15	8.9	27000	0.015	0.03	<1.5	0.48	60	0.03	2200	650
GL12003	1	<0.012	0.035	29	<0.0012	<0.012	0.14	1.2	32	<0.0023	3400	200
GL12002	0.45	<0.011	0.17	51	<0.0011	<0.011	0.12	2.7	150	<0.0023	2700	160
GL12004	2.2	<0.013	0.15	50	0.016	0.059	0.052	2.5	150	0.0052	2200	130
RM08021	12	0.016	0.22	68	0.015	0.033	0.21	2.9	100	<0.013	2300	150
RM08018	0.48	0.022	0.024	32	<0.0024	<0.012	0.085	1.5	23		2900	220

Sample ID	Concentration (mg kg^{-1}; wet weight)											
	Al	**As**	**Ba**	**Ca**	**Cd**	**Co**	**Cr**	**Cu**	**Fe**	**Hg**	**K**	**Mg**
RM13078	7.6	<0.017	420	120000	<0.0017	<0.017	0.1	0.73	73	<0.0035	830	2000
XX14048	0.96	<0.012	<0.12	89	<0.0012	<0.012	0.048	1.5	17	<0.0024	3100	200
XX14053	3.8	<0.016	5.5	3700	<0.0016	0.0032	<0.16	0.53	18	<0.0016	590	110
RM07001	150	<0.013	14	1200	0.01	0.077	3.1	1.7	82		2500	1000
XX12010	41	0.0054	7.2	370	0.0019	0.029	3.5	1.1	70		1600	270
2017-390	30	<0.5	179	360000	0.15	0.3	<5	4.2	420	<0.05	<50	<10
RM08075	3.6	0.015	0.037	43	<0.0025	<0.012	0.025	0.48	8.1		3300	170
2021-220	5.6	<0.14	14	250	0.042	0.042	<1.4	3.1	34	<0.014	2000	240
2021-107	11	<0.28	24	2300	0.028	4.3	<2.8	1.0	11	<0.028	3000	1000
2021-109	12	<0.31	11	860	0.15	0.28	<3.1	1.6	61	<0.031	4700	500
2021-119	82	<0.19	68	7500	0.056	0.30	<1.9	1.4	82	<0.019	1300	1900
2017-360	<1.1	<0.055	80	760	0.033	0.072	<0.55	0.33	680	<0.0055	190	62
2018-686	1.3	0.063	96	1300	0.038	0.089	<0.63	0.58	1100	0.013	250	92
2018-687	2.5	0.13	130	1400	0.044	0.11	<0.63	0.61	1300	0.013	250	89
2018-689	1.3	0.063	140	1100	0.031	0.11	<0.63	0.5	1300	0.013	220	82
2018-701	1.9	0.094	130	1300	0.061	0.051	<0.47	0.54	1800	0.0094	170	77
2018-704	3.3	0.22	150	1300	0.077	0.15	<0.55	0.44	3100	0.016	200	91

[a] Data taken from Medley et al. (2013).

[b] Data taken from (Bollhöfer et al., 2012).

Table B-5 Concentrations of Mn, Na, Ni, P, Pb, Rb, S, Sb, Se, Sr, V and Zn in bush food and wildlife samples from the ARR (Measured by ICP-MS, measurement uncertainty is estimated at 10%). Data from ERISS unpublished results unless otherwise noted.

Sample ID	Concentration (mg kg^{-1}; wet weight)											
	Mn	Na	Ni	P	Pb	Rb	S	Sb	Se	Sr	V	Zn
JE15006	1.8	2900		58000	1.8	18	1200	0.03	0.91	150	<6.1	84
JE15008	3.6	4200		31000	1	91	8300	<0.050	3.5	63	<10	100
JE15007	0.19	720		2200	<0.044	32	2200	<0.011	0.66	0.066	<2.2	17
JE15009	52	4500		5800	3.6	130	4500	<0.050	4.5	26	30	81
JT14002	0.19	340		2000	0.079	1.6	46	<0.0025	<0.025	1.2	<0.49	4.7
DN15008	0.99	1400		8600	<0.066	17	2600	<0.017	0.33	16	<3.3	28
RM08002	0.15	320		1800	0.061	5.1	1800	<0.012	0.14	0.024	<0.012	41
RM08005	0.61	1300		1300	0.042	4.2	1300	<0.011	0.64	0.084	<0.011	12
XX14054	0.16	830	0.016		<0.013			<0.013	0.24	0.26	<0.013	7.5
GN14001	0.11	460	0.17		<0.011			<0.011	0.36	0.19	<0.011	2.7
GN14002												
RM07011[a]	8.7	24		310	<0.014	8.7	310	<0.014	<0.014	3.4	<0.014	5.5
RJX10059[b]	5.8	40		310	0.0099	10	180	<0.0055	<0.0055	1.1	0.0099	3.6
RM07015	2	750		260	0.11	6.1	160	<0.014	<0.014	1.1	<0.014	1.2
RM08046	5.5	16		240	0.18	14	410	<0.014	0.028	4	0.055	3
RM08053	2.2	28		340	<0.055	15	340	<0.014	<0.14	0.055	<2.8	1.8
RM08078	27	170		420	0.021	9.9	310	<0.021	0.034	9.2	<0.021	4.1
RM08080	32	34		500	<0.023	6.4	290	<0.023	0.041	15	0.023	3.9

Sample ID	Concentration (mg kg^{-1}; wet weight)											
	Mn	**Na**	**Ni**	**P**	**Pb**	**Rb**	**S**	**Sb**	**Se**	**Sr**	**V**	**Zn**
RM08082	3.5	59		410	<0.015	17	190	<0.015	0.059	4.6	<0.015	3.1
RM10071	25	61	1.9		0.028			<0.014	0.017	11	0.17	3
RM10072	3	130	0.28		0.014			<0.014	0.028	4.2	0.022	1.9
XX12085	0.89	110		110	0.011	4.2	99	<0.0095	0.017	0.68	0.011	1.2
XX12085S	1.2	200		360	<0.027	11	300	<0.27	0.048	0.53	<0.027	3.7
XX12093	2.2	180		310	<0.0091	8	130	<0.0091	0.0091	6.3	<0.0091	1.4
XX12051	0.44	510		2100	<0.013	2.1	2000	<0.013		0.021	<0.013	12
XX14002	0.48	770	0.08		<0.013			<0.013	0.35	0.027	<0.013	21
XX14003	2.4	910	1.3		0.053			<0.013	0.51	0.08	0.053	24
RM09031	0.25	270		1700	<0.048	0.81	2000	<0.012	0.12	0.024	<2.4	28
RM09033	0.23	360		1900	0.097	15	2000	<0.012	0.79	0.055	<2.4	27
RM09034	0.18	460		1600	1.6	9.7	1900	<0.012	0.12	0.03	<2.4	25
RM13067	0.28	2600		37000	2.5	1.4	140	<0.010	<0.10	160	<2.1	46
RM13066	0.084	450	<0.042		<0.042			<0.042	0.042	0.84	<0.042	1.7
DN15009	2.2	1600		13000	0.29	17	2000	<0.015	0.45	36	<3.0	49
GL12003	0.16	320	1.4	1800	<0.012	14	1600	<0.012	0.22	0.035	0.016	23
GL12002	0.43	860	<0.011	1500	0.057	12	2100	<0.011	0.25	0.085	<0.011	14
GL12004	3.8	990	0.016	2000	0.17	18	2000	<0.013	0.39	0.091	0.013	27
RM08021	4.2	1200		2300	0.53	14	1900	<0.013	0.37	0.093	<0.013	28
RM08018	0.22	350		1800	<0.012	12	1700	<0.012	0.21	0.012	<0.012	16

Sample ID	Concentration (mg kg^{-1}; wet weight)											
	Mn	**Na**	**Ni**	**P**	**Pb**	**Rb**	**S**	**Sb**	**Se**	**Sr**	**V**	**Zn**
RM13078	0.52	5500	0.17		0.8			<0.017	<0.017	210	0.017	45
XX14048	0.13	720	0.012		<0.012			<0.012	0.2	0.096	<0.012	22
XX14053	0.22	610		2500	0.038	2.3	64	<0.0016	<0.016	2.5	0.32	6.2
RM07001	14	72		250	0.31	6.9	600	<0.013	<0.013	18	<0.013	6.1
XX12010	6.4	18		120	0.096	3.9	68	<0.0048		3.6	0.096	3.9
2017-390	908	2100	2	120	0.2	0.24	500	0.25	1	1390	<10	7.5
RM08075	0.12	320		1700	<0.012	12	1500	<0.012	0.27	0.031	<0.012	17
2021-220	40	670	<0.056	1800	<0.056	3.8	1200	<0.014	0.14	2.5	<2.8	43
2021-107	74	<28	0.57	140	<1.1E-1	15	270	<0.028	<0.28	44	<5.7	2.6
2021-109	37	<31	0.37	150	0.37	19	343	0.092	<0.31	17	<6.1	5.2
2021-119	120	37	1.93	190	0.15	3.6	304	<0.019	<0.19	66	<3.7	4.8
2017-360	180	190	<0.22	1100	0.066	0.52	390	0.0055	0.11	9.5	1.1	17
2018-686	270	230	0.051	1600	0.15	0.78	490	0.019	0.13	17	0.25	25
2018-687	340	240	0.051	1700	0.43	0.78	480	0.013	0.13	20	0.25	26
2018-689	290	230	0.05	1500	0.13	0.65	410	0.0063	0.063	19	0.25	24
2018-701	220	220	0.037	1500	0.075	0.61	390	0.0047	0.14	23	0.19	28
2018-704	280	350	0.066	1700	0.11	0.64	450	<0.0055	0.16	24	<0.22	29

[a] Data taken from Medley et al. (2013).

[b] Data taken from Bollhöfer et al. (2012).

Table B-6 Concentrations of Mn, Na, Ni, P, Pb, Rb, S, Sb, Se, Sr, V and Zn in bush food and wildlife samples from the ARR (Measured by ICP-MS, measurement uncertainty is estimated at 10%). All data from ERISS unpublished results.

Sample ID	Concentration (mg kg^{-1}; wet weight)											
	Ce	Cs	La	Lu	Nb	Nd	Re	Sc	Ta	Ti	W	Zr
2021-220			0.0084									
2017-360	0.54	0.0033	0.38	<0.0011	0.0055	0.19	<0.0055	<0.11	0.011	0.055	<0.0055	0.011
2018-686	0.90	0.0038	0.63	<0.0013	<0.0063	0.3	<0.0063	<0.13	0.046	0.063	<0.0063	0.013
2018-687	1.0	0.0025	0.70	0.0025	<0.0063	0.34	<0.0063	<0.13	0.038	0.13	<0.0063	0.013
2018-689	1.1	<0.0013	0.81	<0.0013	<0.0063	0.38	<0.0063	<0.13	0.03	0.13	<0.0063	0.013
2018-701	2.0	<0.0009	1.4	0.00094	<0.0047	0.71	<0.0047	<0.094	0.015	0.14	<0.0047	0.0094
2018-704	3.1	0.0055	2.2	0.0022	<0.0055	1.1	<0.0055	<0.11	0.013	0.11	<0.0055	<0.011

Table B-7 Concentrations of Ag, Al, As, Ba, Be, Bi, Cd, Co, Cr, Cu, Fe, Hg, K and Li in soil samples from the ARR (Measured by ICP-MS, measurement uncertainty is estimated at 10%).

Sample ID	Concentration (mg kg^{-1}; wet weight)													
	Ag	Al	As	Ba	Be	Bi	Cd	Co	Cr	Cu	Fe	Hg	K	Li
2021-218	<5	34000	28	42	0.59	<1	<0.2	6.5	120	6.8	120000	<1	540	8.1
2021-221	<5	15000	<2	37	0.41	<1	<0.2	4.2	120	5.2	17000	<1	1400	7.9
2021-222	<5	5000	<2	11	0.092	<1	<0.2	0.69	53	1.3	1500	<1	630	2
2021-224	<5	14000	<2	33	0.25	<1	<0.2	3.4	64	5.7	17000	<1	1100	4.1
2021-225	<5	10000	<2	56	0.23	<1	<0.2	2.6	130	3	6600	<1	3100	2.3
2021-228	<5	26000	2.5	26	0.26	<1	<0.2	11	110	8.4	34000	<1	590	5.8

Table B-8 Concentrations of Mn, Mo, Ni, Pb, Sb, Se, Sn, Sr, Th, Ti, Tl, V and Zn in soil samples from the ARR (Measured by ICP-MS, measurement uncertainty is estimated at 10%).

Sample ID	Concentration (mg kg^{-1}; wet weight)												
	Mn	**Mo**	**Ni**	**Pb**	**Sb**	**Se**	**Sn**	**Sr**	**Th**	**Ti**	**Tl**	**V**	**Zn**
2021-218	130	2.8	9.4	22	<4	<4	1.5	7.6	9.6	1500	<1	280	2.90
2021-221	64	0.81	8.7	10	<4	<4	<1	6.9	4.7	1100	<1	48	4
2021-222	16	<0.5	<2	<2	<4	<4	<1	14	2.3	280	<1	3.4	<2
2021-224	43	0.57	71	6	<4	<4	<1	7.9	4.5	760	<1	37	2.6
2021-225	63	<0.5	8.7	7.2	<4	<4	<1	9.7	7.9	770	<1	19	4.6
2021-228	100	0.98	12	8.1	<4	<4	<1	10	7.7	3300	<1	93	4.4

Appendix C Concentration ratios and dose

C-1 Region-specific organism geometries

Region-specific organism geometries are shown in Table C-1. The ERICA tool interpolated new DCCs for these inputs from the DCCs of the defined representative organism ellipsoids, the new DCCs were then used for dose calculation. For region-specific organisms, occupancy factors were the same as used in Doering et al. (2019a) and Doering and Bollhöfer (2016b) for the equivalent ERICA reference organism, with Barramundi considered to be a pelagic fish. Except Northern brown bandicoot (*Isoodon macrourus*), which was assumed to be 100% in-soil and Flying fox (*Pteropus* sp.), which was assumed to be 50% on-soil and 50% in-air.

Table C-1 ARR region-specific organism and ERICA default reference organism geometries. A density of 1 g mL^{-1} was assumed; height and width were assumed equal unless otherwise noted.

Species name	Local organism (cm or kg)				Reference organism	ERICA defaults (cm or kg)			
	Height	Length	Width	Mass		Height	Length	Width	Mass
Freshwater environment									
Magpie goose (*Anseranas semipalmata*[a])	12	36	10	2.4	Bird	30	10	8.0	1.3
Freshwater crocodile (*Crocodylus johnstonii*[b])	20	210	43	30	Reptile	18	12	6.0	1.0
Barramundi *(Lates calcarifer*[c])	10	60	7.2	2.2	Pelagic fish	50	8.0	6.0	1.3
Freshwater mussel (*Velesunio angasi*[d])	1.9	6.4	2.9	0.018	Mollusc – bivalve	10	4.5	3.0	0.071
Terrestrial environment									
Green tree snake (*Dendrelaphis punctulatus*[e])	1.8	130	1.8	0.22	Reptile	120	3.5	3.5	0.74
Northern brown bandicoot (*Isoodon macrourus*[f])	14	46	12	3.0	Mammal – small-burrowing	20	6.0	5.0	0.31

Species name	Local organism (cm or kg)				Reference organism	ERICA defaults (cm or kg)			
	Height	Length	Width	Mass		Height	Length	Width	Mass
Green ant (*Oecophylla smaragdina*[g])	0.15	0.80	0.15	9.0×10^{-6}	Arthropod – detritivorous	1.7	0.61	0.30	1.7×10^{-4}
Flying fox (*Pteropus* sp.[h])	6.5	25	6.5	0.54	Mammal – small-burrowing				
Agile wallaby (*Macropus agilis*[i])	70	20	20	15	Mammal – large	130	60	60	245
Rainbow lorikeet (*Trichoglossus moluccanus*[j])	3.3	30	3.3	0.17	Bird	30	10	8.0	1.3

[a] Magpie goose (*Anseranas semipalmata*) body mass taken average of male and female specimens reported by Frith and Davies (1961). Geometry parameters determined using scaling factors for duck from (ICRP, 2008a).

[b] Freshwater crocodile average snout-vent length for the 10 largest female and male adults reported by Tucker et al. (2007). Total length, belly width and body mass derived from allometric relationships for largest size range specimens described in Edwards et al. (2017), height derived from volume of an ellipsoid function.

[c] In the NT juvenile barramundi move upstream, remaining in upper freshwater reaches until mature (Russell and Garrett, 1985), which occurs at a length of about 55–60 cm (Davis, 1982), as such a body length of 60 cm was assumed for dose assessment. Body mass and height/width geometry parameters were determined using scaling factors for salmonid/trout from (ICRP, 2008a).

[d] Freshwater mussel (*Velesunio angasi*) body length taken from average ultimate body length for all billabongs (excluding Sandy Billabong, which is a control site) reported in Bollhöfer et al. (2011). Body mass and height/width geometry parameters were determined using scaling factors for freshwater bivalve mollusc from (Pröhl et al., 2003).

[e] Green tree snake (*Dendrelaphis punctulatus*) snout-vent length from average of male and female specimens reported by Shine (1991), total body length and mass derived from allometric data for snakes reported in Feldman and Meiri (2012).

[f] The Northern brown bandicoot (*Isoodon macrourus*) body mass taken from highest value noted for males in Ingleby (2024). Geometry parameters determined using scaling factors for rat from (ICRP, 2008a).

[g] Green ant (*Oecophylla smaragdina*) body mass taken from average of worker ant from three sites reported in (Medley et al., 2017), body length taken from (Chapuisat and Keller, 2002).

[h] Flying fox (*Pteropus* sp.) data for *Pteropus alecto* species, the larger of two flying fox spp. common to the ARR region from Tedman and Hall (1985).

[i] Agile wallaby (*Macropus agilis*) data taken from Doering and Bollhöfer (2016b).

[j] Rainbow lorikeet (*Trichoglossus moluccanus*) data from (Birdlife Australia, 2023), maximum body length and mass used.

For dose pathways where values differed, a comparison of ^{227}Ac DCCs from the ERICA tool (v2.0) for region-specific organisms and similar default reference organisms is shown in Table C-2. The DCCs are generated for pathways where the occupancy factor is relevant for the organism. Two additional pathways, internal dose from alpha radiation (DCC = 0.0169) and low energy beta radiation (DCC = 1.38×10^{-5}) do not vary between organisms. The very high DCC for internal alpha radiation reflects that this is the dominant dose pathway for alpha emitting radionuclides and that organism geometry has a minimal effect on dose rate.

Table C-2 Comparison of ^{227}Ac DCCs for region-specific organisms and ERICA (v2.0) reference organisms.

Organism	**Dose pathway and associated DCC (μGy hour^{-1} per Bq kg^{-1} × 10^{-4})**			
	External radiation on soil	**External radiation in soil**	**Internal beta gamma**	**External radiation in air**
Green Tree snake	0.807	1.66	5.40	
ERICA Reptile	0.793	1.58	5.77	
Northern brown bandicoot		1.39	6.16	
ERICA Mammal - small burrowing		1.64	5.84	

Organism	Dose pathway and associated DCC (µGy hour^{-1} per Bq kg^{-1} × 10^{-4})			
	External radiation on soil	External radiation in soil	Internal beta gamma	External radiation in air
Green ant	0.791		2.67	
ERICA Insect - detritivorous	0.825	1.76	4.24	
ERICA Insect - flying	0.828		4.78	
Flying fox[a]	0.797		5.90	0.686
Rainbow lorikeet	0.810		5.70	0.734
ERICA Bird[b]	0.784		6.03	0.723
Agile wallaby	0.696		6.50	
ERICA Mammal - large	0.465		7.22	

[a] Assumes height above ground when 'in air' of 6.7 m, which is equal to the lowest roosting height recorded by Tidemann et al. (1999).

[b] Assumes height above ground when 'in air' of 10 m, which is the maximum allowable input value in the ERICA tool (v2.0).

C-2 Tissue:Whole-organism conversion factors

C-2.1 Terrestrial environment – Australian native species

Table C-3 Mammal Tissue:Whole-organism conversion factors for relevant chemical analogues and derived whole organism activity concentrations for ^{227}Ac and ^{231}Pa in Agile wallaby (*Macropus agilis*. Samples GL12003, GL12004, and XX14048 in Table B-1) from unperturbed sites. The highest activity concentration derived for ^{227}Ac and ^{231}Pa is highlighted in bold and was used in environmental dose assessment.

Analogue element	Tissue:Whole-organism conversion factor[a]					Activity concentrations[b] for unperturbed sites (mBq kg^{-1}; wet weight)					
						^{227}Ac			^{231}Pa		
	Tissue	Mean	Min	Max	*n*[c]	Mean	Min	Max	Mean	Min	Max
^{227}Ac[d]	Muscle	12			1	43					
Am	Muscle	13			1	47			9.4	8.5	10
Ce	Muscle	34			1	120					
Pu	Muscle	5.3	2.1	33	6				3.9	1.4	**26**
	Liver	0.24	0.027	9.2	12				0.37	0.019	22
^{231}Pa[d]	Muscle	10.5			1				7.63	6.89	8.4
	Bone	2.06			1				3.29		
Th[d]	Muscle	1.1	0.97	1.4	10	3.9	3.5	5.0	0.80	0.64	1.1
	Liver	0.74	0.13	2.9	9	23	2.3	130	1.1	0.092	7.0
U	Muscle	4.7	4.0	5.6	2	17	14	20	3.4	2.6	4.5
	Liver	4.2	3.5	5.4	2	130	61	**240**	6.5	2.5	13
U[e]	Muscle	2.4	0.98	15	15	8.6	3.5	54	1.7	0.64	12
	Liver	0.84	0.057	2.1	10	26	1.0	94	1.3	0.040	5.0

[a] All values from Yankovich et al. (2010) unless otherwise specified.

[b] Mean is calculated by multiplying the measured value for a given tissue by the conversion factor, where a sample type has more than one measured value, the average of both values is used. Min = Minimum and is calculated by multiplying the lowest conversion factor by the MDL value or by the 95% lower confidence limit of the sample activity concentration (value minus the standard deviation multiplied by 1.96). Max = Maximum and is calculated by multiplying the highest conversion factor by the MDL value or by the 95% upper confidence limit of the sample activity concentration (value plus the standard deviation multiplied by 1.96). Where a sample type has more than one result, the lowest value was used to calculate the minimum and the highest value is used to calculate the maximum.

[c] *n* = Number of samples.

[d] Values derived from ^{227}Ac and ^{231}Pa activity concentrations measured in Northern brown bandicoot (*Isoodon macrourus*) in this study, see Table B-1.

[e] Values from Doering et al. (2018).

Table C-4 Mammal Tissue:Whole-organism conversion factors for relevant chemical analogues and derived whole organism activity concentrations for ^{227}Ac and ^{231}Pa in Agile wallaby (*Macropus agilis*. Samples RM08018, RM08021, and RM13078 in Table B-1) from perturbed sites. The highest activity concentration derived for ^{227}Ac and ^{231}Pa is highlighted in bold.

Analogue element	**Tissue:Whole-organism conversion factor**[a]					**Activity concentrations**[b] **for perturbed sites (mBq kg^{-1}; wet weight)**					
						^{227}Ac			**^{231}Pa**		
	Tissue	**Mean**	**Min**	**Max**	***n***[c]	**Mean**	**Min**	**Max**	**Mean**	**Min**	**Max**
^{227}Ac[d]	Muscle	12			1	20					
Am	Muscle	13			1	25			12		
	Bone	0.83			1	23	12	**33**	6.6		
Ce	Muscle	34			1						
	Bone	0.76			1	21	11	31			
Pu	Muscle	5.3	2.1	33	6				5.0	2.0	31
	Liver	0.24	0.027	9.2	12				0.83	0.057	**44**

Analogue element	Tissue:Whole-organism conversion factor[a]					Activity concentrations[b] for perturbed sites (mBq kg^{-1}; wet weight)					
						^{227}Ac			^{231}Pa		
	Tissue	Mean	Min	Max	*n*[c]	Mean	Min	Max	Mean	Min	Max
^{231}Pa[d]	Bone	0.25	0.084	3.1	11				2.0	0.67	25
	Muscle	10.5			1				9.97		
Th[d]	Muscle	1.1	0.97	1.4	10	2.1	1.8	2.6	1.0	0.92	1.3
	Liver	0.74	0.13	2.9	9				2.5	0.28	14
U	Muscle	4.7	4.0	5.6	2	8.9	7.5	11	4.5	3.8	5.3
	Liver	4.2	3.5	5.4	2				14	7.4	26
	Bone	0.13	0.084	0.26	2	3.5	1.2	10	1.0	0.67	2.1
U[e]	Muscle	2.4	0.98	15	15	4.5	1.8	28	2.3	0.93	14
	Liver	0.84	0.057	2.1	10				2.9	0.12	10
	Bone	0.21	0.18	0.24	2	5.7	2.6	9.6	1.7	1.4	1.9

[a] All values from Yankovich et al. (2010) unless otherwise specified.

[b] Mean is calculated by multiplying the measured value for a given tissue by the conversion factor, where a sample type has more than one measured value, the average of both values is used. Min = Minimum and is calculated by multiplying the lowest conversion factor by the MDL value or by the 95% lower confidence limit of the sample activity concentration (value minus the standard deviation multiplied by 1.96). Max = Maximum and is calculated by multiplying the highest conversion factor by the MDL value or by the 95% upper confidence limit of the sample activity concentration (value plus the standard deviation multiplied by 1.96). Where a sample type has more than one result, the lowest value is used to calculate the minimum and the highest value is used to calculate the maximum.

[c] *n* = Number of samples.

[d] Values derived from ^{227}Ac and ^{231}Pa activity concentrations measured in Northern brown bandicoot (*Isoodon macrourus*) in this study, see Table C-11.

[e] Values from Doering et al. (2018).

Table C-5 Bird Tissue:Whole-organism conversion factors for relevant chemical analogues and derived whole organism activity concentrations for ^{227}Ac and ^{231}Pa in magpie goose (*Anseranas semipalmata*. Samples XX12051, XX14002 and XX14003 in Table B-1) from unperturbed sites. The highest activity concentration derived for ^{227}Ac and ^{231}Pa is highlighted in bold and was used in environmental dose assessment.

Analogue element	Tissue:Whole-organism conversion factor[a]					^{227}Ac[b] (mBq kg^{-1}; wet weight)			^{231}Pa[b] (mBq kg^{-1}; wet weight)		
	Tissue	Mean	Min	Max	*n*[c]	Mean	Min	Max	Mean	Min	Max
Ce	Liver	0.33	0.16	0.78	5	2.0	0.99	4.8			
Eu	Liver	0.74	0.45	0.98	5	4.6	2.8	6.1			
Th[d]	Muscle	1.0	1.0	1.1	3	9.4	9.4	10	39	8.8	**77**
	Liver	0.80	0.26	1.3	3	5.0	1.6	**8.1**	2.2	0.72	3.6
U[d]	Muscle	1.0	1.0	1.0	3	9.4.	9.4	9.4	39	8.8	70
	Liver	0.69	0.52	1.0	3	4.3	3.2	6.2	1.9	1.4	2.8

[a] All values from Yankovich et al. (2010) unless otherwise specified.

[b] Mean is calculated by multiplying the measured value for a given tissue by the conversion factor, where a sample type has more than one measured value, the average of both values is used. Min = Minimum and is calculated by multiplying the lowest conversion factor by the MDL value or by the 95% lower confidence limit of the sample activity concentration (value minus the standard deviation multiplied by 1.96). Max = Maximum and is calculated by multiplying the highest conversion factor by the MDL value or by the 95% upper confidence limit of the sample activity concentration (value plus the standard deviation multiplied by 1.96). Where a sample type has more than one result, the lowest value is used to calculate the minimum and the highest value is used to calculate the maximum.

[c] *n* = Number of samples.

[d] Values from Doering et al. (2018).

C-2.2 Terrestrial environment – Non-native Australian species

Table C-6 Mammal Tissue:Whole-organism conversion factors for relevant chemical analogues and derived whole organism activity concentrations for ^{227}Ac and ^{231}Pa in pig (*Sus scrofa*. Samples RM08002 and RM08005 in Table B-1) from unperturbed sites. The highest activity concentration derived for ^{227}Ac and ^{231}Pa is highlighted in bold.

Analogue element	Tissue:Whole-organism conversion factor[a]				^{227}Ac[b] (mBq kg^{-1}; wet weight)			^{231}Pa[b] (mBq kg^{-1}; wet weight)		
	Tissue	Mean	Min	Max	*n*[c]	Mean	Min	Max	Mean	Min	Max
Am	Muscle	13			1	27	4.1	66	39		
	Bone	0.83			1	2.7	1.2	4.2	1.3		
Ce	Muscle	34			1	71	11	**170**			
	Bone	0.76			1	2.5	1.1	3.9			
Pu	Muscle	5.3	2.1	33	6				16	6.3	**98**
	Bone	0.25	0.084	3.1	11				0.40	0.13	5.0
Th[d]	Muscle	1.1	0.97	1.4	10	1.3	0.45	2.6	3.3	2.9	4.2
U	Muscle	4.7	4.0	5.6	2	5.4	1.8	10	14	12	17
	Bone	0.13	0.084	0.26	2	0.42	0.12	1.3	0.21	0.13	0.42
U[d]	Muscle	2.4	0.98	15	15	2.8	0.45	0.28	7.2	2.9	45
	Bone	0.21	0.18	0.24	2	0.68	0.25	1.2	0.34	0.29	0.38

[a] All values from Yankovich et al. (2010) unless otherwise specified.

[b] Mean is calculated by multiplying the measured value for a given tissue by the conversion factor, where a sample type has more than one measured value, the average of both values is used. Min = Minimum and is calculated by multiplying the lowest conversion factor by the MDL value or by the 95% lower confidence limit of the sample activity concentration (value minus the standard deviation multiplied by 1.96). Max = Maximum and is calculated by multiplying the highest conversion factor by the MDL value or by the 95% upper confidence limit of the sample activity concentration (value plus the standard deviation multiplied by 1.96). Where a sample type has more than one result, the lowest value is used to calculate the minimum and the highest value is used to calculate the maximum.

[c] *n* = Number of samples.

[d] Values from Doering et al. (2018).

Table C-7 Mammal Tissue:Whole-organism conversion factors for relevant chemical analogues and derived whole organism activity concentrations for ^{227}Ac and ^{231}Pa in water buffalo (*Bubalus bubalis*. Samples RM08002 and RM08005 in Table B-1) from unperturbed sites. The highest activity concentration derived for ^{227}Ac and ^{231}Pa is highlighted in bold.

Analogue element	**Tissue:Whole-organism conversion factor**[a]					**^{227}Ac**[b] **(mBq kg^{-1}; wet weight)**			**^{231}Pa**[b] **(mBq kg^{-1}; wet weight)**		
	Tissue	**Mean**	**Min**	**Max**	***n***[c]	**Mean**	**Min**	**Max**	**Mean**	**Min**	**Max**
Am	Muscle	13			1	15	6.0	24	39		
Ce	Muscle	34			1	39	16	**63**			
Pu	Muscle	5.3	2.1	33	6				16	6.3	**100**
	Kidney	0.88	0.46	5.7	7				6.7	1.0	75
Th[d]	Muscle	1.1	0.97	1.4	10	1.3	0.45	2.6	3.3	2.9	4.2
	Kidney	0.75	0.15	2.3	8				5.7	0.33	30
U	Muscle	4.7	4.0	5.6	2	5.4	1.8	10	14	12	17
	Kidney	0.95	0.52	5.8	2				7.3	1.1	76
U[d]	Muscle	2.4	0.98	15	15	2.8	0.45	28	7.2	3.0	45
	Kidney	0.74	0.014	3.6	11				5.7	0.030	47

[a] All values from Yankovich et al. (2010) unless otherwise specified.

[b] Mean is calculated by multiplying the measured value for a given tissue by the conversion factor, where a sample type has more than one measured value, the average of both values is used. Min = Minimum and is calculated by multiplying the lowest conversion factor by the MDL value or by the 95% lower confidence limit of the sample activity concentration (value minus the standard deviation multiplied by 1.96). Max = Maximum and is calculated by multiplying the highest conversion factor by the MDL value or by the 95% upper confidence limit of the sample activity concentration (value plus the standard deviation multiplied by 1.96). Where a sample type has more than one result, the lowest value is used to calculate the minimum and the highest value is used to calculate the maximum.

[c] *n* = Number of samples.

[d] Values from Doering et al. (2018).

C-2.3 Freshwater aquatic environment –Native Australian species

Table C-8 Freshwater reptile (excluding turtles) Tissue:Whole-organism conversion factors for relevant chemical analogues and derived whole organism activity concentrations for ^{227}Ac and ^{231}Pa in freshwater crocodile (*Crocodylus johnstoni*. Samples XX12051, XX14002 and XX14003 in Table B-1) from unperturbed sites. The highest activity concentration derived for ^{227}Ac and ^{231}Pa is highlighted in bold and was used in environmental dose assessment.

Analogue element	Tissue:Whole-organism conversion factor[a]					^{231}Pa[b] (mBq kg^{-1}; wet weight)		
	Tissue	Mean	Min	Max	*n*[c]	Mean	Min	Max
U	Muscle	2.6			1	**7.2**		
U[d]	Muscle	1.1	0.79	1.6	3	3.0	2.2	4.4

[a] All values from Yankovich et al. (2010) unless otherwise specified.

[b] Mean is calculated by multiplying the measured value for a given tissue by the conversion factor, where a sample type has more than one measured value, the average of both values is used. Min = Minimum and is calculated by multiplying the lowest conversion factor by the MDL value or by the 95% lower confidence limit of the sample activity concentration (value minus the standard deviation multiplied by 1.96). Max = Maximum and is calculated by multiplying the highest conversion factor by the MDL value or by the 95% upper confidence limit of the sample activity concentration (value plus the standard deviation multiplied by 1.96). Where a sample type has more than one result, the lowest value is used to calculate the minimum and the highest value is used to calculate the maximum.

[c] *n* = Number of samples.

[d] Values from Doering et al. (2018).

Table C-9 Freshwater fish Tissue:Whole-organism conversion factors for relevant chemical analogues and derived whole organism activity concentrations for ^{227}Ac and ^{231}Pa in the freshwater fish Barramundi (*Lates calcarifer*. Samples GN14001 and GN14002 in Table B-1) from perturbed sites. The highest activity concentration derived for ^{227}Ac and ^{231}Pa is highlighted in bold.

Analogue element	Tissue:Whole-organism conversion factor[a]					^{227}Ac[b] (mBq kg^{-1}; wet weight)			^{231}Pa[b] (mBq kg^{-1}; wet weight)		
	Tissue	Mean	Min	Max	*n*[c]	Mean	Min	Max	Mean	Min	Max
Ce	Liver	0.53	0.30	1.0	7	6.5	1.9	18			
	Muscle	2.0	0.91	6.3	9	13	6.1	42			
Eu	Liver	1.0	0.43	1.7	7	12	2.7	31			
	Muscle	2.3	1.5	4.2	8	15	10	28			
La	Liver	0.43	0.13	0.91	11	5.3	0.83	17			
	Muscle	1.9	0.91	1.1	12	13	6.1	7.3			
Th	Liver	1.7	4.5	2.0	2	21	29	36	1.1	2.9	1.3
	Muscle	2.2	1.0	4.2	41	15	6.7	28	1.6	0.71	3.0
U	Liver	4.8	4.2	5.6	2	59	27	100	3.1	2.7	3.6
	Muscle	2.5	0.91	26	44	17	6.1	170	1.8	0.64	18
U[d]	Liver	4.2	0.23	36	24	51	1.5	**650**	2.7	0.15	**23**
	Muscle	3.0	0.87	18	29	20	5.8	120	2.1	0.61	13

[a] All values from Yankovich et al. (2010) unless otherwise specified.

[b] Mean is calculated by multiplying the measured value for a given tissue by the conversion factor, where a sample type has more than one measured value, the average of both values is used. Min = Minimum and is calculated by multiplying the lowest conversion factor by the MDL value or by the 95% lower confidence limit of the sample activity concentration (value minus the standard deviation multiplied by 1.96). Max = Maximum and is calculated by multiplying the highest conversion factor by the MDL value or by the 95% upper confidence limit of the sample activity concentration (value plus the standard deviation multiplied by 1.96). Where a sample type has more than one result, the lowest value is used to calculate the minimum and the highest value is used to calculate the maximum.

[c] *n* = Number of samples.

[d] Values from Doering et al. (2018).

Table C-10 Freshwater bivalve Tissue:Whole-organism conversion factors for relevant chemical analogues and derived whole organism activity concentrations for ^{227}Ac and ^{231}Pa in freshwater mussel (*Velesunio angasi*. Samples 2017-360, 2017-390, 2018-686, 2018-687, 2018-689, 2018-701, and 2018-704 in Table B-1) from unperturbed sites. The highest activity concentration derived for ^{227}Ac and ^{231}Pa is highlighted in bold and was used in environmental dose assessment.

Analogue element	Tissue:Whole-organism conversion factor[a]					^{227}Ac[b] (mBq kg^{-1}; wet weight)			^{231}Pa[b] (mBq kg^{-1}; wet weight)		
	Tissue	Mean	Min	Max	*n*[c]	Mean	Min	Max	Mean	Min	Max
^{227}Ac	Shell	15.9			1	810	230	1400			
	Soft Tissue	1.07			1	460	260	750			
Ce	Shell	5.4	2.7	9.6	14	280	78	470			
	Soft Tissue	0.66	0.63	0.71	14	280	150	500			
La	Shell	10	2.6	17	14	510	140	880			
	Soft Tissue	0.63	0.61	0.71	14	270	150	500			
Lu	Shell	0.46			1	24	6.6	40			
	Soft Tissue	4.9			1	2100	1200	3400			
Th	Shell	0.70	0.40	5.2	66	362	10	62	7.0	4.0	52
	Soft Tissue	1.3	0.65	160	66	550	160	**11000**	2.2	0.34	**410**
U	Shell	0.83	0.42	2.4	77	42	12	73	8.3	4.2	24
	Soft Tissue	2.0	0.72	11	77	850	180	7700	3.4	0.38	28

[a] All values from Doering et al. (2018), except ^{227}Ac, which was determined from values measured for this project in 3-year old freshwater mussel samples (Sample ID 2017-360 for soft tissue and 2017-390 for shell. See Table C-12).

[b] Mean is calculated by multiplying the measured value for a given tissue by the conversion factor, where a sample type has more than one measured value, the average of both values is used.

Min = Minimum and is calculated by multiplying the lowest conversion factor by the MDL value or by the 95% lower confidence limit of the sample activity concentration (value minus the standard deviation multiplied by 1.96). Max = Maximum and is calculated by multiplying the highest conversion factor by the MDL value or by the 95% upper confidence limit of the sample activity concentration (value plus the standard deviation multiplied by 1.96). Where a sample type has more than one result, the lowest value is used to calculate the minimum and the highest value is used to calculate the maximum.

[c] *n* = Number of samples.

C-2.4 Derivation of mammal and freshwater bivalve whole organism activity concentrations for ^{227}Ac and ^{231}Pa

Table C-11 Tissue data and derived whole organism activity concentrations of ^{227}Ac and ^{231}Pa in Northern brown bandicoot (*Isoodon macrourus*).

Sample ID	Component	Mass (g)	Fraction of total (%)	^{227}Ac activity (wet weight)		^{231}Pa activity (wet weight)	
				Total (mBq)	Concentration (mBq kg^{-1})	Total (mBq)	Concentration (mBq kg^{-1})
JE15002	Heart[a]	5.055	0.4	0.0085±0.0043	<1.7	0.0046±0.0023	<0.91
JE15003	Kidney[a]	4.414	0.3	0.0074±0.0037	<1.73	0.0040±0.0020	<0.91
JE15004	Testicles[a]	9.291	0.7	0.016±0.008	<1.7	0.0085±0.0042	<0.91
JE15005	Liver[a]	10.914	0.8	0.18±0.09	<1.7	0.010±0.05	<0.91
JE15006	Bone[b]	16.316	1.2	0.17±0.09	11±6	0.076±0.035	4.7±2.2
JE15007	Flesh	118.892	9.1	0.20±0.10	<1.7	0.11	<0.91
JE15008	Carcass	1021.72	78	5.4±0.4	5.3±0.4	2.60	2.5±1.1
JE15009	Gastrointestinal tract (including contents[b])	124.85	10	22±12	180±10	9.77	78±25
PSM24009[c]	Whole organism	1310	100	26±11	**19.9±8.3**	12.6±3.3	**9.6±2.5**

[a] ^{227}Ac and ^{231}Pa activity concentrations not measured, assumed to be equal to 'Flesh' activity concentration.

[b] ^{227}Ac activity concentrations not measured, determined from ^{231}Pa values assuming the same ^{227}Ac:^{231}Pa activity ratio for sample JE15008 (Carcass).

[c] The sample ID 'PSM24009' has been assigned to the 'Whole organism' for Northern Brown Bandicoot and the 'Total' activity is calculated as the sum of the products of 'Total' activity reported in the individual tissue sub-samples JE15002–JE15009 and the 'Fraction (%)'; the activity concentration for PSM24009 is calculated by dividing the Total activity by the Mass.

Table C-12 Tissue data and derived whole organism activity concentrations of ^{227}Ac and ^{231}Pa in freshwater mussel (*Velesunio angasi*).

Sample ID	Component	Fraction of total (%)	Activity concentration (mBq kg^{-1}; wet weight)	
			^{227}Ac	^{231}Pa
2017-360	Soft tissue	68.73	347±52	<0.53
2017-390	Shell	31.27	51±19	<10
PSM24010	Total	100	254±36	<3.5

C-3 ^{227}Ac and ^{231}Pa CRs for bush food items from the ARR

Table C-13 ^{227}Ac and ^{231}Pa CRs for terrestrial bush food items from the ARR. Biota activity concentrations are wet weight, soils are dry weight.

Bush food group	Site status	Spatial criterion (m)[a]	Temporal criterion (days)[a]	Tissue	^{227}Ac (Biota and soil Bq kg^{-1})[b]			^{231}Pa (Biota and soil Bq kg^{-1})[b]			*n*[c]
					Biota (×10^{-3})	Soil GM	CR (×10^{-3})	Biota (×10^{-3})	Soil GM	CR (×10^{-3})	
Buffalo	Unperturbed	10000	Any	Flesh	1.1	2.8	0.42	<3.0	2.8	<1.1	1
Buffalo	Unperturbed	10000	Any	Kidney				7.7	2.8	2.8	1
Fruit	Unperturbed	0	0	Flesh	5.6	0.75	7.5	30	0.98	31	5
Pig	Unperturbed	5000	Any	Flesh	3.5	0.84	4.2	<3.0	0.84	<3.6	3/2
Pig	Perturbed	5000	Any	Bone marrow				<2.4	23	<0.10	1

Bush food group	Site status	Spatial criterion (m)[a]	Temporal criterion (days)[a]	Tissue	^{227}Ac (Biota and soil Bq kg^{-1})[b]			^{231}Pa (Biota and soil Bq kg^{-1})[b]			*n*[c]
					Biota (×10^{-3})	Soil GM	CR (×10^{-3})	Biota (×10^{-3})	Soil GM	CR (×10^{-3})	
Wallaby	Unperturbed	200	Any	Flesh	<3.6	2.9	<1.2	<0.66	0.66	<1.0	1/2
Wallaby	Unperturbed	1000	Any	Flesh	<3.6	2.8	<1.3	<0.66	0.66	<1.0	1/2
Wallaby	Perturbed	1000	Any	Flesh	<1.7	32	<0.053	<0.95	32	<0.030	1
Wallaby	Unperturbed	1000	Any	Heart	<6.9	2.8	<2.5	<0.73	2.4	<0.30	1
Wallaby	Unperturbed	1000	Any	Liver	31	2.8	11	1.6	2.4	0.64	1
Wallaby	Perturbed	1000	Any	Liver				3.4	26	0.13	1
Yam	Unperturbed	0	0	Flesh	5.6	0.97	5.8	12	0.97	12	1
Yam	Perturbed	0	0	Flesh				10	2.5	4.2	1

[a] Spatial criterion is the radial distance from each sample collection site, whereas Temporal criterion is the time prior to sample collection. The values used were to determine which soil samples most closely matched the sampling time and location of the biota samples for inclusion in the calculation of the soil activity concentration geometric mean (typical value).

[b] Biota activity concentrations used to derive CRs are from Table B-1, Appendix B Section B-1. Soil values are geometric means of soil activity concentration data for soil samples that mostly closely match the sampling time, location and site status of biota samples and is based on the relevant Spatial and Temporal criterion, and the site status. Where multiple results were available for a tissue type, the maximum activity concentration was used. MDL values were used where a biota activity concentration was <MDL. No soil activity concentrations were <MDL for ^{227}Ac, ^{231}Pa or ^{238}U.

[c] *n* = number of biota samples used to derive CR. Where this differs for each isotope, it is presented as '^{227}Ac/^{231}Pa'.

d Soil GM values for ^{227}Ac and ^{231}Pa were mostly derived by assuming equilibrium with ^{235}U (see Section 5.2.1.2) and will therefore generally be equal. They may differ where actual measurements of ^{227}Ac and ^{231}Pa in soil samples were used, or where the biota samples used for derivation of a CR were collected from different sampling locations (e.g., fruit and wallaby samples were collected from a range of locations and not all were measured for both ^{227}Ac and ^{231}Pa).

Table C-14 ^{227}Ac and ^{231}Pa CRs for freshwater bush food items from the ARR. Biota activity concentrations are wet weight.

Bush food group	Site status	Spatial criterion (m)[a]	Temporal criterion (days)[a]	Tissue	^{227}Ac (Biota and water Bq kg^{-1})[b]			^{231}Pa (Biota and water Bq kg^{-1})[b]			*n*[c]
					Biota (×10^{-3})	Water (×10^{-5})	CR	Biota (×10^{-3})	Water (×10^{-5})	CR	
Barramundi (Fish Group 2)	Perturbed	0	Any	Flesh	6.3	20	31	0.71	20	3.5	1
Barramundi (Fish Group 2)	Perturbed	0	Any	Liver	12	20	60	0.65	20	3.2	1
Crocodile	Unperturbed	25000	Any	Flesh				<2.8	3.1	<89	1
Magpie goose	Unperturbed	50000	Any	Flesh	<9.4	1.7	<540	39	1.7	2100	1
Magpie goose	Unperturbed	25000	Any	Heart	<14	0.48	<3000	<1.4	0.48	<300	1
Magpie goose	Unperturbed	25000	Any	Liver	<6.2	0.48	<1300	<2.8	0.48	<595	1
Mussel	Unperturbed	0	1825	Flesh	340	0.48	72000	<2.5	0.48	<530	5/4

[a] Spatial criterion is the radial distance from each sample collection site, whereas Temporal criterion is the time prior to sample collection. The values used were to determine which water samples most closely matched the sampling time and location of the biota samples for inclusion in the calculation of the water activity concentration geometric mean.

[b] Biota activity concentrations used to derive CRs are from Table B-1, Appendix B Section B-1. Where multiple results were available for a tissue type, the maximum activity concentration was used. MDL values were used where a biota activity concentration was <MDL. The geometric mean of water activity concentrations is used, and no water values were <MDL. 783 water samples with results for ^{226}Ra used to derive ^{227}Ac and ^{231}Pa were in the CR Database (see Section 5.2.1.1), with 24 <MDL for ^{226}Ra. Of these water samples, 128 were collected from 3 sites where bush food items represented here were collected, 7 of which were <MDL. Where no results were available from the billabong where the bush food item was collected, spatial criteria were set to include nearby water courses from which results were available. For most samples ^{226}Ra or ^{227}Ac results for water samples were not available within 10 years of the bush food item sample collection, as such the temporal criteria was set to include all results matching the spatial criteria only (except for freshwater mussel samples).

[c] *n* = number of biota samples used to derive CR. Where this differs for each isotope, it is presented as '^{227}Ac/^{231}Pa'.

C-4 $CR_{WO\text{-}Media}$ values for used for ERICA environmental dose assessment of the RPA

Table C-15 $CR_{WO\text{-}Media}$ values for the terrestrial environment used for ERICA environmental dose assessment of the RPA. Results are from unperturbed sites. Biota activity concentrations are wet weight, soils are dry weight.

ERICA Reference organism	Region-specific organism	Spatial criterion (m)[a]	Temporal criterion (days)[a]	^{227}Ac (Biota and soil Bq kg^{-1})			^{231}Pa (Biota and soil Bq kg^{-1})		
				Biota (× 10^{-3})	Soil GM	CR (× 10^{-3})	Biota (× 10^{-3})	Soil GM	CR (× 10^{-3})
Arthropod - detritivorous	Green ant	10000	0	<2.9	1.6	<1.8	<1.6	1.6	<0.99
Bird - terrestrial	Rainbow lorikeet	10000	365				<3.6	1.9	<1.9
Grasses and Herbs	Mixed herbs	0	0	5.3	1.1	4.9	1.7	1.1	1.6
Grasses and Herbs	Mixed grasses	0	0	17	2.6	6.5	4.2	2.6	1.6
Mammal - small burrowing	Northern brown bandicoot	0	0	20	4.5	4.4	9.6	4.5	2.1
Mammal - large	Agile wallaby	200	365	<240	4.9	<49	<26	4.9	<5.3
Mammal - large	Agile wallaby	1000	365	<240	3.8	<63	<26	3.8	<6.9
Mammal - large	Agile wallaby (Joey)	1000	Any	0.11	0.72	<0.15	<0.42	0.66	<0.64
Mammal - small burrowing	Flying fox	6000	730	<0.39	1.6	0.24	1.6	1.6	0.99
Mammal - small burrowing	Flying fox	20000	365	<0.39	1.1	0.35	1.6	1.1	1.5
Mammal - large	Buffalo	10000	365	<63	3.5	<18	<100	3.5	<29
Mammal - large	Pig	5000	365	<170	0.84	<200	<98	0.84	<120
Reptile - terrestrial	Green tree snake	400	365	7.4	2.3	3.2	<3.8	2.3	<1.6

ERICA Reference organism	Region-specific organism	Spatial criterion (m)[a]	Temporal criterion (days)[a]	^{227}Ac (Biota and soil Bq kg^{-1})			^{231}Pa (Biota and soil Bq kg^{-1})		
				Biota (× 10^{-3})	Soil GM	CR (× 10^{-3})	Biota (× 10^{-3})	Soil GM	CR (× 10^{-3})
Shrub	Mixed shrubs	0	0	8.8	2.6	3.5	1.9	2.6	0.73

[a] Spatial criterion is the radial distance from each sample collection site, whereas Temporal criterion is the time prior to sample collection. The values used were to determine which soil samples most closely matched the sampling time and location of the biota samples for inclusion in the calculation of the soil activity concentration geometric mean.

Table C-16 $CR_{WO\text{-}Media}$ values for the freshwater environment used for ERICA environmental dose assessment. Results are from unperturbed sites, except for Barramundi, which is from a perturbed site. Biota activity concentrations are wet weight.

ERICA Reference organism	Region-specific organism	Spatial criterion (m)[a]	Temporal criterion (days)[a]	^{227}Ac (Biota, Bq kg^{-1}, and water, Bq L^{-1})			^{231}Pa (Biota, Bq kg^{-1}, and water, Bq L^{-1})		
				Biota (× 10^{-3})	Water GM (× 10^{-5})	$CR_{WO\text{-}Media}$ (× 10^{3})	Biota (× 10^{-3})	Water GM (× 10^{3})	$CR_{WO\text{-}Media}$ (× 10^{3})
Pelagic fish	Barramundi (Fish Group 2)	0	Any	<650	2.3	<28	<23	2.3	<1.0
Bird	Magpie goose	25000 / 50000	Any	<8.1	0.43	<1.9	<77	0.95	<8.1
Mollusc - bivalve	Freshwater mussel	0	1825	250	0.89	29	<3.5	0.89	<0.39
Reptile	Crocodile	25000	Any				<7.2	0.95	<0.76

[a] Spatial criterion is the radial distance from each sample collection site, whereas Temporal criterion is the time prior to sample collection. The values used were to determine which water samples most closely matched the sampling time and location of the biota samples for inclusion in the calculation of the water activity concentration geometric mean. For 'Brid' a spatial criterion of 25000 m was used for ^{227}Ac whereas 50000 m was used for ^{231}Pa.

C-5 Variations in derived CRs for different input values

Table C-17 Variations in CRs for fruit flesh samples with different spatial, temporal and MDL multiplication factor values.

Radionuclide /Element	Site status	Spatial criterion (m)[a]	Temporal criterion (days)[b]	MDL factor[c]	GM ($\times 10^{-3}$)	CR Geometric standard deviation	CR Arithmetic mean ($\times 10^{-3}$)	CR Arithmetic standard deviation ($\times 10^{-3}$)	CR Min[d] ($\times 10^{-3}$)	CR Max[d] ($\times 10^{-3}$)	*n*[e]
Ac-227	Unperturbed	0	0		1.5	2.5	2.6	2.9	0.38	7.5	5
Ac-227	Unperturbed	250	365		1.3	2.5	2.6	3.0	0.23	7.5	5
Ac-227	Unperturbed	1000	730		1.4	2.4	2.7	2.9	0.27	7.5	5
Ac-227	Unperturbed	50000	1825		0.93	2.1	1.6	1.4	0.20	3.6	6
Ac-227	Perturbed	0	0				0.23	0.09	0.17	0.30	2
Ac-227	Perturbed	250	365				0.20	0.05	0.17	0.24	2
Ac-227	Perturbed	1000	730				0.11	0.01	0.10	0.11	2
Ac-227	Perturbed	50000	1825				0.085	0.058	0.044	0.13	2
Pa-231	Unperturbed	0	0	1	2.2	3.3	7.4	13	0.38	31	5
Pa-231	Unperturbed	0	0	0.5	1.5	3.0	4.2	6.3	0.19	15	5
Pa-231	Perturbed	0	0	1			0.13				1
Pa-231	Perturbed	250	365	1			1.8	2.4	0.072	3.5	2
Pa-231	Perturbed	1000	365	1			1.2	1.6	0.049	2.3	2
Pa-231	Perturbed	50000	1825	1			0.47	0.64	0.019	0.92	2
Th	Unperturbed	0	0	1	5.4	3.7	33	71	0.20	210	8
Th	Unperturbed	0	0	0.5	4.2	3.8	32	72	0.099	210	8

Radionuclide /Element	Site status	Spatial criterion (m)[a]	Temporal criterion (days)[b]	MDL factor[c]	GM ($\times 10^{-3}$)	CR Geometric standard deviation	CR Arithmetic mean ($\times 10^{-3}$)	CR Arithmetic standard deviation ($\times 10^{-3}$)	CR Min[d] ($\times 10^{-3}$)	CR Max[d] ($\times 10^{-3}$)	*n*[e]
Th	Perturbed	0	0	1			5.8	7.1	0.73	11	2
Th	Perturbed	0	0	0.5			5.6	7.4	0.37	11	2
U	Unperturbed	0	0	1	3.9	2.6	5.8	7.0	1.3	23	8
U	Unperturbed	0	0	0.5	3.6	2.7	5.6	7.1	1.3	23	8
U	Perturbed	0	0	1			1.3	1.3	0.34	2.2	2

[a] Spatial criterion is the radial distance from each sample collection site used to determine samples used to calculate the water activity concentration geometric mean.

[b] Temporal criterion is the time prior to sample collection used to determine samples used to calculate the water activity concentration geometric mean.

[c] MDL factor is the value by which MDL values are multiplied to calculate mean, standard deviation, minimum and maximum values. The MDL factor is irrelevant for ^{227}Ac in unperturbed sites and U in perturbed sites as all values were >MDL.

[d] Min = Minimum; Max = Maximum.

[e] *n* = Number of biota samples used to derive CR.

C-6 Comparison of ^{238}U series and ^{235}U series (^{227}Ac and ^{231}Pa) CRs in bush food items of the ARR

Table C-18 ^{227}Ac, ^{231}Pa and ^{238}U series CRs for terrestrial bush food items from the ARR (unperturbed sites only). Where results were available for more than one sample, arithmetic mean values are shown, followed by minimum–maximum values where available.

Bush food group	**CR**						
Bush food group	**^{227}Ac**[a]	**^{231}Pa**[a]	**Pb**[b]	**Po**[b]	**Ra**[b]	**Th**[b]	**U**[b]
Buffalo (Flesh; × 10^{-3})	0.42	0.54	1.3 0.20–2.9	4.9 1.5–16	0.32 0.20–0.75	0.067 0.046–0.081	0.20 0.081–0.036
Buffalo (Kidney; × 10^{-3})		2.8	6.6 1.7–12	510 85.5–1100	3.7 2.4–5.8	0.14 0.063–0.21	0.24 0.052–0.37
Fruit (flesh; × 10^{-3})	2.6 0.38–7.5	4.2 0.19–15	22 0.078–260	32 0.052–120	27 0.26–170	13 0.012–270	2.3 0.018–14
Pig (Flesh; × 10^{-3})	1.7 0.33–4.2	0.98 0.17–1.8	1.0 0.54–1.8	28 2.9–90	0.30 0.098–0.44	9.3 0.79–27	1.8 0.020–6.6
Agile wallaby (Flesh; × 10^{-3})	1.3	0.33 0.17–0.50	3.8 0.28–20	12 1.2–68	0.51 0.045–2.3	1.0 0.029–2.5	0.15 0.018–0.41
Yam (× 10^{-3})	5.8	12	71 0.59–300	20 7.2–38	180 0.94–980	13 0.45–130	27 0.21–360

[a] Biota activity concentrations used to derive CRs are from Table B-1, geometric mean of soil values from the updated CR database used. The MDL value multiplied by 0.5 was used where a biota activity concentration was <MDL.

[b] Values for these radionuclides reproduced from (Doering et al., 2017).

Table C-19 ^{227}Ac, ^{231}Pa and ^{238}U series CRs for freshwater bush food items from the ARR (unperturbed sites except for Barramundi where none were available). Where more than one result was available for a sample type, arithmetic mean values are shown, followed by minimum–maximum values.

Bush food group	^{227}Ac[a]	^{231}Pa[a]	Pb[b]	Po[b]	Ra[b]	Th[b]	U[b]
Barramundi (Fish Group 2; Flesh)	30.8	3.48	57 0.78–310	220 19–1100	80 5.5–750	62 1.1–260	24 0.43–300
Crocodile flesh		45	9.6	700	12 1.9–39	26 24–28	4.9 1.3–6.7
Magpie goose flesh	270	2100	140 7.6–450	81 46–120	9.3 5.7–18	57 8.0–130	28 2.0–96
Mussel (soft tissue; × 10^3)	37 22–72	0.13 0.017–0.26	16 2.4–71	28 23–37	58 4.6–180	0.24 0.00068–3.6	0.33 0.021–1.5

[a] Biota activity concentrations used to derive CRs are from Table B-1 (half the value if <MDL), geometric mean of soil values from the updated CR database used. The MDL value multiplied by 0.5 was used where a biota activity concentration was <MDL.

[b] Values for these radionuclides reproduced from Doering et al. (2017).

C-7 Comparison of ^{238}U series and ^{235}U series (^{227}Ac and ^{231}Pa) CRs in whole organisms of the ARR

Table C-20 ^{227}Ac, ^{231}Pa and ^{238}U series $CR_{WO\text{-}Media}$ values from the ARR (unperturbed sites except for Barramundi where none were available). Where more than one result was available for a sample type, arithmetic mean values are shown, followed by minimum–maximum values.

Bush food group	^{227}Ac[a]	^{231}Pa[a]	^{210}Pb[b]	^{210}Po[b]	^{226}Ra[b]	^{230}Th[b]	^{238}U[b]
Freshwater environment (× 10^3)							
Barramundi (Fish Group 2)	<28.2	<0.997	1.0 0.0031–240	1.1 0.053–5.4	3.0 0.015–52	0.81 0.0053–11	0.59 0.0029–23

Bush food group	**^{227}Ac**[a]	**^{231}Pa**[a]	**^{210}Pb**[b]	**^{210}Po**[b]	**^{226}Ra**[b]	**^{230}Th**[b]	**^{238}U**[b]
Magpie goose[c]	<1.87	<8.11	0.54 0.023–1.4			0.099 0.023–0.44	0.11 0.0030–0.64
Freshwater mussel	28.6	<0.393	41 0.024–700		56 0.50–200	17 0.70–110	1.8 0.017–46
Crocodile[d]		<0.761	0.21 0.033–0.33	1.8 0.064–4.7	5.3 0.31–25	0.12 0.011–0.31	0.16 0.0016–1.3
Terrestrial environment (× 10^{-3})							
Green ant	<1.78	<0.994	95	56	320	4.1	28
Bird[e]		<1.93	10		11 6.1–17	3.5	
Grasses and Herbs							
Mixed herbs	4.90	1.61	320 160–1200	120 45–250	250 95–500	36 0.47–290	35 1.7–130
Mixed grasses	6.53	1.65					
Ground-dwelling mammals[f]							
Agile wallaby[g]	<49.1	<5.32					
Agile wallaby[h]	<63.3	<6.86					
Agile wallaby (Joey)	<0.153	<0.637	13 0.31–58	85 1.3–630	270 14–790	0.38 0.074–1.6	3.3 0.20–16
Buffalo	<18.2	<28.9					
Northern brown bandicoot	4.41	2.12					
Pig	<203	<117					

Bush food group	^{227}Ac[a]	^{231}Pa[a]	^{210}Pb[b]	^{210}Po[b]	^{226}Ra[b]	^{230}Th[b]	^{238}U[b]
Flying fox (*Pteropus* sp.)	0.240	0.990	97 81–110		59 49–69	0.31	1.2
Green tree snake[i]	3.17	<1.63	39 11–79	84 63–110	240 26–790	0.80 0.50–1.1	2.7 0.62–13
Mixed shrubs	3.48	0.733	490 220–1600	76 24–120	210 120–440	14 0.68–36	21 6.2–43

[a] Biota activity concentrations used to derive CRs are from Table B-1 (half the value if <MDL), geometric mean of soil values used. The MDL value multiplied by 0.5 was used where a biota activity concentration was <MDL.

[b] Values for these radionuclides taken from Medley et al. (2017) for Green ant, from (Supervising Scientist, 2022) for 'Grasses and Herbs' and Shrub, all other terrestrial organisms are from Doering (2019b) and all freshwater organisms are from (Doering et al., 2019a). The ^{230}Th CR is assumed equal to the reported ^{232}Th CR value for Bat (Flying Fox), Bird, Green ant and all freshwater organisms. ^{210}Pb values are derived from ^{210}Pb and stable Pb CR values for all freshwater organisms except freshwater reptile, which uses ^{210}Pb CRs only.

[c] Reported as 'Freshwater bird' in (Doering et al., 2019a) where all values for ^{238}U series are derived from Magpie goose (*Anseranas semipalmata*).

[d] Reported as freshwater reptile in (Doering et al., 2019a) where values for ^{238}U series are from crocodiles (*Crocodylus johnstonii* and *Crocodylus porosus*) file snakes (*Acrochordus arafurae*) and turtles (*Elseya dentate*).

[e] Bird includes Rainbow lorikeet (*Trichoglossus moluccanus*) and Cockatoo (*Cacatua* sp.) for ^{238}U series.

[f] Ground-dwelling mammal ^{238}U series values are a combination of all species listed for ^{227}Ac and ^{231}Pa values.

[g] 200 m spatial range criterion for ^{227}Ac and ^{231}Pa.

[h] 1000 m spatial range criterion for ^{227}Ac and ^{231}Pa.

[i] Reported as terrestrial reptile in Doering (2019b) where values for ^{238}U series are from green tree snake (*Dendrelaphis punctulate*), Keelback snake (*Tropidonophis mairii*), monitors (*Varanus* spp.) and Olive python (*Liasis olivaceus*).

C-8 Above background annual ingestion doses from ^{227}Ac and ^{231}Pa

Table C-21 Above background annual ingestion doses from ^{227}Ac and ^{231}Pa to an adult – Worst case scenario (see Section 5.3.3). Dose coefficients are taken from ICRP (2019).

Food item	kg per person	Bq consumed		Annual ingestion dose (µSv)	
		^{227}Ac	^{231}Pa	^{227}Ac	^{231}Pa
Freshwater bush foods					
Crocodile flesh[a]	3	<0.008	<0.008	<0.008	<0.005
File snake flesh[b]	3	0.002	0.002	0.002	0.002
Fish group 1 flesh[c]	10	0.088	0.020	0.097	0.014
Fish group 2 flesh	20	0.018	0.002	0.019	0.001
Magpie goose flesh	20	<0.308	1.2	<0.339	0.87
Magpie goose liver[d]	2	<0.075	<0.034	<0.083	<0.024
Other waterfowl[e]	3	0.005	1.2	0.006	0.87
Mussels	4	8.2	<0.060	9.0	<0.043
Turtle flesh[b] (pig nose, long neck and snapping)	5	0.008	0.008	0.008	0.005
Turtle liver[b] (long neck only)	0.5	0.001	0.001	0.001	0.001
Water lily[b]	3	0.021	0.021	0.023	0.015
Water	2000	0.036	0.036	0.039	0.025
Terrestrial bush foods					
Buffalo flesh	5	0.005	<0.012	0.005	<0.009
Buffalo kidney[f]	0.5	0.003	0.003	0.004	0.002
Buffalo liver[f]	0.5	0.003	0.003	0.004	0.002
Emu flesh[g]	2	<0.006	<0.004	<0.006	<0.003
Fruit	3	0.050	0.21	0.055	0.15
Flying fox flesh[h]	5	<0.004	0.016	0.004	0.011
Goanna flesh[i]	2	0.014	0.007	0.015	0.005
Pig flesh	25	0.23	<0.20	0.26	<0.14
Agile wallaby flesh	20	<0.057	<0.044	<0.063	<0.031
Agile wallaby liver[d]	2	0.049	0.003	0.054	0.002
Yams	20	0.26	0.54	0.28	0.38
Terrestrial total	83	0.63	1.0	0.69	0.73

Food item	kg per person	Bq consumed		Annual ingestion dose (µSv)	
		^{227}Ac	^{231}Pa	^{227}Ac	^{231}Pa
Freshwater total	72	8.7	2.6	9.6	1.8
Total	155	9.3	3.7	10.3	2.6

[a] Assumes Pa CR for ^{227}Ac values.

[b] Assumes geometric mean Th CR from Doering et al. (2017).

[c] Assumes Fish group 2 CR multiplied by 10, which is the maximum difference in CRs for Fish groups 1 and 2 reported by Martin et al. (1998).

[d] These values not used in summed data and are for information only. They are included as the diet model (ERA, 2023) notes organs are eaten for these animals, though the specific organ and amount consumed is not provided.

[e] Assumes CRs for Ac and Pa for Magpie goose.

[f] Assumes the CR for Pa from Buffalo kidney for Ac and Pa.

[g] Assumes Agile wallaby flesh CRs.

[h] Assumes Whole organism CRs for Flying fox.

[i] Assumes Whole organism CRs for Green tree snake.

C-9 Above background dose rates for region-specific and ERICA default reference organisms

Table C-22 Above background terrestrial dose rates on the RPA for region-specific organisms compared with the ERICA default, Th and U CRs for ERICA reference organisms (dose rates from ^{232}Th and ^{238}U only).

Organism	Dose rate (µGy hour^{-1} × 10^{-4})								
	External		Internal		Total		Total (^{227}Ac + ^{231}Pa)		
	^{227}Ac	^{231}Pa	^{227}Ac	^{231}Pa	^{227}Ac	^{231}Pa	CRs – ^{227}Ac/^{231}Pa	CR – Th	CR – U
Region-specific organisms and CRs[a]									
Green tree snake	2.73	0.280	11.9	1.14	14.6	1.42	16.1	7.26	16.7
Agile wallaby	1.54	0.145	184	3.73	186	3.87	190	6.62	14.3
Flying fox	1.64	0.155	1.31	1.02	2.95	1.17	4.12	6.73	14.4
Grasses and Herbs	1.63	0.181	24.4	1.16	26.4	1.34	27.7	671	520
Green ant	1.75	0.180	6.67	0.696	8.42	0.876	9.30	51.6	427
Northern brown bandicoot	3.07	0.319	16.5	1.48	21.2	1.80	23.0	8.33	16.0
Rainbow lorikeet	1.79	0.171	5.50	1.35	7.29	1.52	8.81	4.05	8.48
Shrub	1.53	0.162	13.1	0.513	14.6	0.675	15.3	267	268
ERICA reference organisms and default CRs[b]									
Amphibian	3.82	0.406	369	68.8	372	69.2	442	6.76	6.24
Annelid	3.87	0.412	461	86.1	465	86.5	551	54.0	156
Arthropod - detritivorous	3.90	0.415	515	96.2	519	96.6	616	54.0	429
Bird	1.74	0.164	106	19.8	108	20.0	128	3.99	8.42

Organism	Dose rate (µGy hour^{-1} × 10^{-4})								
	External		Internal		Total		Total (^{227}Ac + ^{231}Pa)		
	^{227}Ac	^{231}Pa	^{227}Ac	^{231}Pa	^{227}Ac	^{231}Pa	CRs – ^{227}Ac/^{231}Pa	CR – Th	CR – U
Grasses and Herbs	1.63	0.181	564	105	565	105	671	671	520
Flying insects	1.83	0.182	426	79.5	428	79.7	508	15.2	25.2
Lichen and Bryophytes	1.63	0.183	4510	842	4510	842	5350	1680	4050
Mammal - large	1.03	0.0961	103	19.2	104	19.3	123	6.06	13.8
Mammal - small-burrowing	3.63	0.385	103	19.2	106	19.5	126	8.95	16.6
Mollusc - gastropod	1.84	0.181	591	110	593	111	704	51.7	154
Reptile	3.49	0.368	248	46.2	251	46.6	298	8.11	17.5
Shrub	1.53	0.162	225	41.9	226	42.1	268	267	268
Tree	1.29	0.133	35.1	6.55	36.4	6.68	43.1	6.56	30.3

[a] Region-specific CR values derived from direct measurement of whole organism activity concentrations or derivation of whole organism activity concentrations from Tissue:Whole-organism conversion factors, except Rainbow lorikeet CR for ^{227}Ac, which is an assumed value from the ERICA default CR for U.

[b] ERICA reference organism default CRs are used based on a chemical analogue: Cm for ‘Arthropod – detritivorous’ and ‘Tree’, Th for ‘Grasses and Herbs’, U for ‘Shrub’, Am for all others.

Table C-23 Above background freshwater dose rates for region-specific organisms compared with the ERICA default, Th and U CRs for ERICA reference organisms (dose rates from ^{232}Th and ^{238}U only).

Organism	Dose rate[a] (µGy hour^{-1} × 10^{-3})								
	External		Internal		Total		Total (^{227}Ac + ^{231}Pa)		
	^{227}Ac	^{231}Pa	^{227}Ac	^{231}Pa	^{227}Ac	^{231}Pa	$CR_{WO\text{-}Media}$ – ^{227}Ac/^{231}Pa	$CR_{WO\text{-}Media}$ –Th	$CR_{WO\text{-}Media}$ – U
Determined from region-specific organisms and $CR_{WO\text{-}Media}$ values[b]									
Magpie goose	2.49 × 10^{-5}	2.50 × 10^{-6}	42.2	34.1	42.2	34.1	76.3	1.60	2.11
Freshwater crocodile	190	0.255	10.8	3.20	201	3.46	205	203	194
Barramundi	2.58 × 10^{-5}	2.59 × 10^{-6}	636	4.19	636	4.19	640	19.2	4.00
Freshwater mussel	332	0.437	645	1.65	977	2.09	979	797	379
Determined from ERICA reference organisms and default $CR_{WO\text{-}Media}$ values[c]									
Amphibian	3.22 × 10^{-5}	3.20 × 10^{-6}	108	20.1	108	20.1	128	0.589	0.222
Benthic fish	264	0.357	25.6	4.77	290	5.12	295	284	269
Bird	2.63 × 10^{-5}	2.64 × 10^{-6}	65.7	12.3	65.7	12.3	78.0	1.60	2.11
Crustacean	683	0.576	755	141	1440	142	1580	1150	689
Insect larvae	1340	1.14	755	141	2100	142	2240	1810	1390
Mammal	2.35 × 10^{-5}	2.35 × 10^{-6}	108	20.1	108	20.1	128	12.8	3.68
Mollusc - bivalve	309	0.415	756	141	1070	141	1210	775	356
Mollusc - gastropod	366	0.461	375	70.0	741	70.5	812	831	413
Pelagic fish	2.68 × 10^{-5}	2.71 × 10^{-6}	25.6	4.77	25.6	4.77	30.3	19.2	4.00

Organism	Dose rate[a] (µGy hour^{-1} × 10^{-3})								
	External		Internal		Total		Total (^{227}Ac + ^{231}Pa)		
	^{227}Ac	^{231}Pa	^{227}Ac	^{231}Pa	^{227}Ac	^{231}Pa	$CR_{WO\text{-}Media}$ – ^{227}Ac/^{231}Pa	$CR_{WO\text{-}Media}$ –Th	$CR_{WO\text{-}Media}$ – U
Phytoplankton	8.29 × 10^{-5}	4.65 × 10^{-6}	267	49.9	267	49.9	317	317	1.74
Reptile	266	0.359	108	20.1	374	20.5	395	279	270
Vascular plant	612	0.566	1000	187	1610	187	1800	1800	624
Zooplankton	7.85 × 10^{-5}	4.53 × 10^{-6}	754	141	75.4	141	895	464	46.6

[a] Distribution coefficient (K_d) values used to determine sediment activity concentrations from the specified activity concentrations in water are the ERICA default values of 2.00E+07 L kg^{-1} for ^{227}Ac (derived from IAEA, 2001) and 2.68 × 10^{-5} L kg^{-1} for ^{231}Pa derived from Th value.

[b] Region-specific $CR_{WO\text{-}Media}$ values derived from direct measurement of whole organism activity concentrations or derivation of whole organism activity concentrations from Tissue:Whole-organism conversion factors, except Freshwater crocodile CR for ^{227}Ac, which is an assumed value from the ERICA default $CR_{WO\text{-}Media}$ for Th.

[c] ERICA reference organism default $_{WO\text{-}Media}$ values are assumed for a chemical analogue: Cm for 'Arthropod – detritivorous' and 'Tree, Th for 'Grasses and Herbs', U for 'Shrub', Am for all others.

Appendix D Alpha decay data

Nuclear decay data for ^{229}Th and ^{233}U data is from Nichols et al. (2008), from Akovali (1996) for ^{230}Th, from Browne (2002) for ^{230}Th, all other Dulieu et al. (2017).

Table D-1 Alpha particle emission energy and intensity for relevant radionuclides.

Isotope	Main Alpha Energies	Emission intensity	Isotope	Main Alpha Energies	Emission intensity
^{238}U decay series					
^{238}U	4151	22.33	^{226}Ra	4601	5.95
	4198	77.54		4784.34	94.038
^{234}U	4722.4	28.42	^{222}Rn	5489.48	99.92
	4774.6	71.37	^{218}Po	6002.35	99.9769
^{230}Th	4620.5	23.4	^{214}Po	7686.82	99.9895
	4687.0	76.3	^{210}Po	5304.33	99.99876
^{235}U decay series					
^{235}U	4214.7	5.95	^{227}Th	6038.01	24.2
	4322	3.33		6008.8	2.90
	4366.1	18.8		5977.72	23.5
	4397.8	57.19		5959.7	3.00
	4414.9	3.01		5866.6	2.41
	4502.4	1.28		5807.5	1.27
	4556.0	3.79		5756.87	20.4
	4596.4	4.74		5713.2	4.89
^{231}Pa	4680.1	1.8		5708.8	8.3
	4712.3	1.2		5700.8	3.63
	4736.3	8.4		5693.0	1.50
	4853.5	1.4		5668.0	2.06
	4936.0	2.9	^{223}Ra	5434.6	1.6
	4952.6	22.5		5539.43	10.6
	4987.8	1.6		5606.99	25.8
	5015.1	25.3		5715.84	49.6
	5031.2	20		5747.14	10.0
	5033.8	2.8		5871.63	1.0
	5060.7	11.7	^{219}Rn	6424.8	7.85

^{227}Ac	4940.57	0.546		6553.0	12.6
	4953.23	0.658		6819.2	79.4
			^{215}Po	7386.1	99.934
			^{211}Bi	6278.5	16.16
				6622.4	83.56
			^{211}Po	7450.2	98.936
^{232}Th decay series					
^{232}Th	3948.5	21.0	^{220}Rn	6288.22	99.882
	4011.2	78.9	^{216}Po	6778.4	99.9981
^{228}Th	5340.35	26.0	^{212}Bi	6051.04	25.1
	5423.24	73.4		6090.14	9.7
^{224}Ra	5448.80	5.25	^{212}Po	8785.17	100
	5685.48	94.73			
^{237}Np decay series					
^{237}Np	4640	6.43	^{225}Ac	5609.0	1.09
	4665	3.46		5637.3	4.16
	4708.3} 4712.3}	1.174		5682.2	1.31
				5723.1	2.03
	4766.5	9.5		5730.5	1.6
	4771.4	23		5731.6	1.24
	4788	47.64		5731.9	9.0
	4803.5	2.02		5791.7	6.2
	4816.8	2.43		5793.1	18.9
	4872.7	2.41		5829.6	52.4
^{233}U	4729	1.61	^{221}Fr	6126.3	15.1
	4783.5	13.2		6243	1.34
	4824.2	84.4		6341.0	82.8
^{229}Th	4797.8	1.2	^{217}At	7066.9	99.932
	4814.6	9.3	^{213}Bi	5981.0	1.90
	4838	5.0			
	4845.3	56.2			
	4901.0	10.2			
	4967.5	5.97			
	4978.5	3.17			
	5053	6.6			

Contaminant radionuclides					
^{241}Am	5388.25	1.66	^{240}Pu	5123.6	27.16
	5442.86	13.23		5168.13	72.74
	5485.56	84.45	^{242}Pu	4858.2	23.44
^{238}Pu	5456.3	28.85		4902.3	76.53
	5499.03	71.04	^{232}U	5263.48	30.6
^{239}Pu	5105.81	11.87		5320.24	69.1
	5143.82	17.14			
	5156.59	70.79			
Miscellaneous					
^{232}U	5136.64	0.325			
	5263.48	30.6			
	5320.24	69.1			

Appendix E Methods – Sample preparation

E-1 Tracer addition – ^{225}Ac and ^{233}Pa

A yield tracer is added to each sample for analysis of ^{227}Ac and ^{231}Pa, being ^{225}Ac and ^{233}Pa respectively. For ^{227}Ac analysis, the recommended total activity per sample is ~100 mBq. For ^{231}Pa analysis, it is recommended to add sufficient tracer to achieve ~1×10^{10} atoms of ^{233}Pa per sample at the AMS measurement date. Allowing for one half-life between tracer addition and measurement and a chemical recovery of 60% this equates to ~10 kBq of ^{233}Pa per sample.

E-2 Freeze-drying and milling

Biological samples were kept cool during transport to the laboratory and were separated into fractions (i.e., organs and tissues by dissection) as soon as practicable after collection (and after washing where undertaken). Samples were then frozen to between -10 and -20°C followed by freeze drying. Freeze drying times varied depending on the sample size and volume but typically took 3–5 days. Samples were considered sufficiently dry when temperature and pressure had held below -65 °C and 0.02 mBar respectively for at least 24 hours.

After freeze drying samples were milled to a fine powder (an IKA® M 20 Universal mill was used for most samples in this project) and stored in a desiccating cabinet prior to sample analysis.

E-3 Water sample preparation

This method was specific to the sample analysed for this project.

1 Shake sample well then record weight of sample.
2 Transfer ~2 L of unfiltered sample into a 2 L beaker and heat at 80°C to evaporate sample.
    a. Do not allow sample to reach complete dryness.
3 Continue adding sample until sample volume is <1 L.
4 Transfer sample to a 1 L, acid-washed, HPDE sample bottle.
5 Rinse the 2 L beaker with 40–50 mL 2% conc. HNO_3 and combine with sample in HDPE sample bottle. Store until ready to proceed with analysis. Weigh and record the weight of the original sample container to determine total sample mass evaporated.
6 Transfer the sample to a 1 L glass beaker, weigh and record weight.
7 Weigh and add tracer solution to the sample beaker (see Section E-1).
8 Evaporate combined sample and tracer to dryness at 80–90°C.

9 Add sufficient conc. HNO_3 to cover the bottom of the beaker (20–30 mL); cover with a watchglass and heat overnight at 80–90°C.

10 Remove the watchglass and evaporate to semi-dryness. Repeat step 9 once.

11 Add 0.5 mL aliquots of 30% H_2O_2 at 30-minute intervals for 4 hours then continue heating overnight.

12 Remove the watchglass and evaporate to semi-dryness.

13 Add sufficient conc. HNO_3 to cover the bottom of the beaker (20–30 mL), cover with a watchglass and heat at 80–90°C for ~10 minutes to dissolve sample. If a black/brown colour or a high particulate matter content remains, this step can be repeated as necessary.

14 Add high purity water to obtain a concentration of 4 M HNO_3 and filter into a 500 mL beaker through a 0.45 µm pore size PES syringe filter to remove traces of undigested particulate material.

15 Evaporate sample to dryness then add 10 mL 3 M HNO_3, cover with a watchglass and heat at 80–90°C for ~10 minutes to dissolve sample.

    a. At this stage if some fine particulates remain the sample can be centrifuged at 4000 rpm for 5 minutes, then decanted to separate particulates.

16 Dilute with high purity water to ~0.5 L and proceed to $PbSO_4$ coprecipitation (Section E-9).

E-4 Dry-ashing

This method is based on USTUR (1995). Crucibles[58] used for this project were 30 mL or 100 mL and made from 100% Pt, or 95% Pt with 5% Au.

1 Weigh samples into Pt crucibles – fill to 1–2 mm below upper edge. Create a small divot in the centre. Record weight of crucibles empty and after addition of sample.

2 Weigh and add tracer[59] solution dropwise into the central divot (see Section E-1).

3 Allow tracer to soak into the sample, gently fold sample over solution to allow it to soak in. Avoid tracer flowing to the edges of the crucible (to minimise the potential for tracer isotopes to bake onto crucible before adequately mixing with sample).

4 Place in an ashing oven pre-heated to 150°C.

[58] These were used as it is known that Ra has the potential to stick to ceramic crucibles, and although it is unknown if this will also apply to Ac, use of Pt crucibles reduced the potential risk of losses to crucible surfaces.

[59] Dry-ashing is not recommended for ^{231}Pa analysis as it may lead to formation of insoluble Pa oxides.

5 Raise temperature approximately 50°C every 4 hours to 250°C, continue heating overnight. If smoke is produced, pause heating until the smoke stops.
6 Raise temperature approximately 50°C every 4 hours to 300°C, continue heating overnight.
    a. If additional sample material is to be added (generally required for 30 mL crucibles), allow oven to cool to room temperature before removing samples from the oven and repeating steps 1, then 3–5. If no further sample material is required to be added proceed directly to step 7.
7 Raise temperature approximately 50°C every 4 hours to 450°C, continue heating overnight.
8 Raise temperature approximately 50°C over 4 hours to 500°C, continue heating overnight.
9 Turn off oven and allow samples to cool to room temperature.
10 Remove samples from oven, weigh, and record ashed weight.
11 Proceed to step 'Digest of ashed samples' (Section E-5).

E-5 Digest of ashed samples

This method follows from method 'Dry-ashing' (Section E-4).

1 Add 15–30 mL conc. HNO_3 to Pt crucibles containing ashed samples (add enough to fully cover the ashed sample), cover with a watchglass.
2 Heat on a hotplate to ~90°C for 3–4 hours, remove watchglass and evaporate to semi-dryness overnight at 60°C.
3 Add 10 mL 3 M HNO_3 to semi-dried residue followed by 2 × 1 mL 30% H_2O_2, allow bubbling to subside in between additions of 30% H_2O_2.
4 Heat to ~90°C for 2–3 hours. Continue adding 2 × 1 mL 30% H_2O_2 approximately every 30 minutes.
    a. This step may be continued if a black colour persists in the solution which can occur if incomplete combustion of carbon compounds has occurred during the dry-ashing process.
    b. Where excess colour persists, remove watchglass and evaporate to semi-dryness overnight at 60°C and return to step 3. The 3 M HNO_3 may be replaced with conc. HNO_3 to increase the rate of reaction[60].

[60] This may not always be effective as the increased concentration of HNO_3 can lead to a direct reaction with the H_2O_2, preventing decomposition of the carbon (for further information see Kim et al., 2000).

5 When bubbling has ceased, dilute samples to ~50 mL with high-purity water and filter through a 0.45 µm pore size PES syringe filter into 1–2 L beakers.

6 Further dilute samples to 800–900 mL with high-purity water.

7 Proceed to 'Dissolution of soil digest residues' (Section E-8).

   a. If high levels of Ca are expected to be present in the sample digest, an additional coprecipitation step to remove Ca may be required prior to proceeding with $PbSO_4$ coprecipitation (e.g., MnO_2 coprecipitation as per steps 2–4 in E-8, section F-3).

E-6 Microwave-assisted digestion procedure

1 Weigh 0.5–0.6 g of dried sample into a 100 mL PTFE microwave digestion vessel.

2 Add ~0.25 mL tracer solution in 3 M HNO_3 (see Section E-1).

   a. Avoid adding more than 0.25 mL of tracer solution as it may impact the completeness of sample digestion. For ^{231}Pa analysis this may lead to loss of Pa bound to undigested particulates.

3 Add 9 mL conc. HNO_3 and 1 mL 30% H_2O_2.

4 Undertake closed vessel microwave digestion of the solutions.

   a. Program the microwave[61] with a 15-minute ramp-up followed by a 15-minute hold, temperature of 200°C and power at:

      i. 800 W for 3 or less vessels.

      ii. 1200 W for 4–8 vessels.

      iii. 1800 W for 9–15 vessels.

5 Allow to cool to <60˚C before removing the rotor and opening the digestion vessels.

6 Decant digest solution into a 100 mL PTFE beaker and, using the original 100 mL PTFE microwave digestion vessel repeat steps 1–5 until ~2 g of digested material is obtained, combining filtered digest solutions.

   a. Ensure that the equivalent ratio of dried sample to ^{233}Pa tracer solution is maintained for each sub-sample digested and combined.

7 Once all digest solutions have been microwaved and are combined, dilute to <25% total HNO_3 then filter through a 0.45 µm pore size PES syringe filter into a 250 mL PTFE beaker

8 Rinse the 100 mL Teflon digestion vessel with 10 mL 8 M HNO_3 and pass through the filter to rinse the filter, add the rinse to the combined digest solutions.

[61] ETHOS™ Milestone Microwave digestion system with SK-15 rotor using 100 mL PTFE digestion vessels.

9 Evaporate combined digest solutions to dryness overnight at 90˚C.

10 Take up dried residue solution in 10 mL 3 M HNO_3, gently heating (50–60°C) to ensure the solution is fully dissolved, transfer to a 50 mL PP centrifuge tube, rinsing the beaker with 2 × 5 mL 3 M HNO_3. Combine the rinses with the solution to make a total of 20 mL 3 M HNO_3.

11 Proceed with $PbSO_4$ coprecipitation (Section E-9 below).

E-7 Hotplate conc. HNO_3 digest with optional 30% H_2O_2 digest

Hotplate digestion techniques used in initial testing for sample decomposition are detailed below, this method is a general summary. For the tests conducted, various fractions were separated (e.g., collection of particulates by filtration or wiping from beaker walls) to measure losses of ^{233}Pa at various stages of the procedure. This method was only used in preliminary testing and losses of ^{233}Pa were high, it is not recommended for routine analysis of ^{231}Pa in environmental samples.

1 Weigh (~1–1.5 g dry weight) into a 100 mL PTFE beaker then add ^{233}Pa solution to the weighed sample.

2 Add 10–15 mL conc. HNO_3, cover with a watchglass and leave overnight at room temperature to allow for an initial reaction to take place.

3 Place sample on a hotplate and heat overnight at 90°C then remove watchglass, rinsing with high purity water and evaporate to near dryness.

4 Repeat step 3 once. For conc. HNO_3 digestion only proceed to step 5, for additional 30% H_2O_2 digestion proceed to step 7.

5 Add 10 mL 8 M HNO_3, heat at 50–60°C for ~10 minutes to dissolve sample then filter through a 0.45 µm pore size PES syringe filter.

6 Proceed to coprecipitation technique for sample preconcentration.

7 Add 15 mL conc. HNO_3, and heat covered with a watchglass at 90°C for ~10 minutes to dissolve sample. Every 30 minutes for ~4 hours add 1 mL 30% H_2O_2 then remove watchglass and evaporate to near dryness.

8 Repeat step 7 once then return to step 5.

E-8 Dissolution of soil digest residues

1 Heat semi-dried soil digest residue to ~90°C after addition of 10 mL 3 M HNO_3 and 1 mL 30% H_2O_2 for ~1 hour.
    a. This also aids in removing undigested particulates from the beaker wall.
2 Transfer solution to a 50 mL centrifuge tube then centrifuge at 4000 rpm for 5 minutes.
3 Decant solution to a disposable syringe then filter through a 0.45 µm pore size PES syringe filter into a 250 mL PTFE beaker.
4 Rinse filter with ~10 mL high purity water and combine with filtered solution.
5 Repeat steps 1–4 with the residue remaining in the centrifuge tube, combining all filtered solutions.
6 Heat combined solution at 90°C until only 5–10 mL remains.
7 Add 10 mL 3 M HNO_3 and dilute to ~150 mL with high purity water. Proceed with $PbSO_4$ coprecipitation (Section E-9).

E-9 $PbSO_4$ coprecipitation for preconcentration of metals in solution

This procedure proceeds from:

- Sample digestion as per Sections E-5 to E-7 above, or
- Acidified water samples. Note that the acid concentration should be below 0.14 M for acidified water samples or $PbSO_4$ coprecipitation may be affected (Medley et al., 2005).
- HF digest solutions from external laboratory.
    - For this project digest solutions were received as 5% HCl and were diluted with high purity water to 800–900 mL prior to $PbSO_4$ coprecipitation.

Glass beakers are suitable for Ac analysis, use only PTFE beakers for Pa analysis.

1 While gently stirring with a magnetic stirrer bar add:
    a. 2 mL conc. H_2SO_4.
    b. 40 mL 10% K_2SO_4 (4 g K_2SO_4).
2 Precipitate $PbSO_4$ by dropwise addition of 3 mL 0.24 M $Pb(NO_3)_2$.
3 Continue stirring for 10–15 minutes then remove stirrer bar, rinsing with a solution of 0.1 M K_2SO_4 in 0.2 M H_2SO_4.
4 Cover beaker with a watchglass and allow to settle overnight.

5 Decant supernatant to waste and collect the precipitate in a 50 mL centrifuge tube, rinse the precipitate into the centrifuge and from the walls of the beaker using a solution of 0.1 M K_2SO_4 in 0.2 M H_2SO_4.

6 Centrifuge precipitate at 4000 rpm for 5 minutes, then decant and discard the supernatant (re-centrifuge if precipitate loosens during decantation).

7 Wash the precipitate with ~10 mL high purity water twice, centrifuging at 4000 rpm for 5 minutes after washing. Decant and discard the washings.

8 Proceed to 'Separation of ^{227}Ac' (Section F-4.2 below) or 'Pa Separation using TK400® resin' (Section F-2 below).

E-9.1 Modifications to improve weak precipitate formation

For several samples analysed for this project, relatively weak precipitate formation occurred upon addition of $Pb(NO_3)_2$. Several modifications were made to improve precipitate formation in these samples. This included the following steps either individually or in combination until increased precipitation was visually observed:

- Heating the precipitated solutions to 70°C while continuing to stir for ~30 minutes.
- Increasing the diluted sample volume from 800–900 mL to 1.6–1.8 L either
    - prior to precipitation or,
    - after initial precipitation.
    - The solution volumes of H_2SO_4 and K_2SO_4 were increased proportionally for both cases.
- Addition of an extra 1 mL $Pb(NO_3)_2$ and increasing stirring time to 30 minutes.
    - This was undertaken in most cases where increased dilution was performed.

E-9.2 Modifications to improve $PbSO_4$ precipitate solubility for ^{227}Ac and ^{231}Pa separation

For several samples, dissolution of the $PbSO_4$ precipitate was incomplete after vortexing in 20 mL 4 M and 10 M HCl for 'Separation of ^{227}Ac' (Section F-4.2 below) or 'Pa Separation using TK400® resin' (Section F-2 below) respectively. Several modifications were made to improve precipitate dissolution for these samples. This included the following steps either individually or in combination until complete dissolution was visually observed[62]:

[62] Confirmation of complete dissolution through visual means was improved by centrifugation at 4000 rpm for 5 minutes to concentrate any undissolved precipitate. After the additional processing, two samples still had undissolved material and

- An additional 10–20 mL 4 M or 10 M HCl was added and the sample vortexed.
- The HCl solution was heated for up to 2 hours in a hot water bath at 70°C followed by vortexing.
- For ^{227}Ac samples only:
    - Heating samples to 70°C prior to precipitation and increasing up to 95°C if needed.
        - For heated samples, substantial recrystallisation of the precipitate occurred 1–2 hours after heating was stopped.
        - To minimise recrystallisation, the heated samples were cooled to room temperature in a cold-water bath immediately after heating and loaded onto the DGA® resin columns for Ac separation.

E-9.3 Specific issues with $PbSO_4$ for ^{227}Ac sample analysis

Three samples with substantially below average recovery were pig flesh and bone marrow (both at 14±2%) and Agile wallaby bone (12±1%). Although no obvious issues were observed with the pig flesh sample there were for both the bone and bone marrow samples. For these samples, evaporation of the digest solution reached a 'saturation' point where continued heating did not reduce the solution volume and the solutions were a thick milky white colour. To initiate $PbSO_4$ coprecipitation, dilution of the digest solution to ~1.8 L with high purity water was required. A fourth sample, comprising ~34 g dry weight of freshwater mussel shell was treated similarly, however, $PbSO_4$ coprecipitation could not be initiated after dilution and analysis was discontinued.

Use of an alternative preconcentration technique that is less prone to matrix interference effects may improve results for these sample types.

were loaded onto the DGA® resin columns. It was observed for these two samples that the undissolved material was rapidly dissolved in the 10 mL 3 M HNO_3 used to rinse the column prior to elution of Ac.

Appendix F Radiochemistry

F-1 Preparation of a ^{233}Pa tracer – Milking the ^{237}Np cow

This method is also referred to as the 'TEVA® resin separation method' in parts of the thesis. All reagent solutions should be filtered through 0.45 µm to minimise potential for particulate contamination on the ^{237}Np cow. The ascorbic acid solution should always be prepared fresh prior to use to prevent decomposition of the ascorbic acid during storage.

A ^{237}Np cow is prepared using a pre-packed 2 mL TEVA® resin (100–150 µm particle size) column with an internal diameter of 0.8 cm. The cap for the column should be kept and a 1-way polycarbonate stopcock connected to the bottom of the column to allow the ^{237}Np cow to be sealed during storage for ingrowth of ^{233}Pa.

A reducing solution is used to load ^{237}Np as Np(IV) with ^{233}Pa eluted in 3 M HNO_3. The reducing solution is used each time ^{233}Pa is milked from the ^{237}Np cow to ensure Np is maintained in the +4 oxidation state.

1 In a 50 mL PTFE beaker, add 1.3 mL 3 M HNO_3.
    a. When preparing the cow for the first time, the ^{237}Np must be in the load solution, and should be introduced here such that the volume and acid concentration in the load solution is maintained.
2 Add 0.5 mL 1.5 M sulphamic acid, swirl to mix.
3 Add 1.25 mL 1.5 M ascorbic acid, swirl to mix then wait for 3 minutes before proceeding to the next step.
4 Add 0.1 mL of a 5 mg mL^{-1} Fe solution.
    a. A blue/violet colour should briefly appear on addition of the Fe solution indicating the reduction of Np(V) to Np(IV).
5 Add 1 mL 8 M HNO_3 to bring the solution concentration to ~3 M HNO_3. Allow the load solution to rest for 15–30 minutes to ensure complete reduction of Np(V) prior to loading onto the column.
6 Prepare ^{237}Np cow.
    a. When milking the cow this is only setting up the previously prepared cow for extraction of ^{233}Pa.

b. When preparing the cow for the first time, the TEVA® resin column must be equilibrated with 10 mL 3 M HNO_3 prior to adding the load solution and step 7 is not required.

c. A 20 mL reservoir should be connected to the top of the column before proceeding to ensure an adequate flow rate during the procedure. Seal the reservoir with Parafilm® to prevent leakage.

7 Open stopcock valve and let solution drain, collect the solution in a small (e.g., 20 mL) HDPE or PTFE collection container.

8 Load the "load solution" and let it drain into the collection container.

a. A flow rate of 0.5–1 mL per minute should be maintained where possible.

9 Add 1 mL 3 M HNO_3 to the column and let it drain into the collection container.

10 Swap the collection container with a pre-weighed PFA bottle.

11 Reload solution from collection container onto the column and let it drain into the PFA bottle.

12 Rinse collection container with 1 mL 3 M HNO_3, load onto the column and let it drain.

13 Add 20 mL 3 M HNO_3, make a mark on the 20 mL reservoir and then fill it up to just below the top. Ensuring a constant flow by always topping up the 20 mL reservoir with 3 M HNO_3.

14 Once all 3 M HNO_3 has been eluted, record the date and time of milking the cow using the time that the elution of 3 M HNO_3 is completed.

15 Close the stopcock valve to prevent further drainage and remove the 20 mL reservoir. Add ~2 mL 3 M HNO_3 to the column to keep the resin wet and carefully place the cap on (it may be necessary to open the tap and let out a drop or two to allow the pressure to adjust when placing on the cap, these drops can be collected in the PFA ^{233}Pa solution bottle).

16 Weigh the filled bottle.

17 Add 1 mL 30% H_2O_2 to the eluate in the bottle and place on a hotplate at 70–80ºC overnight

a. Leave the lid on the bottle but loosen to achieve reflux-like conditions and to prevent pressure build-up.

18 Remove the bottle from the hotplate and allow to cool, firmly secure the lid then re-weigh the bottle to enable the final solution weight to be calculated. This solution is now stable enough to be shipped to an external laboratory for use. Prior to use for spiking samples, it may be necessary to treat the ^{233}Pa solution further to remove excess carbon (from the ascorbic acid) and to reduce the ^{233}Pa solution volume. For further purification of the solution follow steps 19–25.

19 If a brownish colour persists in the ^{233}Pa tracer solution, add 2 mL 30% H_2O_2 and heat with lid slightly loosened at 90°C for ~3 hours, allow to cool to room temperature before proceeding. If solution is clear proceed to step 21.

20 Transfer the solution to a 100 mL PTFE Beaker, rinsing the PFA bottle with 2 × 5 mL 3 M HNO_3 and combining with the ^{233}Pa solution.

21 Add 3 mL 30% H_2O_2 and evaporate to a few mL at 90°C. Reduce temperature to at 50–60°C and evaporate to dryness (this prevents potential spitting of the solution when drying).

22 Add 10 mL 3 M HNO_3 and with 3 mL 30% H_2O_2 to the dried residue, cover with a watchglass. Raise the temperature to 90°C and heat for 4–5 hours.

23 Remove the watchglass and rinse with high purity water. Evaporate to dryness at 60°C.

24 If a black/brown colour persists in the residue steps may be repeated until no colour remains.

25 Add 3 M HNO_3 to the dried residue to the desired volume of the final solution and heat at 60°C for ~10 minutes to dissolve ^{233}Pa. This solution is ready to use, the activity concentration should be checked before and after use to confirm stability of the solution.

F-2 Pa Separation using TK400® resin

1 Take up $PbSO_4$ precipitate with preconcentrated Pa from $PbSO_4$ coprecipitation (Section E-9) in 10 mL 10 M HCl.

2 Prepare column with 2 mL of TK400® resin[63] (100–150 µm) from a slurry of TK400® resin and high purity water[64].

3 Clean the column with a 10 mL rinse of 1 M HCl.

4 Equilibrate the column with 10 mL 10 M HCl.

5 Add the load solution to the column.

6 Elute Th and U with 20 mL 10 M HCl (where additional 10 M HCl was required to improve dissolution of $PbSO_4$ precipitate an extra 5 mL rinse was used here).

7 Elute Pa with 10 mL 1 M HCl into a 25 mL PTFE beaker.

---

[63] A column internal diameter of 0.8 cm for Eichrom® 2 mL standard columns gives a height of approximately 4 cm.

[64] Initial tests with TK400® resin that had been pre-wetted by soaking in high purity water for several hours failed, with poor separation of Pa. It is noted in Horwitz et al. (2005) that wetting of ion chromatography resins is important for best performance and it is likely that insufficient time was allowed for this process, leading to poor separation for this test. For routine use, TK400® resin is submerged in high purity water for 1–2 weeks prior to use and a transfer pipette is used to collect only the resin that is not floating at the surface of the water (i.e., not exhibiting hydrophobic properties) when filling the separation columns.

a. Record finish time as the date/time of ^{233}Pa separation (also record start time of separation to determine the flow rate if required).

b. To assess breakthrough of Th and U if required, add ^{229}Th and ^{232}U tracers to aliquots of the eluted Pa and then proceed to preparation for alpha spectrometry without further separation (Section F-5 below).

8 Add ~1.5 mg Fe in solution (prepare from anhydrous $FeCl_3$) to the 10 mL 1 M HCl and evaporate to dryness on a hotplate at 90°C. Allow drying for a minimum of 24 hours (Note: It is essential that Fe is added prior to evaporation of this solution to minimise losses of Pa to the beaker surfaces[65]).

a. Count using HRGS for recovery determination if required.

9 Transfer the dried sample to a ceramic crucible and place in an ashing oven.

a. Increase temperature of oven up to 250°C in 4.5 hours, hold at temperature for 2 hours then increase to 800°C in 2.18 hours and hold for 8 hours. Allow to cool to room temperature before removing from ashing oven.

10 Press sample into an Al cathode after mixing dried Fe_2O_3 with 1 mg Al powder (Alfa Aesar, 325 mesh, 99.97% purity).

F-2.1 Preparing ^{231}Pa standard solution

The ^{231}Pa solution, used to determine the ^{233}U relative ion counting efficiency (see Section A-2.1) had similarly unknown provenance to the ^{237}Np used to prepare the ANU ^{237}Np cow and was 'cleaned' to remove potential interferences (including ^{233}U). The TK400® resin separation method above was used and a ^{233}Pa tracer solution from a NIST certified ^{237}Np standard solution (i.e., not milked from the ANU ^{237}Np cow and with a much lower relative activity concentration) was used to determine Pa recovery from the cleaning step. This 'cleaned' fraction was then spiked with a solution milked from the ANU ^{237}Np cow for a second TK400® resin separation. A much higher activity was used for the second spike and there were several months between separation stages, so there was a negligible contribution from the originally spiked ^{233}Pa to the count rate at mass 233 at the time of AMS measurement. The eluted Pa fraction containing both ^{231}Pa and ^{233}Pa was used for determining the relative ion counting

[65] This was only done for the last batch of samples analysed for this project. A discussion of Pa losses throughout the measurement process is in Chapter 3, Section 3.12.4 and Appendix J, Section J-2.

efficiency of $^{233}UO_2^-$ compared to $^{233}PaO_2^-$ (See Chapter 3, Section 3.12.3 and equation in Appendix A, Section A-2.1).

F-3 UTEVA® separation method

This procedure[66] may proceed with varying sample volumes and concentrations of HCl and HNO_3 solutions or acidified water samples. For best results use 0.1–1 M HCl or 0.15–4 M HNO_3. Digest solutions from soil samples or samples with a similarly complex matrix should be diluted to a minimum of 400 mL with high-purity water to prevent interferences reducing chemical recovery. Digest solutions from biota samples may experience inhibited coprecipitation with MnO_2 from incompletely digested organic complexes, dilution to ~1.8 L with high purity water can assist in improving coprecipitation.

1 Prepare sample solution as noted above. Spike with a suitable U isotopic tracer.
   a. ^{232}U and ^{238}U tracers were both used during this project.
   b. Stir for ~1 hour to equilibrate.
2 Continue stirring and add 2 mL 0.2 M $KMnO_4$ solution followed by 2 mL 0.3 M $MnCl_2$ (this is for a sample volume of 1.0 L or less, solution volumes should be increased proportionally for increased sample volumes).
   a. Wait for several minutes. If the 'pink' Mn colour persists, continue to step 3. Otherwise continue adding 0.2 M $KMnO_4$ and 0.3 $MnCl_2$ in 2 mL aliquots (maximum of 10 mL) until the colour persists.
3 Add 15 mL NH_4OH solution (25–30%) to adjust the pH to 8–9 and continue stirring for 30 minutes.
4 Allow to settle overnight.
5 Decant the supernatant and rinse the precipitate into a 50 mL centrifuge tube with high purity water or a weak NH_4OH solution.
6 Centrifuge at 3500 rpm for 3 minutes.
7 Discard the supernatant.
8 Add 10 mL 3 M HNO_3 and gently swirl to dislodge precipitate. Allow vigorous bubbling to subside before proceeding.

[66] This method is based on Queensland Health internal method QIS 32317, with a modification to improve separation of ^{237}Np (Vajda et al., 2003).

9 Add several drops 30% H_2O_2 to the centrifuge tube and gently swirl to continue dissolving the precipitate. Allow vigorous reaction to subside before placing the cap on the centrifuge tube.
    a. Vortexing can be used to dissolve the precipitate, taking care to release the pressure build up frequently.
10 Transfer solution to a 150 mL beaker, rinsing into the beaker with 10 mL 3 M HNO_3.
11 On a hotplate, gently heat at 50°C for 30 minutes while covered to break down H_2O_2.
12 Prepare an ion chromatography column with 1 g UTEVA® resin (100–150 µm).
    a. UTEVA® resin should be soaked in high purity water for a minimum of 24 hours prior to use.
    b. For this project columns with internal diameter 1 cm were filled to 3 cm (density of UTEVA® resin is 0.39 g mL^{-1}).
13 Equilibrate the column by rinsing with 20 mL 3 M HNO_3.
14 Add the sample solution to the column (take care not to disturb the resin in this step and the following steps when adding solutions to the column).
15 Rinse the sample solution beaker twice with 5 mL 3 M HNO_3, adding each rinse to the column.
16 Add 20 mL 3 M HNO_3 to the column.
17 Add 5 mL 9 M HCl to the column.
18 Elute the Th fraction with 20 mL of a 5 M HCl/0.05 M oxalic acid solution.
    a. Retain this fraction if Th is to be analysed. If Np and Th are not to be analysed, this step can be ignored as both are removed with 4 M HCl in step 19.
19 Elute Np with 10 mL 4 M HCl
    a. Retain this fraction if Np is to be analysed. This step was added to the original method to improve Np/U separation (see Section F-3.1).
20 Elute the U fraction with 20 mL 0.01 M HCl.
    a. Retain this fraction if U is to be analysed.
21 For both Th and U fractions, evaporate solution to dryness at 50°C.
22 Add 10 mL 3 M HNO_3 and 2 mL 30% H_2O_2 to the dried residue to break down oxalic acid, cover with a watchglass and heat at 90°C for 2–3 hours.
23 Remove the watchglass and evaporate to dryness.
24 Proceed to source preparation for alpha spectrometry. For this project $Nd(OH)_3$ coprecipitation was used (see Section F-5).

The UTEVA® resin used for Th and U separation can be regenerated for repeated use (4–5 times maximum) using the following steps:

1 Wash the column with 50 mL high purity water.
2 Wash the column with 50 mL 0.1 M EDTA solution (adjusted to pH 7 with 25–30% NH_4OH solution).
3 Wash the column with 50 mL high purity water.
4 Store the column with UTEVA® resin covered with high purity water.

F-3.1 Separation of ^{233}U in ^{233}Pa tracer solutions

As noted in Chapter 3 (Section 3.5.4) purification of the ^{233}Pa tracer solutions milked from the ANU ^{237}Np cow to remove ^{237}Np was undertaken for solutions milked 431 and 774 days after preparation using the TEVA® resin separation method (Section F-1; see also Table 3-5 in Chapter 3). For these solutions, further purification of ^{233}U was undertaken using UTEVA® resin (Section F-3) followed by $Nd(OH)_3$ coprecipitation for alpha spectrometry (Section F-5). The UTEVA® resin separation method should separate Np and U, with Np removed in the Th fraction (see e.g., Eichrom Technologies Inc., 2014). For ^{233}Pa tracer solutions prepared 1367 and 1501 days after preparation of the ANU ^{237}Np cow, the separation of Np and U was not effective, however, and the high activity concentration of ^{237}Np compared to ^{233}U led to interference in the alpha spectrum. For this reason, the measurement uncertainty for ^{233}U in the ^{233}Pa tracer solution prepared 1367 after preparation of the ANU ^{237}Np cow was high (>50%), and no result was available for the solution prepared after 1501 days. An additional eluant (10 mL 4 M HCl; step 19) was added to the UTEVA® resin separation method based on Vajda et al. (2003) to more effectively separate Np and U. This was successful for analysis of ^{233}U in the ^{233}Pa tracer solution prepared at 1962 days.

F-4 Actinium-227 separation method

F-4.1 Preparation of an ^{225}Ac tracer

All ^{229}Th tracer solutions used for this thesis were traceable to the NIST US primary standard.

1 Into a 50 mL glass beaker weigh a volume of ^{229}Th tracer solution equivalent to 1.5–2 Bq of ^{229}Th per sample.
2 Evaporate to dryness at 60°C then take up the residue in 20 mL 4 M HCl, heat at 60°C for 5–10 minutes to ensure complete dissolution of Ac.

a. For this project the ^{229}Th tracer was stored in a HNO_3 solution (10% v/v), if the solution is stored in HCl solution then it can be adjusted to the required concentration without the need for evaporation.

3 Add 1 mg of Fe in 4 M HCl solution.

4 Set up two stacked DGA® resin cartridges (2 mL DGA® resin per cartridge, 50–100 µm particle size) attached to an Eichrom® vacuum box (Figure F-1).

5 Attach a 20 mL cartridge reservoir to the top of the stacked cartridges.

6 Equilibrate the DGA® resin by rinsing with 10 mL 4 M HCl.

a. Adjust flow rate to ~1 mL per minute.

7 Add the solution with ^{229}Th to the reservoir.

8 Rinse the cartridge with 2 × 5 mL 4 M HCl and discard rinse.

9 Rinse the cartridge with 10 mL 3 M HNO_3 and discard rinse.

10 Elute Ac with 20 mL 2 M HCl.

a. Collect the eluate in a pre-weighed, acid washed 20 mL HDPE vial.

b. Record the date and time of final Ac separation.

11 Count the ^{225}Ac solution using HRGS for recovery determination after allowing to sit for 4 hours after separation to allow ^{225}Ac progeny ^{213}Bi ^{221}Fr to reach equilibrium with ^{225}Ac.

a. Prepare a calibration standard with the ^{229}Th solution to determine the counting efficiency of the HRGS system in the same geometry as the ^{225}Ac tracer solution.

b. Analyse gamma spectra using the 440.4 keV (26.4% emission intensity) gamma emission of ^{213}Bi and the 218.4 keV (11.42% emission intensity) gamma emission of ^{221}Fr.

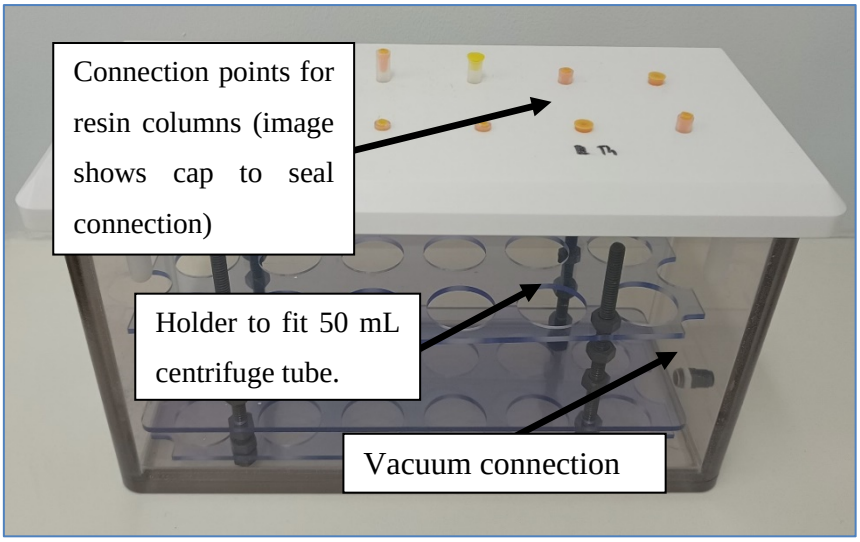

Figure F-1 Eichrom® vacuum box.

F-4.2 Separation of ^{227}Ac

This procedure begins after $PbSO_4$ coprecipitation (Section E-9).

1 Take up the $PbSO_4$ precipitate in 20 mL 4 M HCl.
   a. Additional steps may be required if dissolution is difficult at room temperature in 20 mL of solution. See Section E-9.2 for details.
   b. Ensure the precipitate is fully dissolved and the solution has been cooled to room temperature (e.g., in a cool water bath if heated) before proceeding to the next step.
2 Add 1 mg of Fe in 4 M HCl solution.
3 Set-up a DGA® resin cartridge using an Eichrom® vacuum box (Figure F-1; 2 mL DGA® resin, 50–100 µm particle size). Attach a 20 mL cartridge reservoir to the top of the cartridge.
4 Equilibrate the DGA® resin by rinsing with 10 mL 4 M HCl, discard rinse.
   a. The flow rate can be adjusted at this step and should be kept at approximately 1 mL per minute. Higher or lower flow rates can lead to poor chemical recovery.
5 Add the load solution to the DGA® resin cartridge.
6 Rinse the cartridge with 2 × 5 mL 4 M HCl and discard rinse.
7 Rinse the cartridge with 10 mL 3 M HNO_3 and discard rinse.
   a. Additional 3 M HNO_3 can be added to completely remove Fe if there is remaining yellow colour on the resin.
8 Elute Ac with 20 mL 2 M HCl.

F-5 Source preparation for alpha spectrometry – $Nd(OH)_3$ coprecipitation

Procedures detailed for source preparation of ^{227}Ac, Th, and U for alpha spectrometry are based on the method of Kurosaki et al. (2017).

1 Start with the following solutions in 50 mL beakers:
   a. Ac – 20 mL sample from ‘Separation of ^{227}Ac’ (Section F-4.2) in 2 M HCl solution, in a 50 mL PTFE beaker.
   b. Th – Add 20 mL 2 M HCl to the dried residue from ‘UTEVA® separation method’ Section F-3 above). Gently heat at 50°C for 5–10 minutes to dissolve residue.
   c. U – Add 20 mL 0.01 M HCl to the dried residue from ‘UTEVA® separation method’ (Section F-3 above). Gently heat at 50°C for 5–10 minutes to dissolve residue.

2 Add 0.16 mL of a 0.17 mmol $Nd(NO_3)_3$ solution (equivalent to 25 µg mL^{-1} for a total of 40 µg Nd) and 2 drops of <0.25% bromocresol purple[67] indicator solution. Swirl to mix.
    a. For U samples, add 3 drops of 30% H_2O_2 to one sample only and gently swirl the sample to mix – proceed with one sample at a time to completion to prevent an excessive reaction between the 30% H_2O_2, 0.01 M HCl, and bromocresol purple indicator.
3 While gently swirling continuously, adjust the pH through dropwise addition of 10 M NaOH solution until the indicator's colour change point (orange/yellow changes to purple). To prevent compaction of the precipitate do not excessively agitate solution.
4 Once the colour change is permanent, quickly add 1–2 drops 10 M NaOH solution and swirl gently for 10 seconds and set aside.
5 Set up a PALL™ PES filter unit with a Metricel 0.1 µm pore size, 22.5 mm diameter PP filter.
6 Turn on vacuum pump to a low setting.
    a. Check flow rate throughout procedure to maintain a flow rate of ~1 mL per minute (less than <1 drop every second). Higher flow rates can lead to deep deposition within the filter with potential loss of precipitate (low chemical recovery) and poor resolution of the alpha spectrum.
7 Pre-wet filter with 80% ethanol solution.
8 Add sample in small aliquots (1–2 mL) to prevent adhesion to the walls of the filter funnel.
9 After the sample has filtered, rinse the beaker walls with 4 mL 0.2 M NaOH solution and filter.
10 Rinse the sides of the beaker walls with 4–5 mL 80% ethanol solution and filter.
11 Rinse the sides of the filter holder with 2–3 mL 80% ethanol solution in a circular motion just above the previous aqueous level to wash down any $Nd(OH)_3$ precipitate on the funnel sides.
12 Allow the filter to air-dry before proceeding with alpha spectrometry.
13 For ^{227}Ac analysis, chemical recovery determination using alpha spectrometry should be performed as soon as practicable after the filter is dry. A minimum of 4 hours is required

[67] This indicator is somewhat insoluble in water. Prepare solution by weighing bromocresol purple then adding 2–3 drops 10 M NaOH, swirl (gently to prevent impaction of the precipitate, which can reduce recovery and worsen peak resolution) to dissolve then make to volume (30–50 mL) with high purity water.

for ^{225}Ac to reach equilibrium with progeny. Use the ^{217}At peak at 7067 keV for recovery determination.

F-6 Cleaning of labware

All labware is cleaned in several stages. For new items only step 4 is necessary. Pipette tips, disposable pipettes and disposable syringe filters are rinsed with a small amount of solution to be pipetted or filtered prior to use.

1 If there is visible residue then wipe it off with 96% ethanol and allow to dry

2 Soak in a 3% Decon 90 solution overnight then triple rinse with high purity water.

3 Soak in a 2% conc. HNO_3 acid bath overnight then triple rinse with high purity water and allow to air dry.

   a. For labware used only for ^{227}Ac, further cleaning is not generally required.

   b. For labware used for ^{231}Pa, continue with the remaining procedure.

   c. For labware where relatively high activity concentrations of the analyte of interest (^{227}Ac or ^{231}Pa) have been handled, this additional step may reduce labware contamination: Heat at ~80°C in a 0.2 M alkaline DTPA solution for 1 hour then triple rinse with high purity water and allow to air dry in a covered container to prevent settling of airborne particles.

4 Heat labware for 2 hours in a large beaker, covered with a watchglass, containing conc. HCl to a depth of ~1.5 cm. Heat at a high enough temperature to produce HCl vapour that will reach the surfaces of all labware. After removing from the beaker, triple rinse with high purity water.

5 Soak in a 2% conc. HNO_3 acid bath, prepared with high purity water overnight then triple rinse with high purity water and then oven dry at 70°C. Place all cleaned labware in a covered container if oven drying cannot be undertaken immediately.

6 Place clean, dried labware in sealable plastic bags for storage.

Appendix G Alpha spectrometry – ^{227}Ac analysis

In setting of ROI for alpha spectrometry, typical ranges used for ^{217}At (for recovery determination as progeny of ^{225}Ac) were 6.68–7.13 MeV, and 5.45–6.07 MeV for ^{223}Ra and ^{227}Th combined. Although the alpha spectrum with typical resolution (40–50 keV at FWHM) of ^{223}Ra typically extends out to ~5.34 MeV, the ROI used for this project were truncated to include only counts on the spectrum greater than or equal to 5.45 MeV[68] to remove counts from ^{228}Th. This was because contamination of alpha spectrometers with ^{228}Th and progeny is not uncommon where they have been used for analysis of Th isotopes or where ^{232}U has been used as a tracer for measurement of U isotopes. Such contamination can account for a substantial proportion of the total background counts for low-level alpha spectrometry. Most detectors used for this project had some degree of contamination from ^{228}Th and truncation of the ROI typically reduced the background count rate by half or more. Excluding this region did, however, reduce the total counts from ^{223}Ra + ^{227}Th by 5.8% (assuming an alpha resolution of 103 keV at FWHM as per Figure G-1 below). Overall, truncation of the ROI to remove counts from ^{228}Th led to an improvement in the precision for each measurement and a greater likelihood of results greater than the MDL.

G-1 Radium breakthrough in ^{227}Ac analysis by alpha spectrometry

All alpha spectra for ^{227}Ac analysis were assessed for the presence of ^{226}Ra and ^{228}Th to check that chemical separation had been effective for these isotopes. For most samples there were no above background peaks recognised for these isotopes, however ^{226}Ra was noted for seven samples. These were all five of the freshwater mussel samples (2018-686 to 2018-704), a cluster fig (XX12093) and an Agile wallaby bone sample (RM13078). For all samples except the cluster fig, results for ^{226}Ra were available (Table B-2) and Ra breakthrough could therefore be determined. For the mussel samples Ra breakthrough was 0.47±0.17% with a range of 0.17–0.59%, whereas for the bone sample it was only 0.022%. This breakthrough was higher than expected based on assessment of the effectiveness of separation using the DGA® resin separation method (Dulaiova et al., 2013; see also Chapter 4, Section 4.2.3).

[68] The maximum energy of ^{228}Th is 5.42 MeV, however, the alpha spectrometers used were energy calibrated with the channel with the highest counts equal to the maximum alpha particle energy of that emission, hence the slightly higher cut-off value. The reduced coverage of the ^{223}Ra + ^{227}Th alpha emission by truncating the ROI used was accounted for when determining the alpha spectrometer efficiency.

Given the relatively high Ra activity concentrations in mussels and bones, which can bioaccumulate Ra (e.g., Bollhöfer et al., 2011), this represented a high potential for interference from progeny of both ^{226}Ra and ^{228}Ra. In the case of ^{226}Ra, ^{222}Rn is the direct daughter and, with losses of ^{219}Rn measured at 26%, the far longer half-life of ^{222}Rn indicated losses would potentially be much higher. Modelling was undertaken to determine if ^{222}Rn losses were such that ^{222}Rn and progeny were unlikely to present a risk of interference in the alpha spectrum where ^{223}Ra and ^{227}Th were used to determine ^{227}Ac activity concentrations. This was done by combining the alpha spectra for three mussels (counted in the same alpha chamber). Peak fitting parameters for alpha peak resolution were determined using the method of García-Toraño (2003) for the ^{226}Ra peak at 4.78 MeV (see Chapter 4, Section 4.2.3 for details; alpha resolution at FWHM was 103 keV). The spectrum of ^{226}Ra progeny was then modelled and overlaid on the combined mussel spectrum (Figure G-1), clearly showing that ^{226}Ra progeny are not present at the same activity as the parent isotope in the mussel spectra.

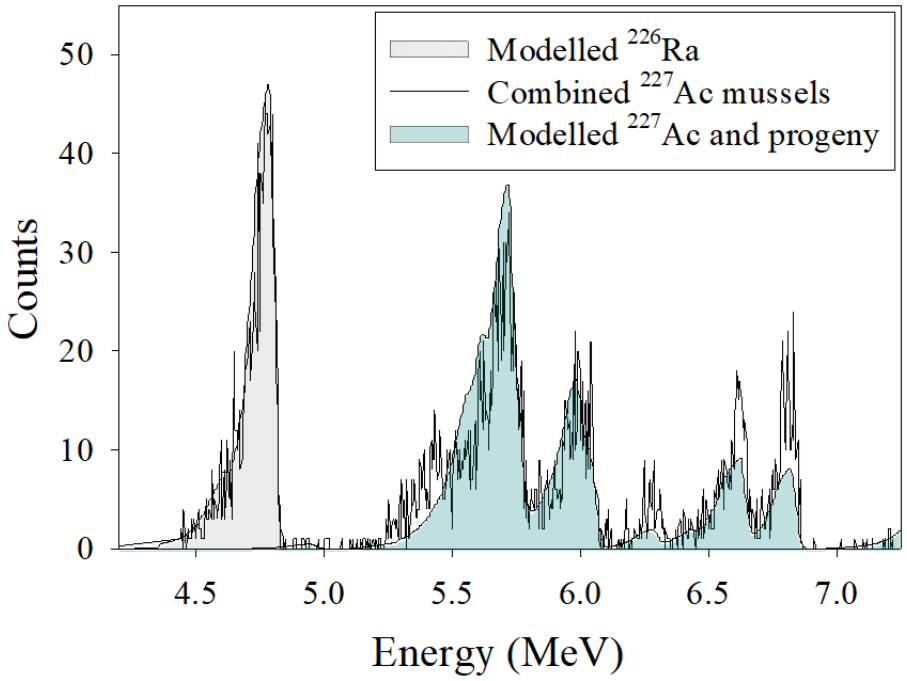

Figure G-1 Modelled ^{226}Ra and progeny overlaid on combined freshwater mussel ^{227}Ac spectra with ^{226}Ra contamination present (FWHM estimated at 103±6 keV using the method of García-Toraño, 2003). Labels correspond to the parent isotopes responsible for each peak.

Further modelling was undertaken to create a spectrum based on an activity of ^{227}Ac and progeny that would match the calculated activity of the combined mussel spectra (Figure G-2). It is apparent that there is a slight increase in counts in the region around 5.1–5.4 Mev. Although this may reflect some contribution from ^{222}Rn, it is more likely that it is from ^{228}Th, present from the decay of ^{228}Ra that, if present, as a beta emitter, must be inferred from progeny.

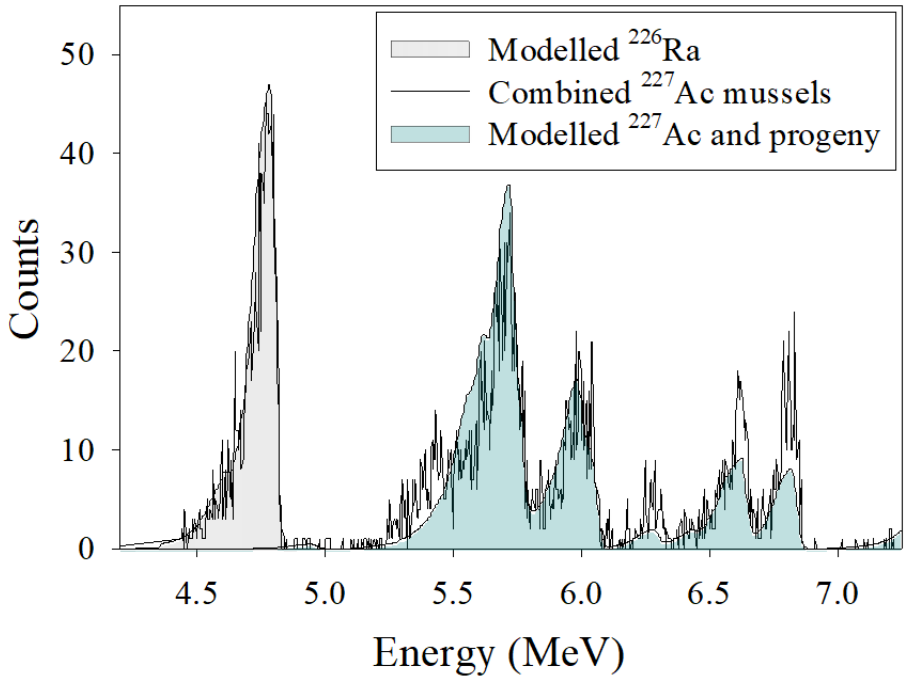

Figure G-2 Modelled ^{226}Ra only overlaid on combined freshwater mussel ^{227}Ac spectra with ^{226}Ra contamination present (FWHM estimated at 103±6 keV using the method of García-Toraño, 2003). Labels correspond to the parent isotopes responsible for each peak.

There is no Rn intermediate between ^{228}Ra and progeny ^{228}Th and ^{224}Ra, both of which have alpha emission energies that overlap to a degree with the '^{223}Ra + ^{227}Th' ROI (see modelled spectra Figure G-3).

The ^{226}Ra:^{228}Ra ratio for biota in the study region, a uranium rich province, is typically >1 (e.g., Bollhöfer et al., 2011). For the samples in this study where results were available the average ratio was 3.4±1.3 (n=14), with mussels at 3.0±0.9 (n=8, with one sample mussel shell, and seven soft tissue results) and higher for non-mussels at 4.0±1.6 (n=6). Thus, counts attributable to ^{226}Ra on the alpha spectrum can be used to infer counts attributable to ^{228}Ra progeny based on the ^{226}Ra:^{228}Ra ratio and relative ingrowth after separation from Ac. Of the seven samples where above background counts of ^{226}Ra were identified, the ^{226}Ra:^{228}Ra ratio was known[69] for six. The number of ^{224}Ra counts attributable to ^{224}Ra decay were determined for these six samples and subtracted from the total counts for ^{223}Ra + ^{227}Th. The counts attributable to ^{228}Th were excluded by routine ROI setting as described above.

[69] For the sample XX12093 less than 10% of the total counts recorded in the ^{223}Ra + ^{227}Th ROI could be attributed to ^{224}Ra, using the ^{226}Ra:^{228}Ra ratio of RM07011, the only fruit sample where this ratio is known from the project samples. This value, however, was not used to correct the reported value, which therefore may be a slight overestimate of the true value.

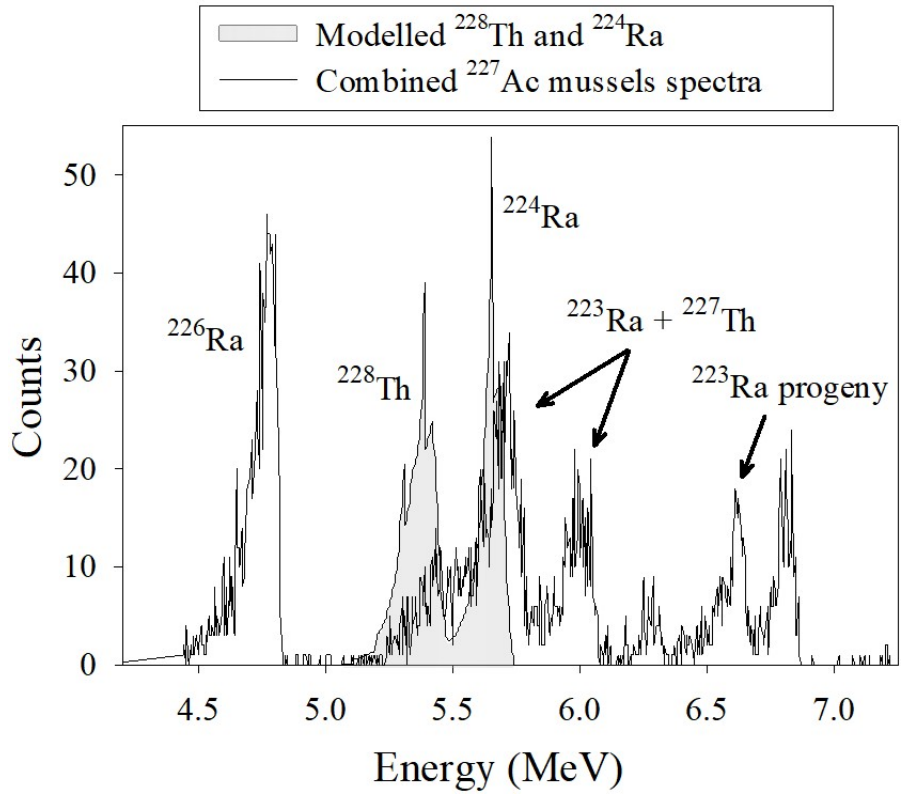

Figure G-3 Modelled progeny of ^{228}Ra (^{228}Th and ^{224}Ra) overlaid on combined freshwater mussel ^{227}Ac spectra with ^{226}Ra contamination present (FWHM estimated at 103±6 keV using the method of García-Toraño, 2003). Labels correspond to the parent isotopes responsible for each peak.

Although there is also the potential for breakthrough of ^{225}Ra during preparation of the ^{225}Ac tracer, activity concentrations of ^{225}Ra at the count time were considered negligible. This is attributed to the use of two stacked DGA® resin cartridges for ^{225}Ac tracer preparation, a further DGA® resin separation for each sample, and a 178-day ingrowth period for ^{223}Ra and ^{227}Th (i.e., with the ^{225}Ra half-life of 15 days, trace amounts would have decayed by the count time).

G-2 Alpha recoil – ^{223}Ra

Alpha recoil was noted on several alpha detectors after counting high activity ^{227}Ac samples (quality control samples spiked with ^{227}Ac; see Section J-3). This was evidenced by the presence of alpha peaks from decay of ^{223}Ra and progeny in chamber background spectra (i.e., an empty alpha chamber with no sample), indicating alpha recoil from decay of ^{227}Th. Subsequent measurements included chamber background counts being conducted prior to counting sample batches for measurement of ^{227}Ac to ensure complete decay of contamination from alpha recoil of ^{227}Th.

Appendix H High-resolution gamma spectrometry

High-resolution gamma spectrometry (HRGS) using planar high purity germanium detectors (HPGe) was undertaken for a range of purposes throughout this thesis and primarily used for measurement of ^{233}Pa and ^{237}Np, but also used for measurement of ^{225}Ac. The detector used for most measurements was an ORTEC™ GMX series HPGe crystal with a diameter of 49 mm and length of 68.2 mm. Calibrated performance gave a resolution of 0.63 keV and 1.75 keV at 5.9 keV and 1.33 MeV respectively. The detector was housed in 101 mm thick Pb shielding with inner liners of 0.5 mm Sn and 1.6 mm Cu.

All detectors used were calibrated for the sample geometry used, with samples and calibration standards placed centrally and directly above the HPGe thin window, with a thin plastic (Glad® Wrap or HDPE cap) cover to prevent contamination of the detector surface.

The most common sample geometry used for ^{233}Pa and ^{237}Np was a 1 mL solution in a 20 mL HDPE vial, double bagged in thin LDPE bags and secured in a PTFE sample holder (see Figure H-1). Where different sample volumes were used, standards were prepared from a calibrated ^{237}Np solution at different volumes. Eluant aliquots were diluted with an appropriate amount of the same solution (e.g., 3 mL HNO_3) to match the volume and matrix of one of the prepared standards.

Figure H-1 A close-up of 1 mL solution in 20 mL HDPE bottle (left) and secured in a PTFE sample holder (right).

The efficiency of the HPGe detector was determined using a 1 mL aliquot of a ^{237}Np NIST certified standard solution. To determine the reproducibility of this sample geometry, the 20 mL HDPE bottle was removed from the sample holder and plastic bags then repacked for counting a total of 20 times. The standard deviation of 1.3% determined was used as the sample counting geometry uncertainty. The gamma emissions used for activity determination throughout this thesis were 29.4 keV for ^{237}Np and 311.9 keV for ^{233}Pa (See Chapter 3, Figure 3-8).

For samples analysed for ^{231}Pa, chemical recovery was determined through comparison of the 311.9 keV counts from ^{233}Pa decay measured in a sub-sample of the cow extract used to spike samples with the counts measured in the eluant from TK400® resin, which contained the ^{231}Pa extracted from the sample.

The ^{237}Np gamma decay photon analysed has the highest emission probability (14.3%) in the decay process but is present in the low energy (29.4 keV) region of the gamma spectrum typically associated with a high background. This is generally owing to elevated counts in the Compton continuum associated with higher gamma energies. The next most probable gamma ray arising from ^{237}Np decay (12.3% at 86.5 keV) is in a lower background region but cannot be effectively resolved from the ^{233}Pa gamma emission line at 86.6 keV, which has an emission probability of 16.1%. All other gamma emissions of ^{237}Np have an emission probability below 0.4%. Hence, determination of ^{237}Np activity was based solely on the 29.4 keV gamma ray.

Where the activity of ^{233}Pa in a measured sample was substantially higher than ^{237}Np, the background in the region around 29.4 keV resulted in a substantially higher detection limit for ^{237}Np. To overcome this issue, where possible, time was allowed for ^{233}Pa and ^{237}Np to reach a state of secular equilibrium such that the 311.9 keV gamma ray from ^{233}Pa decay, which has a higher emission probability (38.3%) and lower system background, could be used to infer the ^{237}Np activity with a lower detection limit.

The sample geometry used for ^{225}Ac was a 20 mL solution in a 20 mL HDPE vial, double bagged in thin LDPE bags and secured in a PTFE sample holder (see Figure H-1). The efficiency of the HPGe detector was determined using a 0.5 mL aliquot of a ^{229}Th NIST certified standard solution diluted to 20 mL with high purity water. The standard deviation of 1.3% derived from the ^{237}Np standard vial (see Figure H-1) was used as the sample counting geometry uncertainty. The gamma emissions used for activity determination throughout this thesis were 440.44 keV for ^{213}Bi and 218.12 keV for ^{221}Fr with emission probabilities of 26.1% and 11.42% respectively.

H-1 Non-standard sample counting geometries

Throughout the project non-standard sample counting geometries were used to provide estimates of the activity of ^{233}Pa throughout the measurement process. The HRGS counting efficiencies for these geometries was less reproducible than the 1 mL standard solution noted above owing to uncertainty in the distribution of ^{233}Pa within the measured item. For example, beakers and resin columns were counted and although the sample counting geometry was

reproducible, the distribution of ^{233}Pa on the resin column or where it may have attached to a beaker (e.g., walls or base) was unknown. This can lead to a substantially different efficiency for the same sample counting geometry (Gilmore, 2008). In light of the effort required to achieve this, it was decided the determination of a reliable calibration for each geometry was not warranted. However, simple calibrations for the different geometries was undertaken, such as by evaporation of a known activity of ^{233}Pa in a beaker or by comparison with a similarly shaped item (see Table J-2 in Section J-2 below). Despite this, substantial variations in counting efficiencies for various items compared to the calibrated value are likely to exist and such measurements were considered semi-quantitative only.

H-2 Distribution of ^{237}Np on the ^{237}Np prototype cow.

A semi-quantitative estimate of the distribution of ^{237}Np on the ^{237}Np prototype cow (Chapter 3, Section 3.3.1.4) was made by counting the TEVA® column using HRGS. The sample geometry used involved placing the column in a Pb cradle with a 6 mm diameter hole in the centre (Figure H-2) to provide a counting window placed centrally and directly above the HPGe thin window. Alternative sections of the column were placed above the hole and repeat HRGS measurements were made. Relative count rates were used to determine the distribution assuming 100% of ^{237}Np was measured.

Figure H-2 Pb cradle with 6 mm diameter centre hole top view (top). A TEVA® resin column prepared for gamma counting (bottom).

Appendix I Accelerator Mass Spectrometry

The methods used for AMS are described in Chapter 3 (Section 3.11), with further details in (Medley et al., 2019). Counting for most sample batches used 'slow-cycling', with total measurement times of 1080 s, starting with 120 s for mass 233 (three runs, total count time 480 s) and alternating to 300 s for mass 231 (two runs, total count time 600 s). For blanks, 300 s for each mass was used, for the ^{231}Pa standard 120 s for each mass was used. For several samples with low ^{233}Pa recovery, the count time per run at mass 233 was increased to 300 s. Count times for 'fast-cycling' measurements of the final batch of samples were 150 s at mass 233 and 375 s at mass 231 for all samples and blanks (Chapter 3, Section 3.12.2).

Appendix J Quality control and Quality assurance for ^{227}Ac and ^{231}Pa measurements

J-1.1 Blank assessment and minimum detection limits

Blank determination can take several paths, typically a surrogate sample that is passed through the full chemical measurement process is used. An alternative approach is to examine each step of a measurement process for contributions from contamination and interference. Importantly, where a tracer is used for blank assessment, it must be recognised that partial recoveries at each stage of a measurement process, may lead to the final tracer recovery not being representative of contaminants and interferences introduced at different stages (Currie, 1995). To overcome some of the challenges in obtaining an appropriate measure of the blank signal different types of blank sample can be run. The samples for blank assessment run over the course of sample processing and analysis for this project are detailed in the following sections.

J-1.2 Blank assessment for ^{227}Ac sample analysis

The following blanks were run throughout sample processing and analysis for ^{227}Ac

- An analytical blank was run with each batch of samples. This comprised an empty Pt crucible for two biota batches, for other biota batches the analytical blank was started at the $PbSO_4$ coprecipitation (see Section E-9 and Chapter 4, Section 4.2.3) stage using 800–900 mL high purity water acidified to 0.5% HCl. For the soil samples this was an empty PTFE beaker beginning at the HF digest stage and processed as per samples.
- Spiked blanks were run with two biota batches, starting at the $PbSO_4$ coprecipitation stage as per analytical blanks at which point ^{225}Ac tracer solution was added with approximately the same activity as samples. A further spiked blank was run with the batch of soil samples, which comprised ^{225}Ac tracer solution added to a PTFE beaker, evaporated to dryness then starting with the HF digest stage and processed as per samples.

Blank count rates were low and in the range of 3±3 counts per day for analytical blanks in the ^{223}Ra + ^{227}Th ROI. The instrument blank accounted for 0.4±0.3 counts per day with the remainder likely attributable to the presence of ^{227}Ac or other radionuclides with alpha emission energies in that range (e.g., ^{210}Po, ^{226}Ra, and progeny of ^{228}Th). These levels are very low and are equivalent to a level of alpha activity of <0.18 mBq at the time of counting after correction

for a detector efficiency of 17%. Note that several of the alpha spectrometers used had a low background contamination of ^{228}Th (see Appendix G).

J-1.3 Blank assessment for ^{231}Pa sample analysis

The following blanks were run throughout sample processing and analysis for ^{231}Pa

- analytical blanks were run with five sample batches. An analytical blank comprised an empty PTFE beaker beginning at the digest stage and processed as per samples,
- analytical blanks were also run for the tracer purification steps with TEVA® (for ^{233}Pa tracer milked 858 days after preparation of the ANU ^{237}Np cow) and TK400® resins (all ^{233}Pa tracers except the one milked 1962 days after preparation), and
- spiked blanks were run with seven sample batches. This comprised an empty PTFE beaker beginning at the digest stage and processed as per samples with addition of ^{233}Pa tracer solution of approximately the same volume and activity concentration as per samples.

Spiked blank measurements were used to correct ^{231}Pa results (see Equation A-9 in Section 6.6, Section A-2 for calculation of ^{231}Pa activity concentrations, including blank correction). For analytical blanks the chemical recovery cannot be determined and, as AMS measures a ratio (e.g., ^{231}Pa/^{233}Pa), the transmission efficiency of Pa cannot be determined, therefore only an absolute blank count rate can be measured for mass 231. This may lead to over-estimation of the blank count rate where transmission efficiency and/or recovery is higher than for samples and vice versa. However, potential contamination at mass 233 could be determined with analytical blanks. Only two analytical blanks recorded counts at mass 233, for ^{233}Pa tracer milked at 858 days a single count was recorded (0.0014 counts per second), whereas for the tracer prepared at 1962 days the analytical blank for Batch 1 recorded six counts (0.0080 counts per second).

For spiked blanks, although the overall chemical recovery (HRGS) and transmission efficiency (AMS) can be determined, partial recoveries at different stages of the measurement process are unknown. They may over-estimate the blank contribution, as there is a limitation with AMS methods in general, particularly where there is limited scope for taking detailed measurements for more accurate blank analysis. For the samples here, the potential amount the blank could be over-estimated is very low, so it is unlikely to have led to substantial differences in the estimated blank signal. There is scope for determining an improved way to correct the blank with low count AMS measurements. An improvement realised in this thesis was the application of the

fast-cycling method (see Appendix I) for counting of samples and blanks with the last sample batch. This substantially increased the number of times the spiked blanks could be counted, leading to greater precision in the measurement of the blank signal.

Data from blank measurements, including the average MDL associated with the blank for each batch of samples is shown in Table J-1. The average MDL was determined by multiplying the uncertainty of the blank signal (σ_B; in atoms) by 4.65 (as per Currie, 1968) then converting to an activity concentration for the dry weight of samples in the batch (~2 g). The MDL achieved was several orders of magnitude lower than typical for alpha spectrometry[70] and is similar to the estimate of 1 mBq kg^{-1} as the required MDL for ^{227}Ac in biological samples from the ARR by Martin et al. (1998).

[70] For a typical detection limit of 1 mBq for alpha spectrometry, 2 g of sample would yield an MDL of 500 mBq kg^{-1}.

Table J-1 Blank data from AMS analysis for ^{231}Pa.

^{233}Pa tracer (number of days after preparation of the ANU ^{237}Np cow the solution was milked)	**858**		**1367**		**1501**		**1962**	
	Batch 1	**Batch 2**	**Batch 1**	**Batch 2**	**Batch 1**	**Batch 2**	**Batch 1**	**Batch 2**
Analytical blank (Avg counts $s^{-1} \times 10^{-4}$)[a]		113±53			1.3	33	1.3±3.0	No counts
Spiked blanks (Avg counts $s^{-1} \times 10^{-4}$)	40.6±1.4		7.1±3.6	5.7±2.5	6.7±1.4	20.6±8.3	22±27	21±83
Spiked blank[b] (^{231}Pa atoms, ^{233}Pa corrected $\times 10^{6}$)	57.4±2.0		11.0±5.6	9.0±4.1	9.1±2.0	23.0±9.6	3.1±4.4	2.4±4.8
Average MDL[c] for batch (mBq kg^{-1})	10.5 (1.9)		8.1 (1.6)	6.0 (2.2)	3.3 (0.6)	15 (4.3)	2.8 (1.9)	3.7

[a] For ^{233}Pa tracer milked at 1501 days, the analytical blank was only measured once, hence no standard deviation from repeated measurements is given. No analytical blanks were run with ^{233}Pa tracer milked on 1367 days. An analytical blank was only run with Batch 2 for ^{233}Pa tracer milked at 858 days with a single count at mass 233 recorded over a total count time of 716 s.

[b] A spiked blank was only run with Batch 1 for ^{233}Pa tracer milked at 858 days.

[c] Approximate sample mass of 2 g, dry weight. MDL average for wet weight of samples in batch is given in parentheses. Average MDL for batch based on '$\sigma_B \times 4.65$'.

J-2 Losses of Pa and chemical recovery of ^{233}Pa

The chemical recovery of ^{233}Pa was determined for each sample. To assess where losses of ^{233}Pa may have occurred in the measurement process and allow the method to be adapted to minimise potential losses, an 'activity balance' was undertaken for all sample batches. This involved HRGS measurement of most laboratory equipment used for sample preparation and chemical separation of ^{231}Pa after the addition of ^{233}Pa tracer solution. The range of this equipment is shown in Figure J-1 and detailed below.

Figure J-1 Laboratory equipment used for sample preparation and chemical separation of ^{231}Pa.

From the left across the top row then bottom row in Figure J-1, the list of equipment is:

1 A 100 mL PTFE digestion vessel. This was sealed with a lid that may have had minimal contact with sample from bubbling during the digestion process.

2 A 50 mL syringe (PP, the gasket is a thermoplastic elastomer and there is a silicone oil lubricant) with a 0.45 µm pore size PES syringe filter (with modified acrylic syringe filter housing).

3 50 mL PTFE beaker.

4 100 mL PTFE beaker.

5 50 mL centrifuge tube (PP) containing supernatant from PbSO4 coprecipitation.

6 50 mL centrifuge tube (PP) containing 3 or 5 mL disposable pipette (PET).

7 2 mL PP columns with 25 mL extension funnel and column connector (these are sealed with Parafilm™.

8 50 mL glass beaker (for collecting the 10 M HCl fraction from TK400® separation.

9 Ceramic crucible (with lid).

10 25 mL PTFE beaker.

11 3 types of 20 mL PFA vials.

In addition to this, PP pipette tips that were used for dispensing ^{233}Pa tracer solution were not measured with HRGS. For some samples, additional centrifuge tubes, syringes and PES filters or PTFE beakers were used if needed (such as when additional particulate material needed to be removed before proceeding to the next stage of the separation procedure). Measurements for these have been combined into a single value (e.g., all results from centrifuge tubes or PES filters for the same sample were combined). The efficiency calibrations for the various sample components used are shown in Table J-2.

Table J-2 Sample counting geometry efficiencies for HRGS measurement of laboratory equipment.

Geometry	**Efficiency (Counts ks^{-1} Bq^{-1})**	**Calibration method**
1 mL HDPE bottle	25.5±0.7	1 mL of ^{233}Pa solution (see Appendix H)
50 mL PTFE beaker[a]	14.8±0.2	Evaporation of ^{233}Pa solution
Centrifuge tubes	10.4±8.6	Average of a centrifuge tube with 11, 18 and 25 mL of ^{233}Pa solution
TK400® resin column[b]	8.3±7.0	As for centrifuge tube with only 18 mL and 25 mL volumes used
PFA Vials (20 mL)		1 mL of ^{233}Pa solution
Round base	12.5±1.1	
Flat base	15.7±0.8	
Conical base	14.9±2.1	
Ceramic crucible	31.8±1.2	Evaporation of ^{233}Pa solution

[a] This geometry also used for 100 mL PTFE digestion vessel, 50 mL glass beaker, 100 mL PTFE beaker, HF digest vessels (used for soils only), and PES filters after double bagging in HDPE bags.
[b] The counting geometry for these was after double bagging in HDPE bags and placing in a 100 mL tall-form sample container standing upright.

Owing to non-standard sample counting geometries as noted above (Section H-1) the accuracy of each measurement is uncertain, and results should be considered as semi-quantitative. As such, direct summation of activities measured in different fractions may be higher or lower than 100%, though many summed results do account for close to 100% of the added activity. However, the sensitivity of HRGS allowed for very high precision in these measurements such that comparison of results for the same sample geometry should generally be quite reliable. Not all pieces of equipment were used for all samples, but in general results shown in Figure J-2 for each piece of equipment or solution are for 30–50 samples.

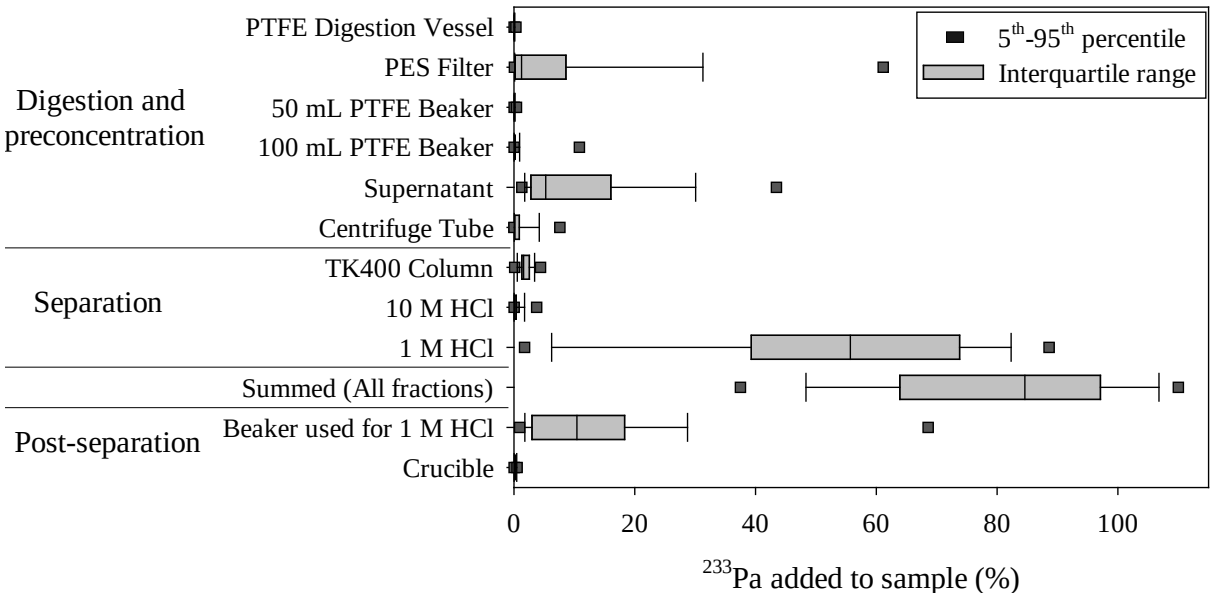

Figure J-2 Boxplots of relative activity of ^{233}Pa in laboratory equipment compared to that added to each sample analysed for ^{231}Pa. Spiked blanks are included in the dataset.

The chemical recovery for ^{233}Pa is the relative recovery shown for the 1 M HCl fraction. As noted in Chapter 3, the highest losses occurred with the PFA vials and PTFE beakers that were used to collect then evaporate the 10 mL of 1 M HCl solution used to extract Pa from the TK400® resin. This was subsequently resolved by addition of Fe prior to evaporation.

The biggest losses on the PES filters were from samples where visible particulates after digestion were observed, suggesting incomplete digestion that could be improved by implementing one or more of the following: longer digestion times, higher temperatures, increased oxidative power (e.g., using a higher volume of H_2O_2).

The biggest losses in the supernatant fraction were samples with high salt loads, i.e., soils, bone samples with high Ca or whole animal samples. This could be improved with further dilution prior to $PbSO_4$ precipitation or using lower sample mass. The use of MnO_2 coprecipitation for samples where Fe concentrations are expected to be low may also yield higher recovery as this

method tends to be less sensitive to the higher salt loads. The highest losses on the PTFE beakers were from the spiked blank samples (e.g., only ^{233}Pa tracer added and no sample material). This may potentially be overcome by a small amount of a carrier element.

J-3 Quality control samples and chemical recovery for ^{227}Ac sample analysis

An additional quality control sample was run with five of the biota sample batches. These were prepared as per spiked blanks (Section J-1.2), with an additional solution of ^{227}Ac tracer added. All ^{227}Ac results for these samples were within uncertainty of the expected ^{227}Ac activity added.

Recoveries for soil samples (95±4%), spiked blanks and the five quality control samples (75±34%), were higher than for all other samples (60±49%). A Student's t-test showed recovery for the two batches of samples analysed in 2020 (freshwater mussels and prawns[71], mean 43±11%) was significantly lower than for all other biota (mean 62±42%), $t(46) = 2.88$, $p = .01$. This may be related to the age of the DGA® resin cartridges used for this batch, which were >5 years old when used. Chemical recovery at the $PbSO_4$ coprecipitation stage may potentially be improved by heating during coprecipitation, with improved recovery using heating noted by (Rogers and Watrous, 1955) and also used by (Dulaiova et al., 2013). However, the relatively high recovery for soil samples, suggests low recoveries may be more likely associated with sample type than the radiochemical procedure. For biota samples, increasing the sample mass may have led to lower recoveries through increased matrix interference, however, linear regression indicated there was no correlation between the sample mass and chemical recovery ($R^2 = 0.001$; Figure J-3). This suggests there is the potential to further increase sample mass to reduce the MDL for ^{227}Ac analysis of biological samples.

[71] These were analysed as part of a different project and included edible flesh and other tissues. Sample masses ranged from 2.1 g dry weight for hepatopancreas to 39.4 g dry weight for whole boiled prawns.

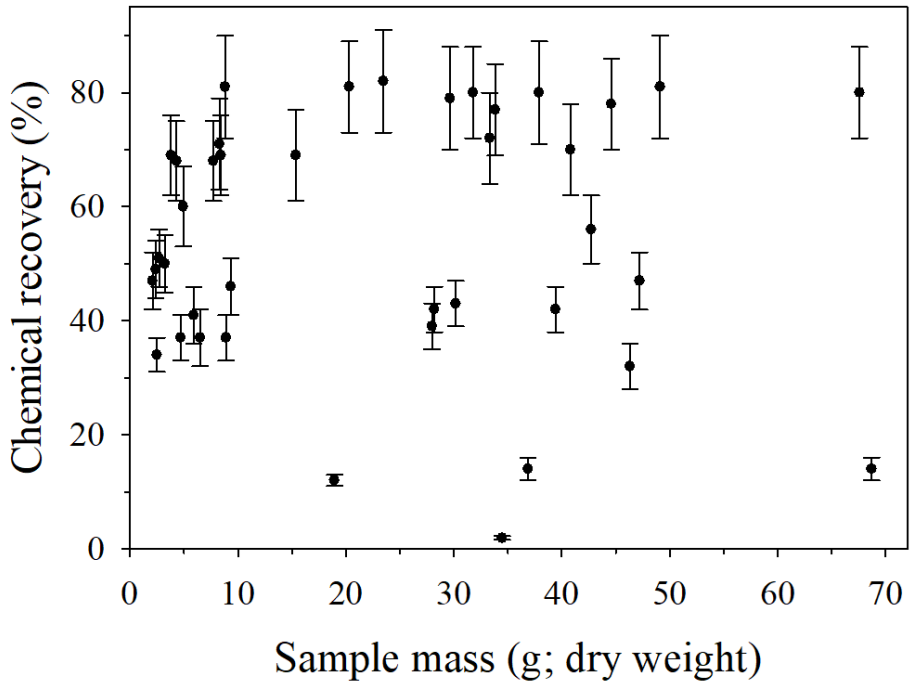

Figure J-3 Comparison of chemical recovery of ^{225}Ac in analysis of ^{227}Ac with sample mass used for analysis of biota samples.

Appendix K Medley et al (2019) publication

The following publication was an outcome of the research conducted for this thesis:

Medley, P., Tims, S.G., Froehlich, M.B., Fifield, L.K., Bollhöfer, A., Wallner, A., Pavetich, S. 2019. Development of ^{231}Pa AMS measurements to improve radiological dose assessment from uranium mining and milling. Nuclear Instruments and Methods in Physics Research Section B: Beam Interactions with Materials and Atoms 438, 66-69.